SPACE SYSTEMS

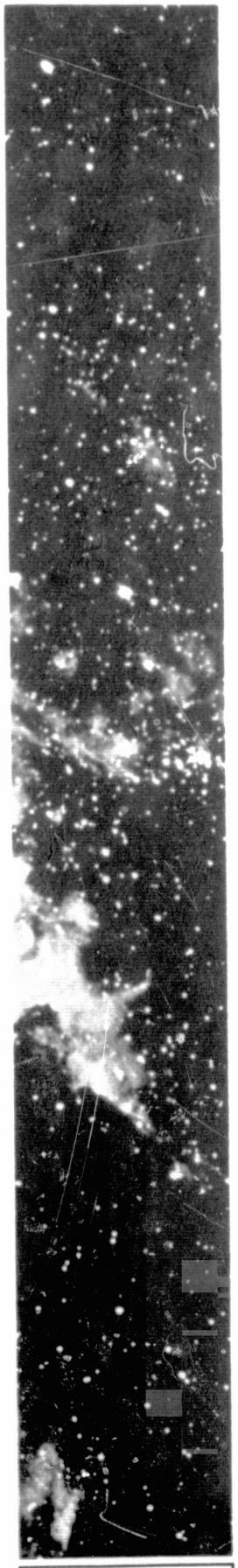

# STUDY FOR PASSIVE GRAVITY STABILIZATION

N69-35262
(ACCESSION NUMBER)
318
(PAGES)
CR-98036
(NASA CR OR TMX OR AD NUMBER)
(THRU)
1
(CODE)
31
(CATEGORY)
FACILITY FORM 602

## FINAL TECHNICAL REPORT

GENERAL ELECTRIC

DOCUMENT NO. 68SD4310
30 AUGUST 1968

# STUDY FOR PASSIVE GRAVITY STABILIZATION FINAL TECHNICAL REPORT

CONTRACT NAS 8-21177

JULY 1967 THROUGH MARCH 1968

APPROVED BY: H. S. Klose

H. KLOSE, MANAGER
STABILIZATION AND CONTROL PROGRAMS

SUBMITTED TO:

ASTRIONICS LABORATORY
MARSHALL SPACE FLIGHT CENTER
HUNTSVILLE, ALABAMA

GENERAL ELECTRIC
MISSILE AND SPACE DIVISION
Valley Forge Space Technology Center
P.O. Box 8555 • Philadelphia, Penna. 19101

PRECEDING PAGE BLANK NOT FILMED.

TABLE OF CONTENTS


| Section | | Page |
|---|---|---|
| 1 | INTRODUCTION | 1-1 |
| | 1.1 Purpose | 1-1 |
| | 1.2 Background for the Study | 1-2 |
| | 1.3 Goals | 1-5 |
| | 1.3.1 Flight Demonstration Goals | 1-5 |
| | 1.3.2 Flight Experiment Goals | 1-5 |
| 2 | SUMMARY OF RESULTS | 2-1 |
| | 2.1 Stabilization Configuration and Performance | 2-1 |
| | 2.1.1 S-IVB Vertical Configuration - 400 KM Orbit Altitude | 2-1 |
| | 2.1.2 S-IVB Vertical Configuration (Preferred Yaw Position) - 400 KM Altitude | 2-3 |
| | 2.1.3 S-IVB Horizontal Configuration - 400 KM Altitude | 2-7 |
| | 2.1.4 Lunar Module Configuration-Synchronous Altitude | 2-7 |
| | 2.2 Rod Flight Experiment Configuration and Performance | 2-11 |
| | 2.2.1 Bending Stiffness | 2-13 |
| | 2.2.2 No Load Straightness | 2-13 |
| | 2.2.3 Thermal Distortion and Impulse | 2-14 |
| | 2.2.4 Extension-Retraction and Damping | 2-14 |
| | 2.2.5 Data Requirements | 2-14 |
| | 2.3 Recommended Flight Experiment | 2-14 |
| | 2.4 Program Plan for Flight Experiment | 2-18 |
| 3 | GRAVITY GRADIENT STABILIZATION CONFIGURATION FOR THE S-IVB STAGE | 3-1 |
| | 3.1 Definition of Properties | 3-1 |
| | 3.1.1 Nominal Orbit | 3-1 |
| | 3.1.2 Definition of the S-IVB Mass/Inertia Properties | 3-4 |
| | 3.1.3 Definition of S-IVB Aerodynamic Torques and Magnetic Torques | 3-9 |
| | 3.2 S-IVB Two Axis Local Vertical Configuration | 3-10 |
| | 3.2.1 Configuration Description | 3-10 |
| | 3.2.2 Configuration Analysis | 3-11 |
| | 3.2.3 Nominal Performance | 3-24 |
| | 3.2.4 Parametric Studies | 3-35 |
| | 3.3 Three-Axis Configuration-Long Axis Vertical | 3-43 |
| | 3.3.1 Configuration Selection | 3-43 |
| | 3.3.2 Nominal Performance | 3-46 |

TABLE OF CONTENTS (Cont'd)


| Section | | | Page |
|---|---|---|---|
| | 3.4 | Alternate S-IVB Vertical Configurations | 3-49 |
| | 3.4.1 | Alternate No. 1 (Appendix B) | 3-49 |
| | 3.4.2 | Alternate No. 2 (Appendix C) | 3-49 |
| | 3.5 | Three-Axis Configuration-Long Axis Horizontal | 3-49 |
| | 3.5.1 | Configuration Selection | 3-49 |
| | 3.5.1.1 | Preliminary Analysis | 3-50 |
| | 3.5.1.2 | Final Analysis | 3-53 |
| | 3.5.2 | Nominal Performance | 3-66 |
| | 3.5.2.1 | Steady State Performance | 3-66 |
| | 3.5.2.2 | Transient Performance | 3-72 |
| | 3.5.3 | Parametric Studies | 3-75 |
| | 3.5.3.1 | Effect of Rod Length and Tip Weight Upon Steady State Performance | 3-75 |
| | 3.5.3.2 | Parametric Damping Characteristics | 3-83 |
| | 3.5.3.3 | Predicted Performance Variation with Altitude | 3-84 |
| 4 | | DESIGN OF A PASSIVE STABILIZATION SYSTEM FOR THE LUNAR EXCURSION MODULE AT SYNCHRONOUS ALTITUDE | 4-1 |
| | 4.1 | Definition of Properties | 4-1 |
| | 4.2 | General Approach | 4-3 |
| | 4.3 | Configuration Selection | 4-3 |
| | 4.3.1 | Gravity Gradient Rods | 4-4 |
| | 4.3.2 | Damper Boom | 4-4 |
| | 4.3.3 | Total Systems Inertias | 4-5 |
| | 4.4 | Nominal Performance | 4-5 |
| 5 | | GRAVITY GRADIENT ROD AND TIP MASS FLIGHT EXPERIMENT | 5-1 |
| | 5.1 | Experimental Goals | 5-1 |
| | 5.1.1 | Possible Flight Measurements | 5-3 |
| | 5.1.2 | Experimental Procedures | 5-7 |
| | 5.1.3 | Static Experiments | 5-7 |
| | 5.1.4 | Dynamic Experiments | 5-10 |
| | 5.1.5 | Rod Requirements | 5-12 |
| | 5.1.6 | Attitude Control System | 5-12 |
| | 5.1.7 | Sensors and Sample Times | 5-12 |
| | 5.2 | Selection of Test Configuration | 5-13 |

TABLE OF CONTENTS (Cont'd)


| Section | | Page |
|---|---|---|
| | 5.3 Analysis of Rod Response to Disturbance | 5-18 |
| | 5.3.1 Disucssion of Sample Calculations | 5-32 |
| | 5.3.2 Limit Cycle Response | 5-38 |
| 6 | COMPONENT DESIGN | 6-1 |
| | 6.1 Deployable Rod Unit | 6-1 |
| | 6.1.1 Deployable Rod Functional Description | 6-2 |
| | 6.1.2 Rod Requirements and Design | 6-5 |
| | 6.1.3 Comparison of Various Rod Types | 6-15 |
| | 6.2 Spherical Magnetically Anchored Damper | 6-18 |
| | 6.2.1 Damper Functional Description | 6-19 |
| | 6.2.2 Damper Design Characteristics | 6-22 |
| | 6.3 Single-Axis Gravity-Anchored Damper | 6-26 |
| | 6.3.1 Damper Functional Description | 6-27 |
| | 6.3.2 Damper Design Characteristics | 6-27 |
| | 6.4 Attitude Sensing Components | 6-30 |
| | 6.4.1 Sensor Selection | 6-31 |
| 7 | FLIGHT EXPERIMENT OPERATIONAL PROCEDURES | 7-1 |
| | 7.1 Preflight Experiment System Test Procedure | 7-1 |
| | 7.1.1 Ground Test Requirements (Acceptance Test Requirements) | 7-2 |
| | 7.1.2 Qualification Test Requirements | 7-4 |
| | 7.1.3 Customer Operational Documentation/Requirements | 7-5 |
| | 7.2 Health Monitor and Experiment Readiness Procedure | 7-6 |
| | 7.3 Flight Experiment Profile | 7-6 |
| | 7.4 Flight Data Collection Profile | 7-11 |
| | 7.4.1 Data Collection | 7-11 |
| | 7.4.2 Saturn IV-B Experiments | 7-11 |
| | 7.4.3 Extendable Rod Experiment | 7-12 |
| | 7.5 Data Reduction and Analysis Procedure | 7-13 |
| | 7.5.1 Software Status | 7-13 |
| | 7.5.2 Long-Term Data System | 7-13 |
| | 7.5.3 Short-Term Data System | 7-17 |
| | 7.5.4 Quick-Look Attitude Determination System | 7-17 |
| | 7.5.5 Quick-Look Spacecraft Health Monitoring | 7-18 |
| | 7.5.6 Data Analysis and Reporting | 7-18 |

TABLE OF CONTENTS (Cont'd)


| Section | | Page |
|---|---|---|
| 8 | PRELIMINARY RESOURCE ANALYSIS . . . . . | 8-1 |
| | 8.1 Design Plan. . . . . | 8-1 |
| | 8.1.1 Spherical Magnetic Damper. . . . . | 8-1 |
| | 8.1.2 Erectable Rod Unit. . . . . | 8-3 |
| | 8.1.3 Gravity-Anchored Single-Axis Damper . . . . | 8-5 |
| | 8.2 Manufacturing Plan . . . . . | 8-7 |
| | 8.2.1 Spherical Magnetic Damper. . . . . | 8-7 |
| | 8.2.2 Erectable Rod Unit. . . . . | 8-3 |
| | 8.2.3 Gravity-Anchored Single-Axis Damper . . . . | 8-9 |
| | 8.3 Test Plan . . . . . | 8-9 |
| | 8.3.1 Spherical Magnetic Damper. . . . . | 8-9 |
| | 8.3.2 Erectable Rod Unit. . . . . | 8-10 |
| | 8.3.3 Gravity-Anchored Single-Axis Damper . . . . | 8-11 |
| | 8.4 Schedule Plan . . . . . | 8-12 |
| APPENDIX A: | S-IVB MASS/INERTIA AND AERODYNAMIC DATA TRANSFORMATIONS . . . . . | A-1 |
| APPENDIX B: | EVALUATION OF S-IVB PERFORMANCE WITH ROTATED SOLAR ARRAY. . . . . | B-1 |
| APPENDIX C: | DAMPING OF THE S-IVB BY USE OF A SINGLE-AXIS GRAVITY-ANCHORED DAMPER. . . . . | C-1 |
| APPENDIX D: | MAGNETIC CHARACTERISTICS OF LARGE DAMPER MAGNETS. . . . . | D-1 |
| APPENDIX E: | STABILIZATION COMPONENT SPECIFICATIONS. . . | E-1 |
| APPENDIX F: | ROD STRESS DURING EXTENSION. . . . . | F-1 |

# SECTION 1
# INTRODUCTION

## 1.1 PURPOSE AND SCOPE

The "Study for Passive Gravity Stabilization" is a design feasibility study for the Marshall Space Flight Center of NASA under contract NAS 8-21177. The purpose of the study is to define attitude stabilization configurations, component designs, and a flight experiment program which will demonstrate the techniques of passive gravity stabilization for large spacecraft, such as the S-IVB Stage of the Saturn Launch Vehicle, and the Lunar Module of the Apollo Spacecraft.

The scope of the study includes selection of configurations for five in-flight stabilization experiments shown in Table 1-1, and the definition of a flight experiment to evaluate the characteristics of the large deployable rod used to position tip weights in gravity gradient stabilization systems. Flight stabilization experiment four (LM-RACK at 400 km) was dropped from consideration during the study to allow more emphasis on the other configurations.

In each of the stabilization flight experiment studies, a rod and tip weight configuration is selected, performance evaluation made, and preliminary designs completed for all new components required for the flight experiment. In the case of the rod flight experiment, the rod configuration most likely to be used for flight stabilization systems has been selected with the approval of MSFC. The rod flight experiment is designed to evaluate the particular size of rod found suitable for all of the stabilization flight experiments. All components required for the rod flight experiment have been specified. Experiment profiles are shown for four flight experiments, along with operational plans and mission requirements. A program plan is included showing tasks required to design and develop new components, integrate the flight experiment components into the spacecraft, complete the flight experiment and analyze results.

Table 1-1. Flight Experiments

| Flight Experiment | Stabilization Position | Orbit Characteristics |
|---|---|---|
| 1) S-IVB Stage 2 Axis Stabilization | Longitudinal Axis Vertical | 400 KM Altitude Circular $28^{o}$ Inclination |
| 2) S-IVB Stage 3 Axis Stabilization | Longitudinal Vertical Solar Panel perpendicular to orbit plane | 400 KM Altitude Circular $28^{o}$ Inclination |
| 3) S-IVB Stage 3 Axis Stabilization | Longitudinal Axis Horizontal Solar Panel Horizontal | 400 KM Altitude Circular $28^{o}$ Inclination |
| 4) LM-RACK 3 Axis Stabilization | RACK Looking Down | 400 KM Altitude Circular $28^{o}$ Inclination |
| 5) LM-RACK 3 Axis Stabilization | RACK Looking Down | Synchronous |
| 6) Deployable Rod | | 400 KM Altitude Circular $28^{o}$ Inclination |

## 1.2 BACKGROUND FOR THE STUDY

The attitude stabilization requirements for large manned space stations of the future will vary widely depending upon the type activity in process at any given time. During periods of celestial observation, high pointing accuracies and low rates are required. During docking activities, medium accuracies and very high restoring torque are required to recover from a missed dock. There will also be long periods of operation when high attitude accuracy or high torque is not required and when it will be very desirable to limit the amount of electrical power used for altitude stabilization and to limit the amount of stored propellant consumed. Passive gravity stabilization offers this combination of characteristics along with extreme long life and high reliability.

Since passive gravity stabilization is accomplished by means of the natural gravity gradient torques which act on a long thin object in orbit, no electrical control signals or sensors or

electromagnetic components are required for steady state operation. The stabilization system consists of several extendable rods which are driven by electric motor and deploy weights at the rod tip into a position to create the mass distribution required for gravity gradient stabilization. These rod units require electrical power only during deployment before gravity gradient stabilization. In addition to the deployed rods, the stabilization system requires a damper to remove the energy of attitude oscillations. The damper consists of a second oriented body coupled to the spacecraft by an energy absorbing medium. The damper requires no electrical control signals, and generally consists of only one moving part. Thus, the stabilization system provides the desirable characteristics of long life, high reliability, and no electrical power or propellant consumption.

Gravity gradient stabilization systems have been successfully flown since 1962 on satellites ranging in weight from below 100 to 775 pounds. A history of the flights is shown in Table 1-2. The many successful flights show that the theory of operation and system implementation is well established for small satellites.

The application of gravity gradient technology to spacecraft in the 20,000 to 100,000-pound class requires design and flight evaluation of components which are considerably larger than any developed thus far. The results of this study represent a first step toward flight proven passive stabilization systems compatible with the requirements of large manned space flights.

## Table 1-2. Summary of Gravity Gradient Stabilized Satellites

| Launch Date | Satellite Designation | GG System Fabrication | GG System Description | GG Damper Description | Orbit | Inclination | Performance |
|---|---|---|---|---|---|---|---|
| 1962-65 | Transit | APL | One Rod Two Axis | Lossy Spring | 740km | - | Satellite Dead GG Oscillations $10^{o}$ - $20^{o}$ |
| 1962-65 | Transit | APL | One Rod Two Axis | Lossy Spring | 740km | - | Satellite Dead GG Oscillations $10^{o}$ - $20^{o}$ |
| 1962-65 | Transit | APL | One Rod Two Axis | Lossy Spring | 740km | - | Satellite Dead GG Oscillations $10^{o}$ - $20^{o}$ |
| Jan 11, 1964 | 1964-1B/GGSE-1 | GE | One Rod Two Axis | Magnetic Viscous Fluid | 935/910km | $69.9^{o}$ | $\pm 5^{o}$ |
| Mar 9, 1965 | 1965-16B/GGSE-2 | GE | One Rod Two Axis | Magnetic Eddy Current | 942/907km | $70.1^{o}$ | $\pm 5^{o}$ |
| Mar 9, 1965 | 1965-16C/GGSE-3 | GE | Three Rod Three Axis | Magnetic Viscous Fluid | 943/906km | $70.1^{o}$ | Pitch $\pm 12^{o}$ Roll $\pm 20^{o}$ Yaw $\pm 32^{o}$ Satellite on a $78^{o}$ bias |
| Nov 6, 1965 | 1965-89A, GEOS-A | GE | One Rod Two Axis | Magnetic Eddy Current | 2600/1300km | $59.4^{o}$ | Pitch and Roll $\pm 7^{o}$ |
| Mar 30, 1966 | 1966-25B/OV1-5 | Convair | Six Rod Vertistat | Gravity Viscous Fluid | 1059/987km | $144.7^{o}$ | |
| June 16, 1966 | 1966-53A/GGTS | GE | Two Rod Two Axis | Magnetic Viscous Fluid | 33835/33683km | $0.09^{o}$ | Pitch and Roll $\pm 6^{o}$ $15^{o}$ Pointing bias over North Pole |
| July 14, 1966 | OV1-7 | Convair | Six Rod Vertistat | Gravity Viscous Fluid | - | - | Failed to orbit |
| 1st Qtr 1967 | OV1-10 | Convair | Six Rod Vertistat | Gravity Viscous Fluid | 555 km | $95^{o}$ | Tumbling once per orbit |
| April 1967 | ATS-A | GE | Six Rod Three Axis | Gravity Eddy Current Hysteresis | 6000km Planned | - | High Elliptic Orbit 6000 mi by 100 mi Vehicle Tumbling |
| June 1967 | Dodge | APL | Ten Rod | Eddy Current Hysteresis | 36,000km Planned | - | (In Orbit, No Specific Information) |

## 1.3 GOALS

### 1.3.1 FLIGHT DEMONSTRATION GOALS

The objectives of a flight demonstration of a gravity gradient stabilization system on an S-IVB/OWS or a LEM are stated as flight experiment goals below.

Demonstrate passive stabilization system performance which is compatible with operational requirements for future large manned space stations

- Initial stabilization (capture and damping) from initial conditions provided by the active control.
- Damping time compatible with mission profiles for periods of passive stabilization.
- Pointing accuracy and rates suitable for as much of the mission as possible.
- Resistance to disturbance torques (internal and external).

Demonstrate Compatibility of Passive Stabilization with Other On-Board Subsystems

- Magnetic effects of damper
- Rod deployment from active control system conditions
- Rod tolerance to astronaut disturbance torques
- Noninterference of stowed passive stabilization system

Demonstrate Applicability of Design and Analysis Techniques to Passive Stabilization of Large Space Stations

- Disturbance torque analysis
- Damping performance
- Flexible structure effects

### 1.3.2 FLIGHT EXPERIMENT GOALS

The objectives of a flight experiment of a rod and tip mass are stated below:

- Obtain basic rod data unavailable from ground testing.
- Demonstrate structural rod properties which are required for large stabilization systems.
- Demonstrate rod, erector and damper performance which will be required for large stabilization systems.
  - Erection rates
  - Damping of rod motion
  - Tolerance to disturbances

# SECTION 2

# SUMMARY OF RESULTS

This final report of "The Study for Passive Stabilization" presents:

1. The design and analysis results which show the feasibility of gravity gradient stabilization of large spacecraft such as the S-IVB stage and Lunar Module

2. The component designs and specifications required for these stabilization systems

3. A program plan for implementation of the experiments

This summary section contains descriptions of the configurations selected for all five (5) flight experiments, performance expected of the flight experiments, discussion of the components required to perform the flight experiments, and the state of development of these components. Recommendations are made for a flight experiment which will demonstrate design and hardware capability for large gravity gradient stabilization systems with a minimum development program by making use of common components on various flight experiments. A complete program plan and logical next phase program is also summarized. A more detailed discussion of all results, and substantiation for all design selections and conclusions is presented in the main body of the report.

## 2.1 STABILIZATION CONFIGURATIONS AND PERFORMANCE

### 2.1.1 S-IV B VERTICAL CONFIGURATION - 400 KM ORBIT ALTITUDE

This stabilization configuration requires only the mounting of a passive damping device on the S-IV B in order to obtain stabilization with the longitudinal axis along the local vertical. The configuration takes advantage of the gravity gradient torques which act on the S-IV B stage because of the differences in moments of inertia between longitudinal and transverse axes. The damping device is a 356 newton (80 lb) spherical, magnetically anchored damper. The damper consists of magnetically oriented sphere which is coupled to the S-IVB by means of a viscous damping oil. The configuration is shown in Figure 2-1 with

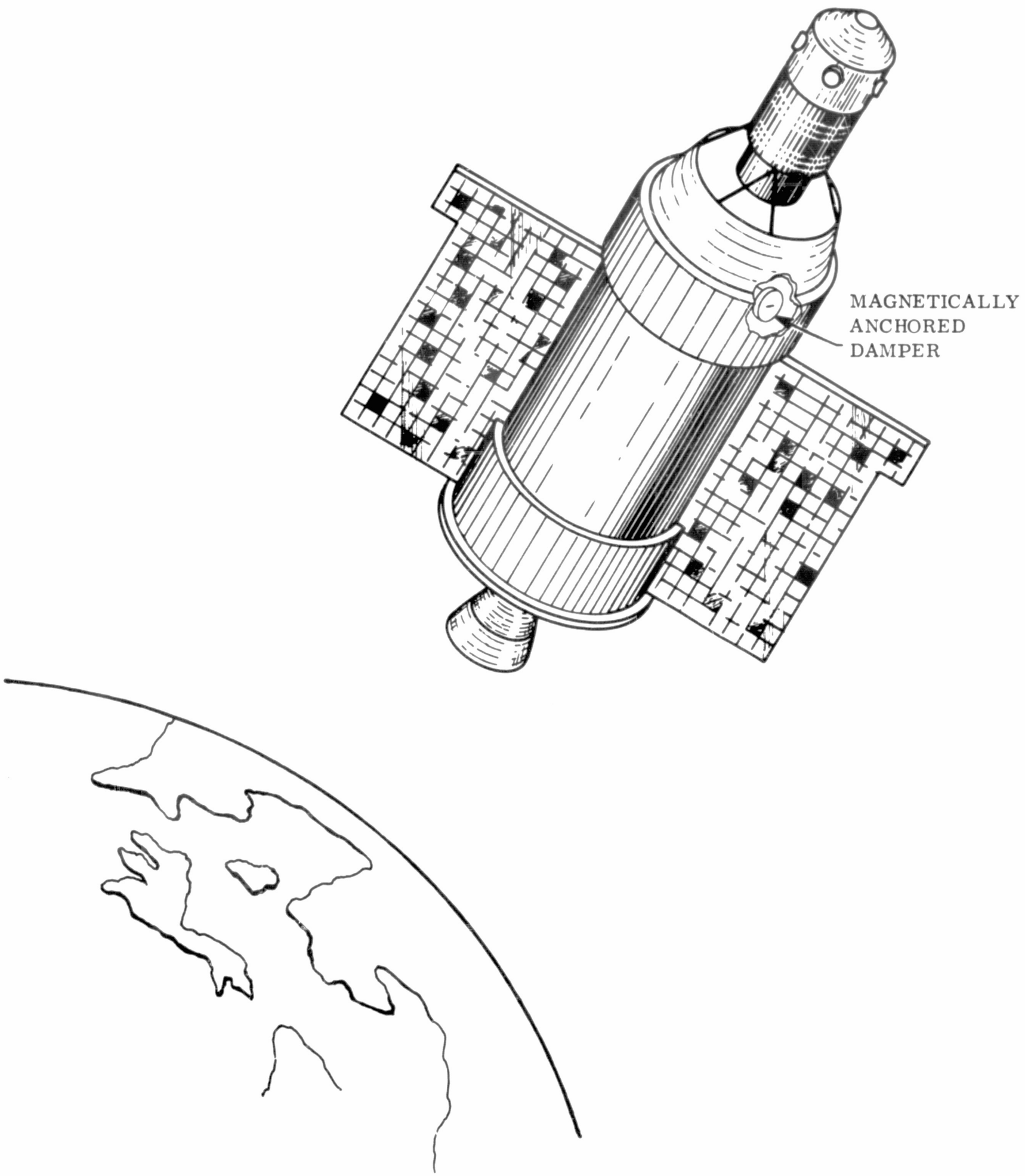


Figure 2-1. S-IVB Vertical Stabilization Configuration - 400 KM Orbit Altitude

the damper mounted in the area inside the Instrument Unit. The stable position shown is with the S-IVB engine nozzle down and the plane of the solar array approximately in the plane of the orbit.

A complete list of components required for performance and evaluation of a stabilization flight experiment is shown in Table 2-1.

The expected transient damping and steady state pointing performance are also summarized in Table 2-1. The damping time to steady state represents the time required to achieve the listed steady state accuracies from initial conditions of 10 degrees error and 0.01 degree per second error rates about all axes. These initial conditions can be supplied by the S-IVB active control systems. Stabilization will be achieved from tumbling conditions, but requires more time. The steady state pointing errors are oscillatory except for the bias shown. Peak body rates are less than 0.015 degree per second in all axes during steady state for all of the S-IVB gravity gradient configurations. Computer simulations of the time histories of damping and steady state performance are shown in Section 3.

### 2.1.2 S-IV B VERTICAL CONFIGURATION (PREFERRED YAW POSITION) - 400 KM ALTITUDE

The S-IV B vertical stabilization configuration described above makes use of existing moments of inertia and results in stabilization with the solar panels nearly in the orbit plane. A vertical stabilization system which provides a preferred yaw position, with the solar array perpendicular to the orbit velocity vector is shown in Figure 2-2. This solar array orientation will provide more power than the orientation of the previous configuration. The preferred yaw position is achieved by deploying a magnetically anchored damper as a tip mass on an erectable tubular rod. The deployed mass serves to alter the moments of inertia of the S-IVB so that the preferred stable orientation about the longitudinal axis is obtained. The deployed tip mass also serves as a damper to damp transient oscillations. The components required for this flight experiment and the expected stabilization system performance are as shown in Table 2-2. The only additional component is the erectable rod. The rod erection unit and damper are fabricated as a single unit including caging

Table 2-1. S-IV B Vertical Stabilization Configuration

Stabilization Components

- Magnetically Anchored Damper
  - Weight - 356 newtons (80 lb)
  - Size - 41 cm. (16 in.) diameter
  - Magnet Strength - 2000 amp. $m^2$ ($2 \times 10^6$ pole cm)
  - Damping Coefficient - 82 newton-m-sec. (60 ft-lb-sec)

Flight Experiment Components

| | WEIGHT | | POWER |
|---|---|---|---|
| | Newtons | Lb | Watts |
| • Earth IR Sensor | 53 | 12 | 12 |
| • Sun Sensor | 27 | 6 | 1 |
| • Magnetometer | 22 | 5 | 1 |
| • Tape Recorder | 44 | 10 | 5 |

Total Experiment Weight

502 newtons (113 lb)

Total Experiment Power

19 watts

Stabilization Performance

- Damping Time Constant - 38 orbits (2.5 days)
- Damping Time to Steady State - 7.5 days
- Steady State Accuracy
  - In Orbit Plane (Pitch) - $\pm 1^{o}$
  - Across Orbit Plane (Roll) - $\pm 3^{o}$
  - About Vertical (Yaw) - $\pm 13^{o}$ with $+9^{o}$ bias

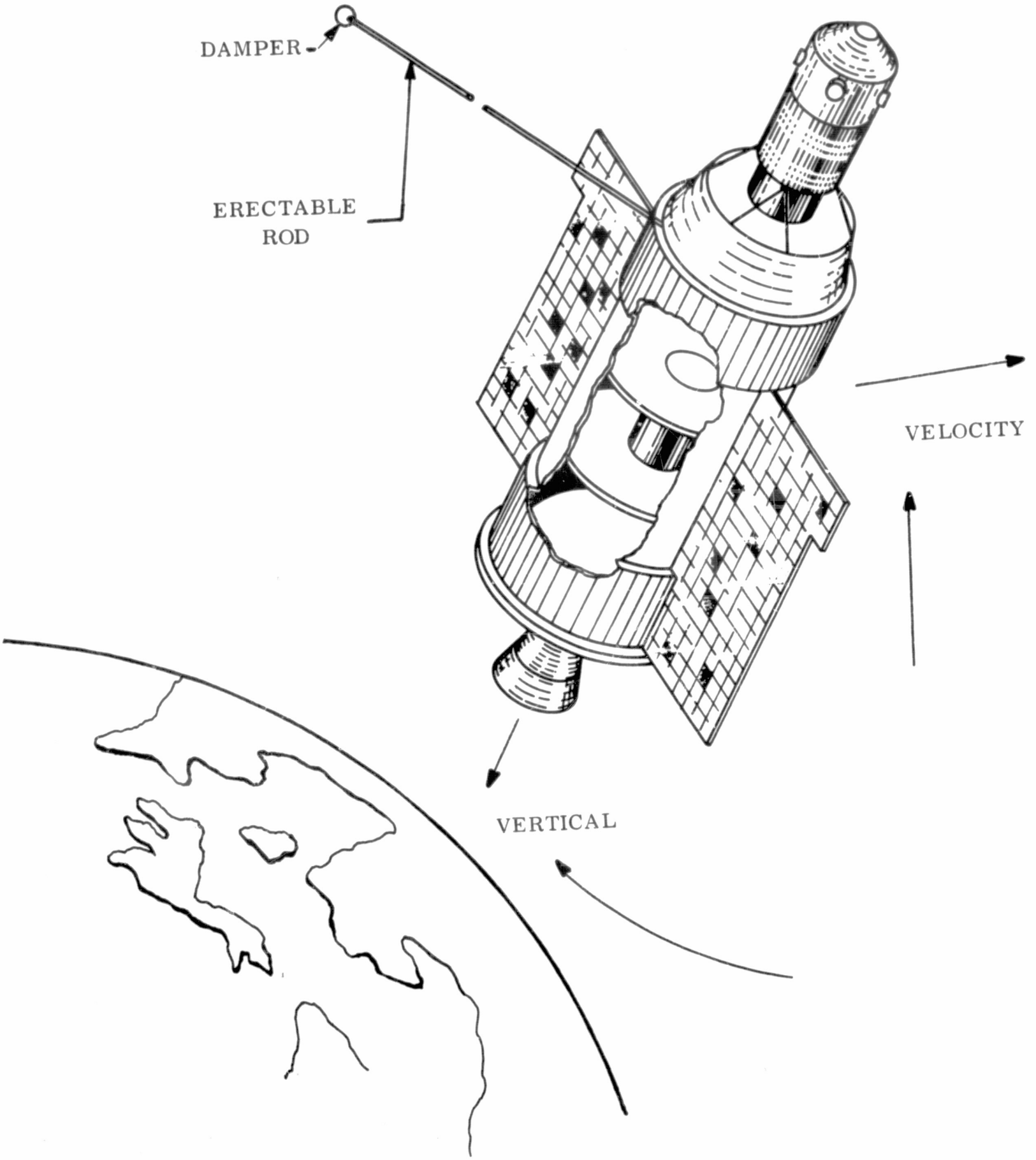


Figure 2-2. S-IVB Vertical Stabilization Configuration (Preferred Yaw Position) - 400 KM Altitude

Table 2-2. S-IV B Vertical Stabilization Configuration (Preferred Yaw Position)

Stabilization Components

- Magnetically Anchored Damper
  - Weight - 1000 newtons (225 lb)
  - Size - 56 cm. (22 in.) diameter
  - Magnet Strength - 6000 amp. $m^2$ ($6 \times 10^6$ pole cm.)
  - Damping Coefficient - 82 newton-m-sec (60 ft-lb-sec)
- Erectible Rod Unit
  - Rod Length x Diameter - 46 m (150 ft) x 7.6 cm (3 in.)
  - Weight Rod and Erection Unit - 550 newton (125 lb)
  - Erection Unit Size - 1.6 x .6 x 0.4 m (66 x 23 x 15 in.)
  - Erection Unit Power - 50 watts operating

Flight Experiment Components

| | WEIGHT Newtons | WEIGHT Lb | POWER Watts |
|---|---|---|---|
| • Earth IR Sensor | 53 | 12 | 12 |
| • Sun Sensor | 27 | 6 | 1 |
| • Magnetometer | 22 | 5 | 1 |
| • Tape Recorder | 44 | 10 | 5 |

Total Experiment Weight

1696 newtons (383 lb)

Total Experiment Power

- During Deployment - 69 Watts
  Constant - 19 Watts

Stabilization Performance

- Damping Time Constant - 40 orbits (2.6 days)
- Damping Time to Steady State - 8 days
- Steady State Accuracy
  - In Orbit Plane (Pitch) - $\pm 12^\circ$ with $+10^\circ$ bias
  - Across Orbit Plane (Roll) - $\pm 5^\circ$
  - About Vertical (Yaw) - $\pm 8^\circ$ with $+5^\circ$ bias

and release mechanism for the damper. This unit constitutes a stabilization subsystem and is all that is required for passive gravity stabilization. The damper weight and rod size selected for this single-rod configuration can be flown with development of a single, stabilization subsystem design.

### 2.1.3 S-IVB HORIZONTAL CONFIGURATION - 400 KM ALTITUDE

Stabilization of the S-IV B with the longitudinal axis along the velocity vector is accomplished in this configuration by deploying two (2) rod and tip mass subsystems as shown in Figure 2-3. This configuration flies with the solar array horizontal where the amount of solar power absorbed is greater than either of the previous configurations. The two (2) deployable rods are oriented so that both gravity gradient torques and aerodynamic torques help to orient the spacecraft. The flight experiment components and predicted stabilization system performance are shown in Table 2-3.

### 2.1.4 LUNAR MODULE CONFIGURATION - SYNCHRONOUS ALTITUDE

The passive gravity gradient stabilization configuration designed for the Lunar Module and Experiment Rack (LM-RACK) is shown in Figure 2-4. This configuration is designed for use at synchronous altitude and makes use of a different damping concept than the 400 km altitude S-IV B configurations. The LM-RACK configuration consists of four (4) erectable rods with tip masses, rigidly attached to the LM-RACK so as to orient the SPAR experiment package looking earthward with a clear field of view. The tip masses of this system do not contain magnetically anchored dampers, since the solar magnetic storm disturbances at synchronous altitude cause large disturbances to a passive system using this type damper. The damping system used for the LM-RACK configuration consists of two (2) erectable rods with tip masses which are attached to the spacecraft by means of a suspension system which provides a single axis of rotational motion. The damper rotational suspension system also contains a frictional loss device so that relative motion between the spacecraft and damper boom generates torques which damp the motion. The damper boom rotational axis is positioned so that motion of the spacecraft about any axis will induce rotation across the damper suspension and thus be damped. The damper must also be located to permit $\pm$45 degrees free rotation of the damper boom about the damper axis.

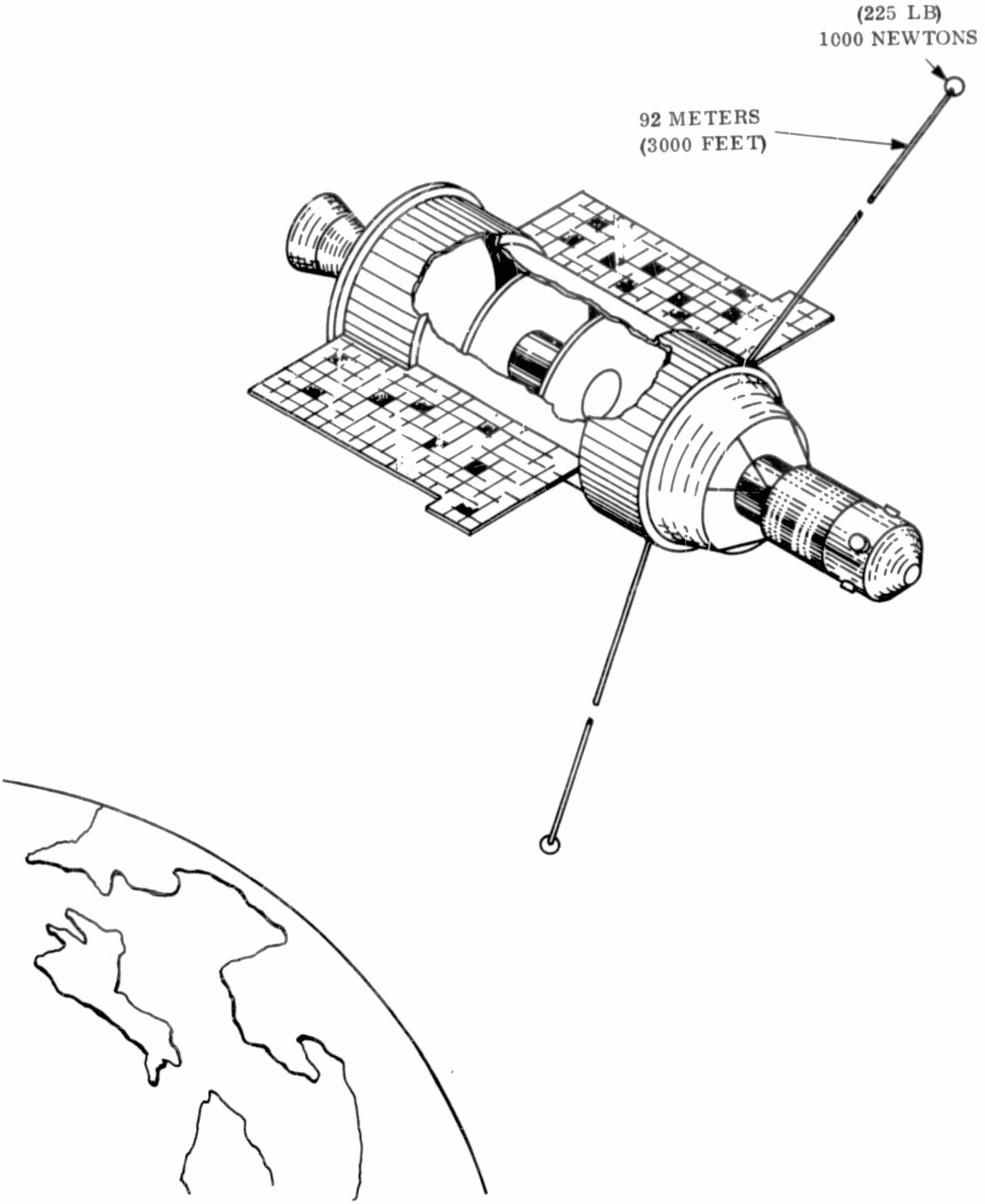


Figure 2-3. S-IVB Horizontal Configuration

Table 2-3. S-IV B Horizontal Configuration

Stabilization Components

- Two (2) Magnetically Anchored Dampers

| | | | |
|---|---|---|---|
| Weight | - | 1000 newtons (225 lb) | each damper |
| Size | - | 56 cm. (22 in.) diameter | each damper |
| Magnet Strength | - | 6000 amp. $m^2$ | each damper |
| Damping Coefficient | - | 41 newt-m-sec (30 ft-lb-sec) | each damper |

- Two (2) Erectible Rod Units

| | | | |
|---|---|---|---|
| Rod Length x Diameter | - | 92 m (300 ft) x 7.6 cm (3 in.) | each unit |
| Weight (rod and erection unit) | - | 890 newtons (200 lb) | each unit |
| Erection Unit size | - | 1.7 x .6 x .4 m (66 x 23 x 15 in.) | each unit |
| Erection Unit power | - | 50 watts operating | |

Flight Experiment Components

| | WEIGHT Newtons | WEIGHT Lb | POWER Watts |
|---|---|---|---|
| • Earth IR Sensor | 53 | 12 | 12 |
| • Sun Sensor | 27 | 6 | 1 |
| • Magnetometer | 22 | 5 | 1 |
| • Tape Recorder | 44 | 10 | 5 |

Total Experiment Weight

3926 Newtons (883 lb)

Total Experiment Power

- During Deployment - 119 Watts
  Constant - 19 Watts

Stabilization Performance

- Damping Time Constant - 46 Orbits (3 Days)
- Damping Time to Steady State - 9 Days
- Steady State Accuracy
  - In Orbit Plane - $\pm 7^{o}$
  - Across Orbit Plane - $\pm 6^{o}$
  - About Vertical - $\pm 20^{o}$

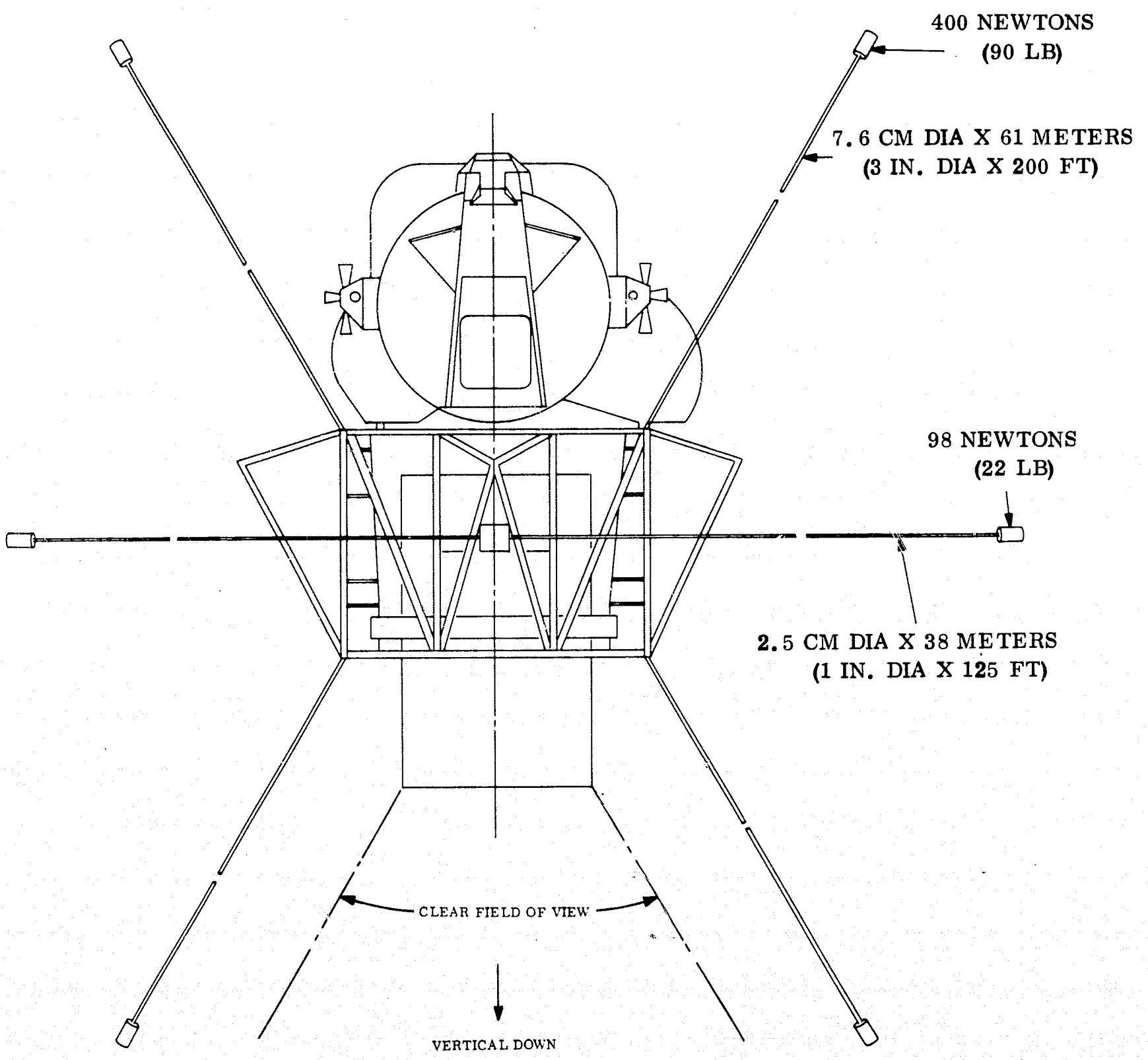


Figure 2-4. LM-RACK Synchronous Configuration

The flight experiment components and predicted stabilization system performance are shown in Table 2-4. The damping time to steady state represents the time to achieve the listed steady state accuracies from any nontumbling conditions. Body rates must be lower than 0.004 degree/sec to prevent tumble. Stabilization will be achieved from tumbling conditions, but longer times are required. The steady state errors are oscillatory with peak body rates of less than 0.0004 degree/sec in all axes.

## 2.2 ROD FLIGHT EXPERIMENT CONFIGURATION AND PERFORMANCE

This flight experiment is designed to evaluate the structural characteristics of an erectable rod which will meet the requirements of the stabilization system previously described. The rod selected for the flight experiment is a 7.6-cm (3-in.) diameter tubular rod of beryllium copper similar in design to the 1.3-cm (1/2-in.) diameter rods which have been used for smaller passive gravity gradient stabilization systems on previous flights. This larger rod makes use of a tab lock feature at the overlap seam of the tubular section, which gives better torsional strength and straightness than the overlapped seam which has been used on previous smaller flight units.

This rod has been selected for flight evaluation because of the broad history of flight experience with rods of this type and because it satisfies all of the requirements of the stabilization system. A comparison with other types of rods is made in Section 6.

The purpose of the rod flight experiment is to conduct structural tests under controlled conditions which are not obtainable when the rod is used as part of a stabilization system.

The structural tests are designed to measure the following rod characteristics:

a. Bending stiffness

b. No-load straightness

c. Thermal distortion (static)

d. Thermal impulse (dynamic

e. Extension-retraction motion

f. Rod damping

Table 2-4. LM-RACK Stabilization Configuration

Stabilization Components

- Four Erectible Main Rod Units with Tip Mass

| (each rod) | | | |
|---|---|---|---|
| | Rod Length x Diameter | - | 61 m (200 ft) x 7.6 cm (3 in.) |
| | Weight (complete unit) | - | 1070 newtons (240 lb) |
| | Erection Unit Size | - | 1.7 x .6 x .4 m (66 x 23 x 15 in.) |
| | Erection Unit Power | - | 50 watts operating |

- Two Erectible Damper Rod Units with Tip Mass

| (each rod) | | | |
|---|---|---|---|
| | Rod Length x Diameter | - | 38 m (125 ft) x 2.5 cm (1 in.) |
| | Weight (complete unit) | - | 133 newtons (30 lb) |
| | Erection Unit Size | - | 38 x 10 x 10 cm (15 x 4 x 4 in.) |
| | Erection Unit Power | - | None (self-erecting) |

- Single-Axis Hysteresis Damper

| | | |
|---|---|---|
| Weight | - | 222 newtons (50 lb) |
| Size | - | 61 Diameter x 86 long - cm (24 diameter x 34 long - in.) |

Flight Experiment Components

| | WEIGHT newtons | WEIGHT lb | POWER watts |
|---|---|---|---|
| • Earth IR Sensor | 53 | 12 | 12 |
| • Sun Sensor | 27 | 6 | 1 |
| • Magnetometer | 22 | 5 | 1 |
| • Tape Recorder | 44 | 10 | 5 |

Total Experiment Weight

4914 Newtons (1103 lb)

Total Experiment Power

- During Deployment - 219 Watts
  Constant - 19 Watts

Stabilization Performance

- Damping Time Constant - 3 Days
- Damping Time to Steady State - 9 Days
- Steady State Accuracy
  - In Orbit Plane - $\pm 7^{o}$
  - Across Orbit Plane - $\pm 1.5^{o}$
  - About Vertical - $\pm 3.8^{o}$

These structural tests are selected to determine detail design data so that long deployable rods may be used for a variety of large stabilization systems as well as other space-structure applications such as deployable remote instrumentation packages or manipulators. A brief description of each test and expected results is presented in the following paragraphs.

### 2.2.1 BENDING STIFFNESS

The rod and tip mass are deployed with the active control system disabled, and rod oscillations are allowed to damp. When a relatively quite rod condition is achieved, a controlled torque pulse is applied to the S-IVB by the active control system. Bending displacement and period of the rod are recorded photographically and used with known mass characteristics to determine the distributed rod stiffness. A predicted first bending mode period of five (5) minutes and a maximum tip deflection of 6.1 meters (20 feet) have been achieved by selection of rod length of 76 meters (250 feet) and disturbance magnitude. The rod characteristics and tip mass are those of the S-IVB horizontal stabilization configuration.

### 2.2.2 NO LOAD STRAIGHTNESS

S-IVB is nominally positioned by the active control system so that the rod will deploy along the antivelocity vector. The active control system is disabled and the rod deployed and allowed to damp oscillations. Straightness data is taken during eclipsed portion of the orbit so that thermal flux does not cause rod distorition. Rod position is recorded photographically with an illuminated tip target and the rod illuminated by an S-IVB mounted light source. Effects of oscillatory motion are removed by recording several full-cycle positions. The effects of imperfect rod orientation (gravity gradient and aerodynamic bending are removed by calculation). Rod straightness to within 2 degree half-cone angle is expected.

### 2.2.3 THERMAL DISTORTION AND IMPULSE

The rod is deployed along the antivelocity vector with the active control system disabled. Rod oscillations are allowed to damp and data is taken at local satellite noon so that the solar flux is nearly perpendicular to the rod longitudinal axis. Rod position is recorded photographically and data is corrected for oscillatory rod motion, gravity and aerodynamic forces, and actual angle of solar flux. Temperature data is taken circumferentially around the rod to evaluate heat load.

### 2.2.4 EXTENSION-RETRACTION AND DAMPING

Extension and retraction of the rod is required between experiments since the fully deployed rod is not compatible with the torque levels of the active control system (rod maximum bending torque is 270 newton meters (200 ft-lb). Dynamic excitation of the rod during a full length 122 meter (400 ft) deployment and retraction will be photographically recorded in order to identify any potentially high stress conditions. Decay of the motion of the fully deployed rod will also be observed to evaluate rod structural damping.

### 2.2.5 DATA REQUIREMENTS

S-IVB position and rate data are required throughout all experiments to allow evaluation of effects on the rod caused by rod orientation and the effects on the rod of any disturbance torques generated within the S-IVB.

A summary of rod flight experiment equipment is presented in Table 2-5.

## 2.3 RECOMMENDED FLIGHT EXPERIMENTS

Of the five (5) experiment configurations studied, the rod structural experiment and the S-IVB horizontal stabilization are recommended as flight experiments. The rod structural experiment will provide detailed design information on the deployable rod and provide a basis for a wide variety of applications. The S-IVB horizontal configuration demonstrates the components, system design, and operational characteristics of gravity gradient stabilization systems. The S-IVB horizontal configuration has been selected in preference to other stabilization configurations because it places the most severe requirements on the deployable rods and demonstrates stabilization on the largest system.

Table 2-5. Rod Flight Experiment Equipment

| | Weight (newton (lb)) | | Power (watts) |
|---|---|---|---|
| • Rod Erection Unit and 122 m (400 ft) Rod | 1100 | (250) | 50 |
| • Tip Mass and Target | 510 | (200) | -- |
| • Earth Sensor | 53 | (12) | 12 |
| • Sun Sensor | 27 | (6) | 1 |
| • Magnetometer | 22 | (5) | 1 |
| • Illumination Light and Camera | 220 | (50) | 15 |

(Rate data assumed available from S-IVB inertial performance)

These two (2) flight experiments can be flown separately on different S-IVB flights or combined into a single flight experiment. The rod structural test cannot be performed on a rod with a spherical damper at the tip since the structural damping of the rod will be masked by the tip damper. A combined experiment configuration would consist of three (3) rods, two (2) with spherical dampers mounted to form the S-IVB horizontal configuration, and a single rod and tip mass mounted to deploy along the antivelocity vector. The combined experiment configuration is shown in Figure 2-5. Several advantages arise from combining the experiments into a single flight. First, the gravity gradient stabilization system orients the S-IVB during the rod structural experiment so that the active control is not required, and it is not necessary to retract the rod and return the S-IVB to proper position between each step of the rod structural experiment. Second, presence of the third rod and tip mass can be used to obtain a variable stabilization configuration in flight and thus investigate the actual versus predicted changes in stabilization performance for different configurations. The effect on the stabilization system of deploying the structural rod and tip weight will be to decrease the pitch gravity gradient orienting torque and to increase the pitch aerodynamic orienting torque. Yaw orienting torques will be increased, and roll orienting torques will be unaffected.

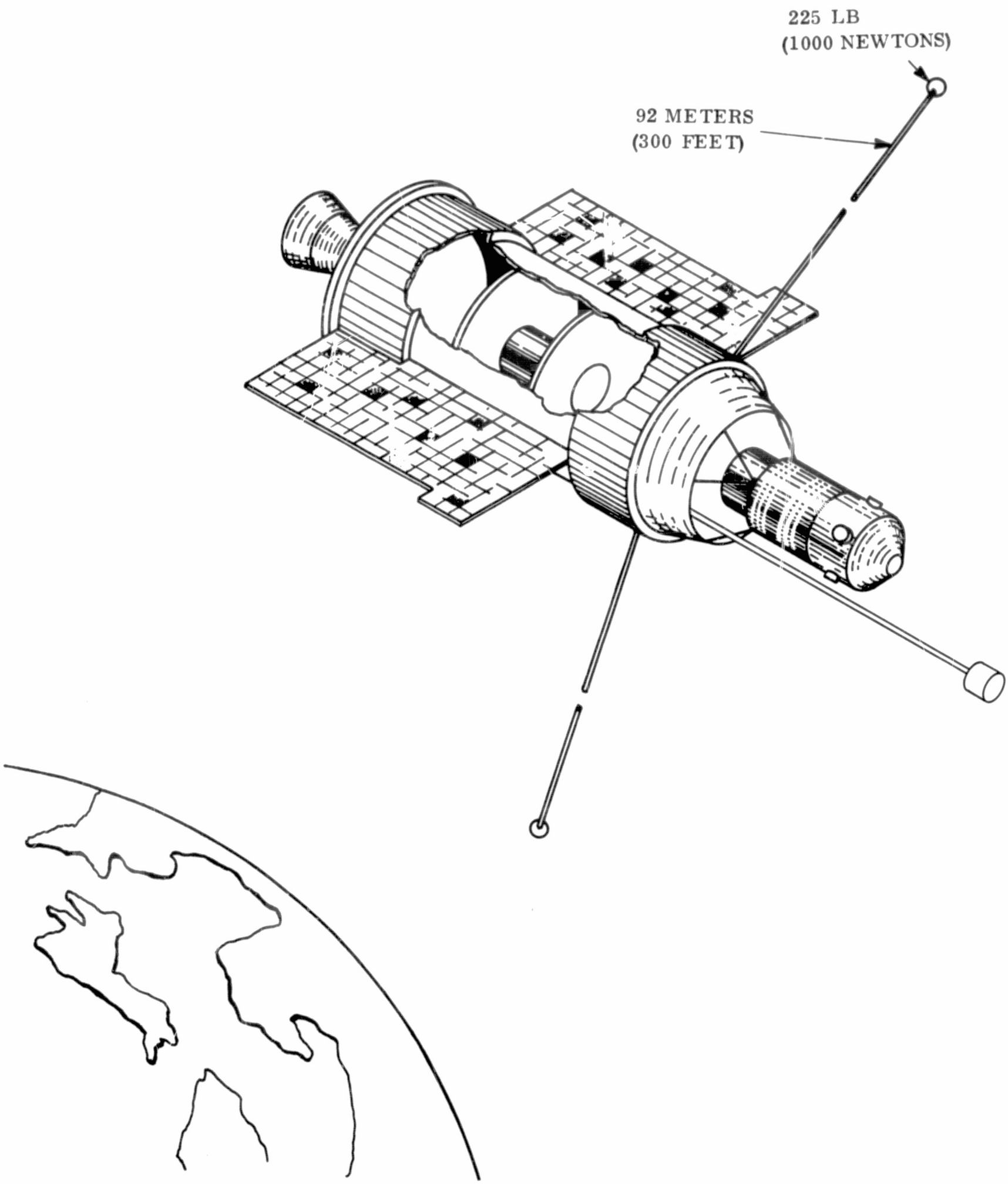


Figure 2-5. S-IVB Combined Configuration

The experiment sequence for a combined experiment would consist of passive stabilization first, followed by the rod structural experiment, and finally a variable configuration stabilization experiment. A summary sequence of events and time span is shown in Table 2-6.

Table 2-6. Profile of Recommended Flight Experiment

| Event | Time Start | Time Stop |
|---|---|---|
| Passive Stabilization Experiment | | |
| 1. Active Control Positions S-IVB | 0 Hours | 1 Hour |
| 2. Deploy Two Rods with Dampers | 1 Hour | 2 Hours |
| 3. Evaluate Passive Damping | 2 Hours | 8 Days |
| 4. Evaluate Passive Steady State | 8 Days | 20 Days |
| Rod Structural Experiment | | |
| 5. Deploy Structural Test Rod - 250 ft | 0 Hours | 0.7 Hour |
| 6. Conduct Rod Structural Tests | 0.7 Hour | 6 Days |
| Variable Configuration Experiment | | |
| 7. Evaluate Passive Stabilization | | |
| Structural Rod at 250 ft | 0 Hours | 16 Days |
| Structural Rod at 400 ft | 16 Days | 32 Days |
| Total time required for three (3) experiments = 60 days | | |

The components required for the combined flight experiment consist of a single set of instrumentation including attitude sensors, rod illumination lights, camera, and tape recorder, and the experimental components themselves. S-IVB attitude and rate information is a common requirement for all of the experiments. The only components requiring design and fabrication of prototype hardware are the erectible rod and the magnetically anchored spherical damper.

## 2.4 PROGRAM PLAN FOR FLIGHT EXPERIMENT

The results of this design feasibility study show that passive gravity stabilization of large spacecraft such as the S-IVB and LM RACK is a practical technique and requires only the development of scaled-up versions of the stabilization components previously used on successful flights of smaller spacecraft. Because all of the other components are available as off-the-shelf hardware, the logical next effort is the design and development of the erectable rod unit and magnetically anchored spherical damper. This effort will result in flight-qualified components with complete interface definitions for integrating the components into the S-IVB spacecraft. The stabilization component development program is subsequently summarized as part of the Integrated Program Plan which defines the required effort to conduct and evaluate a complete passive gravity stabilization flight experiment. A milestone schedule is shown in Figure 2-6.

### PROGRAM PLAN TASKS

1.0 Stabilization Components

A. Design

- Requirements and Analysis
- Design Definition

B. Prototype Components

- Make or Buy Decisions
- Fabrication and Assembly
- Functional and Environmental Tests

C. Qualification Components

- Design of Flight Components
- Fabrication and Assembly
- Functional and Qualification Testing

D. Flight Components

- Fabrication and Assembly
- Acceptance Testing
- Interface and Integration Definition

2.0 Instrumentation Components

A. Design

- Requirements and Analysis
- Interface and Integration Definition

B. Flight Components

- Procurement and Acceptance Testing

3.0 Flight Experiment System

A. Design

- Requirements and Analysis
- Interface and Integration Definition

B. Flight System

- Integration and Test
- System Buyoff and Delivery
- Launch Site Test
- Flight Experiment

C. Experiment Analysis and Correlation

MILESTONE SCHEDULE

PASSIVE STABILIZATION EXP. (NAME) ENGINEERING PROPOSAL/PROGRAM

FORM I-9511 REV. (2-61)

PAGE ___ OF ___

| "B" LEVEL OPER. NO. | OPER. NAME | PREPARED BY | DATE | APPROVED BY | DATE | ISSUE NO. |
|---|---|---|---|---|---|---|
| | | | | | | |

| TASK NO. | SUB-TASK NO. | DESCRIPTION OF DETAIL MILESTONES |
|---|---|---|
| 1.0 | A | DESIGN |
| | B | PROTOTYPE |
| | C | QUALIFICATION |
| | D | FLIGHT |
| | | |
| 2.0 | A | DESIGN |
| | B | FLIGHT |
| | | |
| 3.0 | A | DESIGN |
| | B | FLIGHT |
| | C | ANALYSIS |
| | | |
| | | STAB. COMPONENTS QUALIFIED |
| | | FLIGHT EXPERIMENT |
| | | |

ELAPSED TIME SCHEDULE

(INDICATE YEARS) FISCAL 1969 — FISCAL 1970

(SPECIFY CATEGORY) MONTHS/ WEEK

1 2 3 4 5 6 7 8 9 10 11 12 13 14 15 16 17 18 19 20 21 22 23 24 25 26 27 28 29 30

△ START ▽ COMPLETE ▭ TIME PERIOD OF WORK

⇩ MAJOR ITEM EVENT (REPORT, HARDWARE DELIVERY, FLIGHT TEST, ETC.) - INDICATE ITEM NAME NEXT TO ARROW.

Figure 2-6. Milestone Schedule

# SECTION 3

# GRAVITY GRADIENT STABILIZATION CONFIGURATIONS FOR THE S-IVB STAGE

This section describes the deployable rod and tip mass configurations selected for passive stabilization of the S-IVB stage. Rod lengths, positions, tip weights, damper magnet strength, and damping coefficient are selected to meet the steady state accuracy requirements of ±15 degrees and damping time requirements of 10 days to steady state while maintaining minimum weight. The flight performance of each configuration is simulated by digital computer using the large angle equations of motion, and including the following disturbance effects:

a. Aerodynamic torques on central body and thermally curved rods

b. Damping torques caused by the damper following the Earth's magnetic field

c. Solar pressure torques on thermally curved rods

d. Magnetic torques on vehicle magnetic dipole

## 3.1 DEFINITION OF PROPERTIES

The nominal orbit conditions for which all three S-IVB stage stabilization configurations are to be designed are defined in this section. The nominal characteristics of the S-IVB are also defined.

### 3.1.1 NOMINAL ORBIT

The nominal orbit specified for the S-IVB stabilization study is circular at 400 km (216 nautical miles) with an inclination of 28 degrees. The detailed parameters specifying local time, season, and atmospheric density are shown in Table 3-1.

In Jacchia's density model, the peak of the diurnal density bulge is located 30 degrees from the solar subpoint in the direction of rotation of the earth. A plot of the atmospheric density versus orbit angle for the specified orbit is shown in Figure 3-1. The value of the 20 cm

Table 3-1. Nominal Orbit Definition

| | | |
|---|---|---|
| Orbit Altitude | = | 400 km (216 nm) |
| Orbit Inclination | = | 28 degrees |
| Season | = | Spring Equinox |
| Orbit Ascending Node | = | On Earth-Sun Line |
| GMT at Injection (t = 0) | = | GTM = 0 |
| Injection at Ascending Node | | |
| Precession of Orbital Plane | = | 0 |

Atmospheric Density Model

Proposed by Jacchia, L. G., Journal of Geophysical Research, Vol. 65, p. 2775 (1960)

$$\rho = \rho_o F_{20} \left[ 1 + .19 \left( e^{0.0055h} - 1.9 \right) \cos^6 \psi/2 \right]$$

$$\log \rho_o = -13.021 - 0.001985h + 6.363e^{-0.0026h}$$

$F_{20}$ = 20 cm solar flux constant = 3.0

h = Altitude (kilometers)

P = Atmospheric density ($kg/m^3$)

$\psi$ = angle from peak of diurnal bulge

solar flux constant was chosen as a maximum to provide the worst-case disturbance torque due to variation in atmospheric density.

Since all large angle, nonlinear computer simulations performed in this study include the effect of the Earth's oblateness in the atmospheric density computations, two curves are shown, one with and one without the oblateness effect.

INCLINATION: $28^{o}$

SPRING EQUINOX

RT. ASC. OF ASCENDING NONE AT INJECT: $224^{o}$

$30^{o}$ BETWEEN ATMOS. BULGE & SUBSOLAR POINT

SOLAR FLUX CONSTANT ($F_{20}$) = 3.0

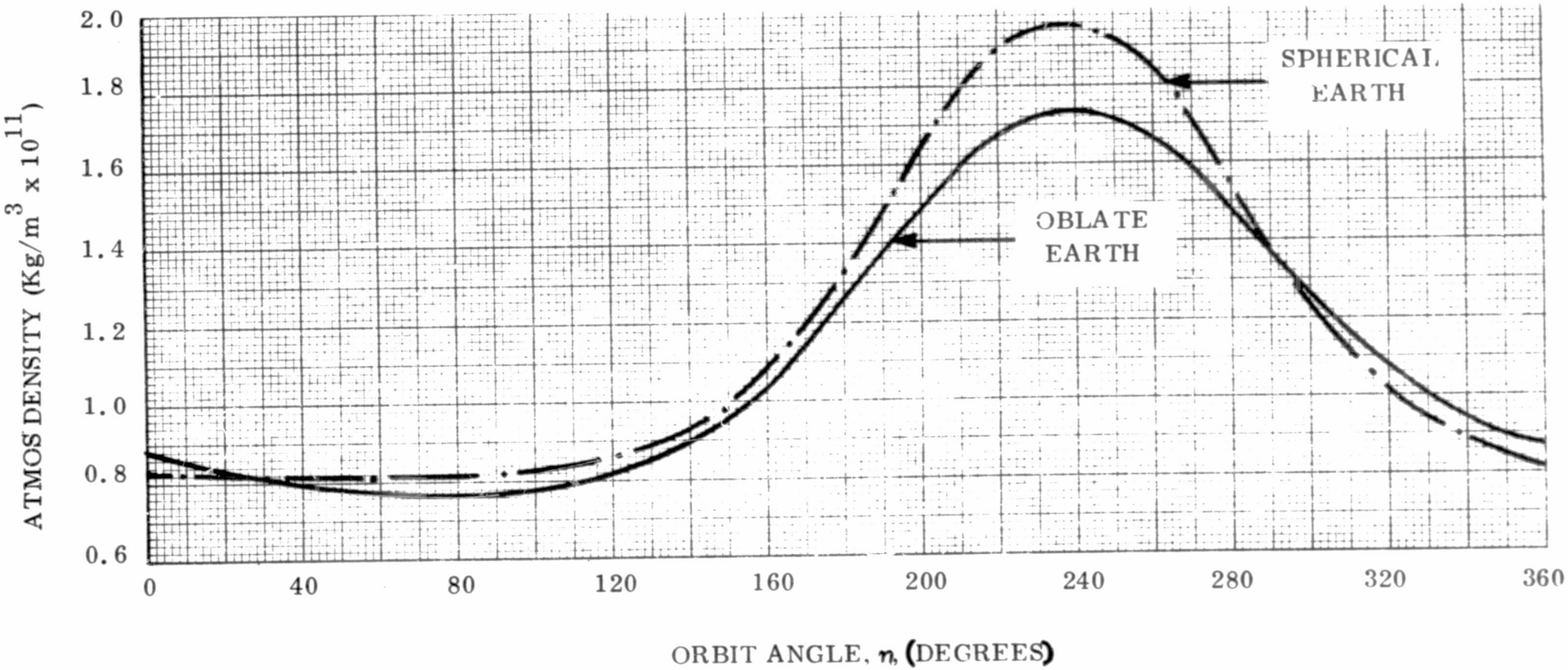


Figure 3-1. Atmospheric Density Model

### 3.1.2 DEFINITION OF THE S-IVB MASS/INERTIA PROPERTIES

The mass and inertia properties of the S-IVB configuration to be used in the study (S-IVB Stage, Instrument Unit, Air Lock, Multiple Docking Adapter) were received from MSFC and are reproduced below in Table 3-2.

Table 3-2. S-IVB Mass/Inertia Properties

| | | |
|---|---|---|
| Wt. | $2.2056 \times 10^5$ newtons | $0.495820 \times 10^5$ lb |
| $X_{CG}$ | 10.8800 meters | (35.695 ft) |
| $Y_{CG}$ | 0.1321 meters | (0.4334 ft) |
| $Z_{CG}$ | -0.0660 meters | (-0.2165 ft) |
| $I_{xx}$ | $0.162109021 \times 10^6$ kg-m$^2$ | (119565.13 slug-ft$^2$) |
| $I_{yy}$ | $0.119847985 \times 10^7$ kg-m$^2$ | (883950.90 slug-ft$^2$) |
| $I_{zz}$ | $0.119181699 \times 10^7$ kg-m$^2$ | (879036.7 slug-ft$^2$) |
| $I_{xy}$ | $-0.174242866 \times 10^5$ kg-m$^2$ | (-12851.36 slug-ft$^2$) |
| $I_{xz}$ | $+0.184811460 \times 10^4$ kg-m$^2$ | (+1363.0959 slug-ft$^2$) |
| $I_{yz}$ | $-0.132197614 \times 10^5$ kg-m$^2$ | (-9750.367 slug-ft$^2$) |

These moments of inertia are defined for a set of reference axes shown in Figure 3-2.

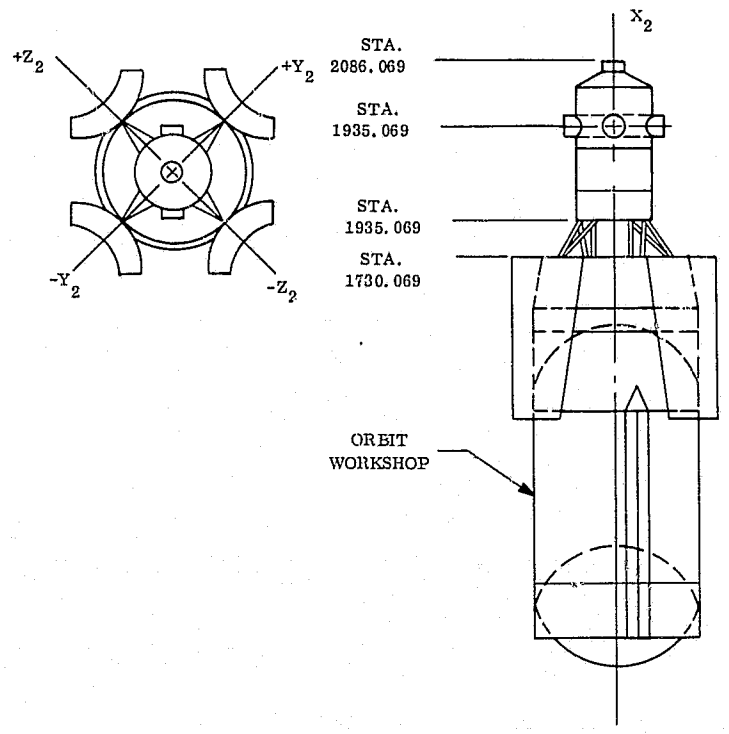


Figure 3-2. S-IVB Mass/Inertia Reference Axes

These moments and products of inertia are used to define the inertia dyadic as follows:

$$I_{xx} = \Sigma\ m\ (Y^2 + Z^2)$$

$$I_{xy} = -\Sigma\ m\ XY$$

$$\Phi = \begin{bmatrix} I_{xx} & I_{xy} & I_{xz} \\ I_{yx} & I_{yy} & I_{yz} \\ I_{zx} & I_{zy} & I_{zz} \end{bmatrix}$$

In order to use the mass/inertia characteristics as inputs to the GE computer program, they were transformed to a new set of body fixed reference axes. This transformation is made in two steps for simplicity. First the mass/inertia data is transformed to the reference axes used for the aerodynamic data, shown in Figure 3-3. This transformation is shown as A below. The second transformation is used to refer both mass/inertia and aerodynamic data to the set of body fixed axes used in the GE computer program. The set of body fixed axes, used in the GE computer program,is oriented with respect to an orbit reference frame set by three Euler angles: pitch ($\theta_p$), roll ($\theta_r$), yaw ($\theta_y$) in sequence, as shown in Figure 3-4. In order to keep the values of these Euler angles below 90 degrees when the S-IVB is at stable null, the S-IVB and aerodynamic reference axes are rotated by -90 degrees about $Y_3$ (J2 gimbal down), and +90 degrees about the new position of $X_3$ (offset solar panel away from direction of flight). The new position of the S-IVB with respect to the GE body axes set is shown in Figure 3-4. The transformation from the aerodynamic body axes to the GE body axes is given by $[B]$. The method of transformation and numerical results are described in Appendix A.

$$\left.\begin{matrix} X_1 \\ Y_1 \\ Z_1 \end{matrix}\right] \quad \text{reference axes of Figure 3-4 (GE computer program)}$$

$$\left.\begin{matrix} X_2 \\ Y_2 \\ Z_2 \end{matrix}\right] \quad \text{reference axes of Figure 3-2 (mass data)}$$

$$\left.\begin{matrix} X_3 \\ Y_3 \\ Z_3 \end{matrix}\right] \quad \text{reference axes of Figure 3-3 (aero data)}$$

$$\left.\begin{matrix} X_1 \\ Y_1 \\ Z_1 \end{matrix}\right] = [T] \left[\begin{matrix} X_2 \\ Y_2 \\ Z_2 \end{matrix}\right]$$

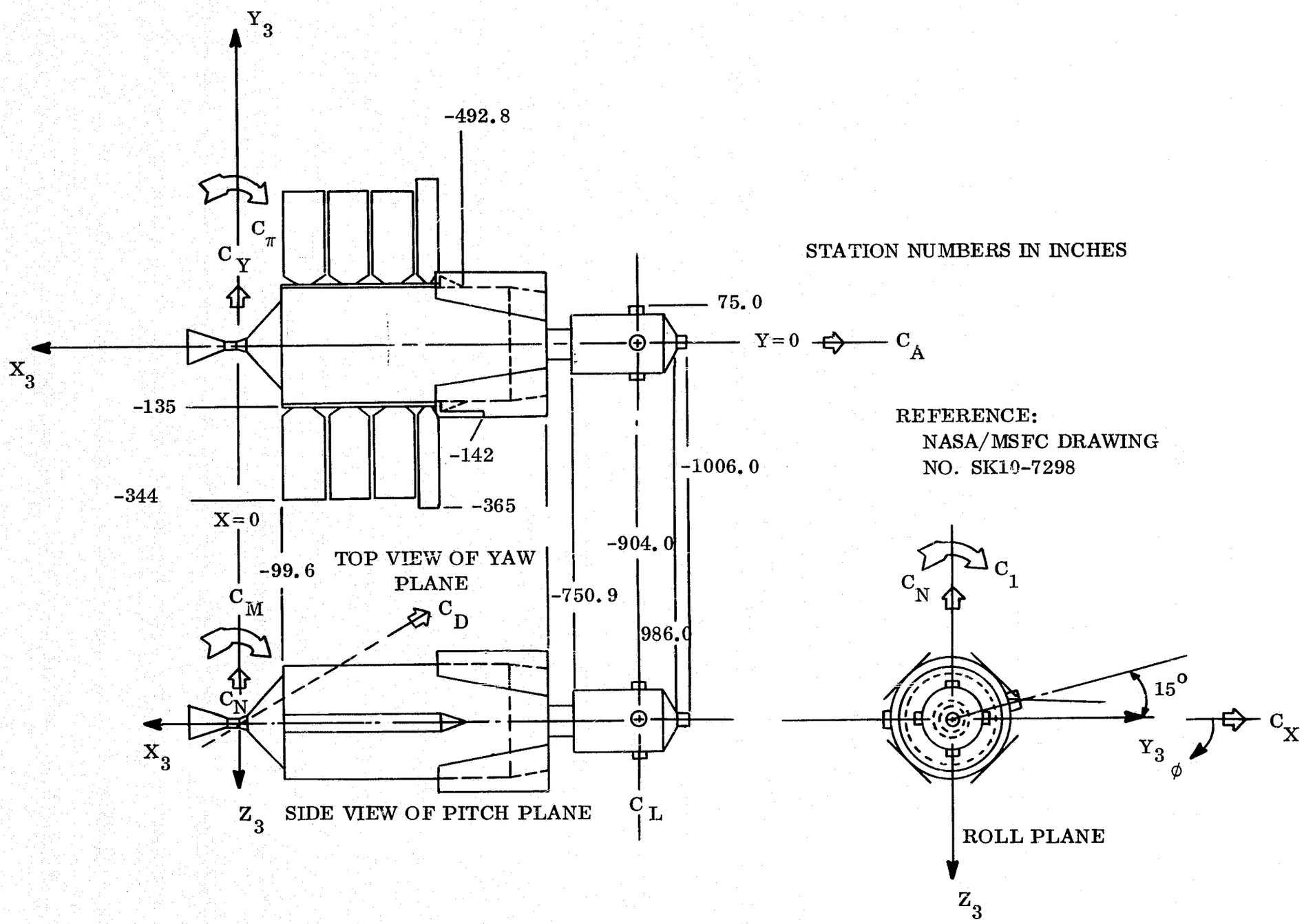


Figure 3-3. Aerodynamic Body Deference Axes

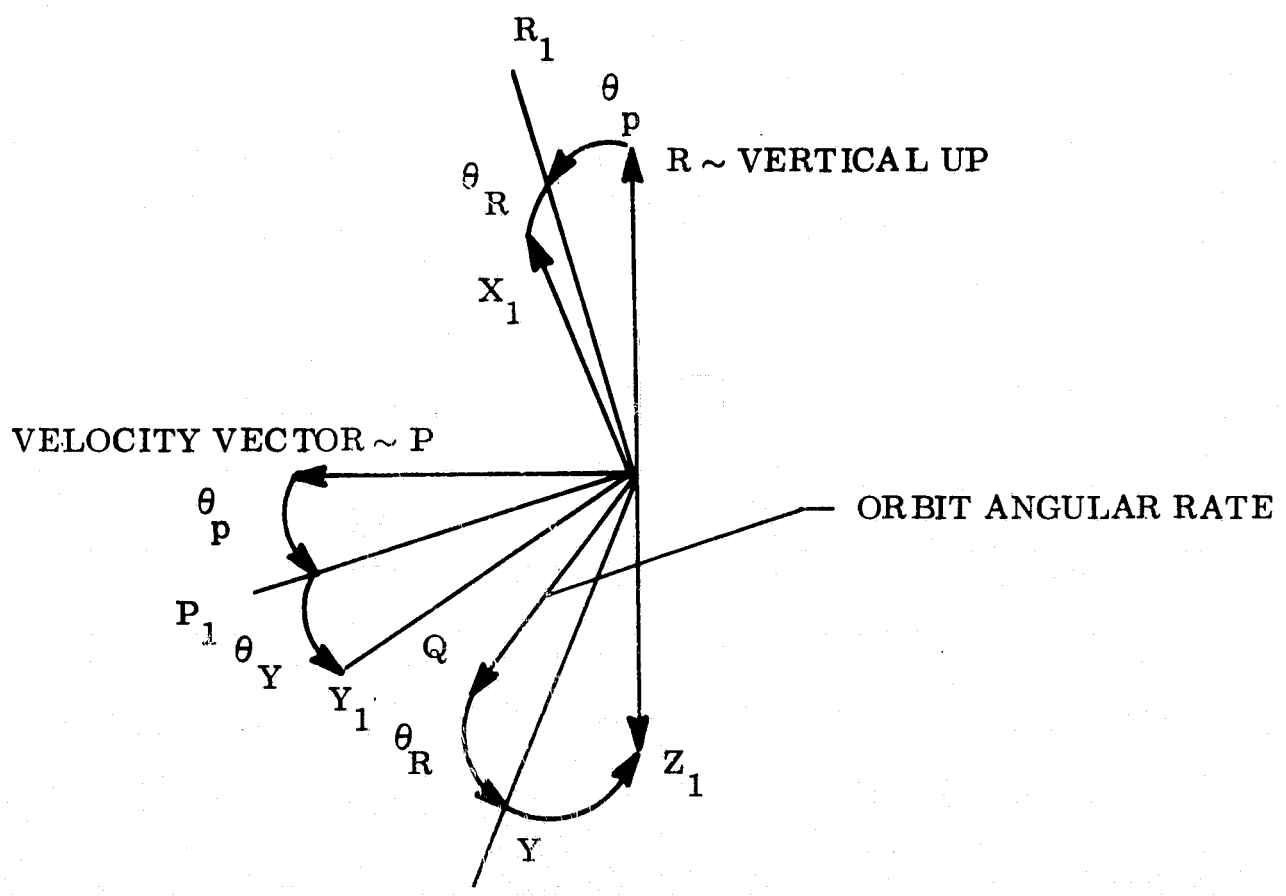


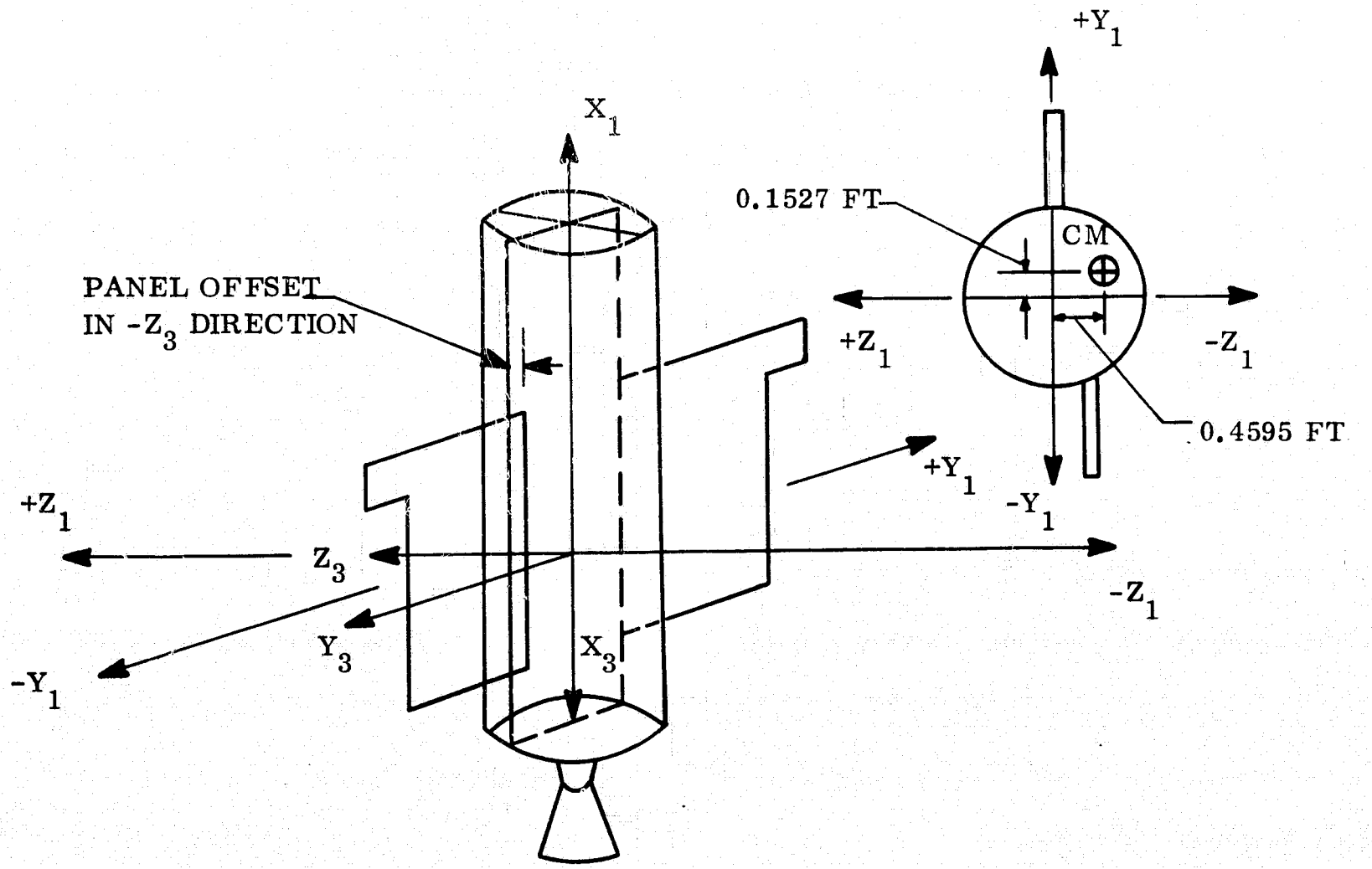


Figure 3-4. General Electric Body Axes

$$\begin{bmatrix} X_3 \\ Y_3 \\ Z_3 \end{bmatrix} = [A] \begin{bmatrix} X_2 \\ Y_2 \\ Z_2 \end{bmatrix}$$

$$\begin{bmatrix} X_1 \\ Y_1 \\ Z_1 \end{bmatrix} = [B] \begin{bmatrix} X_3 \\ Y_3 \\ Z_3 \end{bmatrix}$$

$$[A] = \begin{bmatrix} -1 & 0 & 0 \\ 0 & -0.707 & -0.707 \\ 0 & -0.707 & -0.707 \end{bmatrix}$$

$$[B] = \begin{bmatrix} -1 & 0 & 0 \\ 0 & -1 & 0 \\ 0 & 0 & +1 \end{bmatrix}$$

$$[T] = [B]\,[A] = \begin{bmatrix} 1 & 0 & 0 \\ 0 & +0.707 & +0.707 \\ 0 & -0.707 & +0.707 \end{bmatrix}$$

### 3.1.3 DEFINITION OF S-IVB AERODYNAMIC TORQUES AND MAGNETIC TORQUES

The aerodynamic torques which act on the S-IVB body are computed from data supplied by MSFC. This data is included in the Appendix. Force and moment coefficients, are stored as tables in the digital computer simulations, as a function of angle of attack, and angle about the longitudinal axis. Aerodynamic moments are computed as a function of relative velocity, atmospheric density and center of gravity positon which varies due to rod thermal bending.

The magnetic moment of 50 amp. meter (50,000 pole cm) is assumed based on a figure of 1 pole cm/lb which is normal for smaller spacecraft. Since most of the S-IVB weight is in the structure, this figure is probably conservative.

## 3.2 S-IVB TWO AXIS LOCAL VERTICAL CONFIGURATION

### 3.2.1 CONFIGURATION DESCRIPTION

For two-axis control about the local vertical, with the long axis of the S-IVB stage oriented nominally coincident with the local vertical, the natural gravity gradient torques may be advantageously used to stabilize the spacecraft. Rods and tip masses are not required. However, by means of the large angle, nonlinear, dynamic simulation (digital computer) it has been established that aerodynamics play an important role in performance. Two preferred yaw orientations have been demonstrated to be stable. Referring to Figure 3-4 for axis definition, the stable yaw positions appear to be +10 and +155 degrees about the $+X_1$ axis. That is, the spacecraft will achieve stable orientation with the plane of the solar panels rotated +10 or +155 degrees about the $X_1$ axis. Steady state oscillations about the stable point will naturally occur.

It has also been established that a certain minimum amount of damping is necessary to maintain stability during the initial acquisition phase with initial rates of 0.01 deg/sec about all three axes, and initial angles at 10 degrees (all axes) from the desired orientation. These rates and angles are those obtainable with the active attitude control system onboard the S-IVB.

The characteristics of a magnetically anchored, spherical viscous damper which will adequately provide the required damping performance of 10 days decay to steady state and allow steady state performance requirements to be met are as follows:

| | |
|---|---|
| Sphere outer diameter | 41 cm (16 in.) |
| Total weight | 356 Newtons (80 lb) |
| Damping coefficient | 82 Newton-meter-second (60 ft-lb-sec) |
| Magnet strength | 2000 amp-meter$^2$ ($2 \times 10^6$ pole-cm) |

A single damper with these characteristics serves as the entire passive stabilization subsystem for this configuration.

### 3.2.2 CONFIGURATION ANALYSIS

The analysis and evaluation method leading to the selection of the design parameters listed above is summarized in the following paragraphs.

#### 3.2.2.1 Preliminary Analysis

In the design of a magnetically anchored viscous damper for a particular application, three primary considerations exist:

a. Required damping time to reach steady state conditions

b. Steady state pointing error

c. Passive stabilization system weight

The two design parameters which establish the damping capability of such a system are the rate damping coefficient, expressed as torque per unit rate: Newton-Meters per radian/sec (or ft-lb per radian/sec), and the magnet strength, expressed as ampere-meters$^2$ (or pole-centimeters). The selection of a damping coefficient involves a tradeoff between damping time from large angle oscillations to steady state conditions and the damper-induced steady state error amplitude. This "damper-induced" steady state error results from the fact that the magnet within the damper casing follows the Earth's magnetic field whereas the casing, rigidly attached to the spacecraft, follows the local vertical. The viscous torque due to the relative motion becomes a disturbance torque.

Concerning damping time, the linearized dynamic equations of motion, including damping torques may be solved and a damping time constant determined as a function of damping coefficient, b, for a particular magnet strength. For generalization, b is normalized to the system pitch inertia (largest) and the orbital rate (in essence, altitude); magnet strength is normalized to pitch inertia only. The results can then be shown as a generalized plot of damping time constant ($\tau$, number of orbits) as a function of $b/I_p \omega_o$ for lines of constant $m/I_p$. (See Figure 3-5.) However, since the amplitude of the magnetic torque, which causes the magnet to follow approximately the Earth's magnetic field, is dependent upon the Earth's field strength, this analysis must be done also as a function of orbit

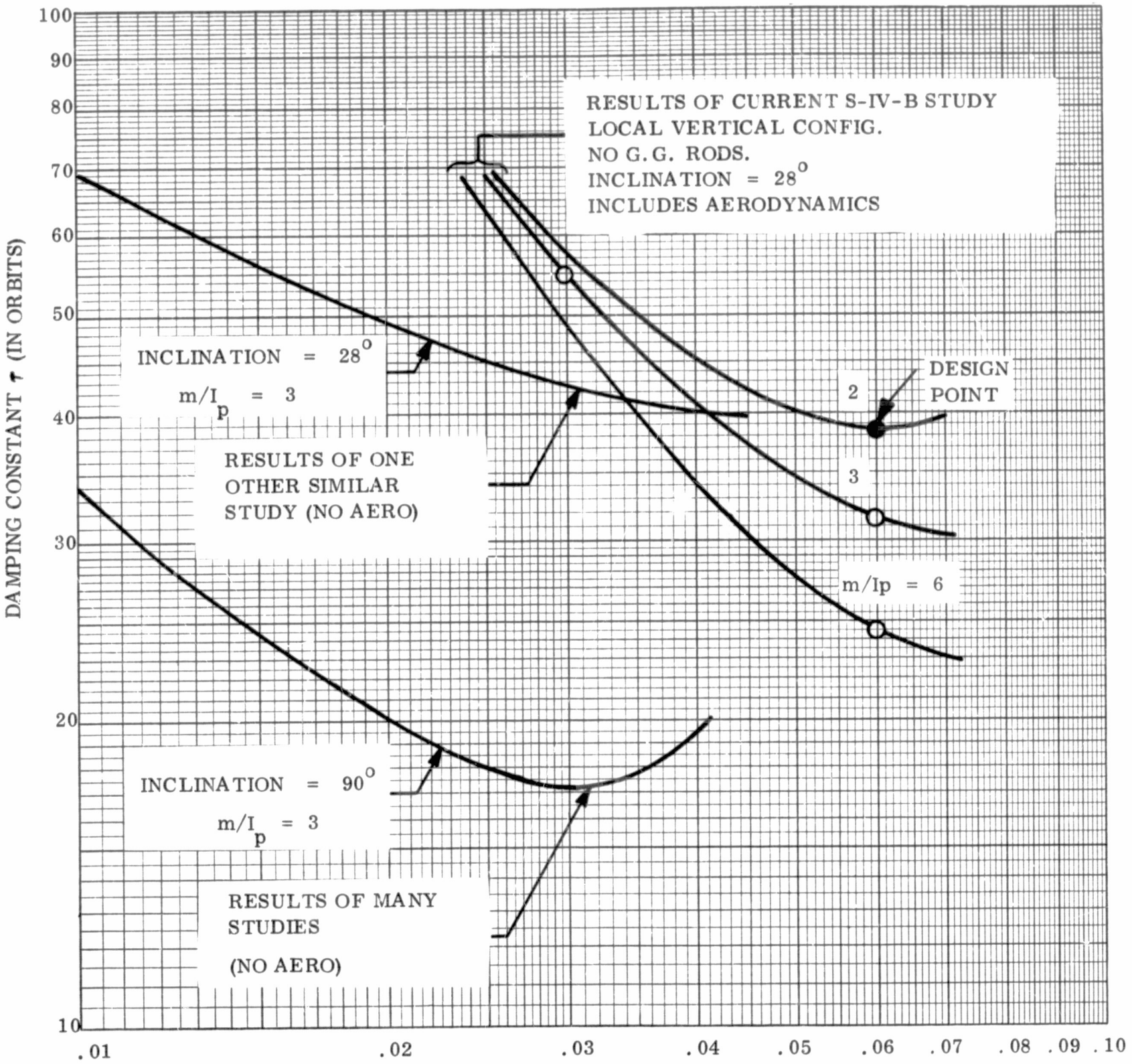


$$\text{DAMPING PARAMETER} = \frac{b}{I_p \omega_o}$$

b = DAMPING COEFF (FT LB SECS)
$I_p$ = PITCH INERTIA (SLUG $FT^2$)
$\omega_o$ = ORBITAL RATE (RAD/SEC)
m = MAGNET STRENGTH (POLE CMS)

Figure 3-5. Damping Time Constant Vs Damping Parameter

inclination. This had been done previously for a polar orbit and one in which aerodynamics is of no significance (altitude > 750 km). However, for the S-IVB application (400 km) aerodynamics is a significant disturbance and, therefore, to some extent modifies, the linearized analysis. This fact was verified in the early phases of this study, in that significantly more damping is required in the presence of aerodynamics than without it, as demonstrated by the use of the large angle, nonlinear digital computer simulations.

The damping investigation carried out for this two-axis local vertical configuration before release of the mid-term report led to the specification of a damper with the following characteristics:

a. Damping coefficient = 82 NMS (60 ft-lb-sec)

b. Magnet strength = 6000 amp meter$^2$ ($6 \times 10^6$ pole cms)

c. Weight 1000 Newtons (225 lb)

Subsequent to this phase of the study, an error was found in the atmospheric density model used in the computer simulations. The error occurred in the diurnal "bulge" term which simulates the solar heating of the atmosphere and therefore affected only a fraction of the orbit. However, the error magnified the peak density in the bulge by eight times. This imposed a significantly greater once orbital disturbance on the system than should exist, thus causing higher oscillation amplitudes and higher body rates. This led to higher viscous damping torques and, therefore, required a magnet strength greater than actually needed to "hold" the earth's magnetic field.

After correcting the atmospheric model, steady state and transient performance was re-evaluated with the originally selected damper parameters. Steady state performance and damping time improved to the extent that a smaller and lighter damper appeared feasible. Since steady state pointing accuracies could be met with a damping coefficient of 82 Newton-meter seconds (60 ft-lb-sec), full advantage of the performance margin available could be taken in the form of a smaller and lighter damper magnet.

3.2.2.2 Final Analysis

Four large-angle, non-linear, transient computer simulations were made using the following damping characteristics:

a. b = 82 NMS (60 ft-lb-sec), M = 5500 amp $m^2$ (5.5 x $10^6$ pole cm)

b. b = 82 NMS (60 ft-lb-sec), M = 2750 amp $m^2$ (2.75 x $10^6$ pole cm)

c. b = 82 NMS (60 ft-lb-sec), M = 2000 amp $m^2$ (2 x $10^6$ pole cm)

d. b = 41 NMS (30 ft-lb-sec), M = 2750 amp $m^2$ (2.75 x $10^6$ pole cm)

The results of these runs are shown in Figures 3-6 through 3-9, respectively. Damping time constants were computed for each assuming exponential decay of the form:

$$\theta_f = \theta_o e^{-t/\tau}$$

Figure 3-5 shows these points plotted in generalized form as a function of damping parameter ($b/I_p \omega_o$) with estimated characteristic shapes superimposed.

The damping parametric curves are straight lines independent of M where damping level is low and magnet strength is large, because $\tau$ is inversely proportional to b for a perfectly anchored damper. As b increases and M remains constant the lines curve through a point of maximum obtainable damping for a given magnet size.

For reference purposes, the normalized characteristic damping curve for a polar orbit is also shown.

Figure 3-10 shows the actual damping time constant for the S-IVB Two-Axis Local Vertical Configuration in a $28^o$ inclined orbit with the selected damping coefficient of 82 NMS (60 ft-lb-sec) as a function of magnet strength. The same information is shown in Figure 3-11 in terms of time to reach steady state as a function of total damper weight.

FOLDOUT FRAME |

S-IVB TWO-AXIS LOCAL VERTICAL CONFIGUR
PLANE OF SOLAR PANELS IN ORBIT PLA

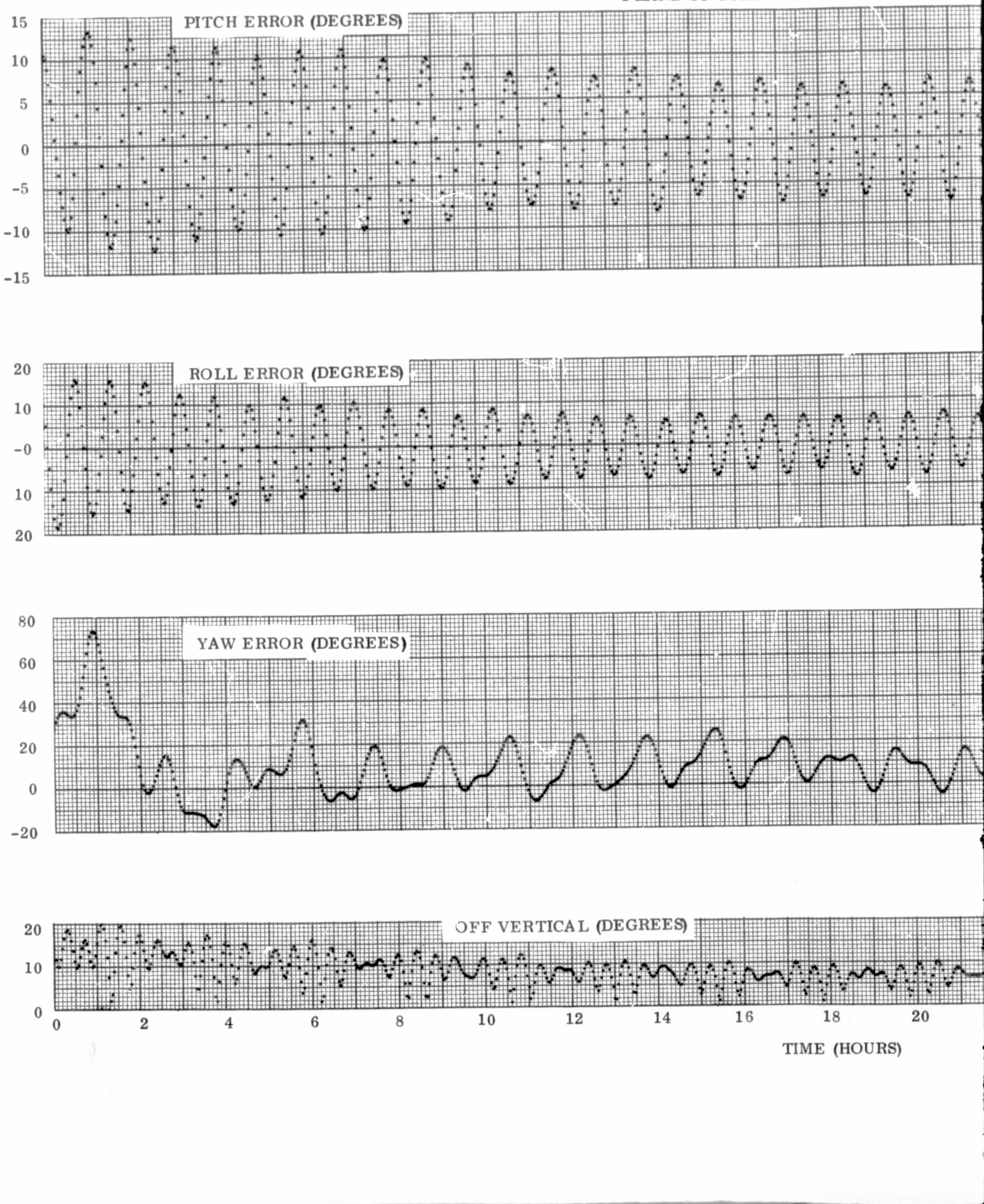

FOLDOUT FRAME 2

CAL VERTICAL CONFIGURATION
R PANELS IN ORBIT PLANE

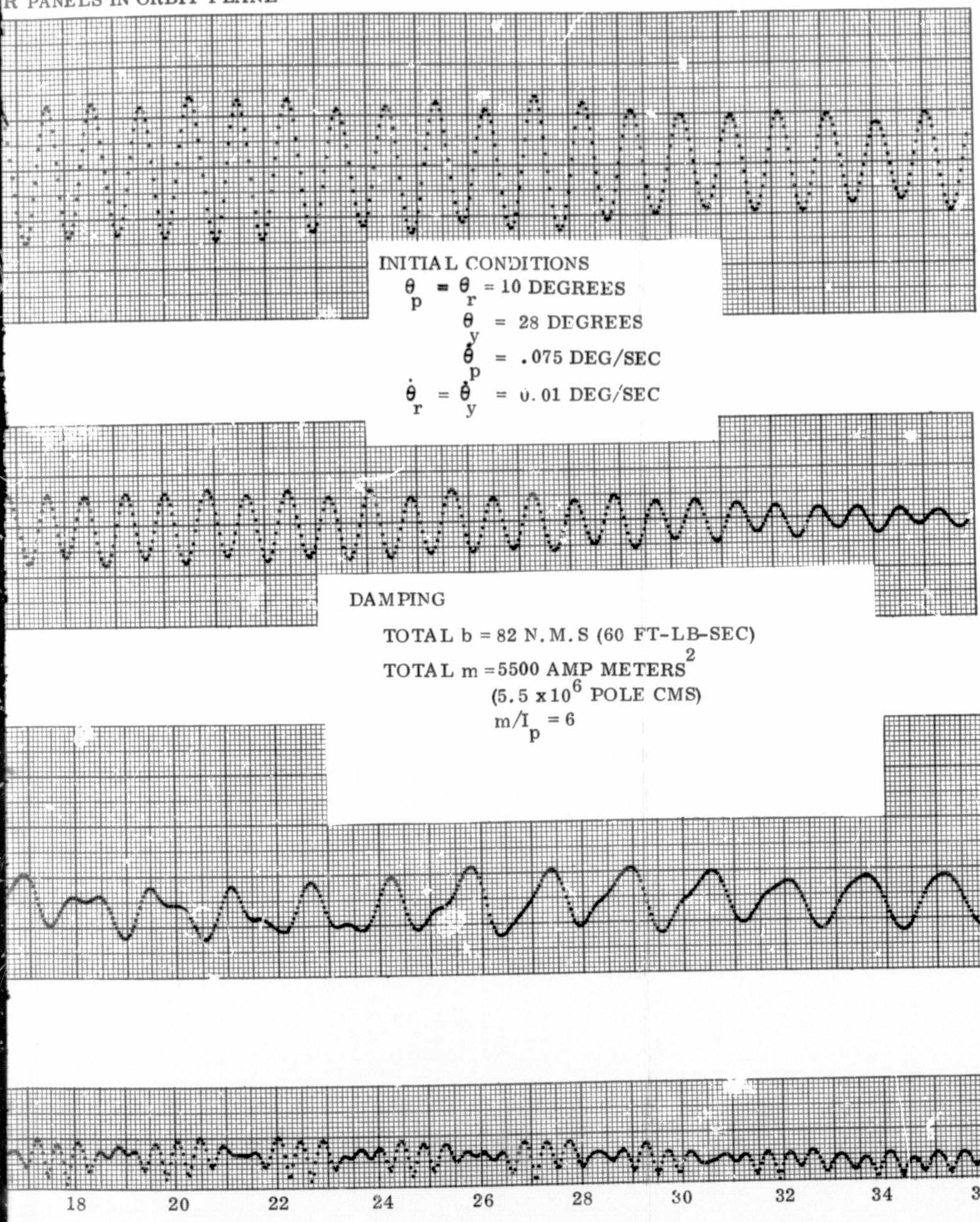


Figure 3-6. Transient Performance
b = 82 N.M.S. (60 ft-lb-sec) $M/I_p = 6.0$

FOLDOUT FRAME

S-IVB TWO AXIS LOCAL VERTICAL CONFIGURAT
PLANE OF SOLAR PANELS IN ORBIT PLANE

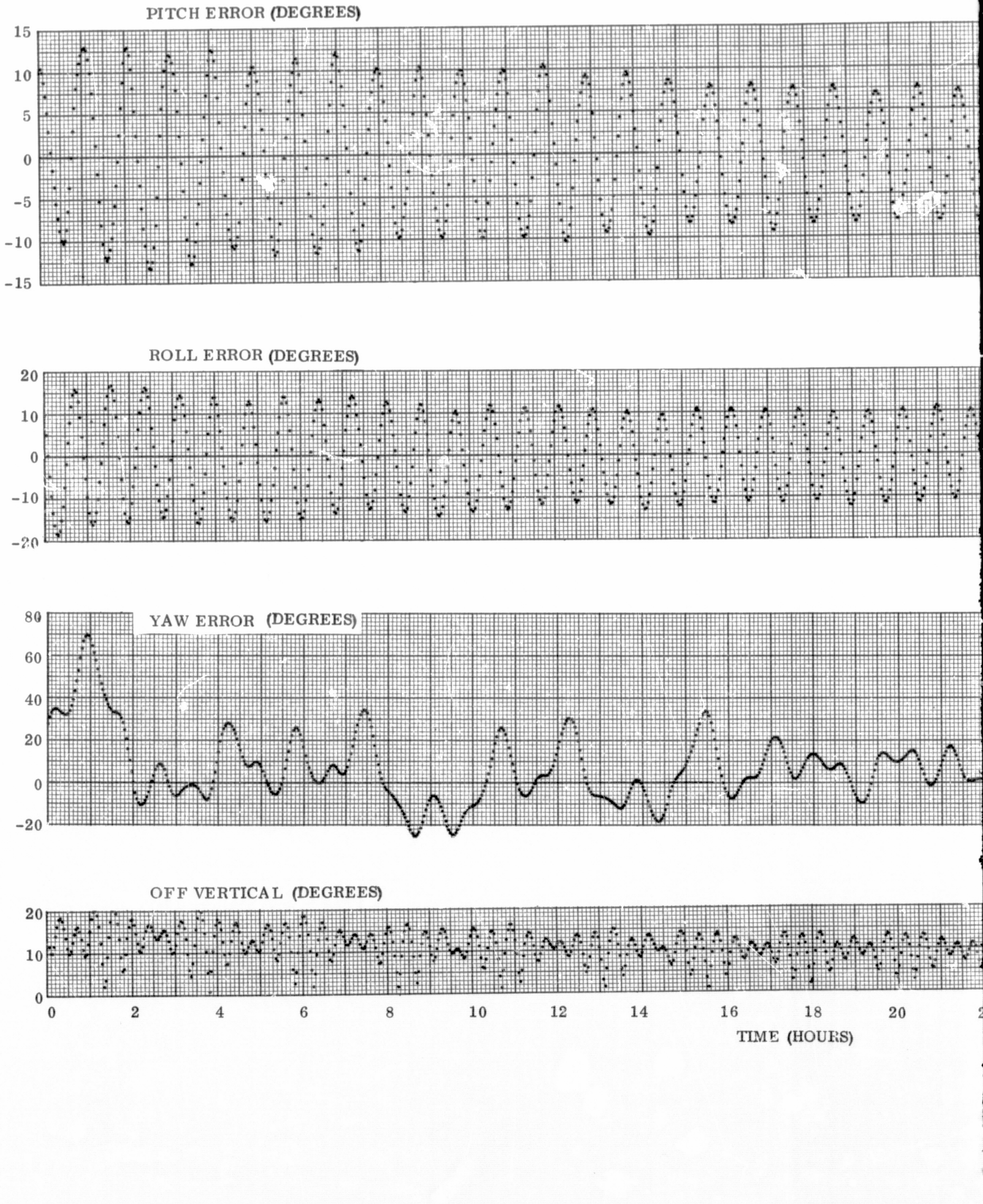

FOLDOUT FRAME 2

ICAL CONFIGURATION
IN ORBIT PLANE

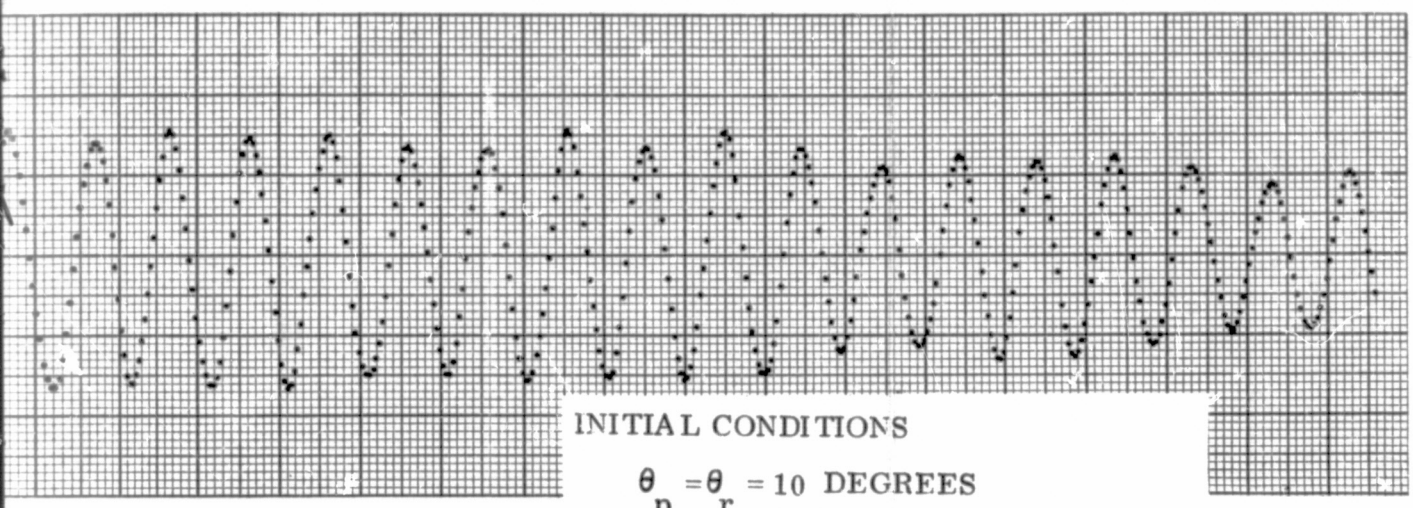

INITIAL CONDITIONS

$\theta_p = \theta_r = 10$ DEGREES

$\theta_y = 28$ DEGREES

$\dot{\theta}_p = 0.075$ DEG/SEC

$\dot{\theta}_r = \dot{\theta}_y = 0.01$ DEG/SEC

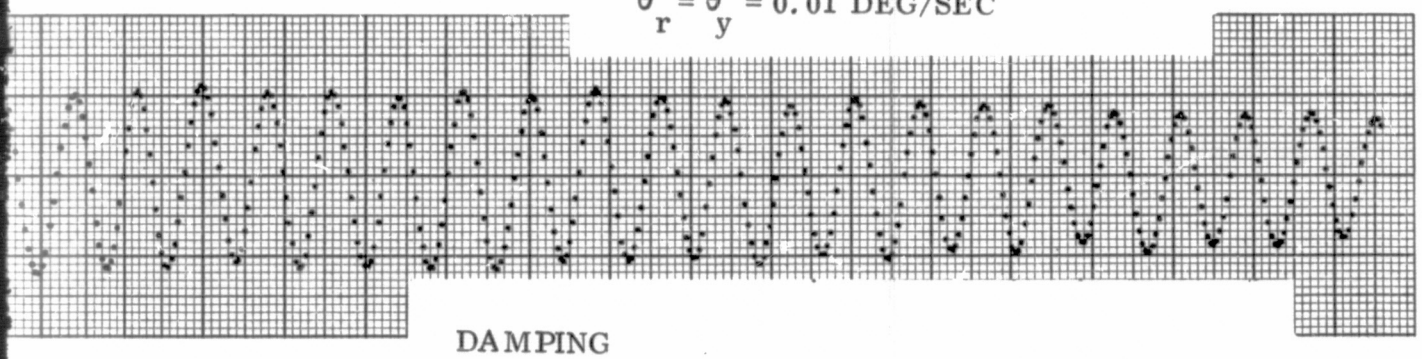

DAMPING

TOTAL b = 82 N.M.S. (60 FT-LB-SEC)

TOTAL m = 2750 AMP METERS$^2$
(2.75 x $10^6$ POLE CMS)

$m/I_p = 3$

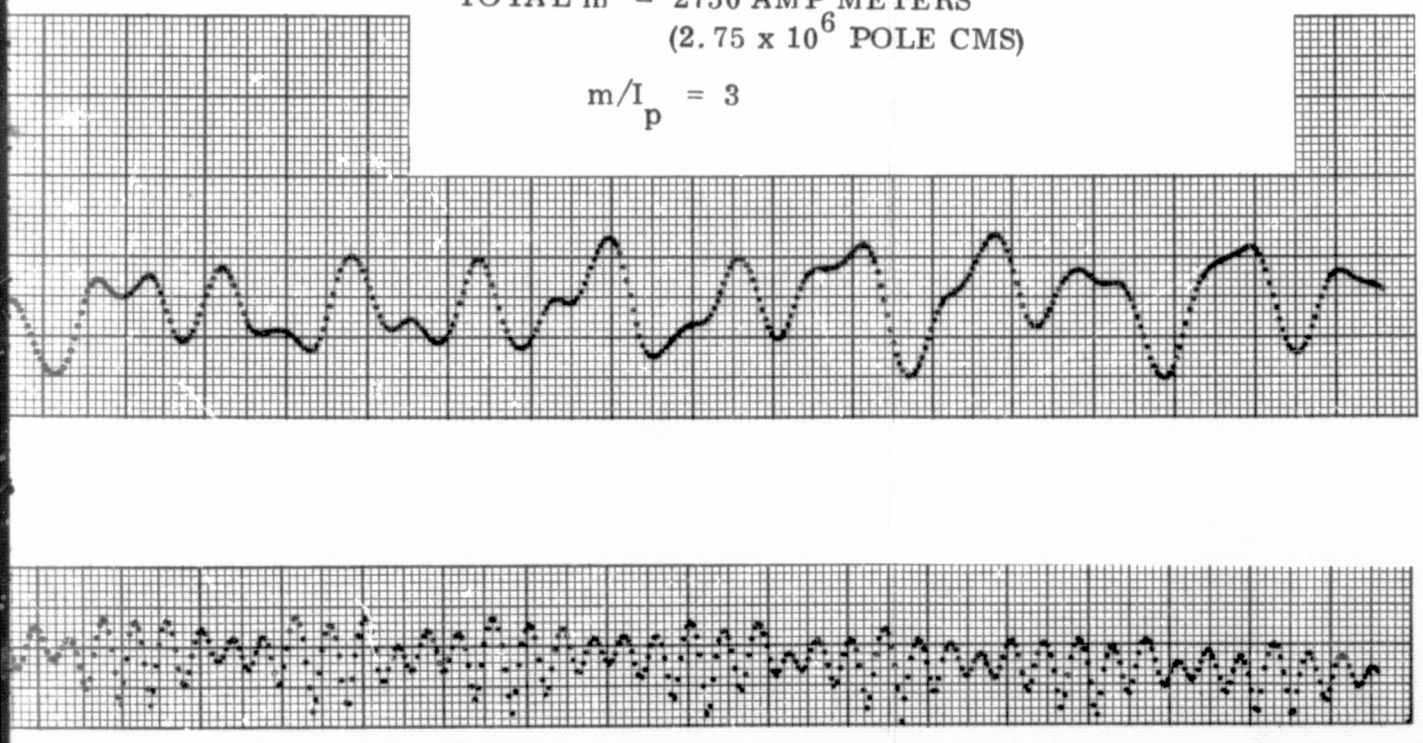



20 22 24 26 28 30 32 34 36

S)

Figure 3-7. Transient Performance, b = 82 N.M.S. (60 ft-lb-sec) $M/I_p = 3.0$

FOLDOUT FRAME 1

S-IVB TWO AXIS LOCAL VERTICAL CONFIG
PLANE OF SOLAR PANELS IN ORBIT P

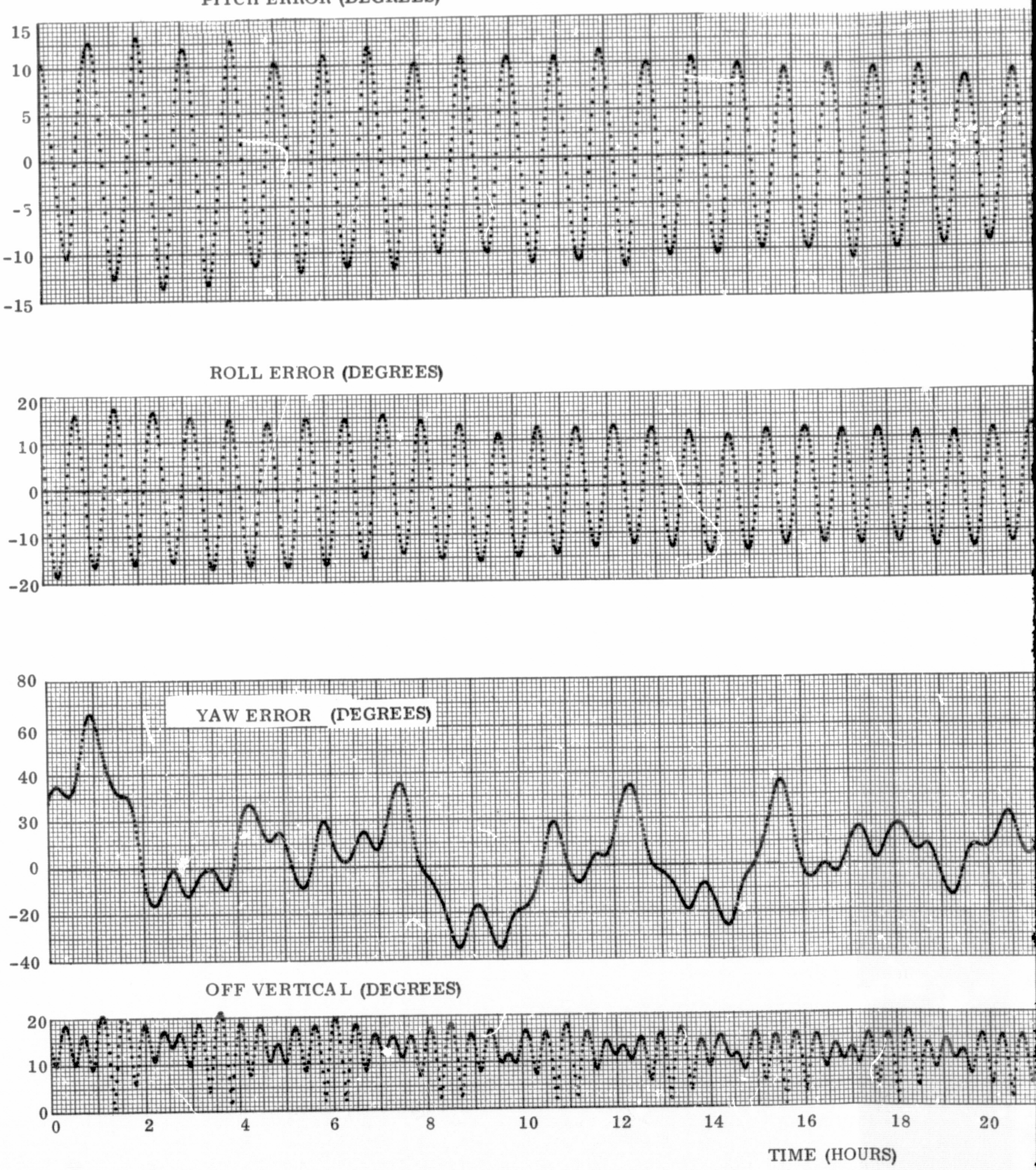

FOLDOUT FRAME 2

ERTICAL CONFIGURATION
NELS IN ORBIT PLANE

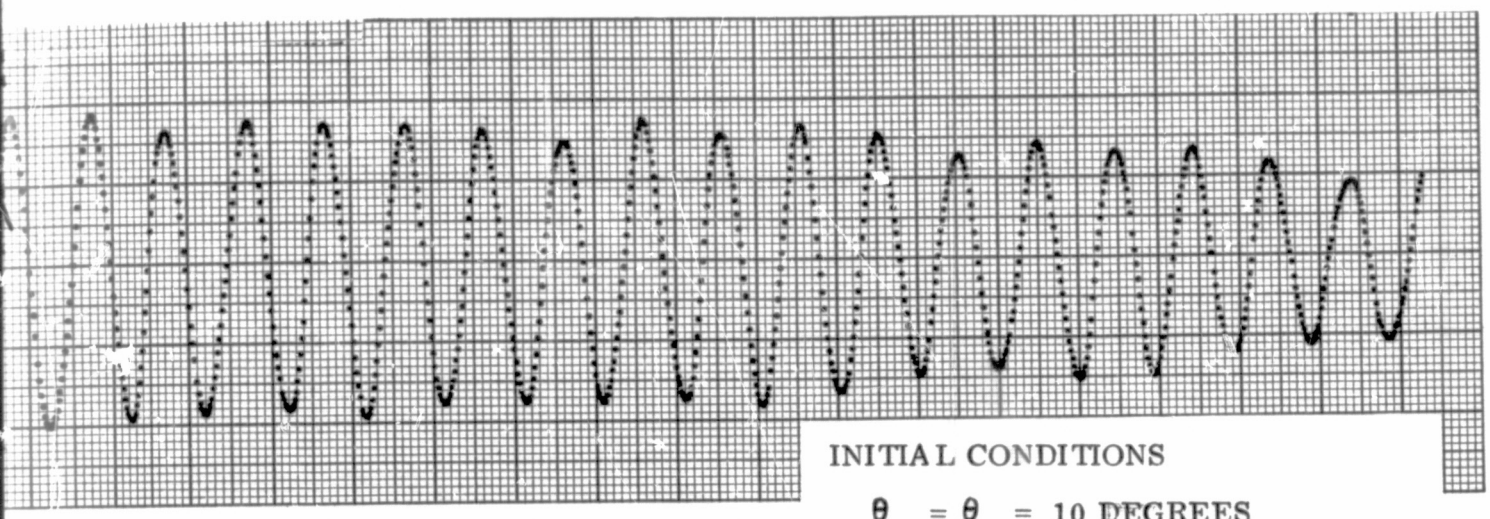

INITIAL CONDITIONS

$\theta_p = \theta_r$ = 10 DEGREES

$\theta_y$ = 28 DEGREES

$\dot{\theta}_p$ = 0.075 DEG/SEC

$\dot{\theta}_r = \dot{\theta}_y$ = 0.01 DEG/SEC

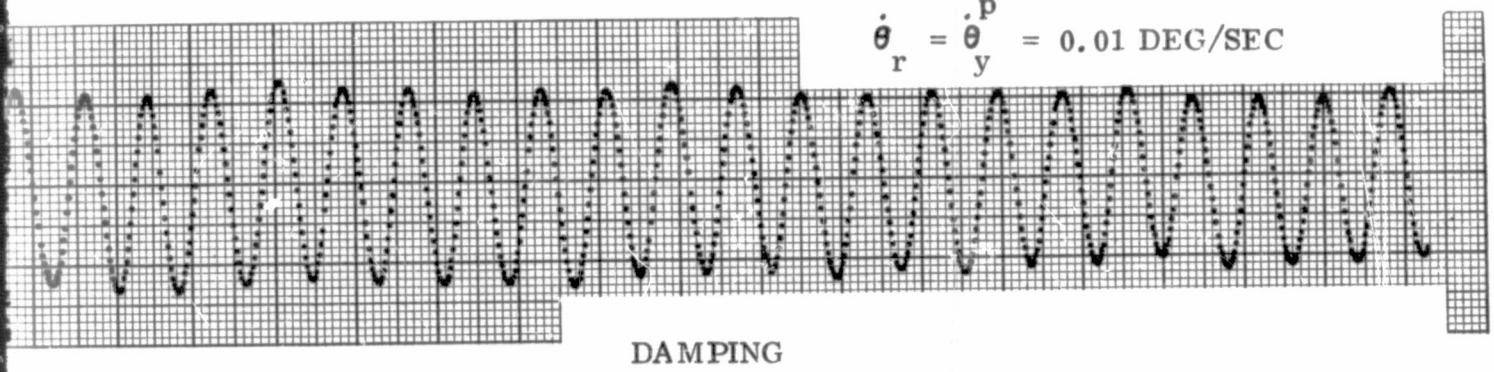

DAMPING

TOTAL b = 82 N.M.S. (60 FT-LB-SEC)

TOTAL m = 2000 AMP METERS$^2$
(2 X $10^6$ POLE CMS)

$m/I_p$ = 2.24

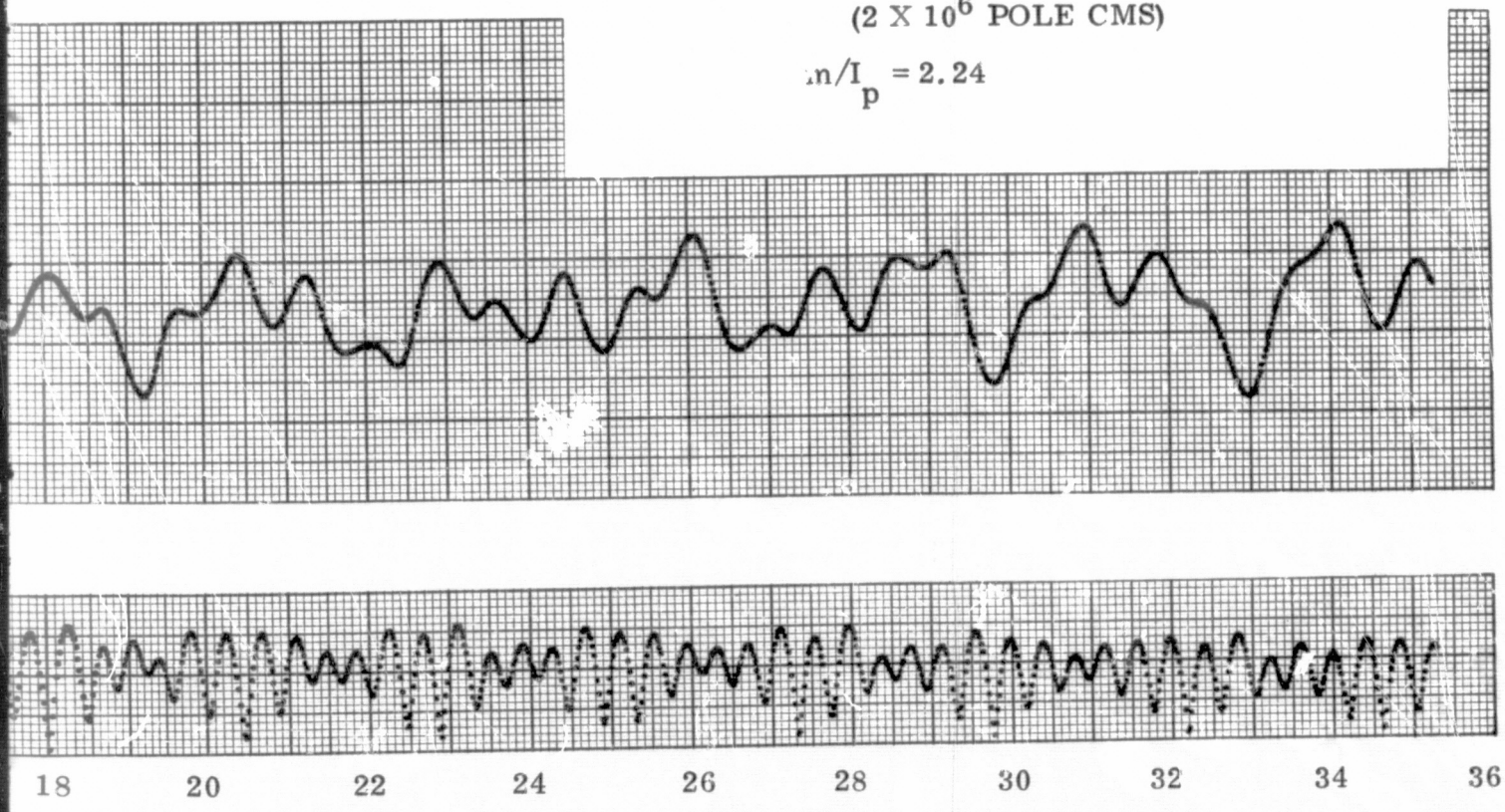

18 20 22 24 26 28 30 32 34 36

S)

Figure 3-8. Transient Performance, b = 82 N.M.S. (60 ft-lb-sec) $M/I_p$ = 2.24

FOLDOUT FRAME /

S-IVB TWO-AXIS LOCAL VERTICAL CONF
PLANE OF SOLAR PANELS IN ORBIT

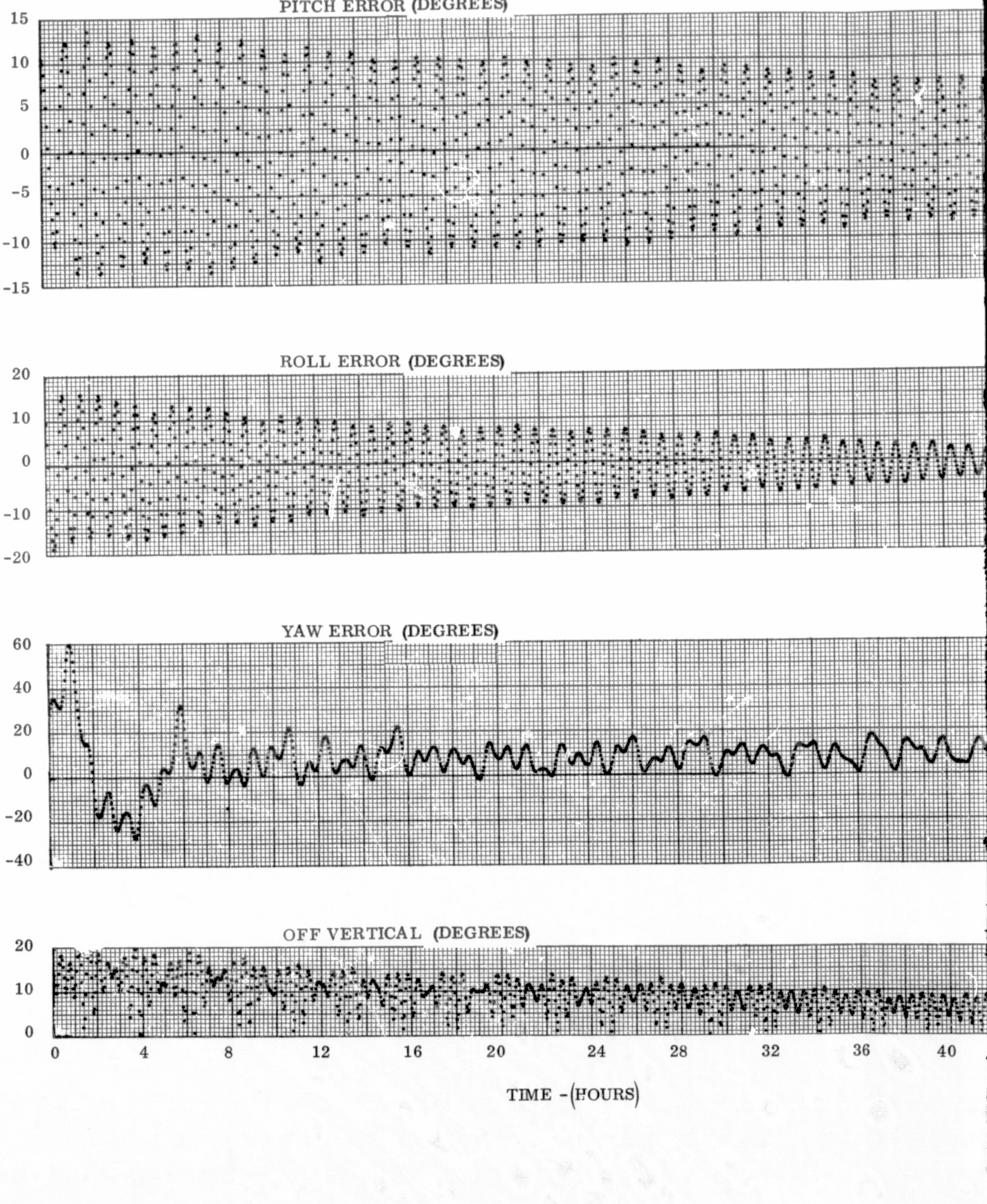

FOLDOUT FRAME 2

CAL CONFIGURATION
IN ORBIT PLANE

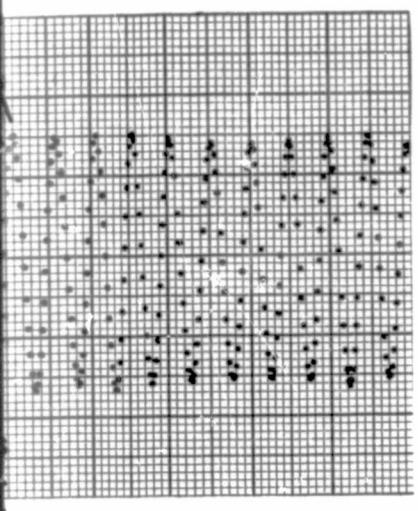

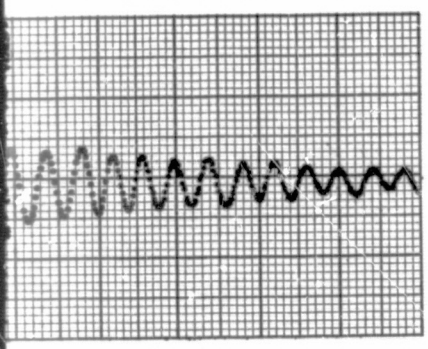

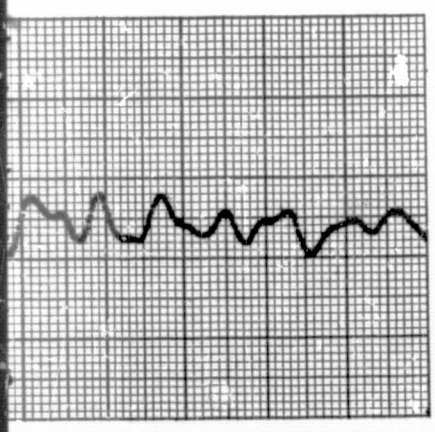

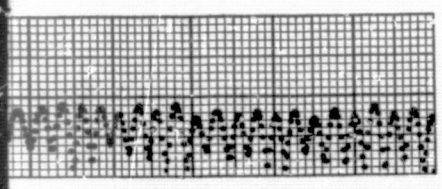

40 44 48

INITIAL CONDITIONS

$\theta_p = \theta_r$ = 10 DEGREES

$\theta_y$ = 28 DEGREES

$\dot{\theta}_p$ = .075 DEG/SEC

$\dot{\theta}_r = \dot{\theta}_y$ = .01 DEG/SEC

DAMPING

TOTAL b = 41 N.M.S. (30 FT-LB-SEC)

TOTAL m = 2750 AMP $M^2$ ($2.75 \times 10^6$ POLE CMS)

$M/I_p$ = 3

Figure 3-9. Transient Performance, b = 41 N.M.S. (30 ft-lb-sec) $M/I_p = 3.0$

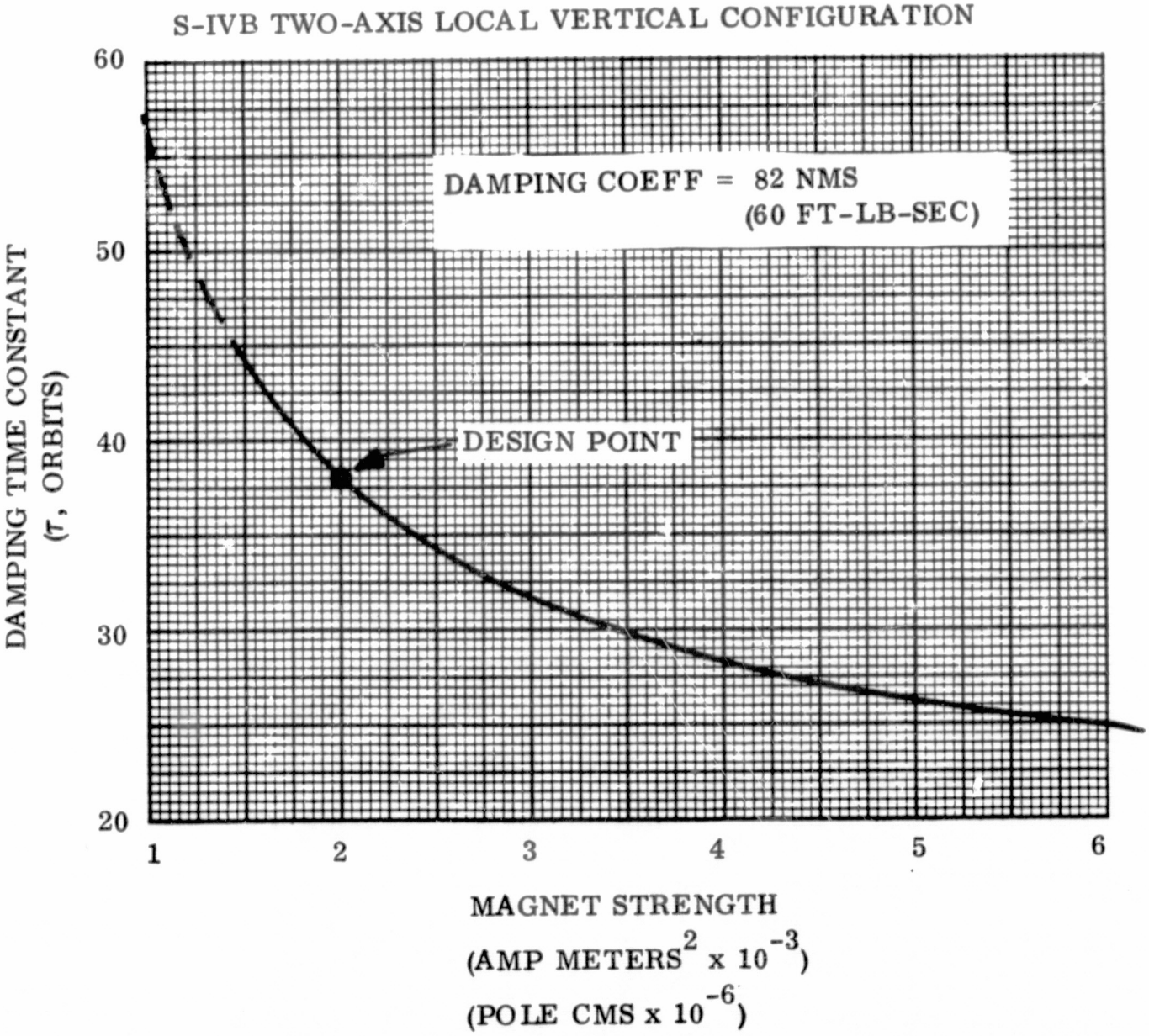


Figure 3-10. Damping Time Constant Vs Magnet Strength

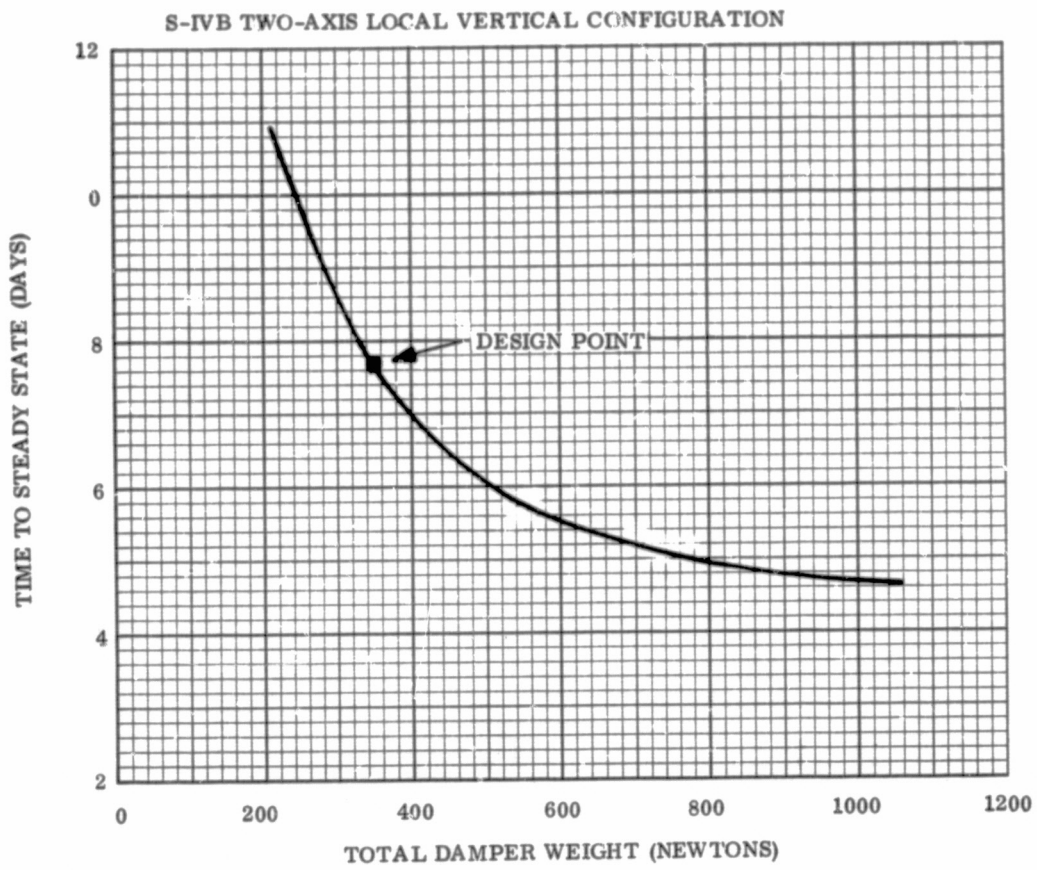


Figure 3-11. Damping Time to Steady State Vs Damper Weight

Based upon these damping characteristics and upon the nominal steady state performance the damper selected for this configuration which will meet all performance requirements is one with the following characteristics:

| | | | |
|---|---|---|---|
| a. | Damping coefficient | = | 82 NMS (60 ft-lb-sec) |
| b. | Magnet strength | = | 2000 amp-$m^2$ (2 x $10^6$ pole-cm) |
| c. | Approximate weight | = | 356 Newtons (80 lb) |

A complete description of such a damper is given in Section 6.

### 3.2.3. NOMINAL PERFORMANCE

The basic tool used to evaluate both transient and steady state performance, in regard to stabilization and attitude pointing accuracy of the S-IVB in orbit, is a large, nonlinear, digital computer program. It includes all significant disturbance forces acting on the

orbiting body. Individual torques are computed and summed; the resulting angular accelerations and rates are sequentially integrated to determine body position as a function of time. The output of the program consists of Euler angle time histories, which at small angles, are representative of body pointing errors relative to an orbiting reference frame.

3.2.3.1 Steady State Performance

The steady state pointing accuracies obtainable with the selected damper design are as follows:

a. Pitch: $\pm 0.7^{o}$ on a $-0.2^{o}$ bias

b. Roll: $\pm 3.0^{o}$ on a $-0.5^{o}$ bias

c. Yaw: $\pm 13^{o}$ on a $+9.0^{o}$ bias

d. Tilt Angle: $3.0^{o}$ (off local vertical)

The results of a 150-hour computer simulation are shown in Figure 3-12A and B. Based upon the computed time constant of 38 orbits, this simulation corresponds to slightly more than 2.5 time constants. Some transient motion existing at the beginning of the run has been damped by the end of the run, which verifies the computed time constant and the predicted time to reach steady state. Steady state oscillations about spacecraft pitch and yaw axes will be a predominantly orbital rate; whereas roll oscillations will be twice the orbital rate.

Although the original intent for this configuration was a two-axis stabilization with no provision for yaw control, the particular inertia relationships exhibited by the S-IVB vehicle, do in fact result in yaw stabilization. Even though yaw pointing error is significantly greater than either pitch or roll error, it is still less than the original requirement of $\pm 15$ degrees specified for a three-axis system.

The reference orientation (i.e., $\theta_p = \theta_r = \theta_r = \theta_y = 0^{o}$) for Figure 3-12 is that position in which the long axis of the vehicle is parallel to the local vertical with the J-2 gimbal toward

Earth and the plane of the solar panels in the orbit plane. (Off-set solar panel aft relative to flight direction). The +9 degree average bias angle on yaw means the S-IVB vehicle will orient itself (i. e., "fly") with the plane of the solar panels rotated +9 degrees out of the orbit plane. Positive yaw is counter clockwise looking earthward.

The disturbances used in the steady state simulation are:

a. Aerodynamics on the S-IVB vehicle.

b. Solar pressure (CP-CM offset).

c. Damper torques.

d. Vehicle magnetic dipole (50 amp-$m^2$/50,000 p. cms).

In order to assess the relative magnitudes of the individual contributors to the overall pointing errors, use was made of a linearized error determination program. This program was originally written as a preliminary design tool in order to establish approximate disturbance magnitudes for purposes of preliminary system sizing. It was modified to include aerodynamics on large bodies. The basic philosophy used in the program leads to pointing errors which are conservatively larger than actually expected.

The following "error budget" was compiled for this S-IVB configuration including the selected damper. The arithmetic total shown assumes that static and oscillatory components of all contributors may be added directly. However, it has been found that better agreement with the large angle, nonlinear digital program is obtained if the RSS (root of the sum of the squares) value is used. It is also to be recognized that good agreement is extremely difficult to obtain when total errors are less than 2 to 3 degrees.

As expected the largest single contributor to overall pointing error is that due to damper-induced torques; approximately 70 percent of the pitch and yaw error and 90 percent of the roll error. Aerodynamics, assumed to be strictly a disturbance in this linearized analysis, may account for 20 to 25 percent of the pitch and yaw errors; whereas, roll is not significantly

FOLDOUT FRAME 1

S-IVB TWO-AXIS LOCAL VERTICAL CONFIG
PLANE OF SOLAR PANELS IN ORBIT P

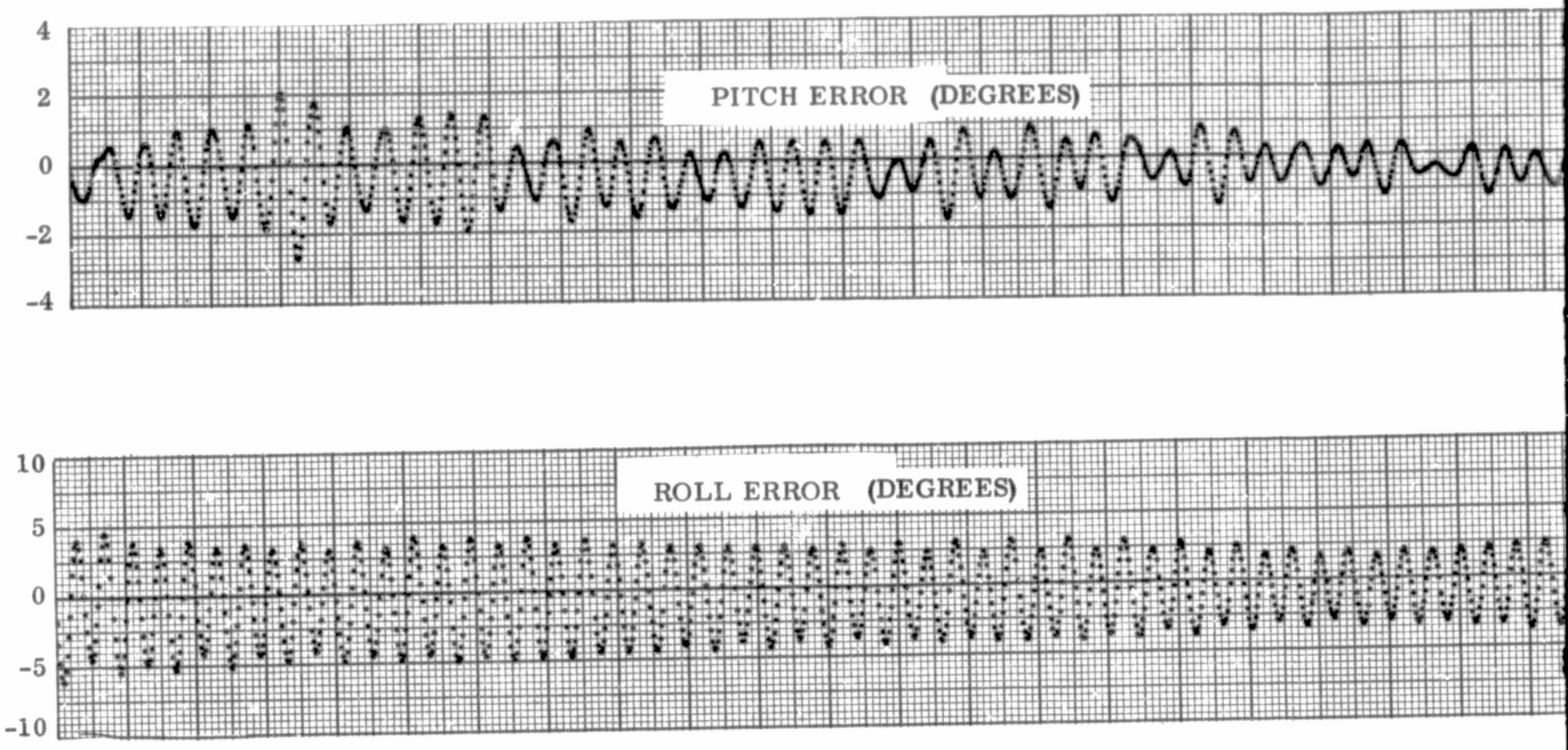

VERTICAL CONFIGURATION
ANELS IN ORBIT PLANE

FOLDOUT FRAME 2

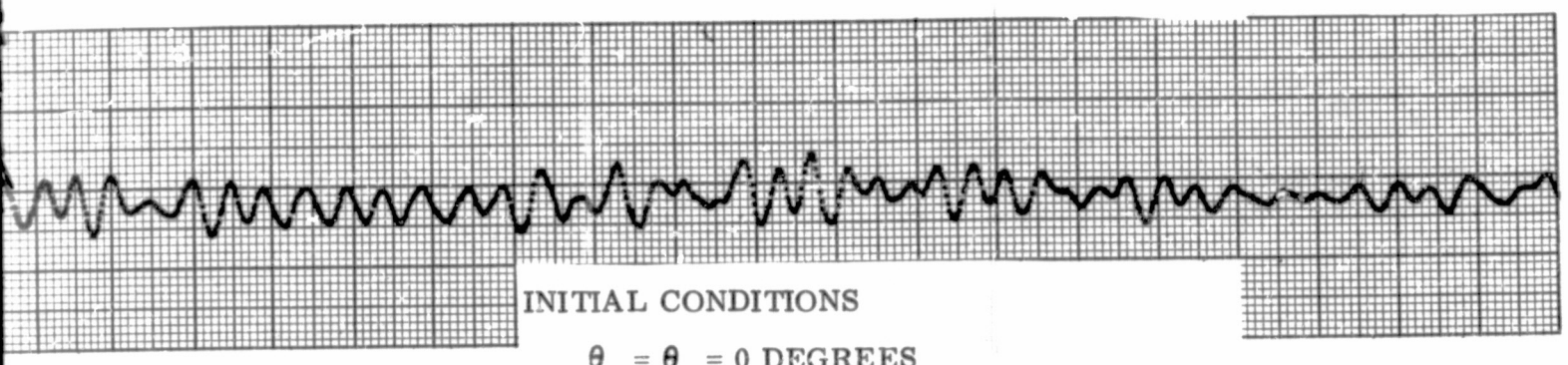

INITIAL CONDITIONS

$\theta_p = \theta_r = 0$ DEGREES

$\theta_y = 10$ DEGREES

$\dot{\theta}_p$ = ORBITAL RATE

$\dot{\theta}_r = \dot{\theta}_y = 0$ DEG/SEC

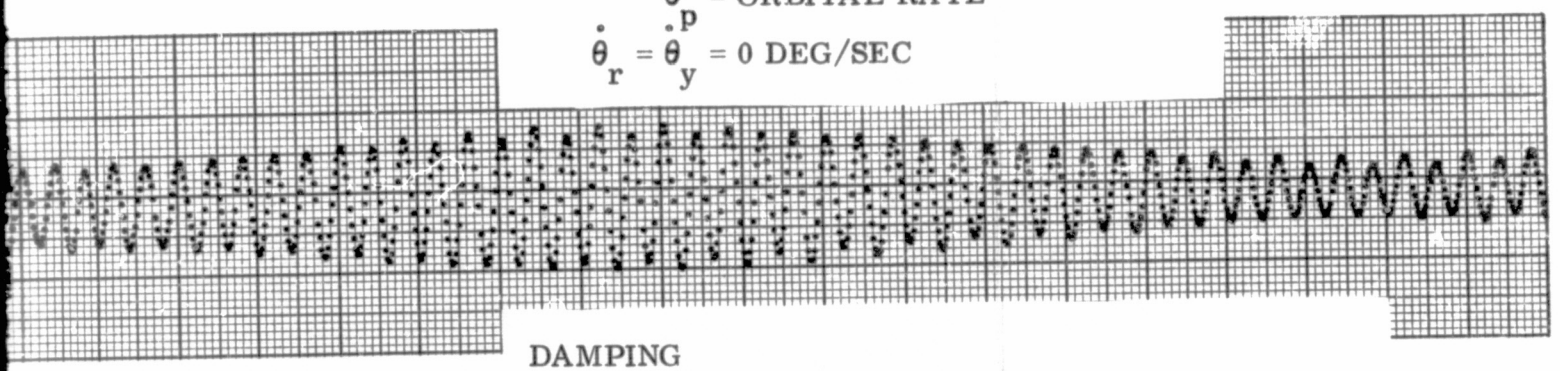

DAMPING

TOTAL b = 82 N.M.S. (60 FT-LB-SEC)

TOTAL m = 2000 AMP $M^2$ ($2 \times 10^6$ POL CMS)

$M/I_p = 2.24$

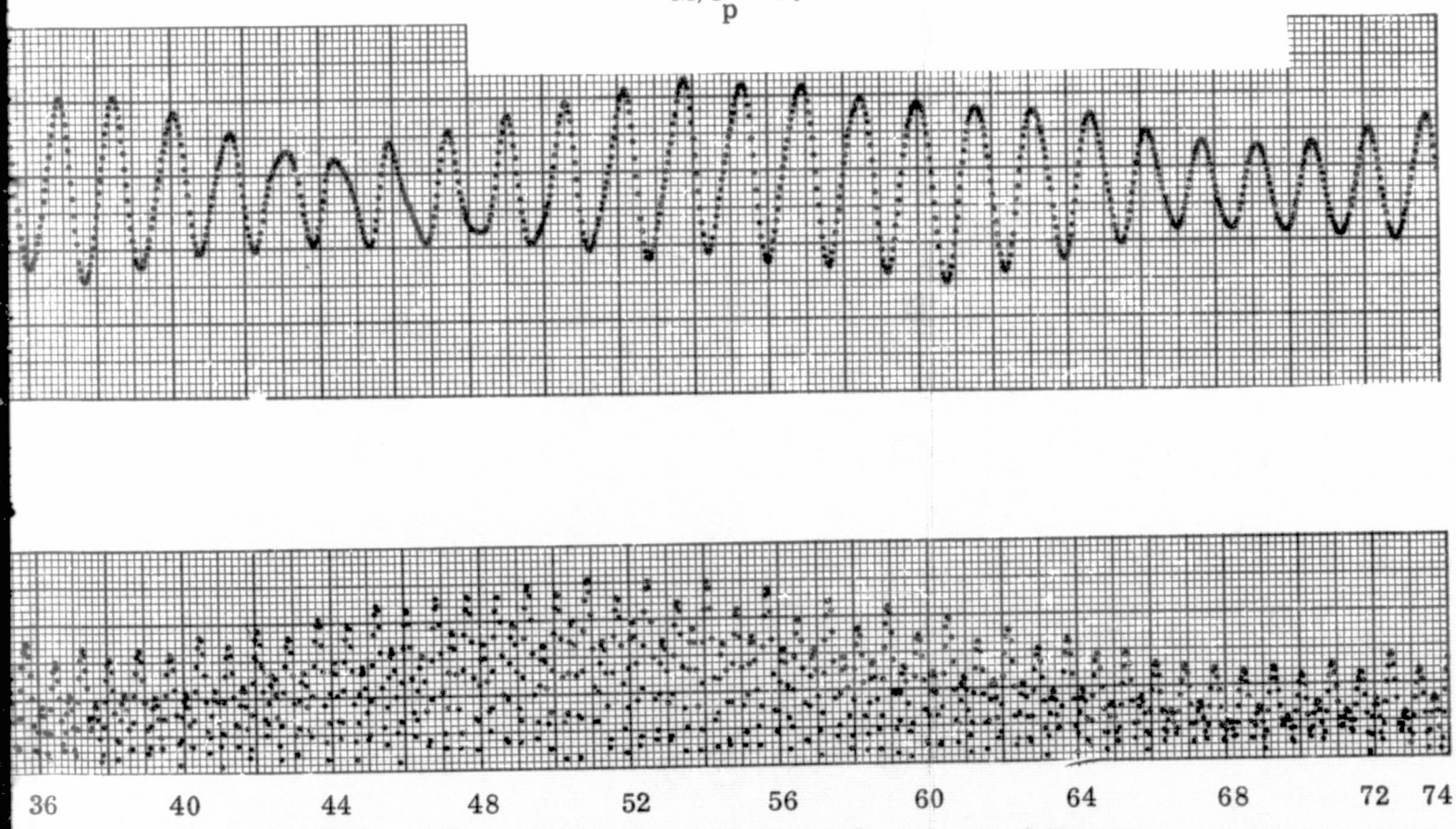

36 40 44 48 52 56 60 64 68 72 74

Figure 3-12. (A) Steady State Performance of Selected Configuration (Split Time Scale)

FOLDOUT FRAME 1

S-IVB TWO-AXIS LOCAL VERTICAL CO
PLANE OF SOLAR PANELS IN ORBI

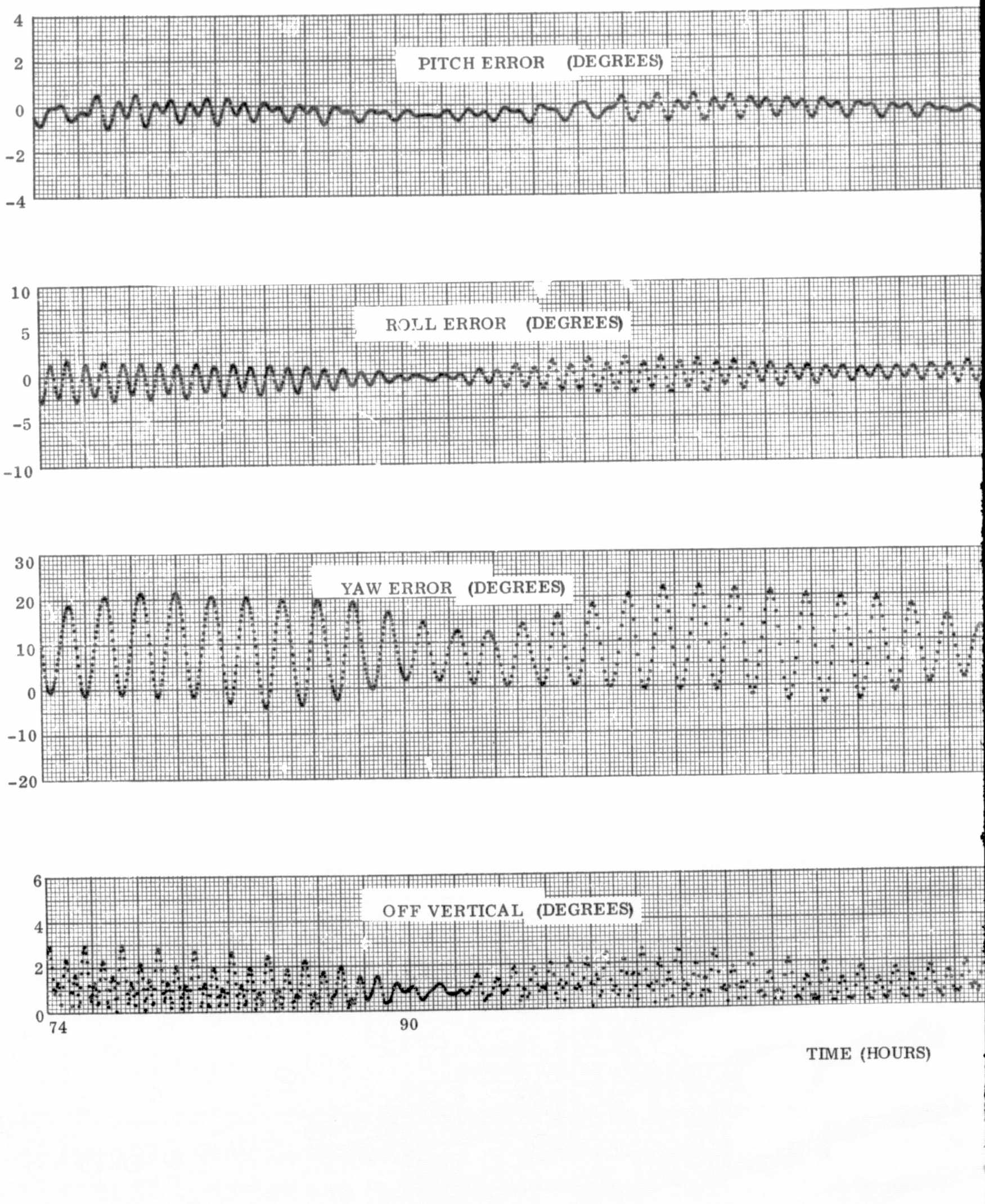

ERTICAL CONFIGURATION
NELS IN ORBIT PLANE

FOLDOUT FRAME 2

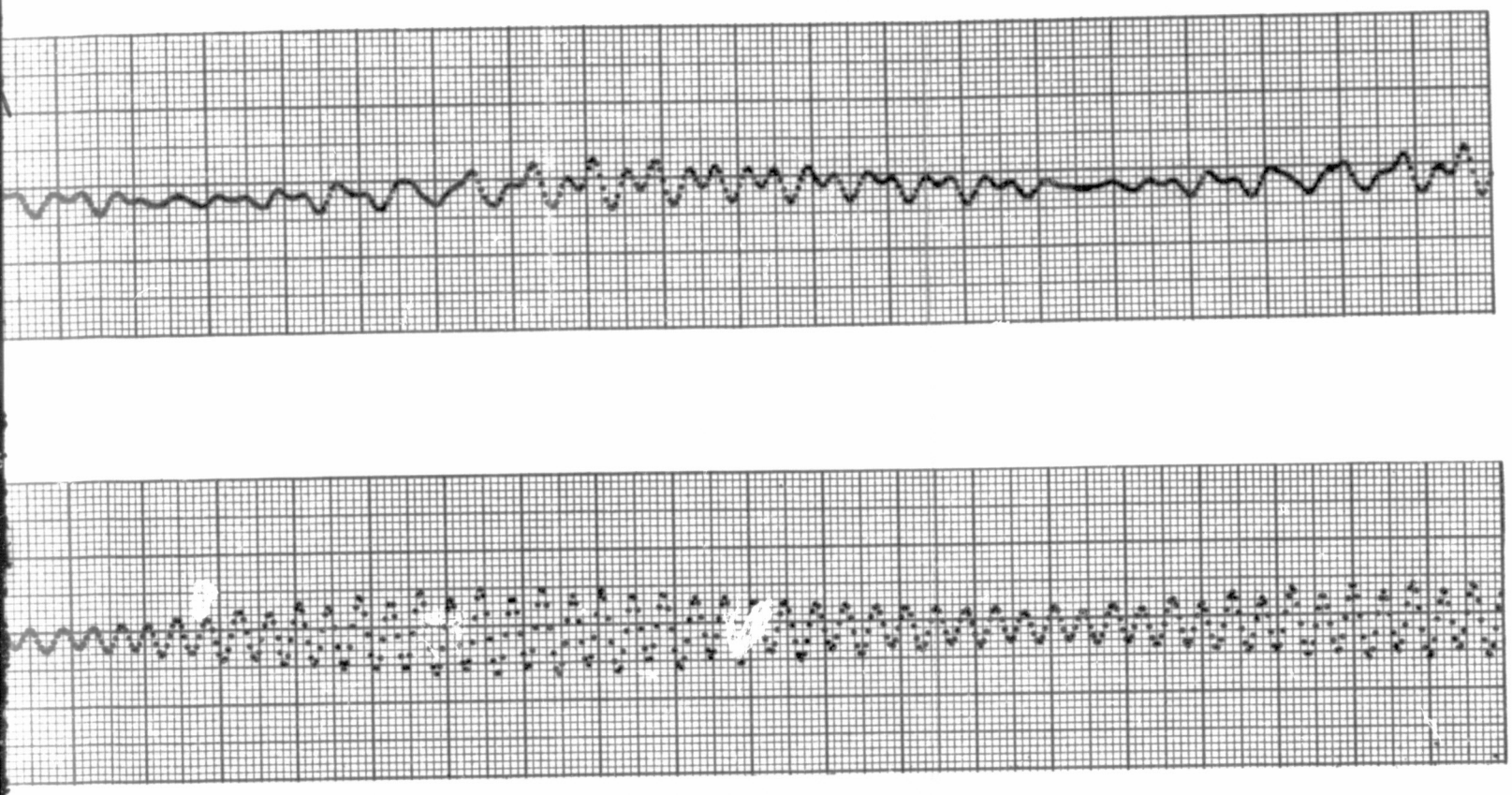

116

150

HOURS)

Figure 3-12. (B) Steady State Performance of Selected Configuration (Split Time Scale)

Table 3-3. Two Axis Local Vertical Linearized Error Budget

| Disturbances | Errors (deg) Pitch | Roll | Yaw |
|---|---|---|---|
| Damper | 1.75 (73%)* | 1.62 (89%) | 14.24 (66%) |
| Aerodynamic | 0.55 (23%) | 0.11 (6%) | 4.36 (20%) |
| Magnetic | 0.08 (3-1/2%) | 0.06 (3%) | 2.89 (13%) |
| Solar | 0.01 (1/2%) | 0.04 (2%) | 0.08 ( </2%) |
| Arithmetic Total | 2.39° | 1.83° | 21.57° |
| RSS Total | 1.84° | 1.63° | 15.17° |
| Nonlinear Results: (Figure 3-12B) | 0.7° | 3.0° | 13° |

* Percent of the total arithmetic error.

affected. The magnetic error component was computed on the assumption of a 50 ampmeter$^2$ (50,000 pole cms) vehicle residual dipole moment. Worst-case orientation was assumed for each individual axis. Solar errors were computed based upon the following assumed surface characteristics:

| | Solar cell surfaces | All other surfaces |
|---|---|---|
| Absorptivity ($\alpha$) | 0.65 | 0.2 |
| Specular Reflectivity ($P_s$) | 0.35 | 0.4 |
| Diffuse Reflectivity ($P_d$) | 0 | 0.4 |

Compared to the damper induced and aerodynamic errors, the solar torque errors are insignificant.

3.2.3.2 Transient Performance

Transient performance of the system with the selected damper design was also evaluated by means of the large angle, nonlinear, computer simulation. The initial position and body rates assumed at the start of the problem were set equal to those capable of being achieved by the active control system on board the S-IVB vehicle. They are 0.01 deg/sec about all three body axes and each axis at 10 degrees from the preferred orientation.

Figure 3-8 shows the result of 36 hours of damping, making use of the 2000 amp $m^2$ ($2 \times 10^6$ pole cms) magnet strength and with the damping coefficient of 82 NMS (60 lb-ft-sec). The initial pitch amplitude increases to $\pm$13 degrees; but after 30 to 32 hours this error has decayed to approximately 7 to 7.5 degrees. This rate of decay indicates a damping time constant, (i.e., the time required to reach approximately 37 percent of its original amplitude) of 38 orbits. Steady state conditions (normally 3$\tau$) will, therefore, be reached within 7.5 days.

3.2.3.3 Detumble Performance

To demonstrate damping capability during a spacecraft tumbling mode, a computer simulation was made. A spacecraft tumble rate in the positive pitch direction (forward tumble - same direction as orbit rate) was assumed as an initial condition. The damper used is the selected design: damping coefficient of 82 NMS. (60 ft-lb-sec) magnet strength of 2000 amp $meters^2$ ($2 \times 10^6$ pole cms).

The results of a 36-hour problem (23 orbits) are shown in Figure 3-13. The usual pitch, roll, and yaw euler angles are plotted, as well as the spacecraft pitch rate relative to inertial space. The initial rate of 0.2 deg/sec (three times orbital rate) resulted in an average inertial rate of 0.175 deg/sec. After 36 hours, this has been reduced to 0.14 deg/sec. Although the decrease in rate appears to be somewhat cyclic, the average linear deceleration is $0.97 \times 10^{-3}$ deg/sec per hour. Based upon this rate of damping, it would

FOLDOUT FRAME /

S-IVB TWO-AXIS LOCAL VERTICAL CONFIGUR
PLANE OF SOLAR PANELS NOMINALLY IN ORBI

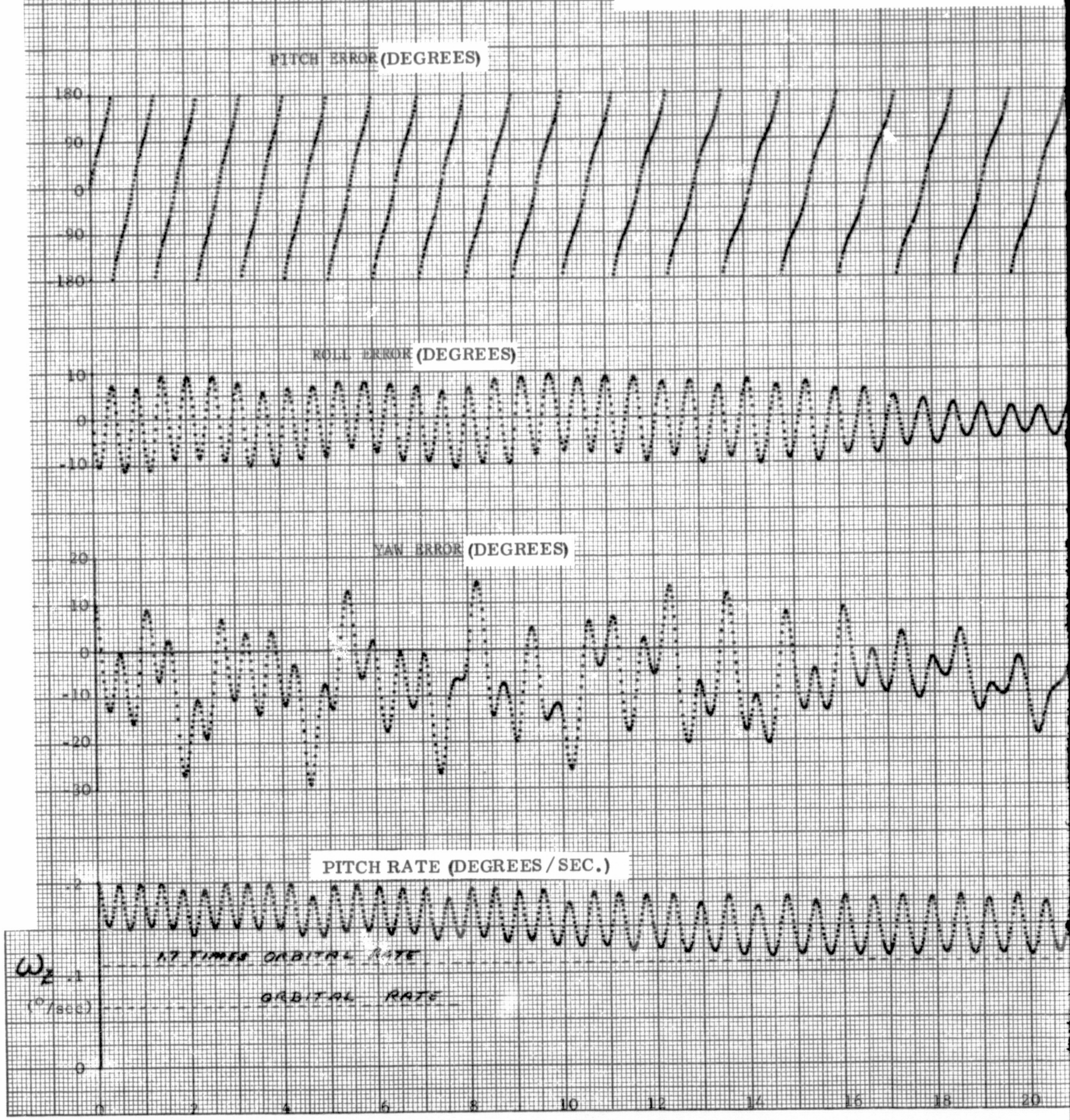


TIME - HOURS

FOLDOUT FRAME 2

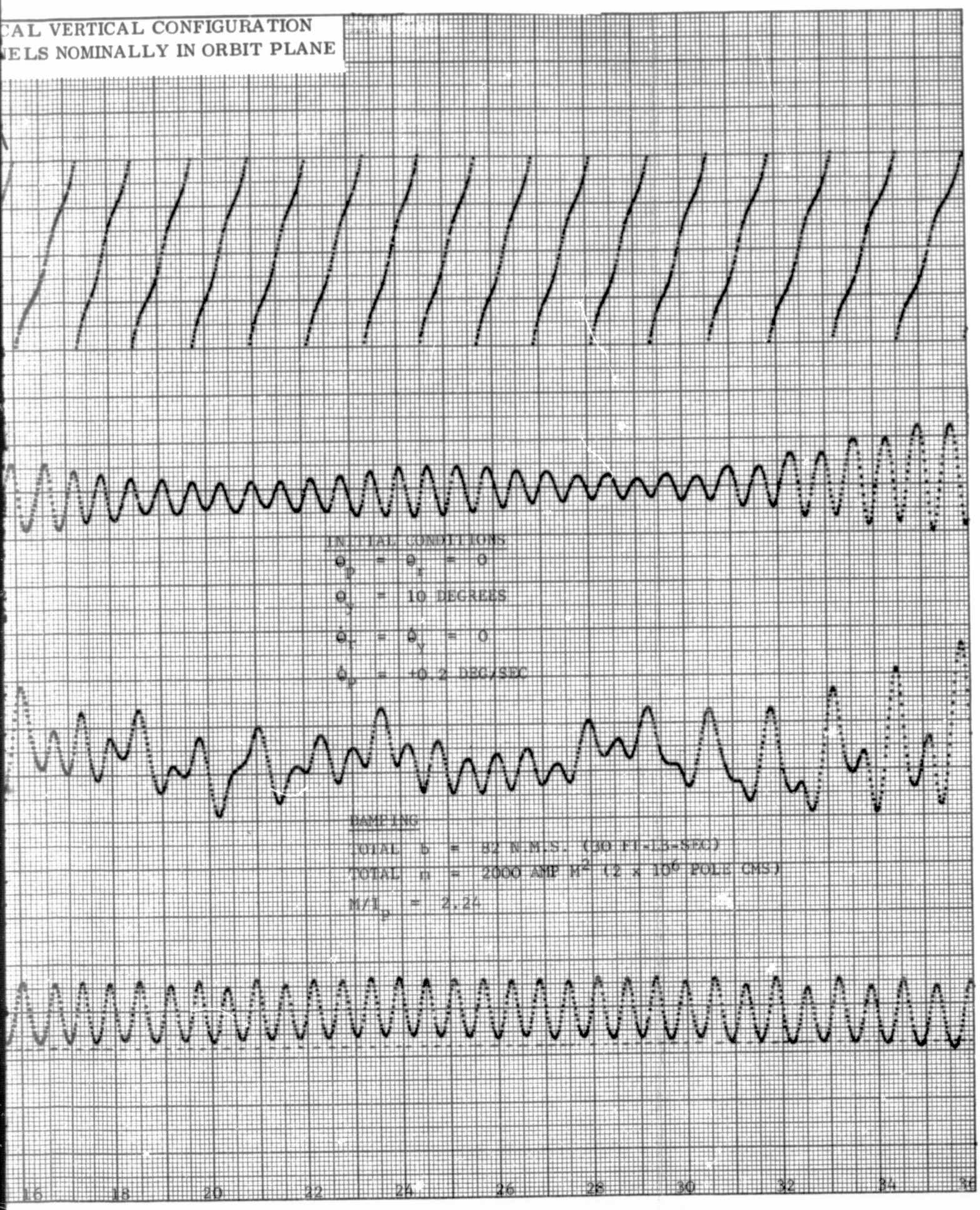


Figure 3-13. Detumble Damping Performance

require approximately 5 days until the peak rate falls below 0.11 deg/sec (1.7 times orbital rate) which is the rate at which capture theoretically occurs for forward pitch tumble.

An upper limit of tumble rate exists beyond which the damper magnet will not "hold" the Earth's magnetic field and damping will be reduced. The assumed rate of three times orbital was chosen for the actual simulation because it is high enough to tumble the magnet and is a representative rate.

### 3.2.4 PARAMETRIC STUDIES

For this two axis system with the long axis vertical and for which no deployed rods and tip weights are necessary, the only parametric tradeoff study involves the damper weight, damping time, damper-induced error relationship. The damping time, weight tradeoff was covered under damper selection (Figure 3-11). Steady state damper-induced error is summarized in Section 3,2.4.1. Also included in this section is the predicted performance as a function of altitude and brief comments on seasonal performance variations.

#### 3.2.4.1 Steady State Damper Induced Error

As stated previously, relative motion between the damper magnet and damper casing exists even after steady state conditions have been achieved because the magnet follows the Earth's magnetic field whereas the spacecraft follows the local vertical. The resulting viscous damping torque is then a disturbance torque. The magnitude of the induced error is a linear function of the damping level; i.e., damping coefficient, moment of inertia of the spacecraft, the orbital rate ($\omega_o$) and the dynamic response of the system. For the two-axis configuration, in the nominal 400 km (216 nm) orbit, the results of the linearized program were scaled to agree with the nonlinear results for the selected damping coefficient of 82 nms (60 ft-lb-sec). The predicted damper driven error as a function of damping coefficient is shown in Figure 3-14.

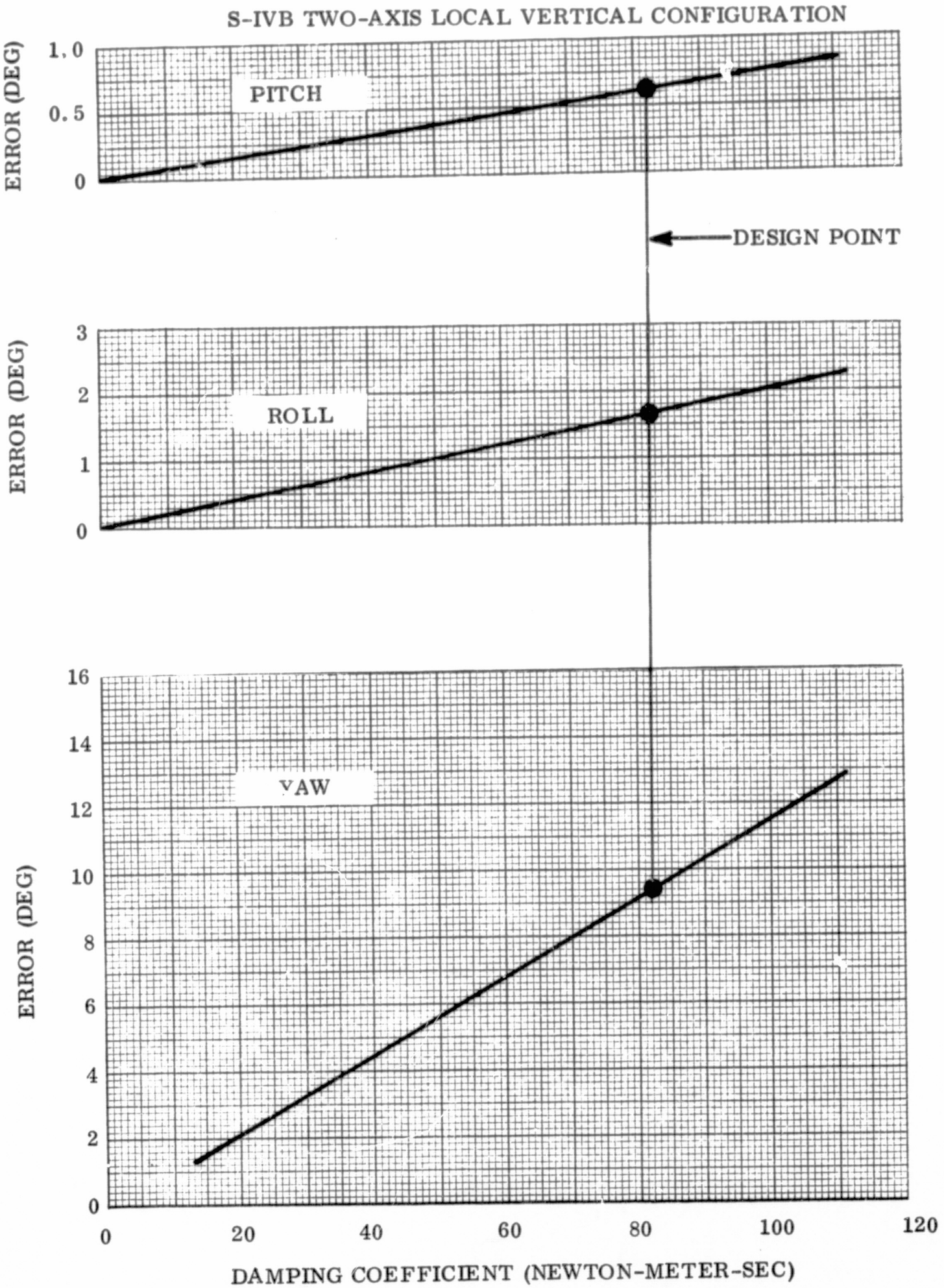


Figure 3-14. Damper Induced Error versus Damping Coefficient

The slopes of the individual errors are:

Pitch: $\frac{\alpha\theta p}{b}$ = 0.006 deg/NMS (.0082 deg/ft lb sec)

Roll: $\frac{\alpha\theta r}{b}$ = 0.020 deg/NMS (.0273 deg/ft lb sec)

Yaw: $\frac{\alpha\theta y}{b}$ = 0.116 deg/NMS (.1585 deg/ft lb sec)

With the induced errors as a function of damping coefficient and the estimated damping characteristic from Figure 3-5, steady state damper errors may be shown as a function of damping time to reach steady state. Making use of the damping characteristic for the selected damper, M = 2000 amp meters$^2$ (2 x $10^6$ pole cms) and $M/I_p$ = 2.24, Figure 3-15 was generated. It is assumed that three time constants are required to reach steady state.

3.2.4.2 Altitude Effect Upon Performance

The most significant effect of altitude is the reduction in aerodynamic effect as higher altitudes are considered. Aerodynamic disturbances become negligible at altitudes higher than 750 km (400 NM). However, an additional effect is a reduction in the gravity gradient stabilization torques. Although a particular system will experience no aerodynamic errors at the higher altitudes, other contributors to overall pointing inaccuracies may increase. The net result, however, is usually smaller errors outside the range of aerodynamics. The effect of altitude upon the performance of the S-IVB in this orientation was evaluated by a nonlinear computer simulation at 750 km (400 nm), making use of the 5500 amp-meters$^2$ (5.5 x $10^6$ pole cms) damper with a coefficient of 82 NMS (60 lb-ft-secs). The results of this steady state run are shown in Figure 3-16 representing approximately 47 orbits (3 days). Comparing this to Figure 3-17, which is the identical system but represents 400 km (216 nm) and includes aerodynamics, the following results are obtained:

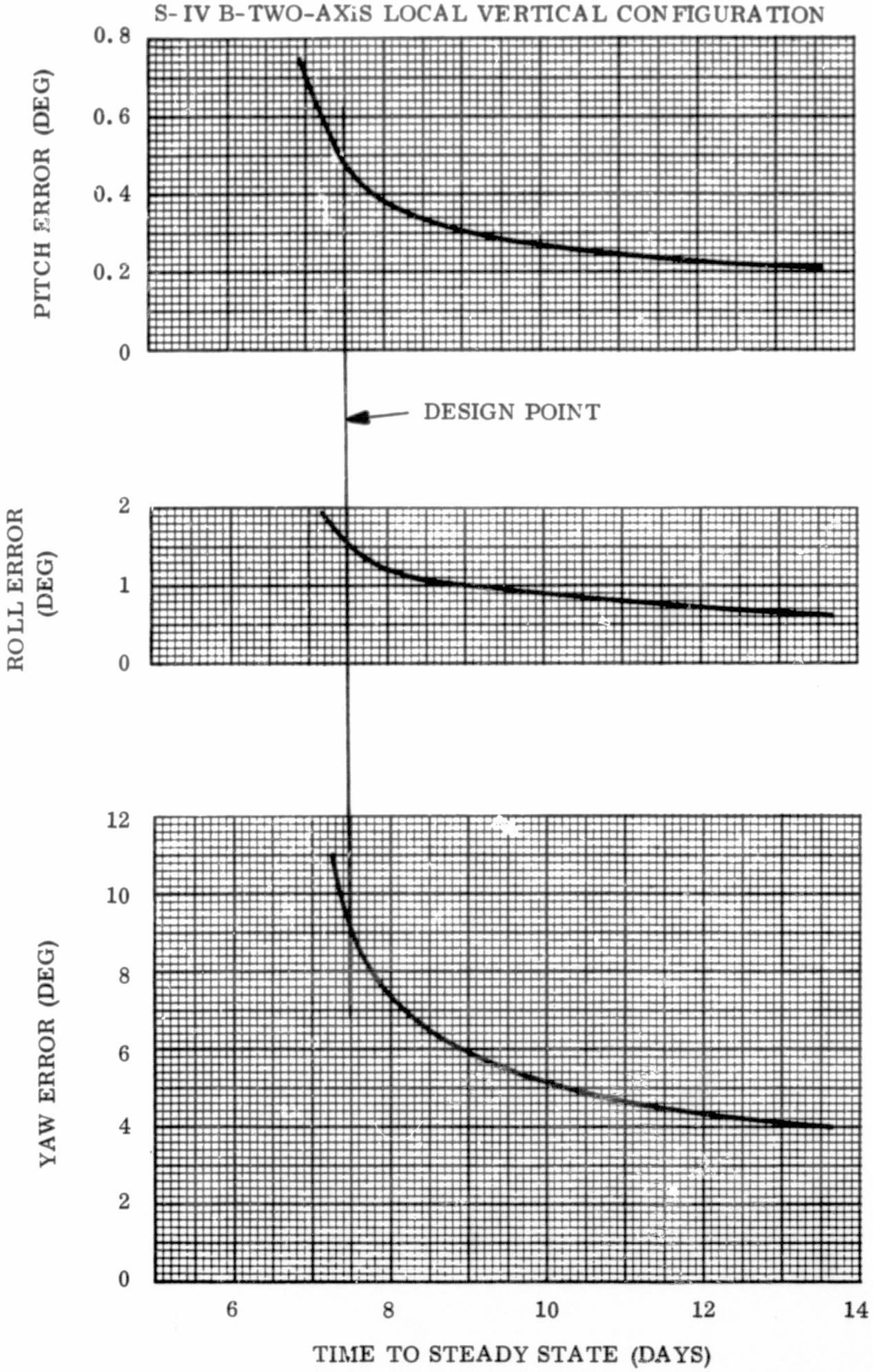


Figure 3-15. Damper Induced Error Versus Damping Time to Steady State

FOLDOUT FRAME 1

S-IVB TWO-AXIS LOCAL VERTICAL CONFIGURATIO
PLANE OF SOLAR PANELS IN ORBIT PLANE

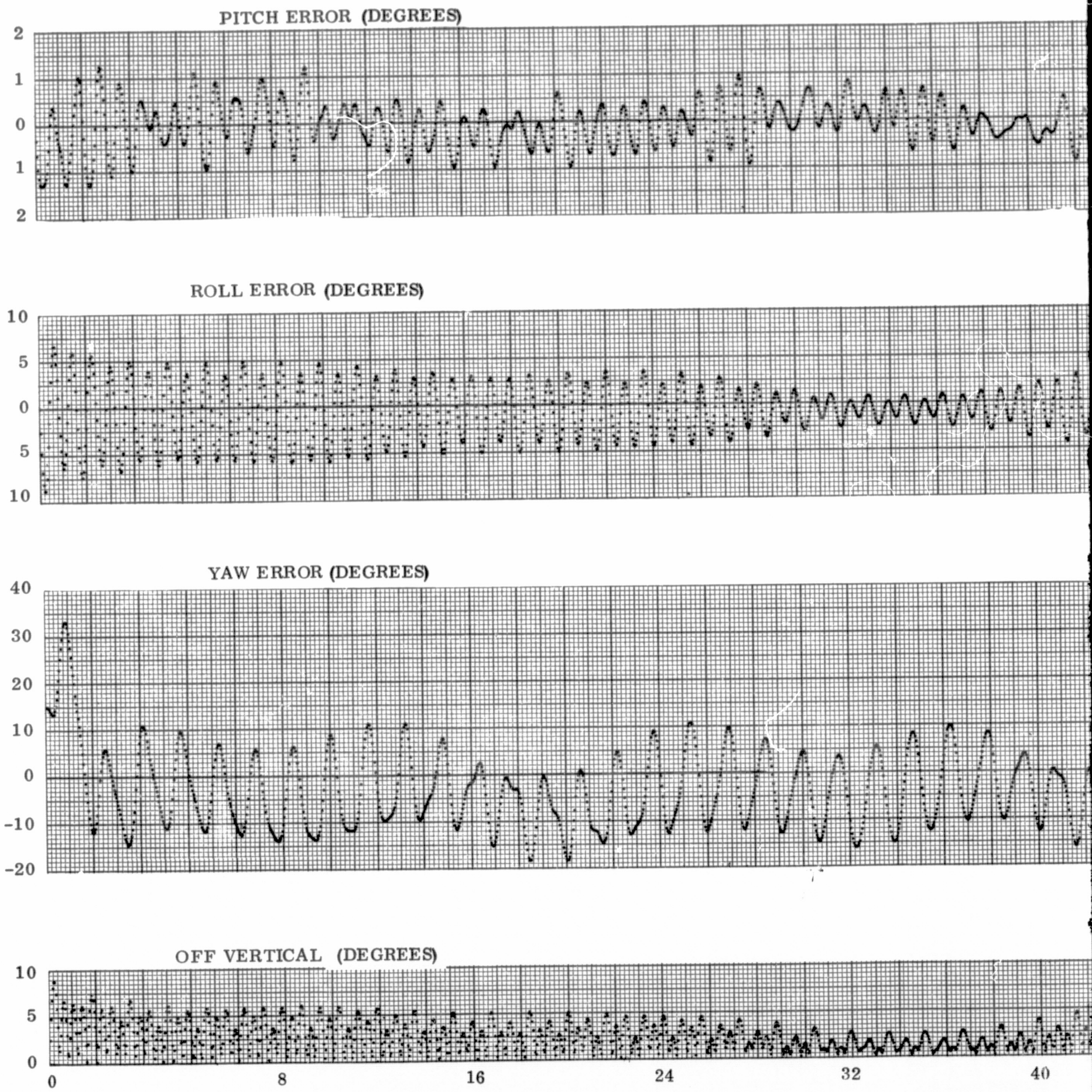

FOLDOUT FRAME 2

L CONFIGURATION
ORBIT PLANE

NO AERODYNAMICS

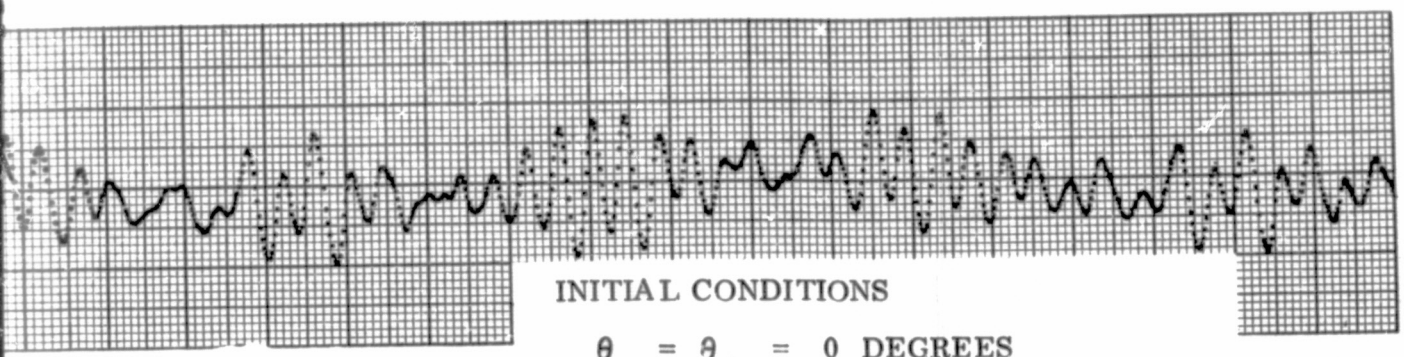

INITIAL CONDITIONS

$\theta_p = \theta_r$ = 0 DEGREES

$\theta_y$ = 15 DEGREES

$\dot{\theta}_p$ = ORBITAL RATE

$\dot{\theta}_r = \dot{\theta}_y$ = 0 DEG/SEC

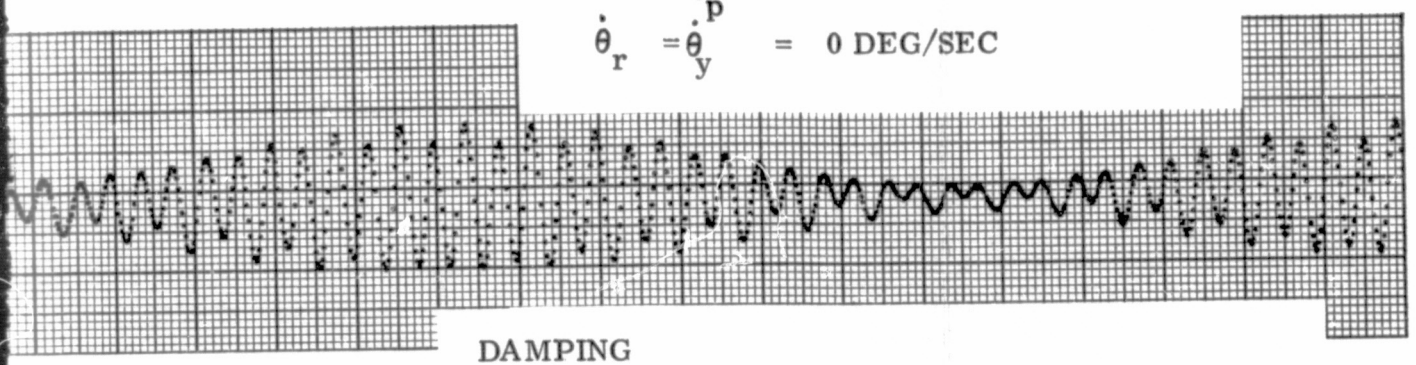

DAMPING

TOTAL b = 82 N. M. S. (60 FT-LB-SEC)

TOTAL m = 5500 AMP METERS$^2$
(5.5 x $10^6$ POLE-CMS)

$m/I_p$ = 6

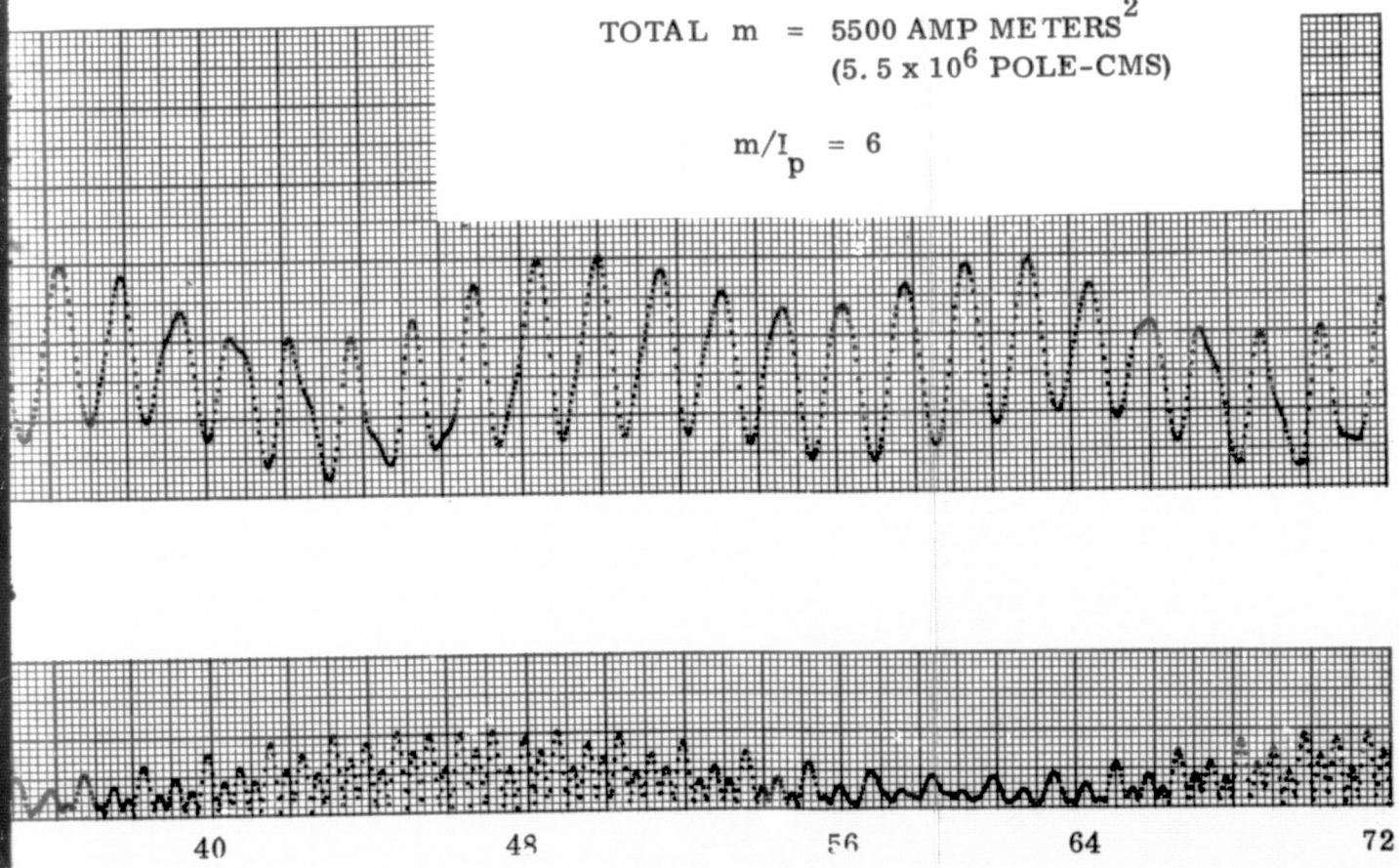



40 48 56 64 72

TIME (HOURS)

Figure 3-16. Steady State Performance at 750 Km (400 N. M)

FOLDOUT FRAME /

S-IVB TWO AXIS LOCAL VERTICAL CONF
PLANE OF SOLAR PANELS IN ORBIT

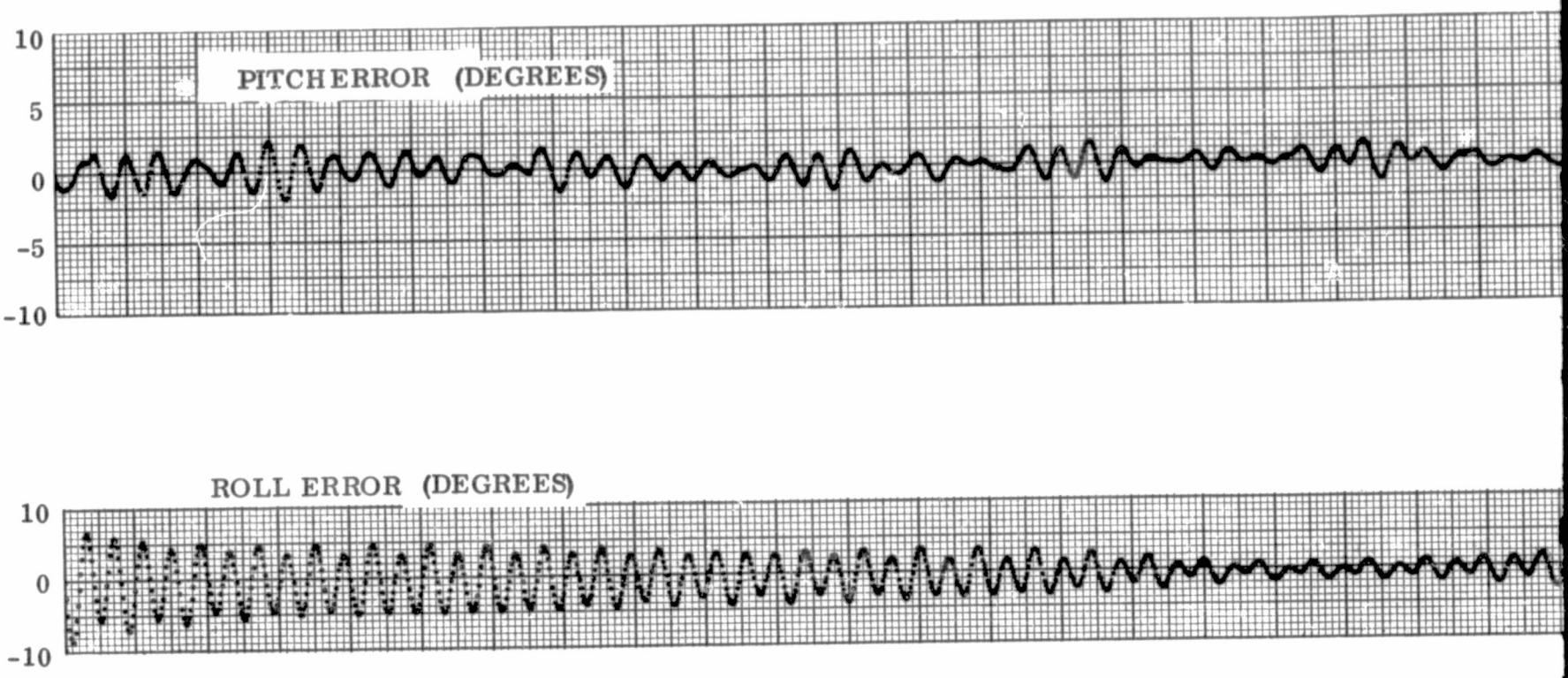

L VERTICAL CONFIGURATION
PANELS IN ORBIT PLANE

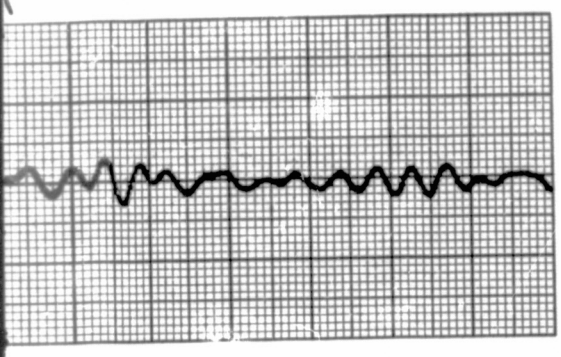

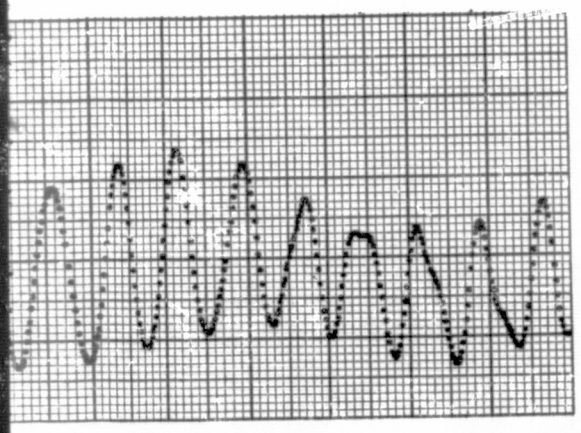

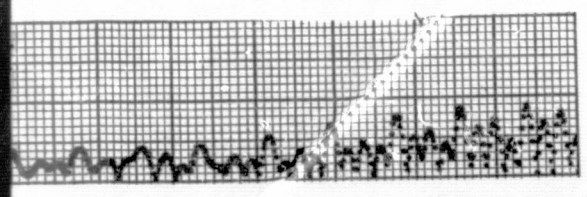

36 40 44 48

INITIAL CONDITIONS

$\theta_p = \theta_r = 0$ DEGREES

$\theta_y = 15$ DEGREES

$\dot{\theta}_p =$ ORBITAL RATE

$\dot{\theta}_r = \dot{\theta}_y = 0$ DEG/SEC

DAMPING

TOTAL b = 82 N.M.S. (60 FT-LB-SEC)

TOTAL m = 5500 AMP METERS$^2$
($5.5 \times 10^0$ POLE CMS)

$m/I_p = 6$

Figure 3-17. Steady State Performance at 400 Km (216 N.M.)

| | 400 km (216 nm) | | 750 km (400 nm) | |
|---|---|---|---|---|
| | Amplitude ($^{o}$) | Bias ($^{o}$) | Amplitude ($^{o}$) | Bias ($^{o}$) |
| Pitch Error | ±1.3 | -0.2 | ±0.9 | -0.05 |
| Roll Error | +4 | -0.5 | ±4 | -0.05 |
| Yaw Error | ±14 | ±10.0 | ±13 | -3.0 |

Pitch and yaw amplitudes are slightly lower at 750 km; no significant difference in roll performance can be detected. However, the most predominant difference between the two sets of performance is the shift in the yaw bias angle from +10$^{o}$ to -3$^{o}$ at 400 km and 750 km, respectively, caused by the removal of the yaw bias aerodynamic torque. The expected performance variation with altitude was derived as follows. The nonlinear results shown above were used in conjunction with the linearized program from which slopes were determined. The final curves were then scaled to the performance expected from the smaller damper. These are shown on Figure 3-18.

## 3.3 THREE AXIS CONFIGURATION - LONG AXIS VERTICAL

As a secondary effort relative to the two axis system, long axis vertical, a configuration was investigated which will maintain long axis vertical, but will also orient the plane of the solar panels perpendicular to the orbit plane. This configuration will provide more favorable conditions for solar power collection. Although this was only a secondary effort, sufficient analysis and evaluation was performed to demonstrate feasibility and to specify a configuration which will meet the same performance requirements as the previous configuration.

### 3.3.1 CONFIGURATION SELECTION

Preliminary analysis and performance evaluations indicated that requirements for this configuration could be met by incorporating one gravity gradient rod and one magnetically anchored viscous damper also serving as a tip mass. The rod is mounted from the end of the instrumentation unit at a 45 degree angle from both the S-IVB longitudinal axis and the perpendicular to the solar panel plane. Relative to the orbiting reference frame, the configuration appears as depicted on Figure 3-19.

S-IVB TWO-AXIS LOCAL VERTICAL CONFIGURATION

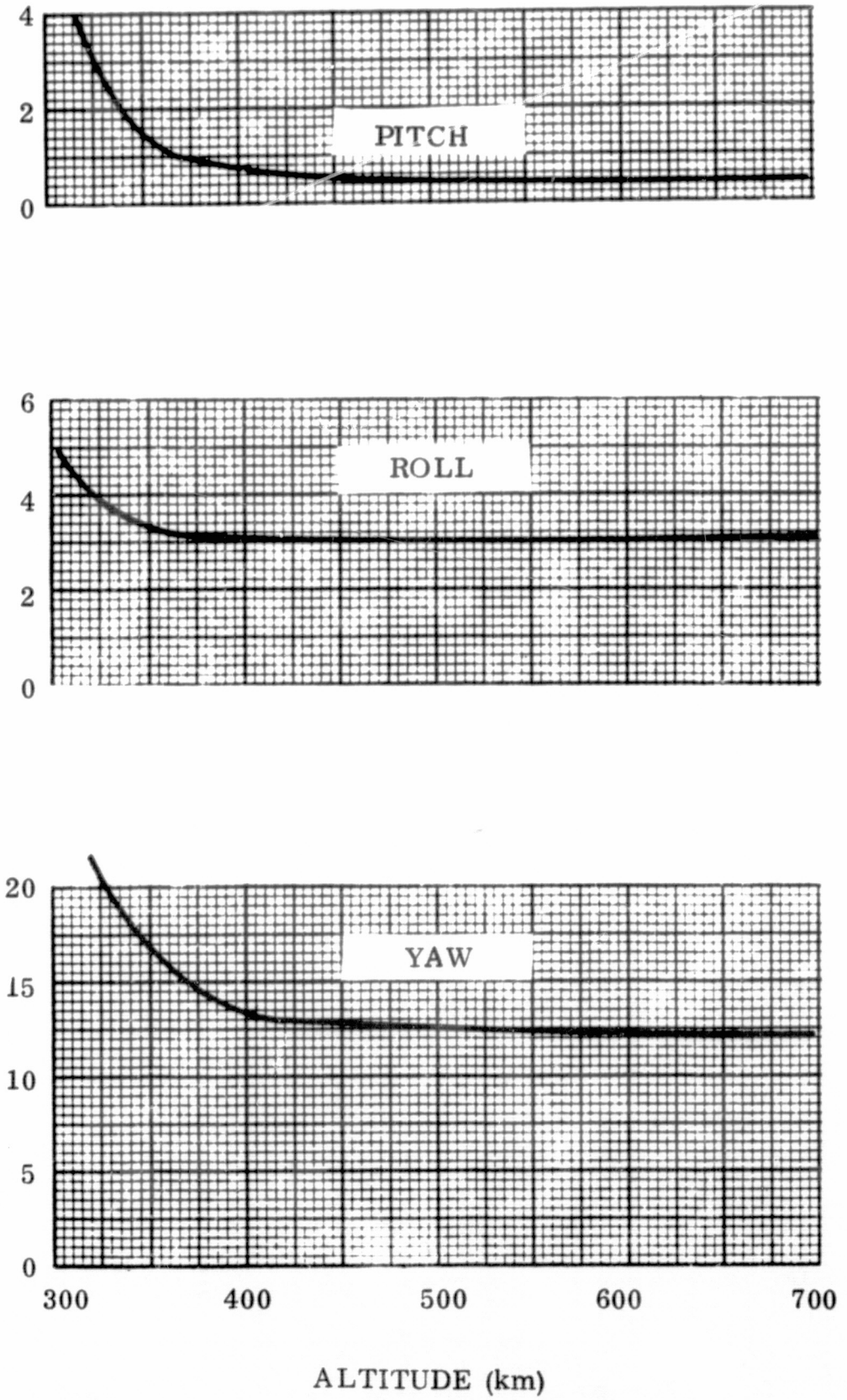


Figure 3-18. Predicted Performance Versus Altitude

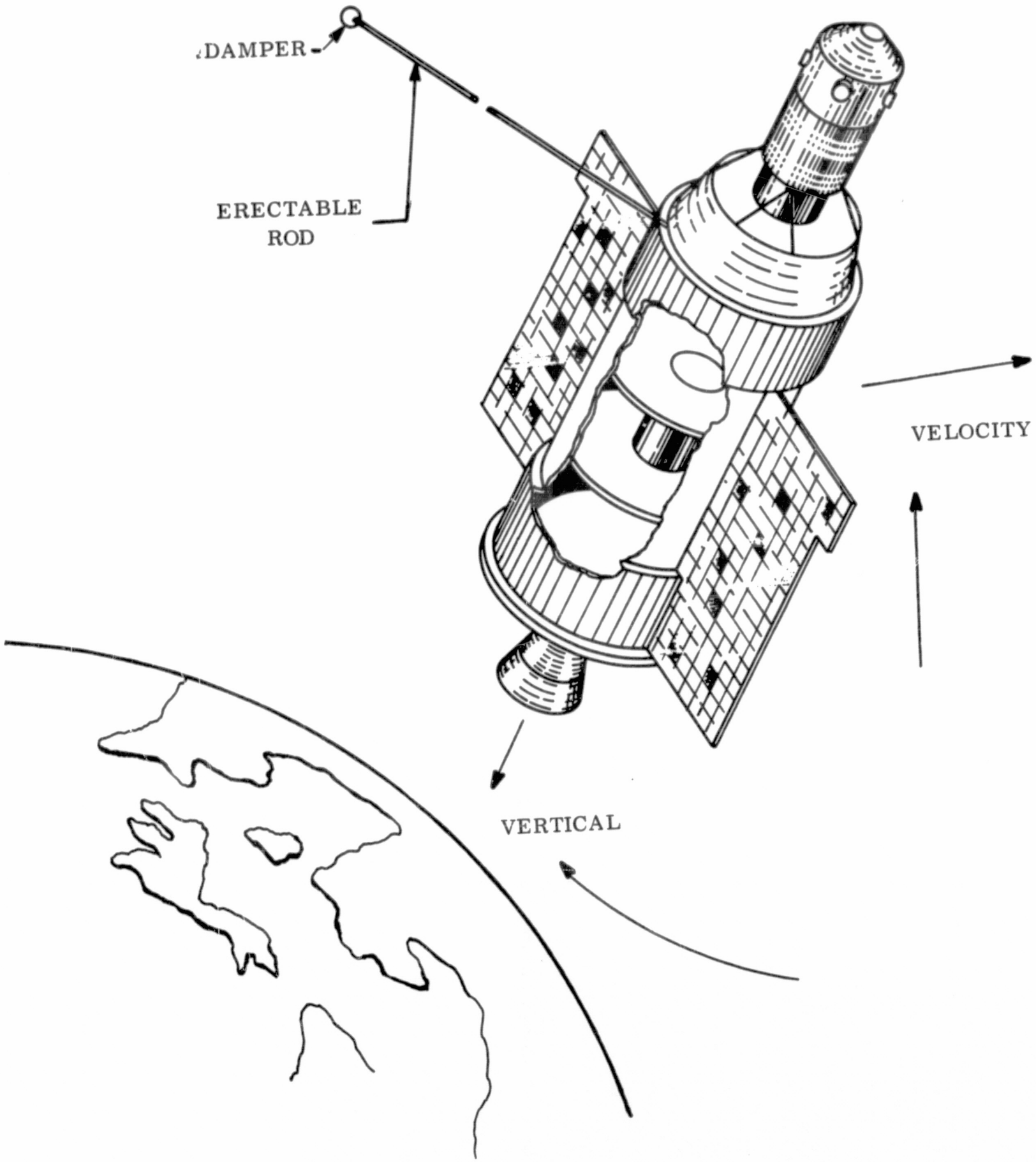


Figure 3-19. Three Axis Local Vertical Configuration

Based upon moment of inertia relationship requirements and upon results of linearized computer studies, the following configuration was selected to be evaluated by means of the large angle, nonlinear digital computer simulation program:

Gravity Gradient Rod (1)

| | |
|---|---|
| Length | 46 meters (150 ft.) |
| Approximate weight | 7.7 Newtons/meter (0.53 lbs/ft) |
| Approximate diameter | 7.6 cm (3 inches) |

Spherical Viscous Damper (1)

| | |
|---|---|
| Weight | 1000 Newtons (225 lb) |
| Approximate diameter | 56 cm (22 inches) |
| Damping Coefficient | 82 NMS (60 lb-ft-sec) |
| Magnet Strength | 6000 amp $m^2$ ($6 \times 10^6$ pole cm) |

### 3.3.2 NOMINAL PERFORMANCE

Making use of the configuration selected above in the large angle, nonlinear computer program, a transient performance evaluation was performed. Again, initial rates were set equal to 0.01 deg/sec and the spacecraft positioned at 10 degrees from the preferred orientation, all axes. Although this is a relatively short simulation, 36 hours (23 orbits), the amount of damping is evident, (see Figure 3-20). The pitch amplitude decay rate indicates a 40-orbit time constant resulting in less than 8 days to reach steady state.

Pointing accuracies after 23 orbits are as follows:

| | |
|---|---|
| Pitch: | $\pm 12^\circ$ on a $+10^\circ$ bias |
| Roll: | $\pm 5^\circ$ no bias |
| Yaw: | $\pm 8^\circ$ on a $+5^\circ$ bias |
| Tilt: | $20^\circ$ ($10^\circ$ due to pitch bias) |

Within 3 days, all oscillations will be significantly less than $\pm 10$ degrees.

FOLDOUT FRAME 1

PLANE OF SOLAR PANELS PERPENDICULAR T

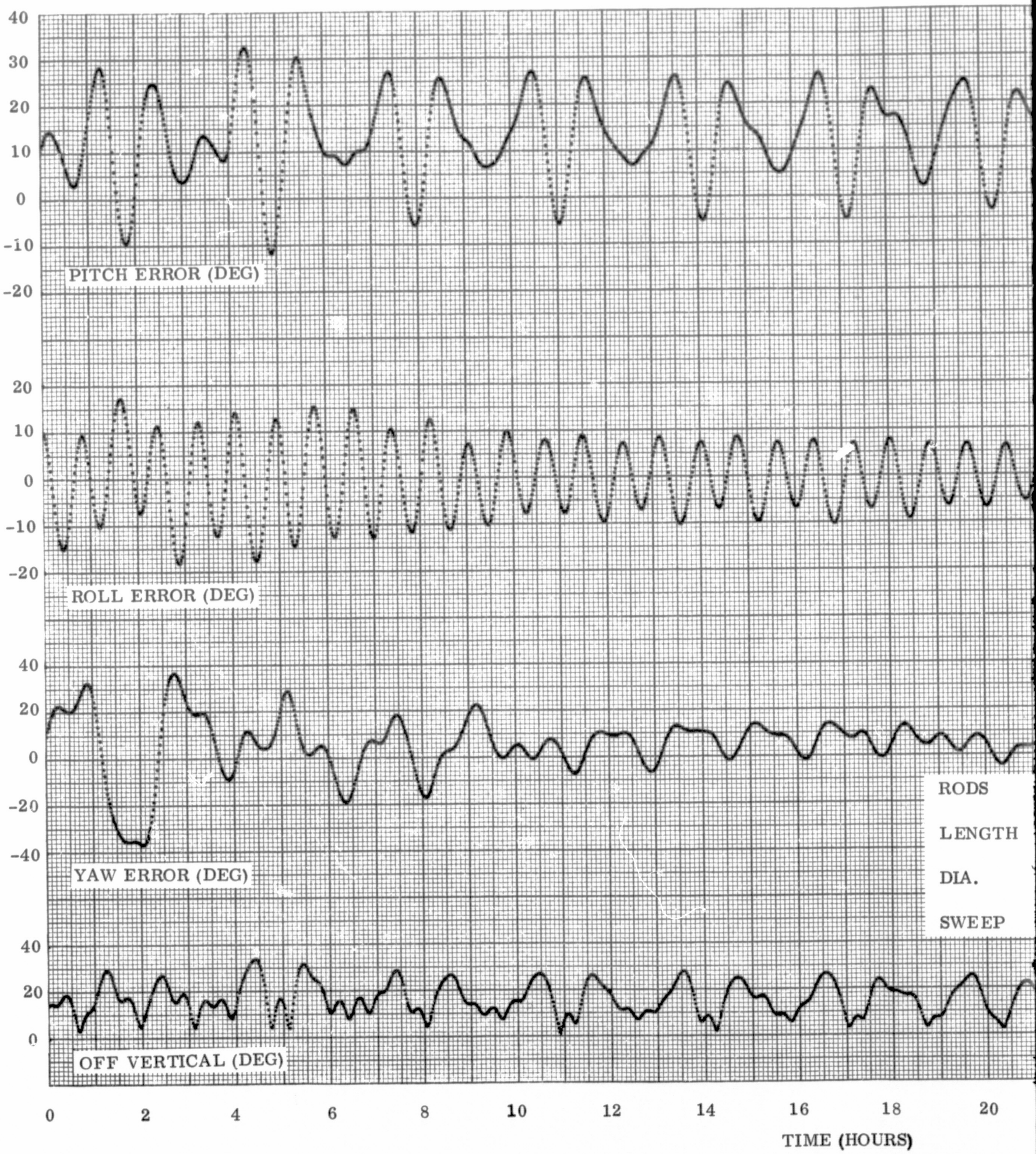

FOLDOUT FRAME 2

PERPENDICULAR TO ORBIT PLANE

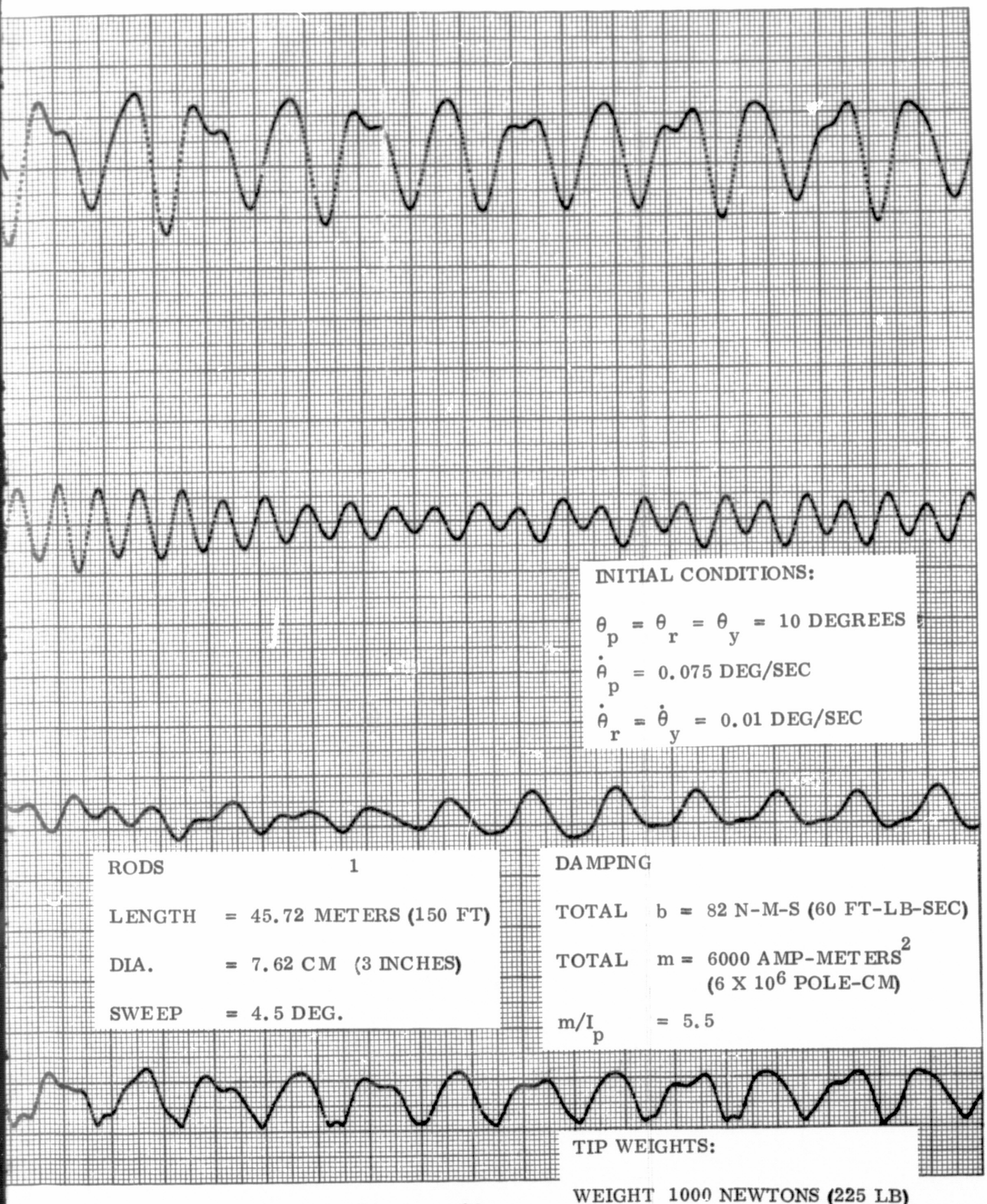


Figure 3-20. Three-Axis Local Vertical Configuration Transient Performance

## 3.4 ALTERNATE S-IVB VERTICAL CONFIGURATIONS

Preliminary design studies were conducted on two (2) alternate configurations for vertical stabilization of the S-IVB. These two (2) studies are discussed in Appendices B and C. The results are summarized below.

### 3.4.1 ALTERNATE NO. 1 (APPENDIX B)

The possibility of gravity gradient stabilization of the S-IVB with no damping present was studied briefly. The mass/inertia and aerodynamic characteristics of the Orbiting Workshop (solar panels perpendicular to the longitudinal axis) were used in two (2) large angle digital computer simulations. Starting from zero error angle and rate initial conditions, error angles grew slightly during 24 hours but did not reach significant amplitudes. Starting from 10 degrees position errors and 0.01 degrees/second rate errors, the S-IVB lost yaw stabilization in eight (8) orbits but remained vertically oriented. No conclusions were drawn as to the period of time required for instability to cause loss of vertical orientation; however, it is concluded, based on a linearized analysis also presented in Appendix B, that the system is unstable.

### 3.4.2 ALTERNATE NO. 2 (APPENDIX C)

An alternate S-IVB stabilization configuration was investigated using a single-axis, gravity-anchored damper in place of the spherical magnetically anchored damper. The results of the study show that this system provides more rapid damping and somewhat less damper induced error than the magnetically anchored damper at about the same weight. This system is not recommended, however, because of the much more restrictive mounting interface caused by the requirement to have $\pm 45$ degree free rotational motion of the 42-meter (140-ft) long damper boom.

## 3.5 THREE-AXIS CONFIGURATION-LONG AXIS HORIZONTAL

### 3.5.1 CONFIGURATION SELECTION

As part of this study, a three-axis passive system was selected and evaluated which will maintain a vehicle orientation with the long axis of the S-IVB parallel to the local velocity

vector, the J-2 gimbal forward and the plane of the solar panels perpendicular to the local vertical and facing away from the earth. This orientation has advantages over the vertical configuration from the aspect of solar power collection and in regard to orbit decay rate.

Because the basic S-IVB moment of inertia relationships will not permit the spacecraft to assume this orientation, gravity gradient rods and tip masses must be added to alter the moment of inertia characteristics.

3.5.1.1 Preliminary Analysis

In the design of a three-axis gravity gradient stabilization system for low earth orbit applications, it is general practice to select a configuration within the following guidelines:

a. Rod and tip mass configuration is such that the total system inertia relationships result in gravity gradient restoring torques about all three axes.

b. Rod configuration is selected so that advantage may be taken of the aerodynamic forces to supplement pitch and yaw restoring torques. This is accomplished by maintaining the system center of pressure aft of the center of mass (weather vane effect).

c. Rod length and tip masses are also selected to achieve favorable moment of inertia differences relative to system natural frequencies. This is necessary to avoid the problem of resonance. If the natural frequency of the system about any of the body axes is equal to that of a disturbance about that axis, poor stabilization will result.

For purposes of preliminary configuration selection, which involves the consideration of system moment of inertia relationships and natural frequencies, it is most convenient to make use of a "natural frequency map." This is a plot of moment of inertia ratios, roll to pitch versus yaw to pitch, showing lines of constant natural frequencies about each of the principal axes. Such a map is shown on Figure 3-21, with the natural frequencies normalized to orbital frequency since all significant sinusoidal disturbances are either once or twice orbital rate. These natural frequencies were determined by the solution of Euler's dynamic equations of motion of a rigid body under the influence of gravity gradient torques. No other external restoring torques are included.

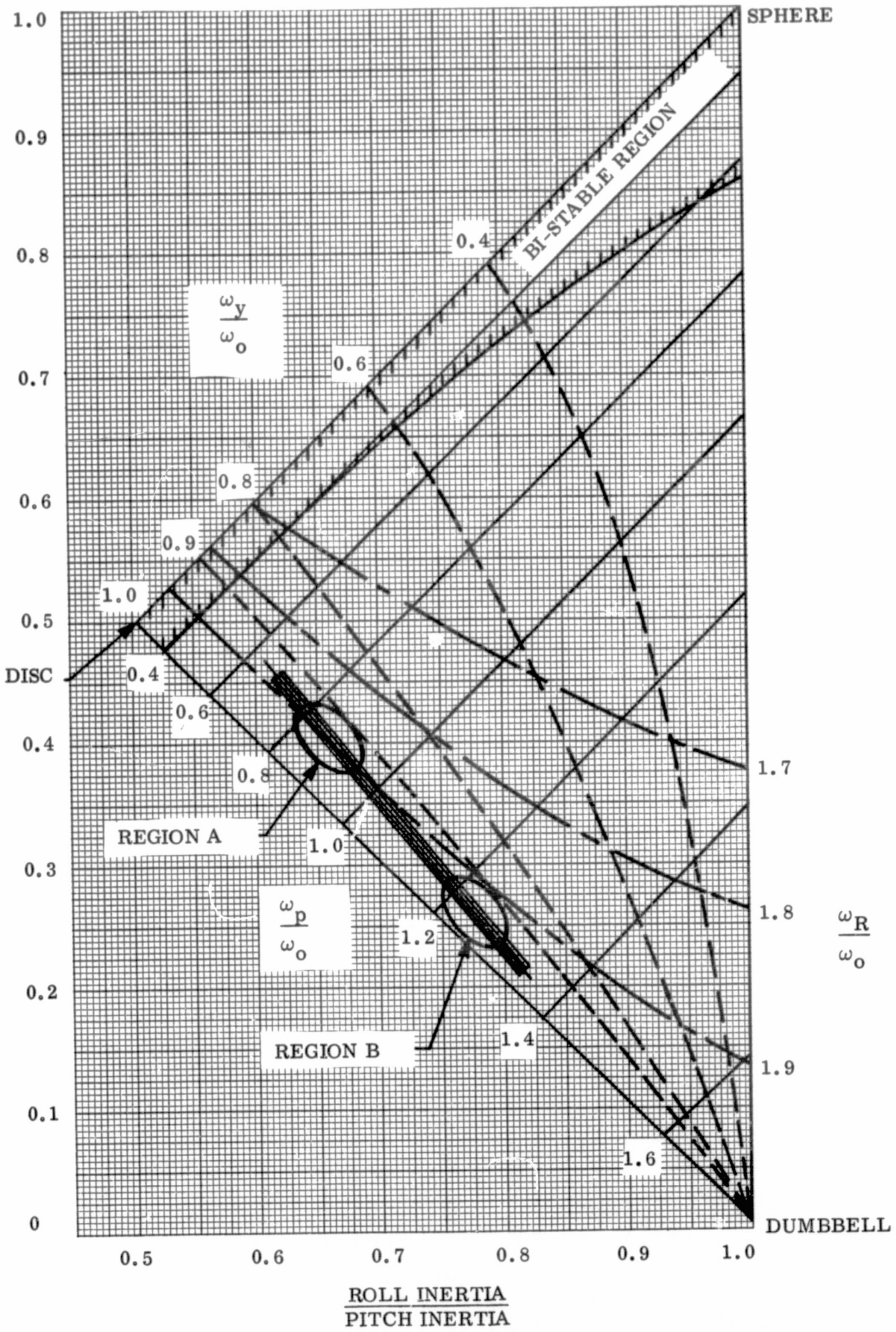


Figure 3-21. Natural Frequency Map

Since it is always desirable to minimize the number of gravity gradient rods and tip masses added to a spacecraft and keeping in mind the preferred center of pressure, center of mass relationship, a two-rod swept configuration immediately becomes evident as an attractive candidate. A two-rod configuration designed with sufficient moment of inertia differences to handle all significant disturbances generally becomes a near planar system. This would appear on a line nearly coincident with the Dumbbell-Disc Line on Figure 3-21. However, enough "out-of-plane" moment of inertia must be maintained in order to avoid the once orbital yaw resonance line. Reducing the yaw natural frequency to the 0.8 + 0.9 range is usually adequate.

Consideration of various rod lengths, sweep back angles and tip masses mounted from the instrumentation unit of the S-IVB in its preferred orientation resulted in all practical configurations falling within the shaded area of Figure 3-21. Since the once-orbital pitch natural frequency must be avoided, two possible regions of operations exist; that is, a system with a pitch natural frequency less than once orbital or one with it greater than once orbital. Again, referring to Figure 3-21 and making the preliminary assumption that the final configuration will fall in proximity of the line $(\frac{\omega_y}{\omega_o}) = 0.9$, certain additional facts become evident.

a. The lower limit of region A and the upper limit of region B is restricted by the proximity of the once orbital pitch natural frequency.

b. The upper limit of region A is limited by the approach to the "Bistability region." This is the area in which roll and yaw moments of inertia approach equality and the spacecraft may assume either one of two orientations (roll and yaw interchange).

c. The lower limit to region B is established by the approach to the twice orbital roll natural frequency line.

d. The lower-left limit of both regions is restricted to the proximity of the once orbital yaw natural frequency line.

e. The upper right limit of both regions is established by the relative amount of "out of plane" moment of inertia present.

   To extend this boundary outward would require additional rods and tip masses.

As a result of considering rod lengths from 60 m (200 ft) to 152 m (500 ft), tip weights from 445 Newtons (100 lb) to 1000 Newtons (225 lb) and sweep angles from 10 to 30 degrees, typical configurations falling in region B are:

| | | |
|---|---|---|
| Rod Length | 122 m (400 ft) | 152 m (500 ft) |
| Tip Weights | 890 Newtons (200 lb) | 445 Newtons (100 lb) |
| Sweep Angle | $10^{o}$ | $10^{o}$ |

Typical of configurations falling in Region A:

| | |
|---|---|
| Rod Length | 91 m (300 ft) |
| Tip Weight | 890 Newtons (200 lb) |
| Sweep | $10^{o}$ |

3.5.1.2 Final Analysis

The discussion thus far has been limited to systems having gravity gradient forces as the only external restoring torques acting on the spacecraft. If, as in this application, other external restoring torques (aerodynamics) do exist, the natural frequencies will be affected. The result will be an altered or shifted natural frequency map.

The basic effect of aerodynamics is to increase the pitch and yaw natural frequencies; roll is virtually unaffected. The magnitude of the effect depends upon the value of the aerodynamic restoring torque coefficient (slope of the torque - position curve) relative to the gravity gradient torque coefficient. Because the aerodynamic torque is a linear function of atmospheric density, the system performance must be evaluated over the entire range of densities expected to be encountered. Variations will obviously be experienced during a single orbit with eccentricity, but even for a circular orbit, density will vary due to the Earth's oblateness and especially due to the solar induced atmospheric bulge. This bulge is the result of solar heating of the sun-lit atmosphere which causes expansion and pushes the lower layers of dense air to higher altitudes. The total variation around the orbit may involve a factor of 2 or more.

In order to determine the extent of natural frequency shift due to aerodynamics, an approximate frequency determination program was written specifically for two-rod configurations with rods swept aft within the roll - yaw plane. A computer was used to allow many cases to be evaluated as a function of atmospheric density.

To establish the accuracy of the frequency computations, the results for a particular configuration were compared to frequencies computed from the results of a large angle nonlinear computer run. Good agreement was found and, hence, the approximate frequency determination program serves its purpose. Figure 3-22 and 3-23 show the computed pitch and yaw natural frequencies, respectively, normalized to orbital rate for various rod lengths and tip weights at minimum and maximum dynamic pressure for the nominal 400 km (216 nm) orbit. The pitch natural frequencies are practically insensitive to the variation in atmospheric density around the orbit; therefore, those shown are for an average density. The yaw frequencies are not significantly affected by tip weight in the range of 400 newtons to 1000 newtons.

The actual natural frequencies were then computed at incremental steps around the nominal orbit for each of the two possible configurations found to fall in regions A and B of Figure 3-21 in the preliminary analysis section. As stated above, the variation in pitch frequency is insignificant. For the smaller system, with 91-meter (300-ft) rods pitch natural frequency varies from 0.93 to 0.94 of orbital rate; for the larger system, 122-meter (400-ft) rods the variation is from 1.24 to 1.25 times orbital. The variation in yaw frequency is shown in Figure 3-24 as a function of time around the orbit. The time weighted average yaw frequency is greater than once orbital for the longer rod system and less than once orbital for the smaller rod system. Past experience has indicated that a resonant frequency may be passed through during an orbit and instability will not build up if the time weighted average frequency is not too near the resonance point. Therefore, from Figure 3-24 it may be concluded that the shorter rod system will produce smaller yaw oscillation than the longer rod system.

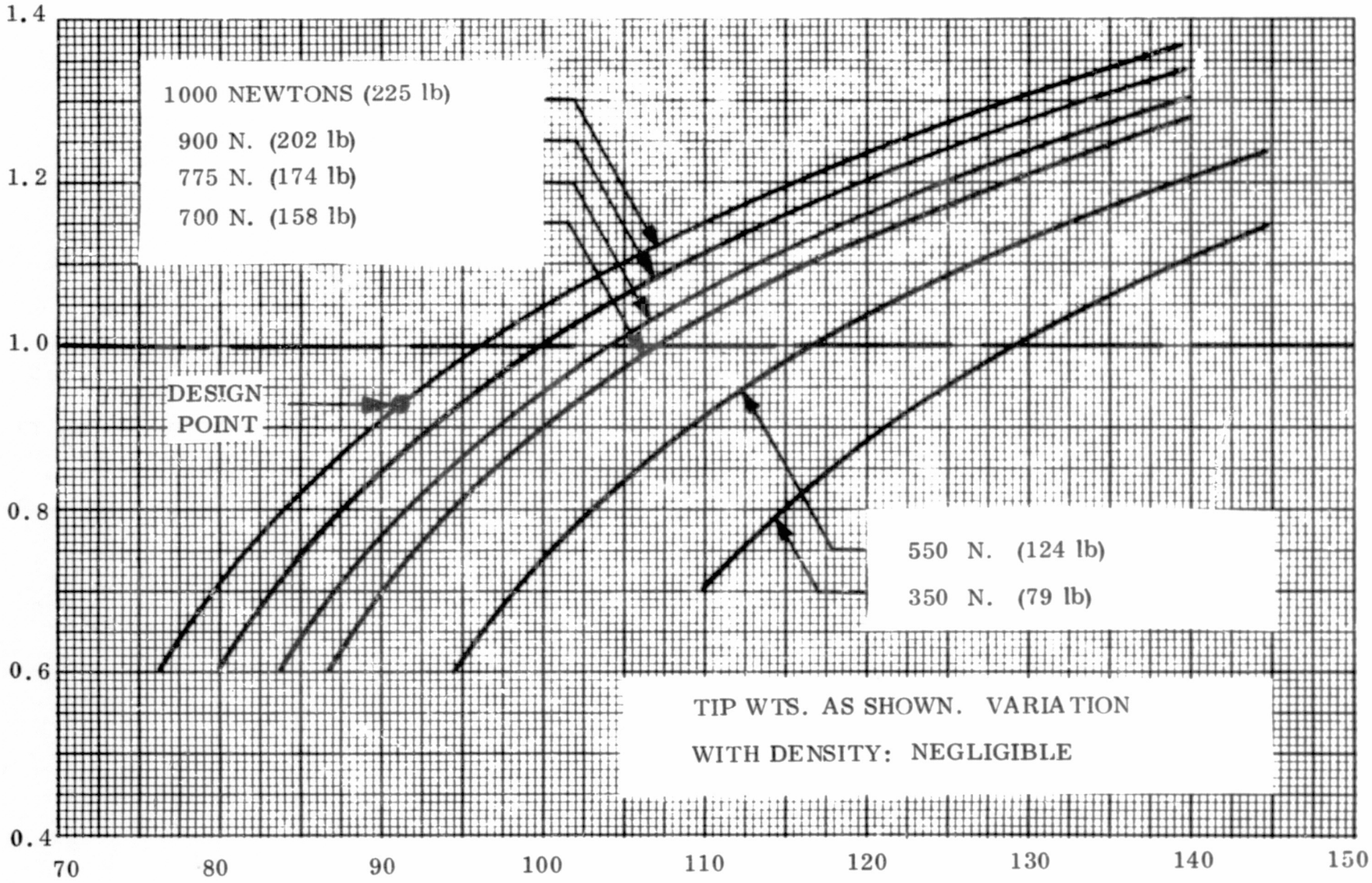


Figure 3-22. Pitch Natural Frequency Versus Rod Length, Various Tip Weights

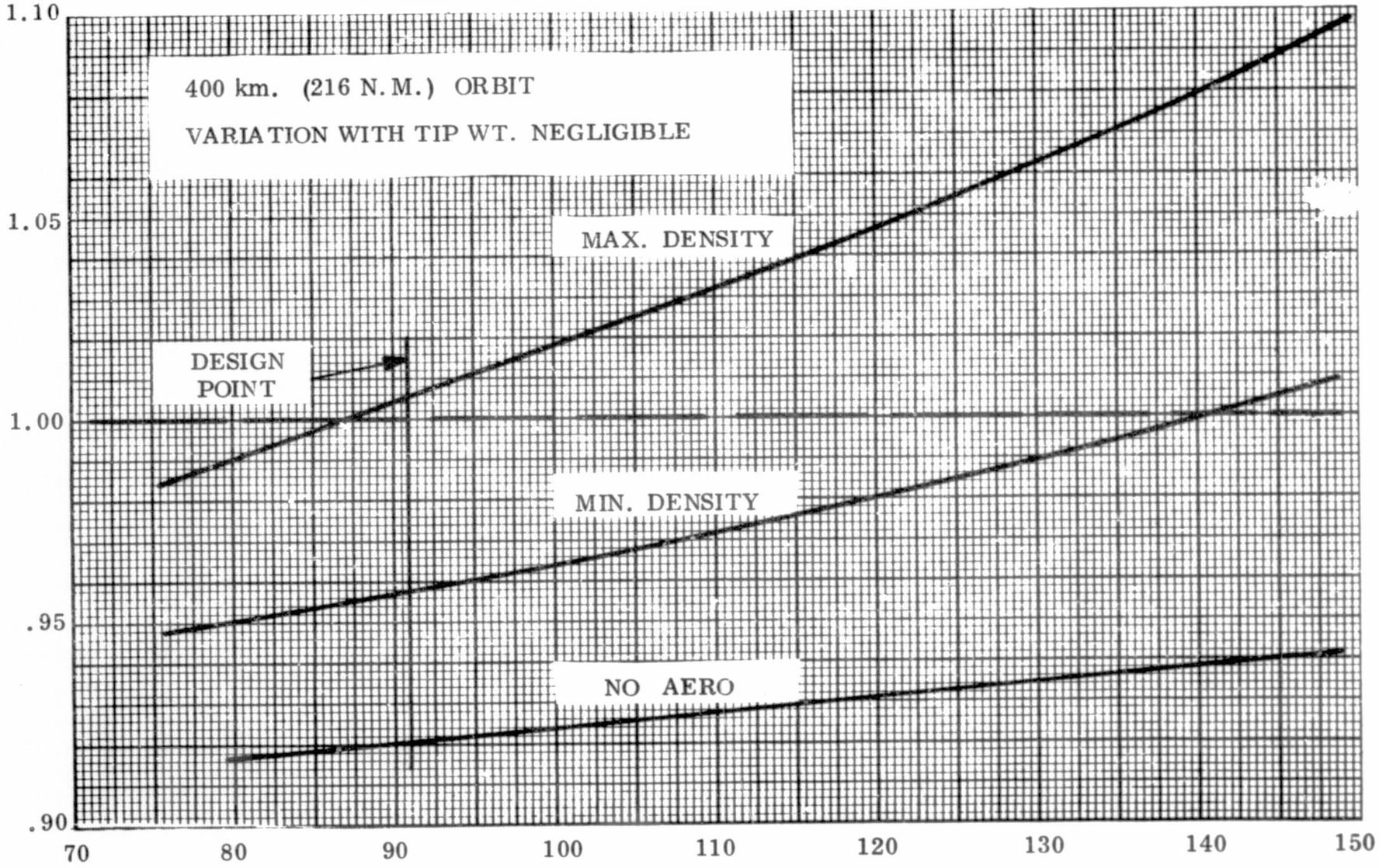


Figure 3-23. Yaw Natural Frequency Versus Rod Lengths

ROD LENGTH: AS SHOWN
DAMPER WT. = 1000 NEWTONS (225 LB)
SWEEP ANGLE = $10^{o}$

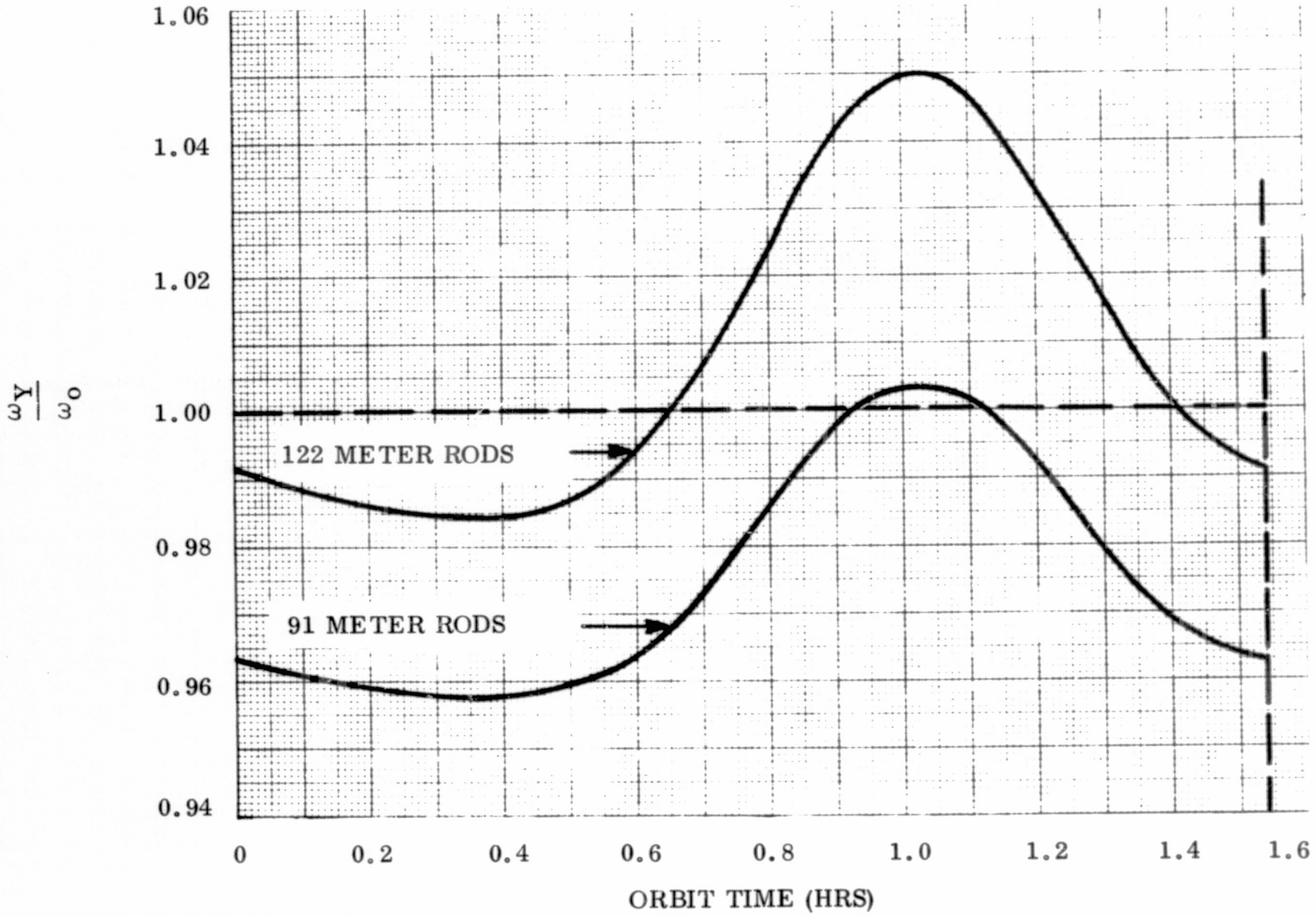


Figure 3-24. Yaw Natural Frequency Versus Orbit Time

These two systems were selected to be evaluated by means of the large angle nonlinear digital computer program, the results of which verified the linear analysis and led to the final configuration selection. The performance time histories for the 122-meter (400-ft) configuration and the 91-meter (300-ft) configuration are shown in Figures 3-25 and 3-26, respectively. Each simulates a steady state 2-day problem (31 orbits). All system characteristics are identical, except rod length. The actual value of damping coefficient, however, was halved for the shorter rod case in order to maintain the same relative damping (time to steady state less than 10 days). As may be observed pitch and roll amplitude appear to be nearly identical for both cases: $\pm$ 4 degrees in pitch and $\pm$ 3.3 degrees in roll. Yaw performance, however, is quite different. For the longer rod case, yaw oscillations reach $\pm$ 38 degrees to $\pm$ 39 degrees. This amplitude is repeated identically on the second "24-hour envelope," showing no indication of decay. For the shorter rod case, initial yaw amplitudes reach only $\pm$ 22 degrees during the first envelope and only $\pm$ 18 degrees on the second, indicating perhaps smaller amplitudes on successive 24-hour cycles. This performance comparison agrees with the linear analysis.

Further comparison of the two systems shows the shorter rod configuration to have several advantages over the longer rod case.

a. Although pitch and roll pointing accuracies will be satisfactory for both configurations, yaw pointing will meet or nearly meet the $\pm$ 15 degree requirement on the shorter rod system.

b. For the 7.6-cm (3-inch) rod, weighing approximately 7.7 Newtons/meter (0.53 lb/ft), an additional 30.5 meters (100 ft) on each of two rods means 445 Newtons (100 lb) of additional weight.

c. Another strong advantage of the shorter rod case is in regard to natural frequency changes at higher altitudes. Because aerodynamics tends to increase pitch and yaw natural frequencies, these will decrease as altitude increases. Since both pitch and yaw frequencies are less than once orbital at the minimum altitude (400 km), they will move away from the once orbital value at the higher altitudes. The reverse is true for the longer-rod system because at the low altitude these are greater than 1.0 and will decrease toward 1.0 as altitude is increased.

d. At high altitudes where aerodynamics were less signficant, rod thermal bending error may become a more significant contributor to overall pointing error. For the shorter rods, this error component will be less than for longer rods.

Based upon the foregoing analysis, the final configuration selected for this S-IVB orientation, long axis horizontal, is as follows. Two gravity gradient rods mounted from the aft section of the instrumentation unit, positioned in the roll-yaw plane; one up and one down, both swept back at an angle of 10 degrees from the local vertical. Each rod will have a spherical viscous damper mounted at its extreme tip. Figure 3-27 depicts the configuration. Weights and sizes will be as follows:

| | |
|---|---|
| Gravity Gradient Rods (2) | |
| Length: | 9 meters (300 ft) |
| Approximate diameter: | 7.6 cms. (3 inches) |
| Approximate weight: | 7.7 Newtons/meter 0.53 lb/ft) |
| Spherical Viscuous Dampers (2) | |
| Weight: | 1000 Newtons (225 lb) |
| Approximate diameter: | 56 cm (22 inches) |
| Damping coefficient: | 41 NMS (30 lb-ft-sec) each |
| Magnet strength: | 6000 amp $m^2$ ($6 \times 10^6$ pole cm) each |

The resulting total system moments and products of inertia about the nominal reference axes for this configuration are:

FOLDOUT FRAME 1

S-IVB THREE-AXIS HORIZONTAL CONFIG
PLANE OF SOLAR PANELS PERPENDICULAR TO O

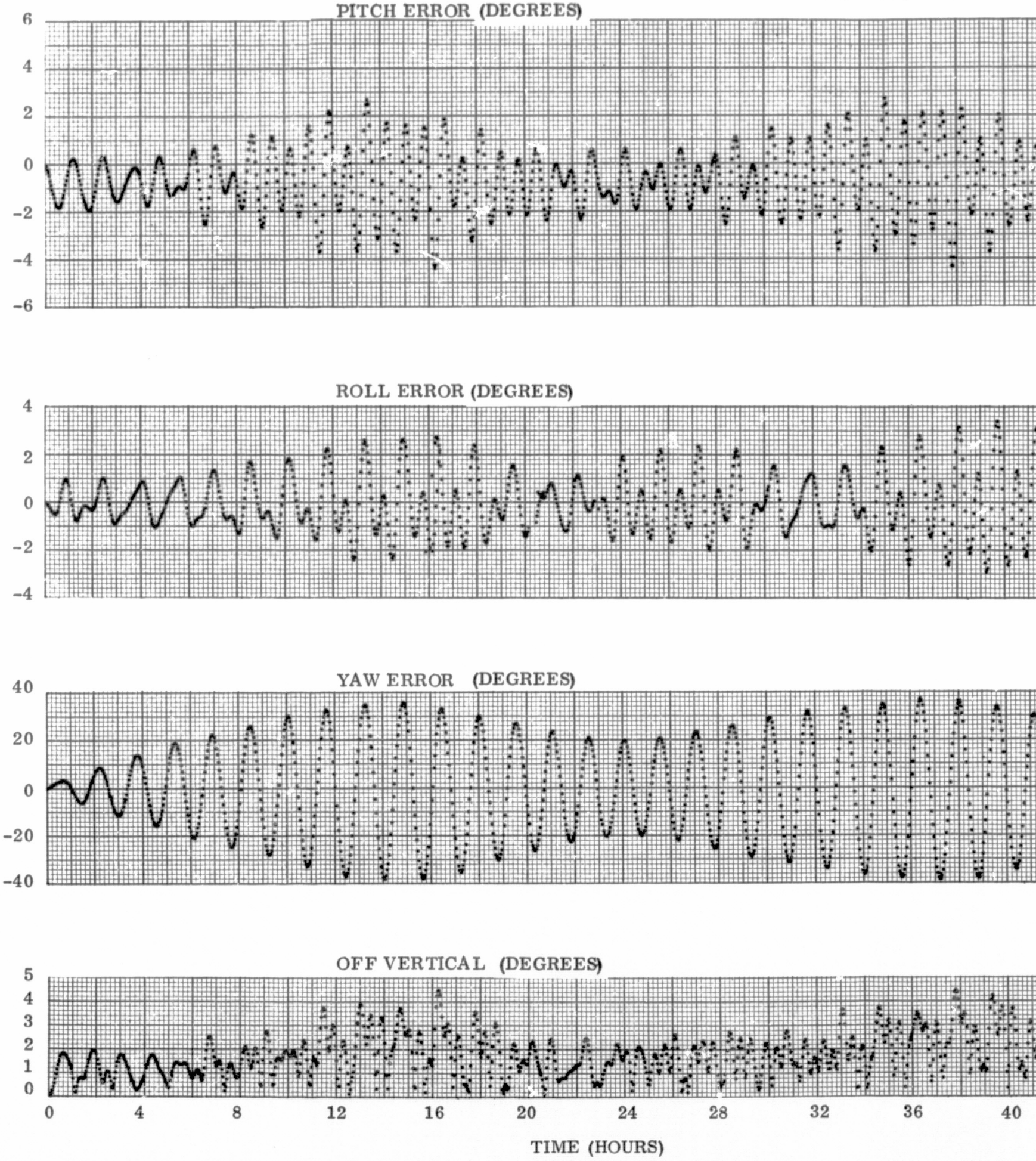

FOLDOUT FRAME 2

ONTAL CONFIGURATION
DICULAR TO ORBIT RADIUS VECTOR

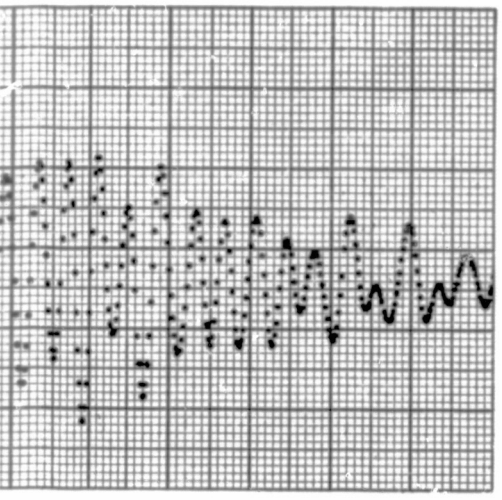

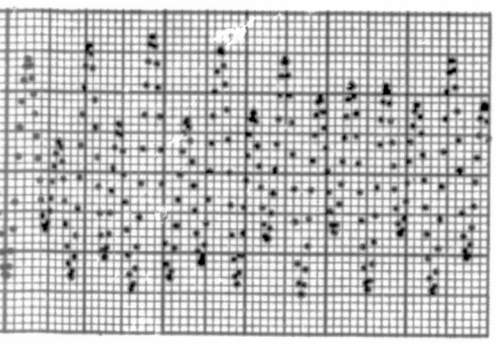

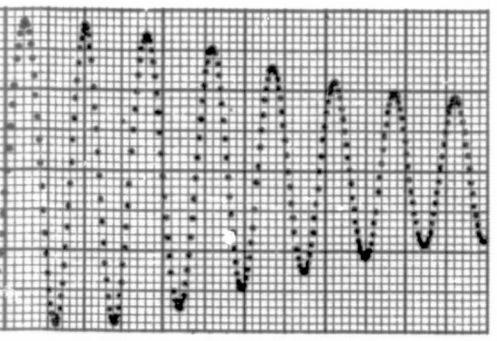

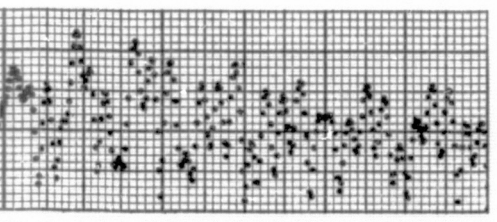

6 40 44 48

INITIAL CONDITIONS

$\theta_p = \theta_r \quad \theta_y = 0$ DEGREES

$\dot{\theta}_r = \dot{\theta}_y = 0$ DEG/SEC

$\dot{\theta}_p = 0.065$ DEG/SEC

TOTAL DAMPING

b = 164 N.M.S. (120 FT-LB-SEC)

m = 12000 AMP $M^2$ ($12 \times 10^6$ POLE CMS)

$M/I_p = 3$

GRAVITY GRADIENT RODS (TWO)

LENGTH = 122 METERS (400 FT)

DIAMETER = 7.6 CMS (3 INCHES)

SWEEP ANGLE = 10 DEGREES

TIP WEIGHTS (TWO)

WEIGHT = 1000 NEWTONS (225 LB)

DIAMETER = 56 CMS (22 INCHES)

Figure 3-25. Steady State Performance
122 m (400 ft) rods, b = 164 N.M.S.
(120 ft-lb-sec)

FOLDOUT FRAME 1

S-IVB THREE-AXIS HORIZONTA
PLANE OF SOLAR PANELS PERPENDICULA

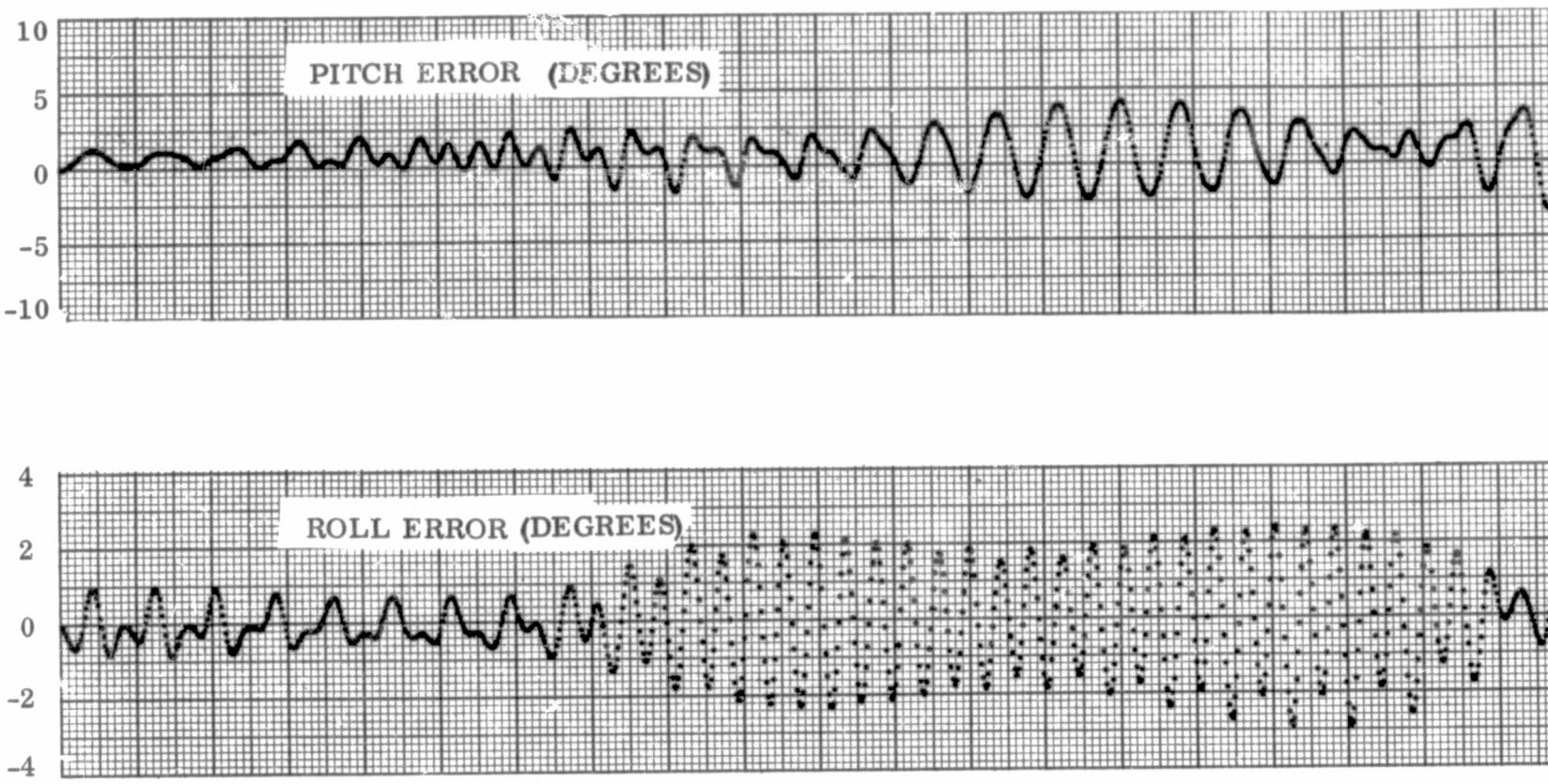

HORIZONTAL CONFIGURATION
RPENDICULAR TO ORBIT RADIUS VECTOR

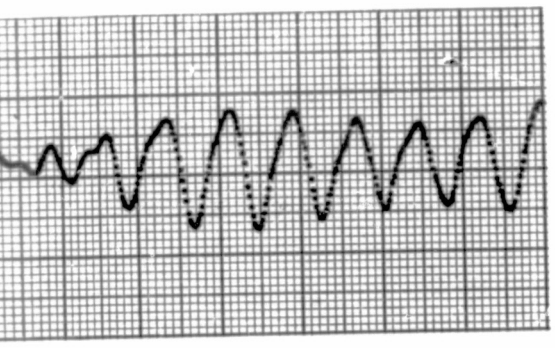

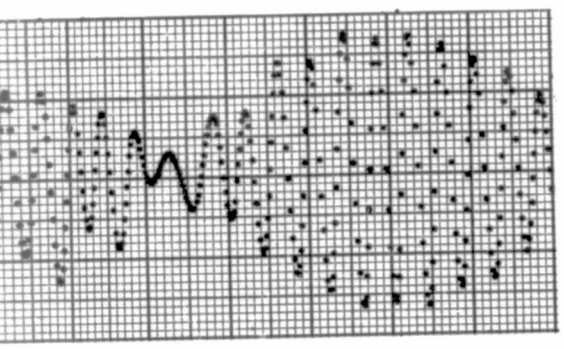

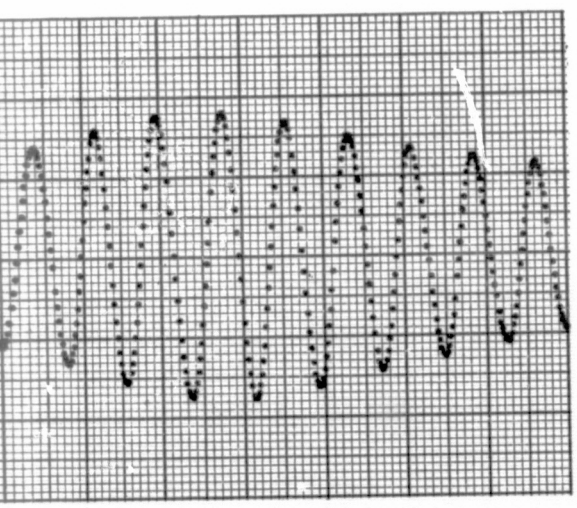

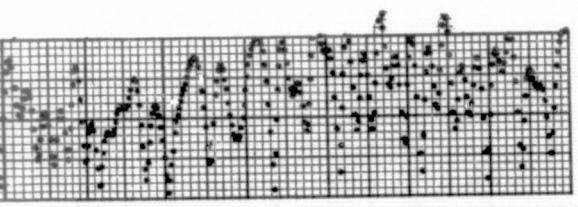


INITIAL CONDITIONS

$\theta_p = \theta_r = \theta_y = 0$ DEGREES

$\dot{\theta}_r = \dot{\theta}_y = 0$ DEG/SEC

$\dot{\theta}_p = 0.065$ DEG/SEC

TOTAL DAMPING

b = 82 N.M.S. (60 FT-LB-SECS)

m = 12000 AMP $M^2$ ($12 \times 10^6$ POLE CMS)

$M/I_p = 3$

GRAVITY GRADIENT RODS (TWO)

LENGTH = 91 METERS (300 FT)

DIAMETER = 7.6 CMS (3 INCHES)

SWEEP ANGLE = 10 DEGREES

TIP WEIGHTS (TWO)

WEIGHT = 1000 NEWTONS (225 LBS)

DIAMETER = 56 CMS (22 INCHES)

Figure 3-26. Steady State Performance
91 m (300 ft) rods, b = 82 N.M.S.
(60 ft-lb-sec)

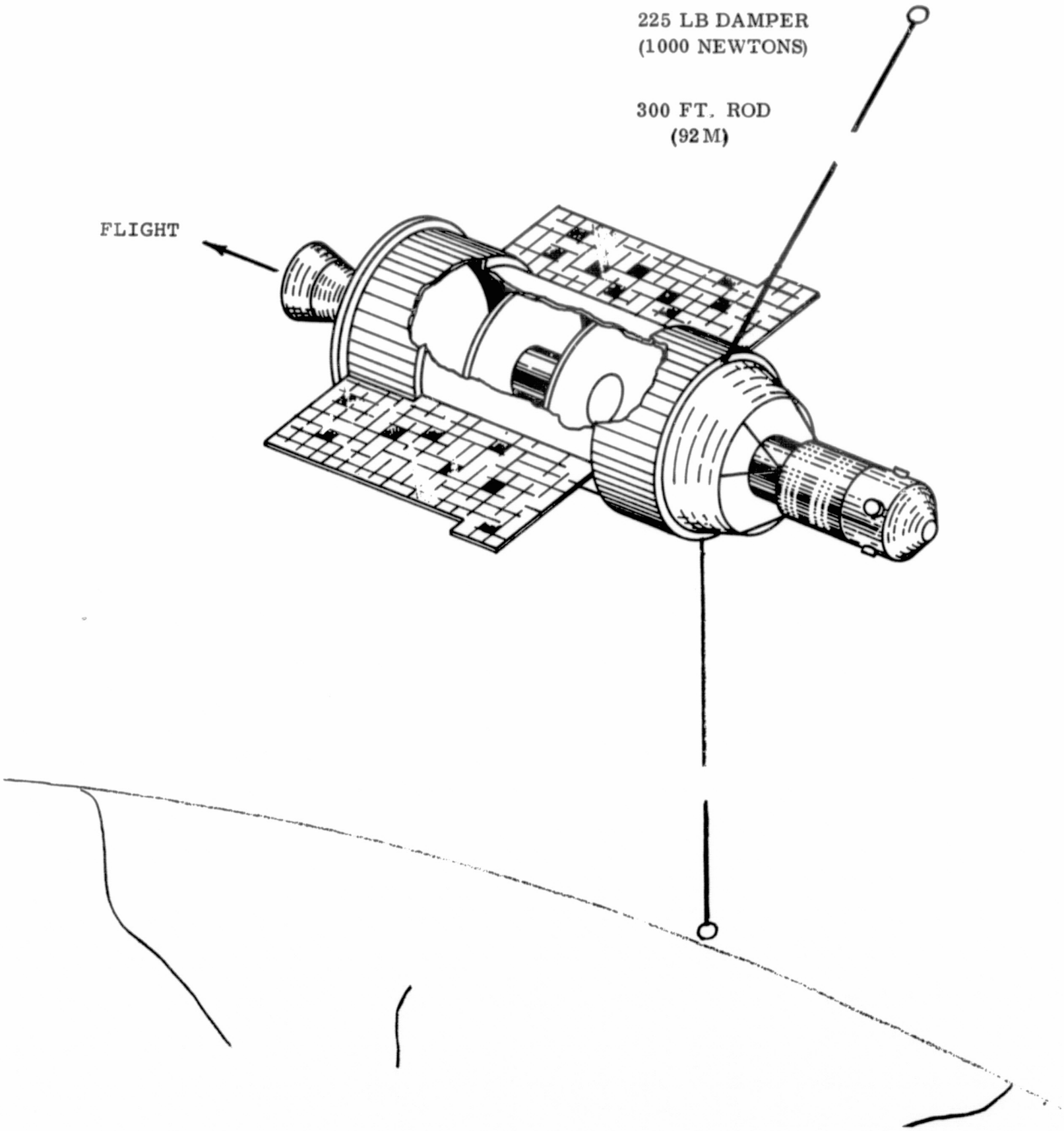


Figure 3-27. S-IVB Horizontal Stabilization Configuration

$$I_{pitch} = 3.52078 \times 10^6 \text{ kg m}^2 \ (2.59681 \times 10^6 \text{ slug-ft}^2)$$

$$I_{roll} = 2.36357 \times 10^6 \text{ kg m}^2 \ (1.743291 \times 10^6 \text{ slug-ft}^2)$$

$$I_{yaw} = 1.34576 \times 10^6 \text{ kg m}^2 \ (1.992587 \times 10^6 \text{ slug-ft}^2)$$

$$I_{yaw\text{-}roll} = 1.47777 \times 10^3 \text{ kg m}^2 \ (1.0899 \times 10^3 \text{ slug-ft}^2)$$

$$I_{yaw\text{-}pitch} = 3.32987 \times 10^3 \text{ kg m}^2 \ (-2.456 \times 10^3 \text{ slug-ft}^2)$$

$$I_{roll\text{-}pitch} = -107041 \times 10^4 \text{ kg m}^2 \ (-7.895 \times 10^3 \text{ slug-ft}^2)$$

## 3.5.2 NOMINAL PERFORMANCE

### 3.5.2.1 Steady State Performance

The steady state performance of the selected design, i.e., 91.4-meter (300-ft.) rods with tip-mounted dampers weighting 1000 Newtons (225 lb) each, was evaluated for the nominal orbit by means of the large angle, nonlinear program. This particular run extends to 135 hours of simulated orbit time (nearly 90 orbits). It is about three times longer than the run shown in Figure 3-26, in order to demonstrate that the conclusions drawn from the shorter run are indeed valid.

The results are shown in Figures 3-28A and 3-28B in two parts for clarity; B is a time continuation of the same computer runs.

As may be observed, pitch error appears to be approaching $\pm$ 6 degrees, roll $\pm$ 5 degrees and yaw $\pm$ 19 degrees. The general conclusions drawn from the shorter run are correct: pitch and roll errors are significantly less than requirements and yaw errors will be in 18 to 19 degree range. Careful examination of each 24-hour cycle on Figure 3-28B reveals the fact that $\pm$ 15 degrees in yaw will be exceeded for less than 10 percent of the total time.

It appears that final steady state conditions have not quite been reached during the 135 hours. The envelope peaks seem to be still increasing slightly at the end of the run. A plot of these increasing envelope peaks as a function of time, shown in Figure 3-29,

FOLDOUT FRAME 1

S-IVB THREE AXIS HORIZONTAL CONFIGURATION
PLANE OF SOLAR PANELS PERPENDICULAR TO ORBIT RADI

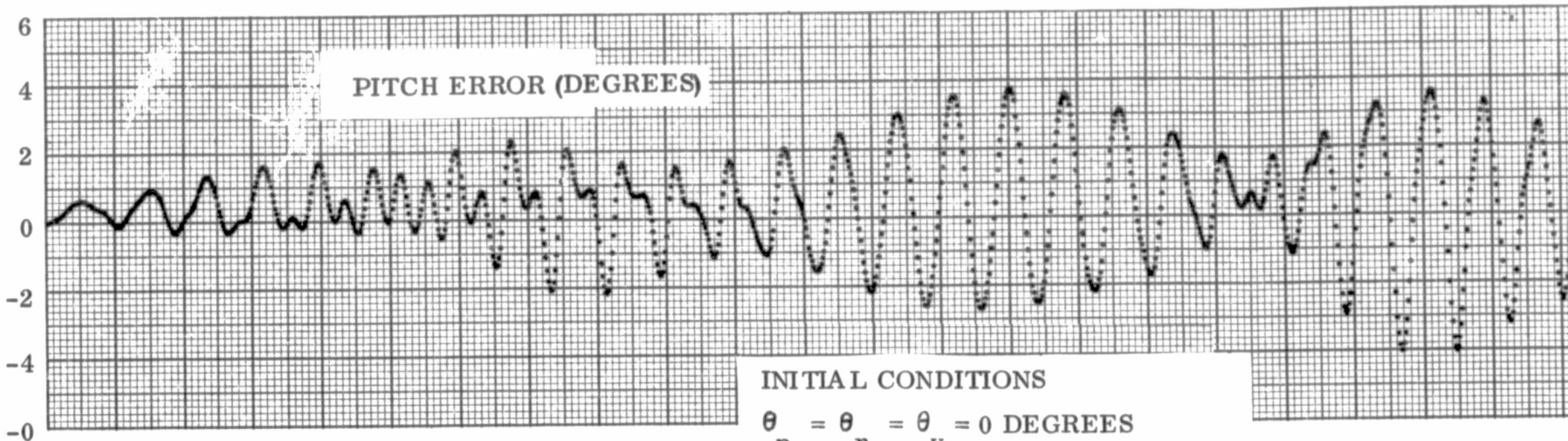


INITIAL CONDITIONS

$\theta_p = \theta_r = \theta_y = 0$ DEGREES

$\dot{\theta}_r = \dot{\theta}_y = 0$ DEG/SEC

$\dot{\theta}_p = 0.065$ DEG/SEC

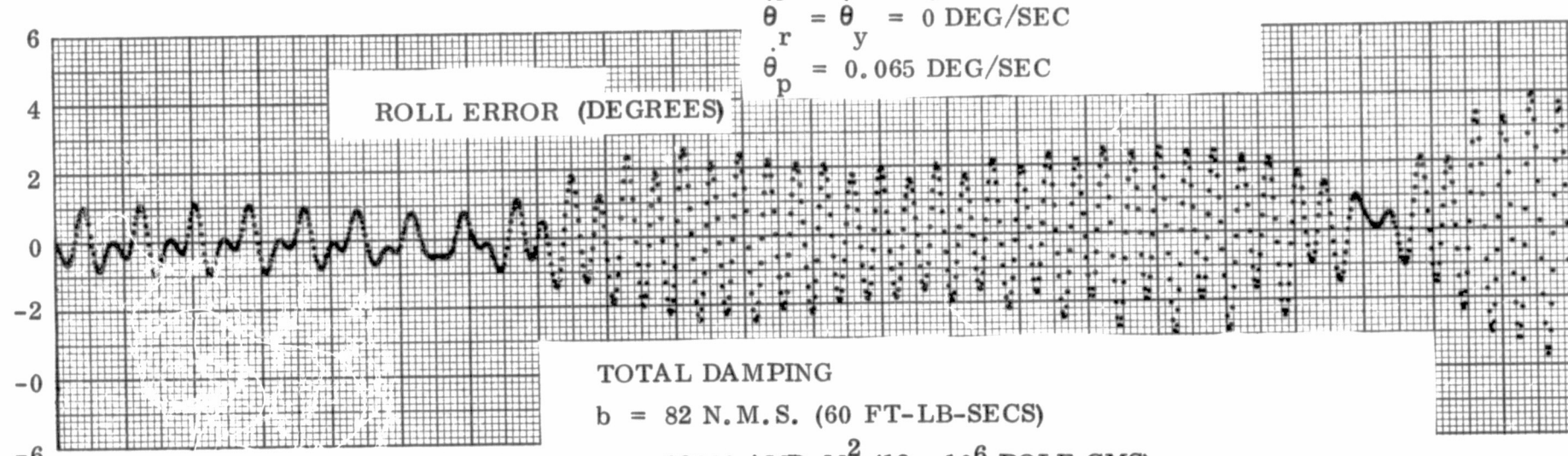


TOTAL DAMPING

b = 82 N.M.S. (60 FT-LB-SECS)

m = 12000 AMP $M^2$ ($12 \times 10^6$ POLE CMS)

$m/I_p = 3$

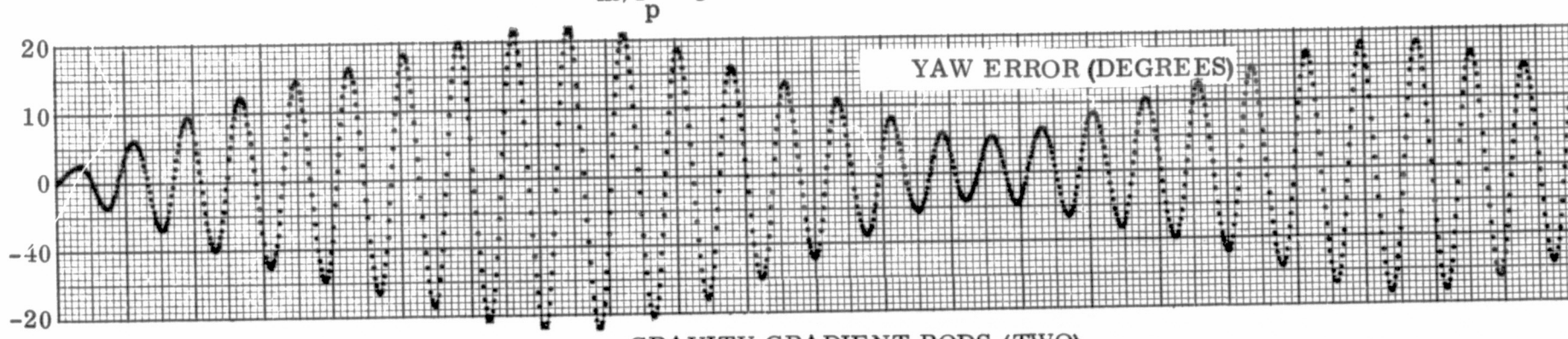


GRAVITY GRADIENT RODS (TWO)

LENGTH = 91 METERS (300 FT)

DIAMETER = 7.6 CMS (3 INCHES)

SWEEP ANGLE = 10 DEGREES

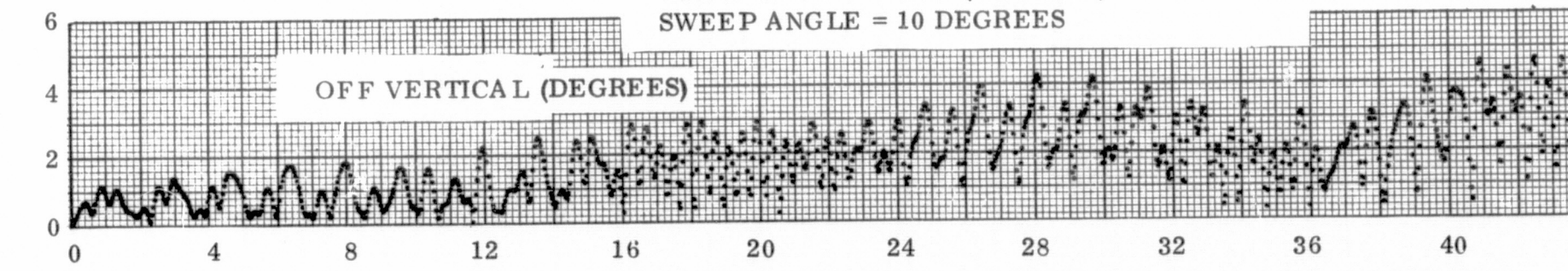

CONFIGURATION
R TO ORBIT RADIUS VECTOR

FOLDOUT FRAME 2

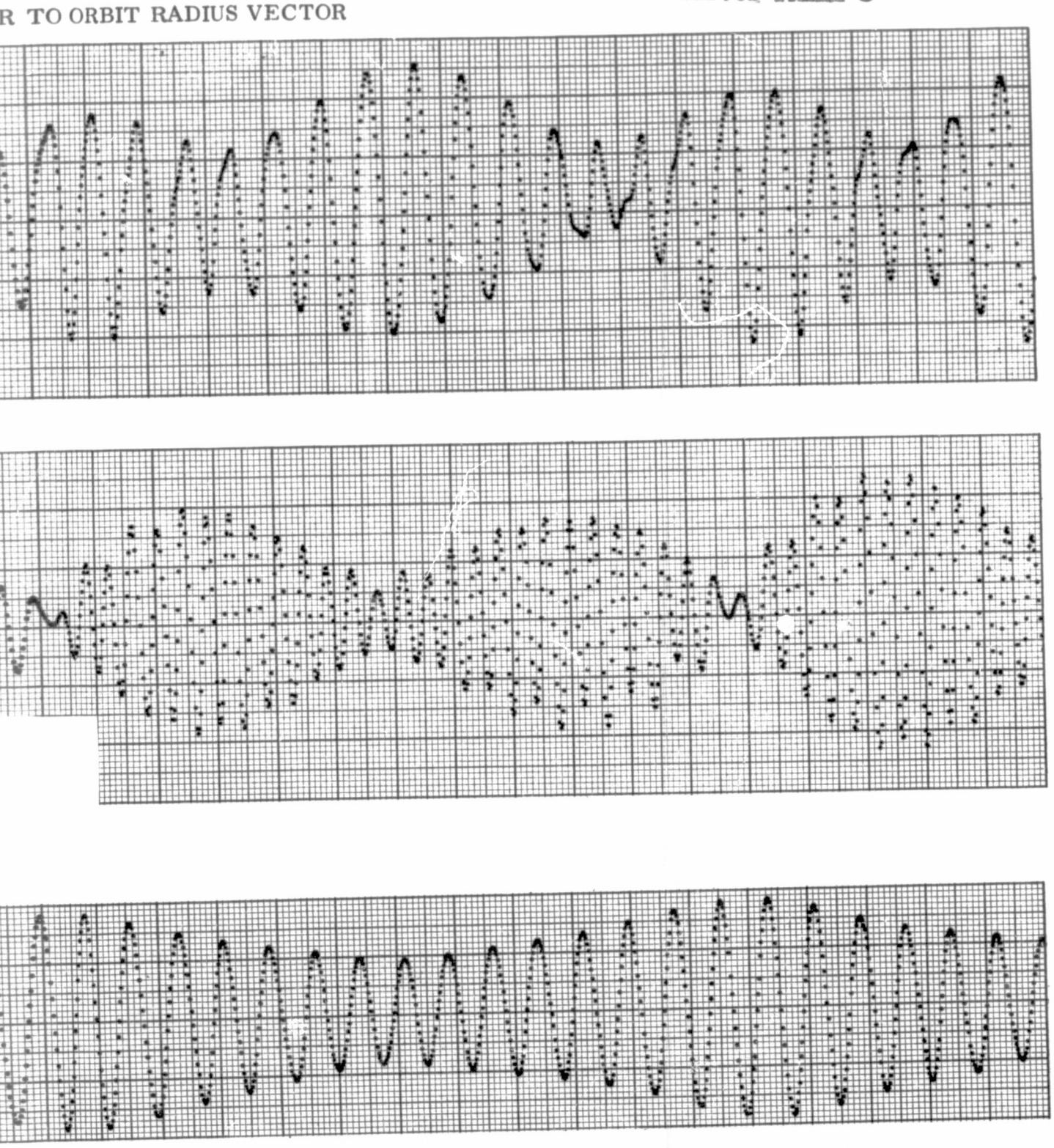

TIP WEIGHTS (TWO)
WEIGHT = 1000 NEWTONS (225 LB)
DIAMETER = 56 CMS (22 INCHES)

6 40 44 45 52 56 60 64 68 72

(HOURS)

Figure 3-28A. Selected Configuration, Steady State Performance

FOLDOUT FRAME /

S-IVB THREE AXIS AXIS HORIZONTAL CONFIGU
PLANE OF SOLAR PANELS PERPENDICULAR TO ORBIT RA

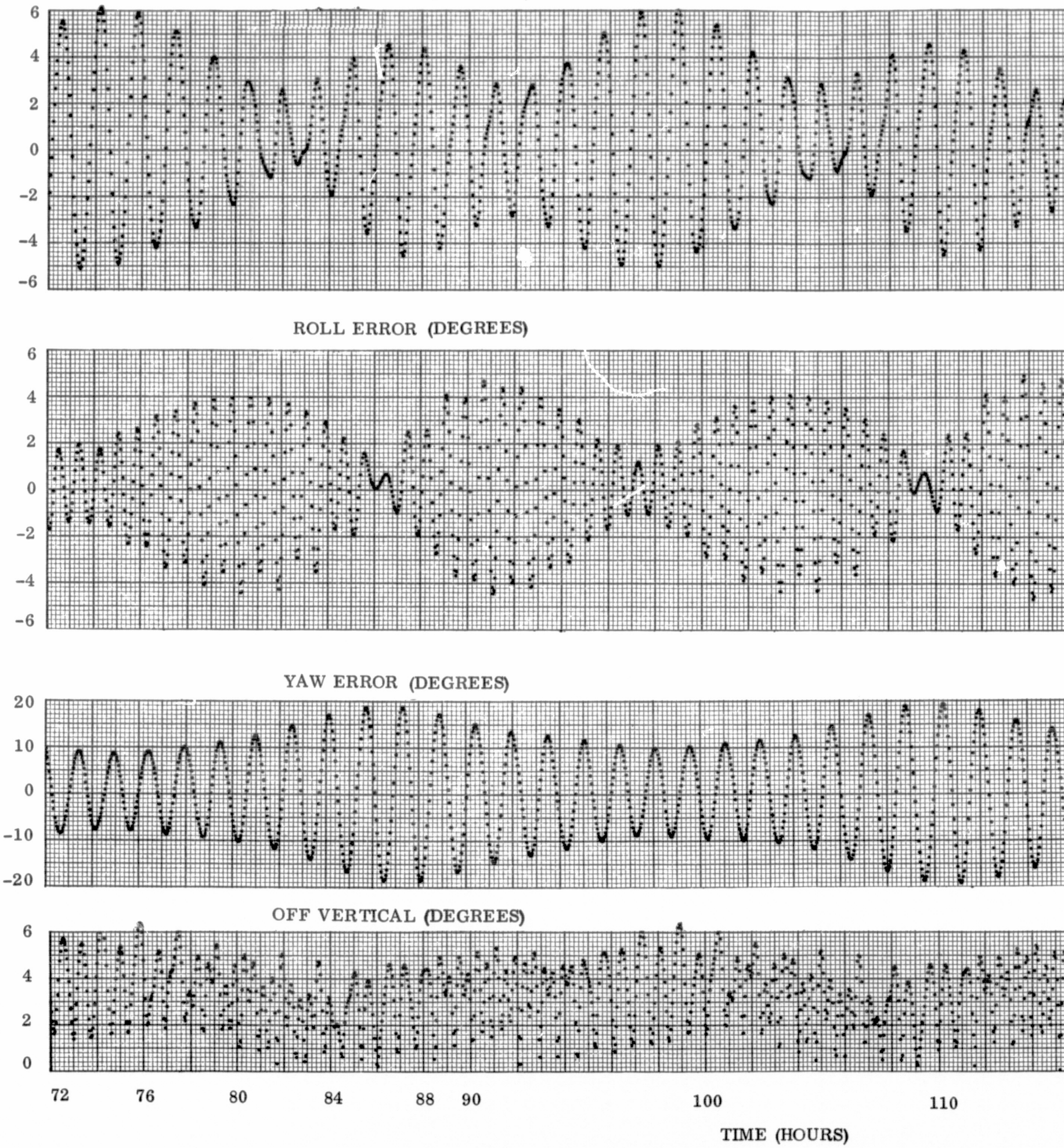

L CONFIGURATION
O ORBIT RADIUS VECTOR

FOLDOUT FRAME 2

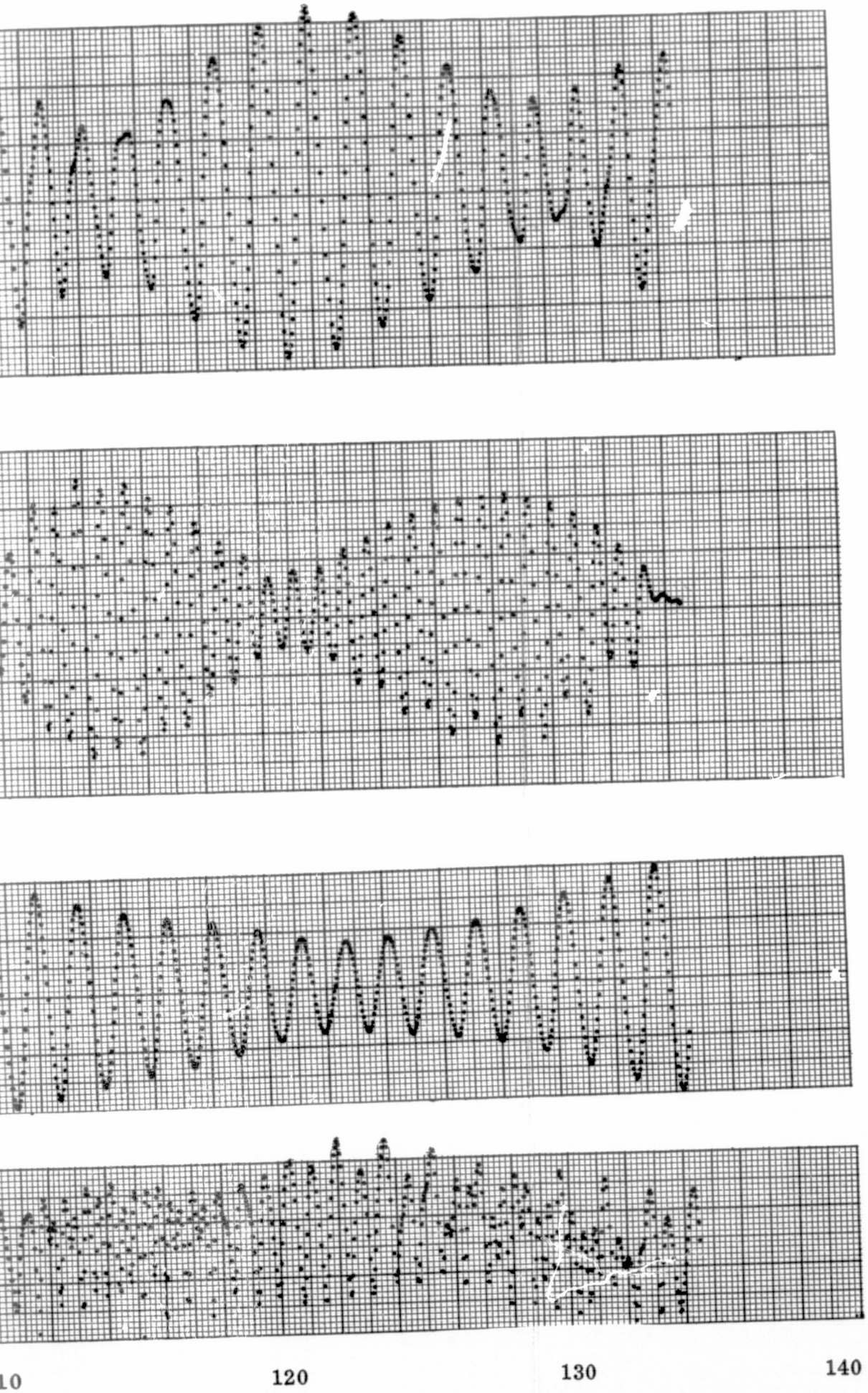


Figure 3-28B. Selected Configuration, Steady State Performance

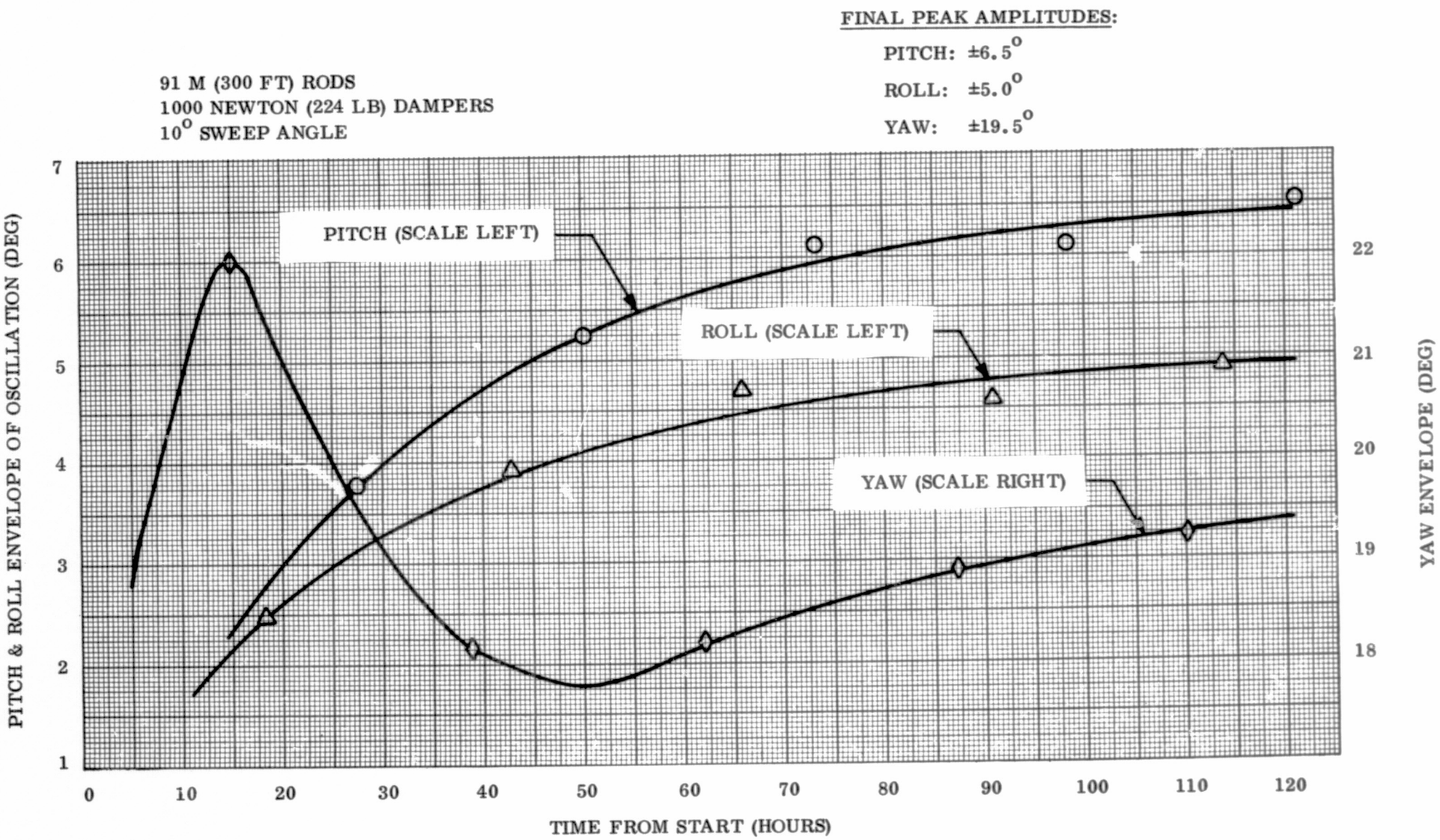


Figure 3-29. Selected Configuration Initial Steady State Error Buildup

indicates that each is becoming asymptotic to constant values. It is concluded that final steady state pointing accuracies for this configuration will be as follows:

Pitch ---------- $\pm 6.5^{o}$ on + 0.5 bias
Roll ---------- $\pm 5.0^{o}$ negligible bias
Yaw ---------- $\pm 19.0^{o}$ negligible bias
Tilt angle -------- less than $7^{o}$ (off vertical)

The performance of this configuration was also evaluated at an altitude of 750 km (400 nm) where, for the purpose of simulation, aerodynamic effects are assumed nonexistent. The results of a 3-day (46 orbits) run are shown on Figure 3-30. All system characteristics are identical to those of Figure 3-28.

It is expected that the rate of increase in peak envelope amplitudes observed for the nominal altitude run (Figure 3-28) may also occur at the 750 km (400 nm) altitude. Assuming the same percent increase from the 70-hour point to the asymptotic final values also exist at the higher altitude, pointing accuracies in the 750 km (400 nm) orbit will be:

| | | |
|---|---|---|
| Pitch: | $\pm 4^{o}$ | on + $0.5^{o}$ bias |
| Roll: | $\pm 3.5^{o}$ | negligible bias |
| Yaw: | $\pm 14^{o}$ | on +0.5 bias |
| Tilt: | $5^{o}$ | |

3.5.2.2 Transient Performance

Transient performance of the selected configuration in the nominal 400 km (216 nm) orbit was evaluated by the same means as steady state performance. The only exception being the initial spacecraft orientation and body rates relative to the orbiting reference frame. These were set equal to the capability of the active control system: $0.01^{o}$ /sec about all axes and each of the fixed body axes at 10 degrees from the nominally preferred orientation.

FOLDOUT FRAME 1

DLDOUT FRAME 2

FOLDOUT FRAME

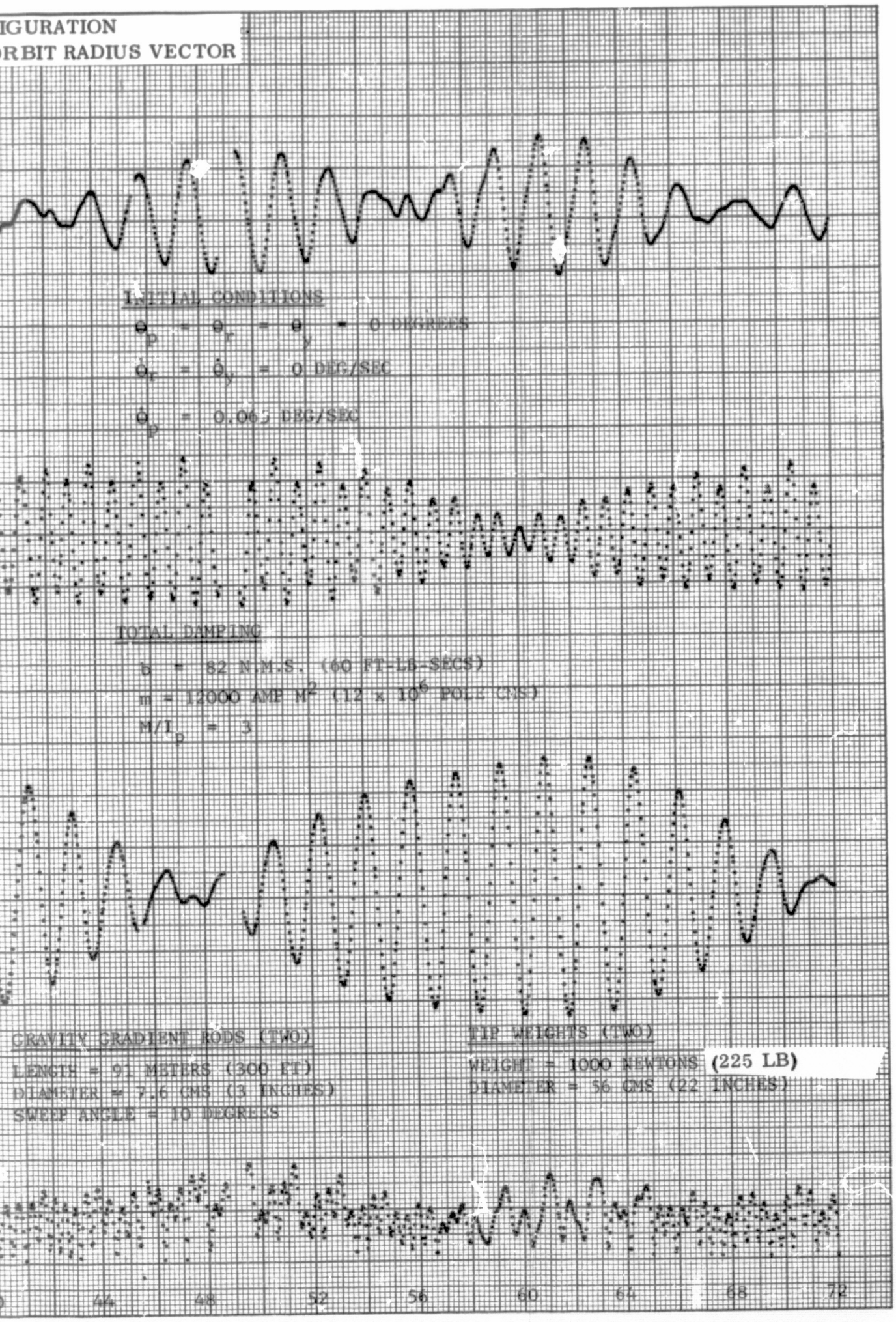


Figure 3-30. Selected Configuration Steady State Performance at 750 km (400 N. M.)

The results of a 2-day simulation are shown in Figure 3-31. Even though it is a relatively short simulation, damping is evident. Based upon the decay of the pitch envelope from the peak at the 5-hour point to the peak at the 20-hour point, a 53 orbit time constant is indicated. Although this is a very short time on which to base a time constant estimate, it is believed to give results within $\pm$ 20 percent. Therefore, the estimated damping time to reach steady state is 10 days $\pm$ 2 days.

### 3.5.3 PARAMETRIC STUDIES

#### 3.5.3.1 Effect of Rod Length and Tip Weight Upon Steady State Performance

In order to predict performance, that is total pointing errors about each of the fixed body axes, use was made of the linearized error determination program.

The individual disturbance for which errors were computed to arrive at a total pointing error about each axis are:

a. Aerodynamics on the S-IVB vehicle, rods and tip masses

b. Solar pressure on S-IVB, including deployed solar panels, rods and tip masses

c. Vehicle magnetic dipole: 50 amp $m^2$ (50,000 pole cm)

d. Damper-induced torques

In addition to the capability of estimating errors as a function of rod lengths and tip masses, parameters may be varied at small enough increments to pinpoint any points of resonance due to external torques other than gravity gradient torques. Another feature of the linear program is the fact that overall estimated damping time may be held constant as the geometry (inertias) are varied.

Linearized Pitch Error Analysis Figure 3-32 is a plot of the predicted pitch error as a function of rod lengths from 70 meters (230 ft) to 150 meters (492 ft) for various tip weights from 550 newtons (124 lb) to 1000 newtons (225 lb). In general, the error should decrease

with increasing system size (rod length and tip weights). However, as may be observed for each value of tip weight, a specific rod length exists for which the system natural frequency in pitch is exactly equal to orbital frequency.

A comparison between the actual pitch errors obtained on the large angle, nonlinear simulations and those of the linear evaluation shows reasonably good agreement. The nonlinear evaluations for the 91-meter (300-ft) rods and the 122-meter (400-ft) rods, discussed in previous sections and shown in Figures 3-25 and 3-28 may be compared directly to the linear errors of Figure 3-32, for the 1000 newton (224 lb.) tip weights:

| | 91-meter rods (300 ft) | 122-meter rods (400 ft) |
|---|---|---|
| Pitch Error, Nonlinear | $\pm 6.5^{o}$ | $\pm 3.5^{o}$ |
| Pitch Error, Linear | $\pm 6^{o}$ | $\pm 2.0^{o}$ |

Based upon the linear results, pitch pointing error can be further optimized by minor, but perhaps desirable, system alterations. For example, holding the 91-meter (300-ft) rod length and reducing tip weight to 778 newtons (175 lb) or holding tip weight at 1000 newtons (225 lb) and reducing rod length to 84 m (275 ft) will reduce the pitch error to near optimum of approximately 4 degrees.

Extending the linearized pitch error analysis, Figure 3-33 is a plot of rod length versus tip weight for the line of once orbital pitch resonance. The shaded area represents error exceeding 10 to 12 degrees. Also shown is the minimum error line of 4 degrees; below this line errors begin increasing again representing systems which are too low in moment of inertia to produce good pitch pointing accuracy. Based upon this analysis, the configuration for optimum pitch performance should theoretically fall on the 4 degree line. However, a lower limit to tip weight does exist from the practical aspect of the minimum damper magnet strength needed to meet damping time requirements. It is estimated that this minimum is in the 778 newton (175 lb) to 890 newton (200 lb) range, allowing no margin in the 10-day requirement.

FOLDOUT FRAME 1

S-IVB THREE-AXIS HORIZONTAL CONFIGURA
PLANE OF SOLAR PANELS PERPENDICULAR TO ORBIT P

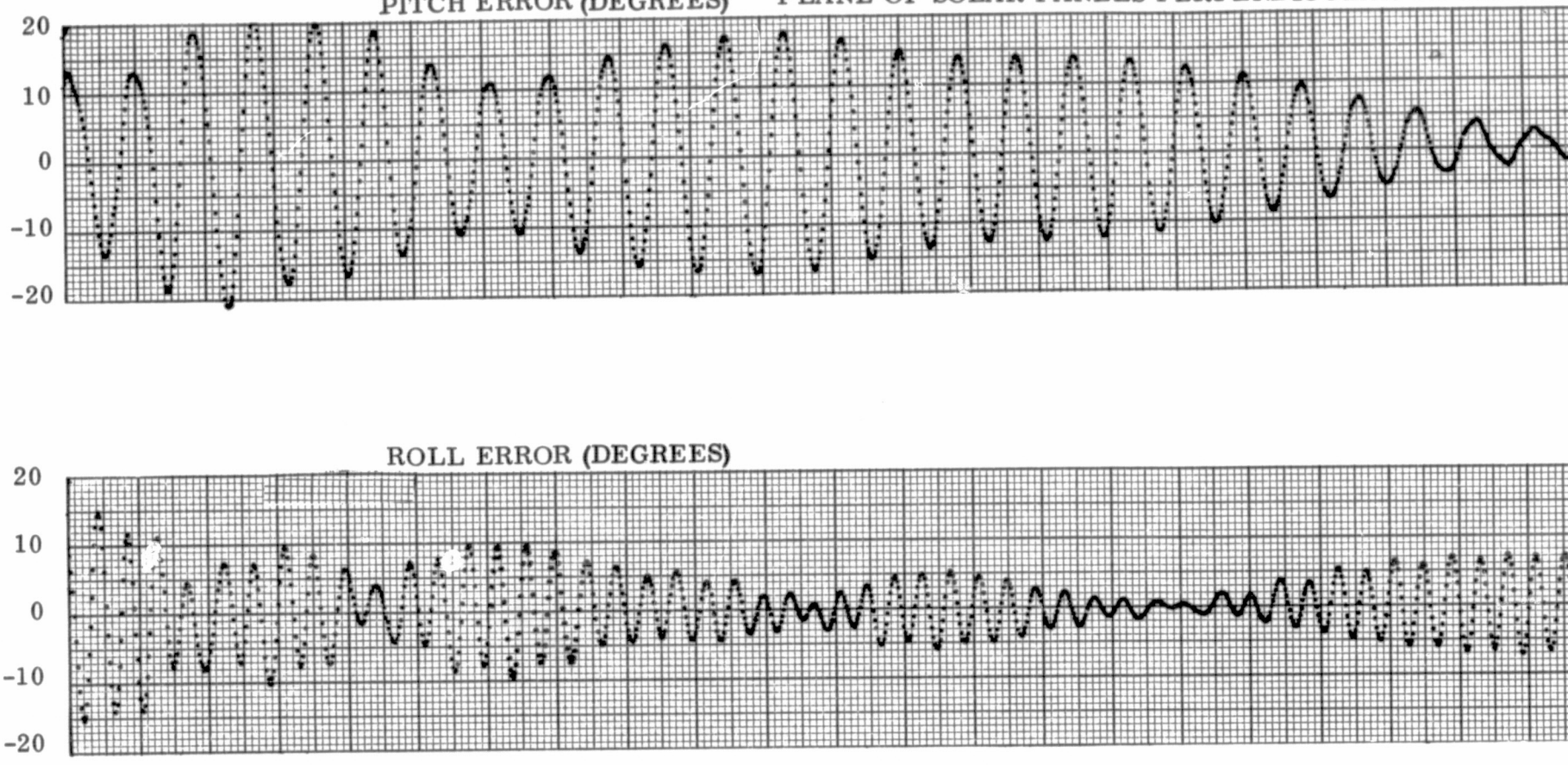

FOLDOUT FRAME 2

AL CONFIGURATION
LAR TO ORBIT RADIUS VECTOR

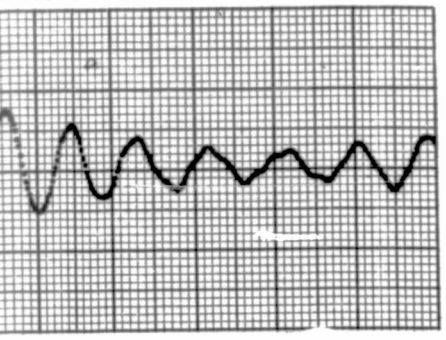

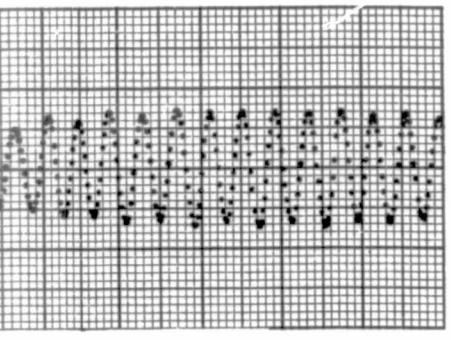

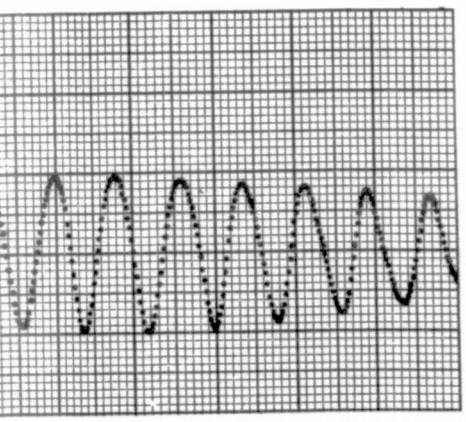

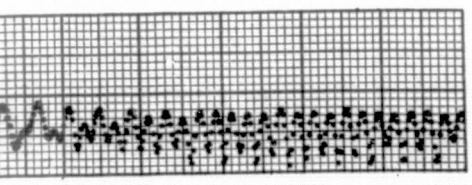

40 44 48

INITIAL CONDITION

$\theta_p = \theta_r = \theta_y = 10$ DEGREES

$\dot{\theta}_r = \dot{\theta}_y = 0.01$ DEG/SEC

$\dot{\theta}_p = 0.075$ DEG/SEC

TOTAL DAMPING

b = 82 N. M. S. (60 FT-LB-SECS)

m = 12000 AMP $M^2$ ($12 \times 10^6$ POLE CMS)

$M/I_p = 3$

GRAVITY GRADIENT RODS (TWO)

LENGTH = 91 METERS (300 FT)

DIAMETER = 7.6 CMS (3 INCHES)

SWEEP ANGLE = 10 DEGREES

TIP WEIGHTS (TWO)

WEIGHT = 1000 NEWTONS (225 LB)

DIAMETER = 56 CMS (22 INCHES)

Figure 3-31. Selected Configuration Transient Performance at 750 km (216 N. M.)

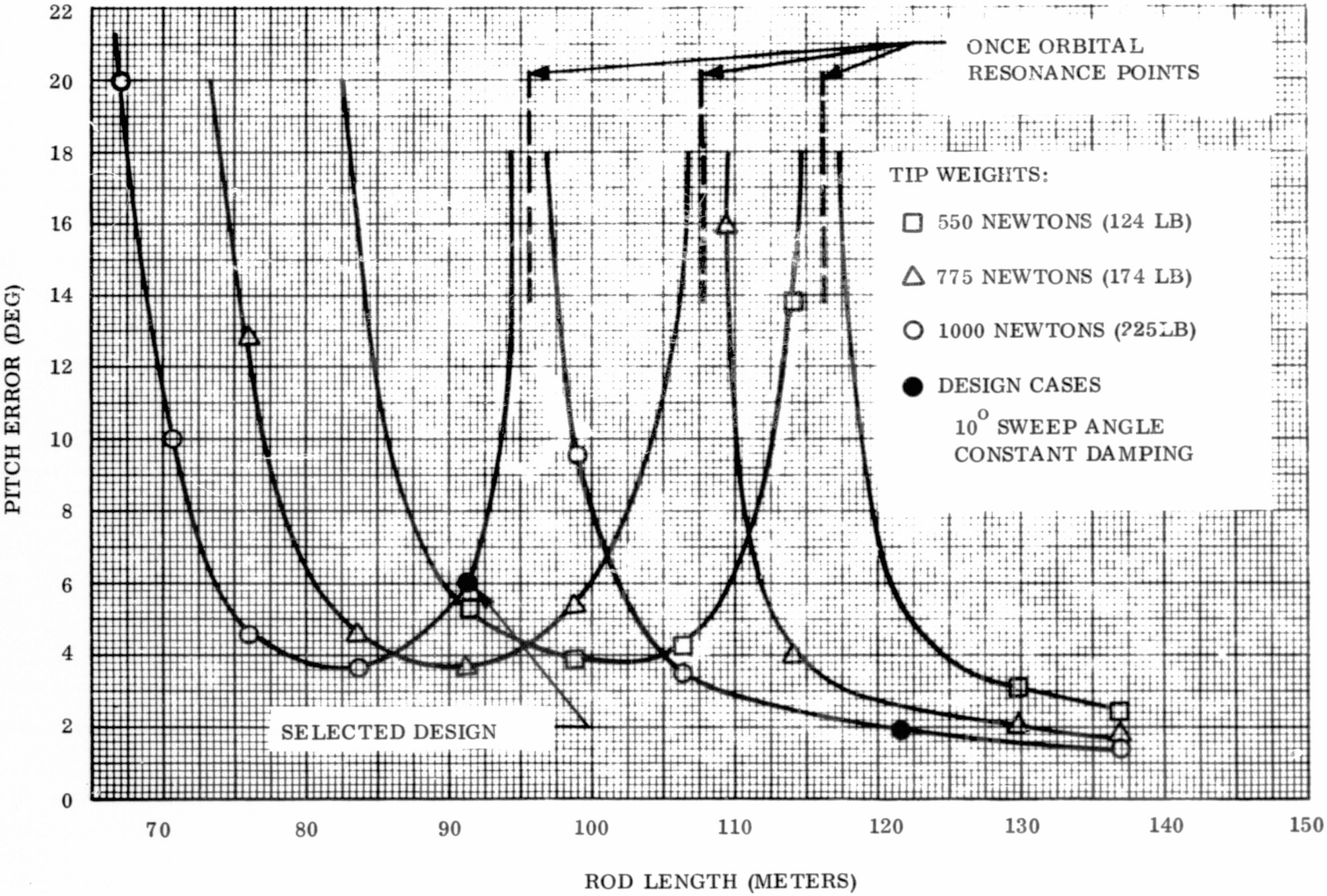


**Figure 3-32.** Linearized Pitch Error Versus Rod Length, Various Tip Weights

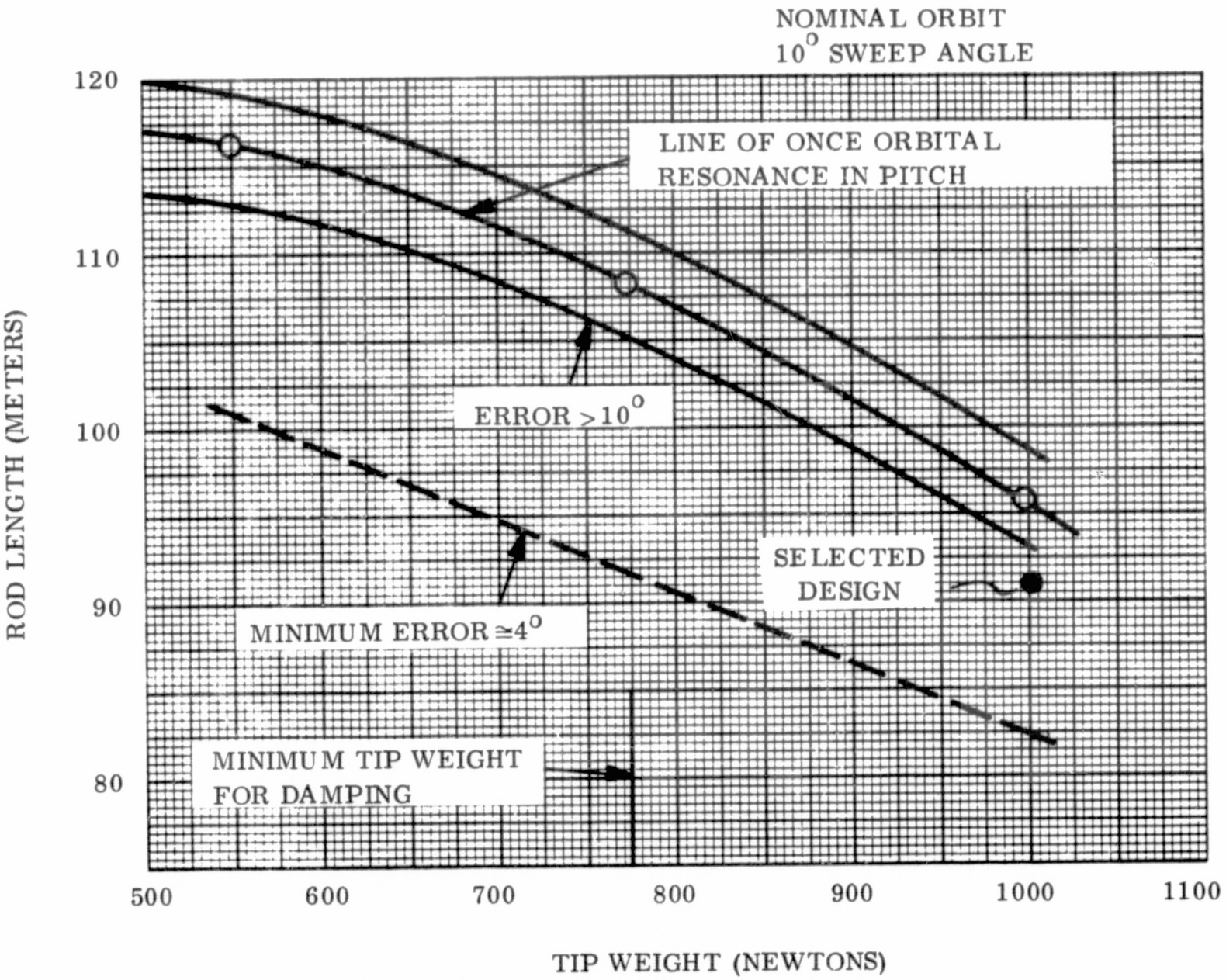


Figure 3-33. Linear Results: Rod Length Versus Tip Weight For Pitch Resonance

Linearized Yaw Error Analysis Figure 3-34 shows the predicted yaw error as a function of rod length for various tip weights as determined by the linearized error determination program. Over the range of rod lengths investigated, the error is increasing with length; this indicates that for rod lengths out to the 122-meter (400-ft) range, the yaw response to a once orbital disturbance is still increasing.

A comparison between the linear predictions and nonlinear results shown in Figures 3-25 and 3-28 shows rather poor agreement compared to that seen in the comparison of pitch performance.

| | 91-meter rods (300-ft) | 122-meter rods (400-ft) |
|---|---|---|
| Yaw Error, Nonlinear | 19.5° | 38° |
| Yaw Error, Linear | 14.6° | 23° |

In both cases, the linearized errors are 60 to 70 percent of the nonlinear results. However, the linearized slopes are nearly correct, and indications are that yaw performance could be improved by decreasing the system size somewhat. This is also what is required for optimizing pitch performance. It is estimated that to obtain yaw pointing errors under 15 degrees would require a rod length of approximately 84 meters (275 ft) with a tip weight of 789 newtons (175 lb).

Linearized Roll Error Analysis The linearized roll analysis shows that the variation in roll error with rod length and tip weight is similar to that in yaw. As the deployed moment of inertia becomes smaller, the total moment of inertia of the configuration becomes less planar and the roll natural frequency drops further below twice orbital frequency.

Conclusions From the Linearized Analysis The linearized analysis has shown that pitch-pointing accuracy can be optimized with the pitch natural frequency either above or below orbital frequency. Optimization with pitch frequency less than orbital frequency results in poorer pitch accuracy but better roll and yaw accuracy, as well as a lighter overall system weight. The optimum design considering weight and performance has the following rod lengths and tip weights:

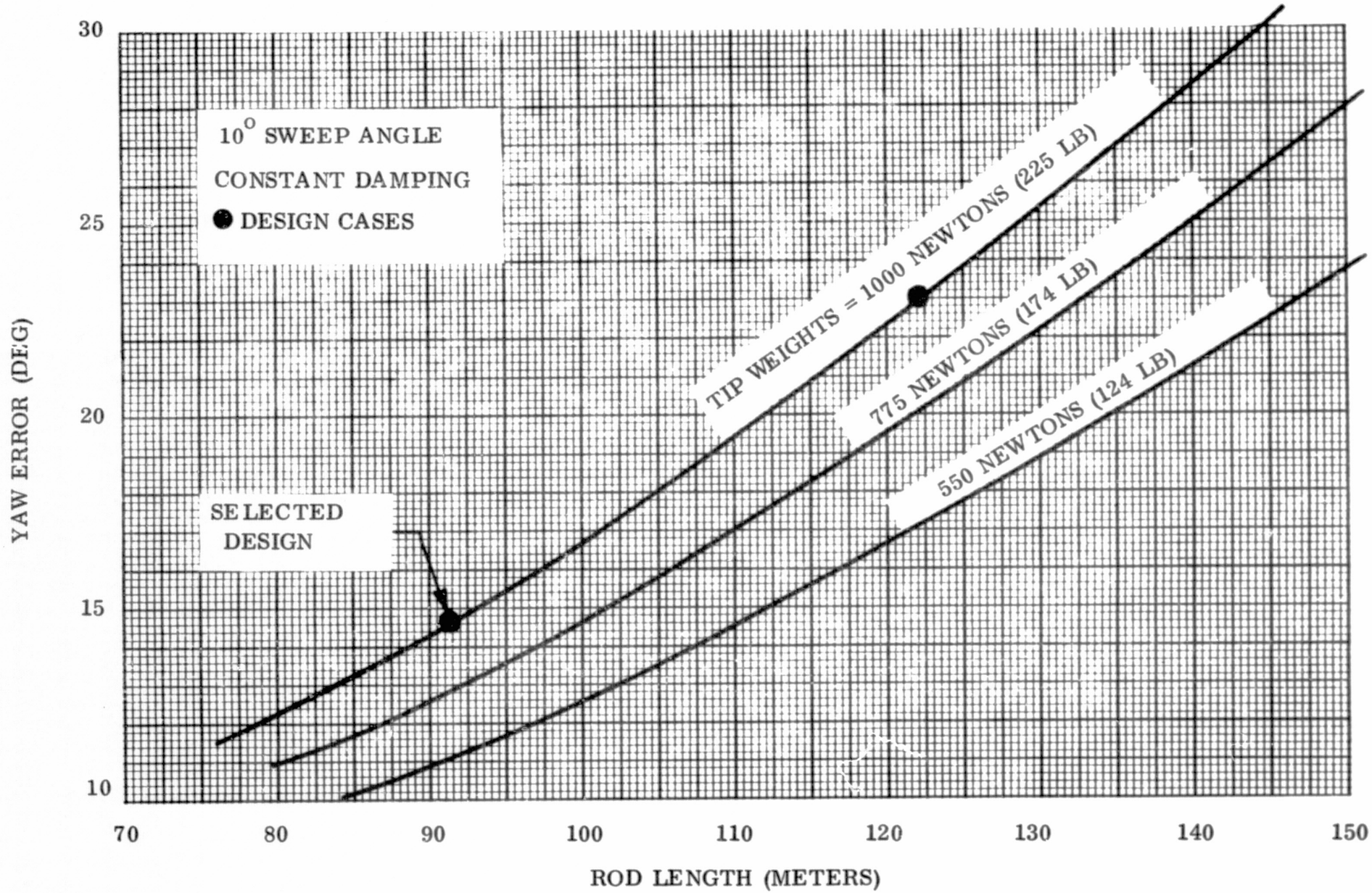


Figure 3-34. Linearized Yaw Error Versus Rod Length, Various Tip Weights

Table 3-4. Optimized S-IVB Horizontal Configuration

| |
|---|
| Rod Length - 91 meters (300 ft) |
| Rod Weight with Erection Unit - 890 newtons (200 lb) |
| Damper Weight - 780 newtons (174 lb) |
| Total Stabilization System Weight |
| (2 rods with erection units) - 3300 newtons (748 lb) |
| (2 dampers) |

3.5.3.2 Parametric Damping Characteristics

The results of a transient damping evaluation using a damping coefficient of 164 NMS. (120 ft-lb-sec) and a magnet M = 1200 amp $m^2$ (12 x $10^6$ pole cms), equivalent to a $(b/I_p \omega_o)$ = 0.026 and an $M/I_p$ = 3 are shown in Figure 3-35. The computer time constant for this run is 40 orbits. This point is shown on the damping characteristic curves in Figure 3-36. Also shown are the results of two other computer simulations. The point at a $(b/I_p \omega_o)$ = 0.02 is taken from the run shown in Figure 3-31.

The shape of the characteristics determined in previous studies is the basis for this S-IVB configuration, characterized through the points shown. Actually, this is a conservative estimate in that three of the four points shown are based upon $M/I_p$ = 3, whereas, the selected system has a value of 4.6.

Based upon the linearized error analysis, the damper induced-error as a function of damping coefficient is shown in Figure 3-37.

Combining the information of Figures 3-36 and 3-37, one obtains the damper-induced errors as a function of overall damping time to reach steady state shown in Figure 3-38. The assumption is again made that three time constants are required.

3.5.3.3 Predicted Performance Variation with Altitude

The predicted performance as a function of altitude between 400km (216 nm) and 750 km (405 nm) was established by using the performance as determined by the large angle, nonlinear program at the end points and by the slopes of the curves, between those altitudes, as determined by the linearized error program. The results appear in Figure 3-39.

S-IVB THREE AXIS HORIZONTAL CO
PLANE OF SOLAR PANELS PERPENDICULAR

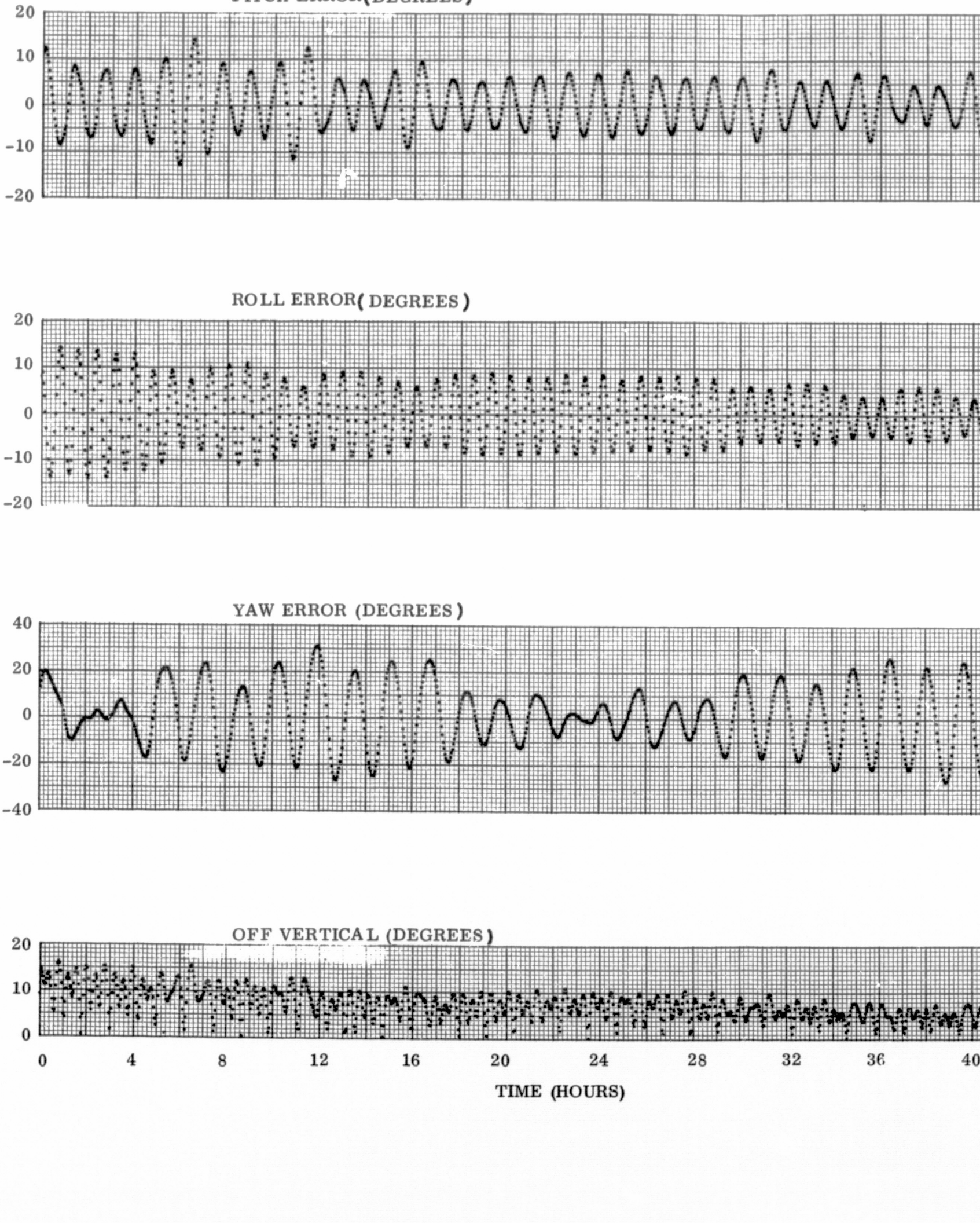

FOLDOUT FRAME 2

ORIZONTAL CONFIGURATION
RPENDICULAR TO ORBIT RADIUS VECTOR

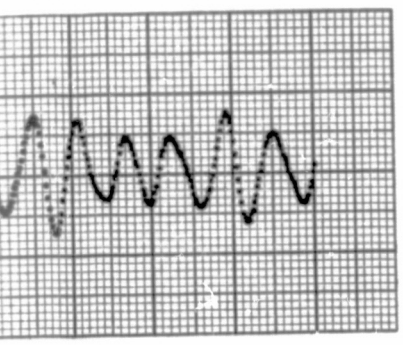

INITIAL CONDITIONS

$\theta_p = \theta_r = \theta_y = 10$ DEGREES

$\dot{\theta}_p = 0.075$ DEG/SEC

$\dot{\theta}_r = \dot{\theta}_y = 0.01$ DEG/SEC

TOTAL DAMPING

b = 164 N.M.S. (120 FT-LB-SEC)

m = 12000 AMP $M^2$ (12 X $10^6$ POLE CM)

$M/I_p = 3$

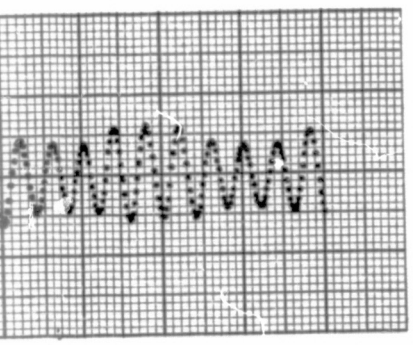

RODS (TWO)

LENGTH = 122 METERS (400 FT)

DIAMETER = 7.62 CMS (3 INCHES)

SWEEP ANGLE = 10 DEGREES

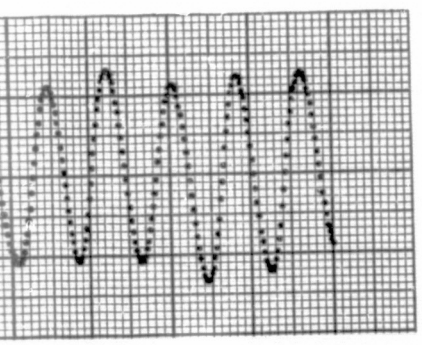

TIP WEIGHTS (TWO)

WEIGHT = 1000 NEWTONS (225 LBS)

DIAMETER = 55.9 CMS (22 INCHES)

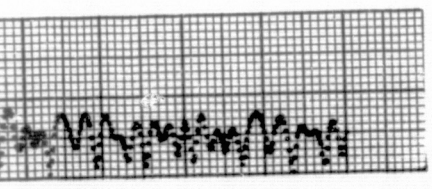


Figure 3-35. Transient Performance
b = 164 N.M.S. (120 ft-lb-sec) $M/I_p = 3$

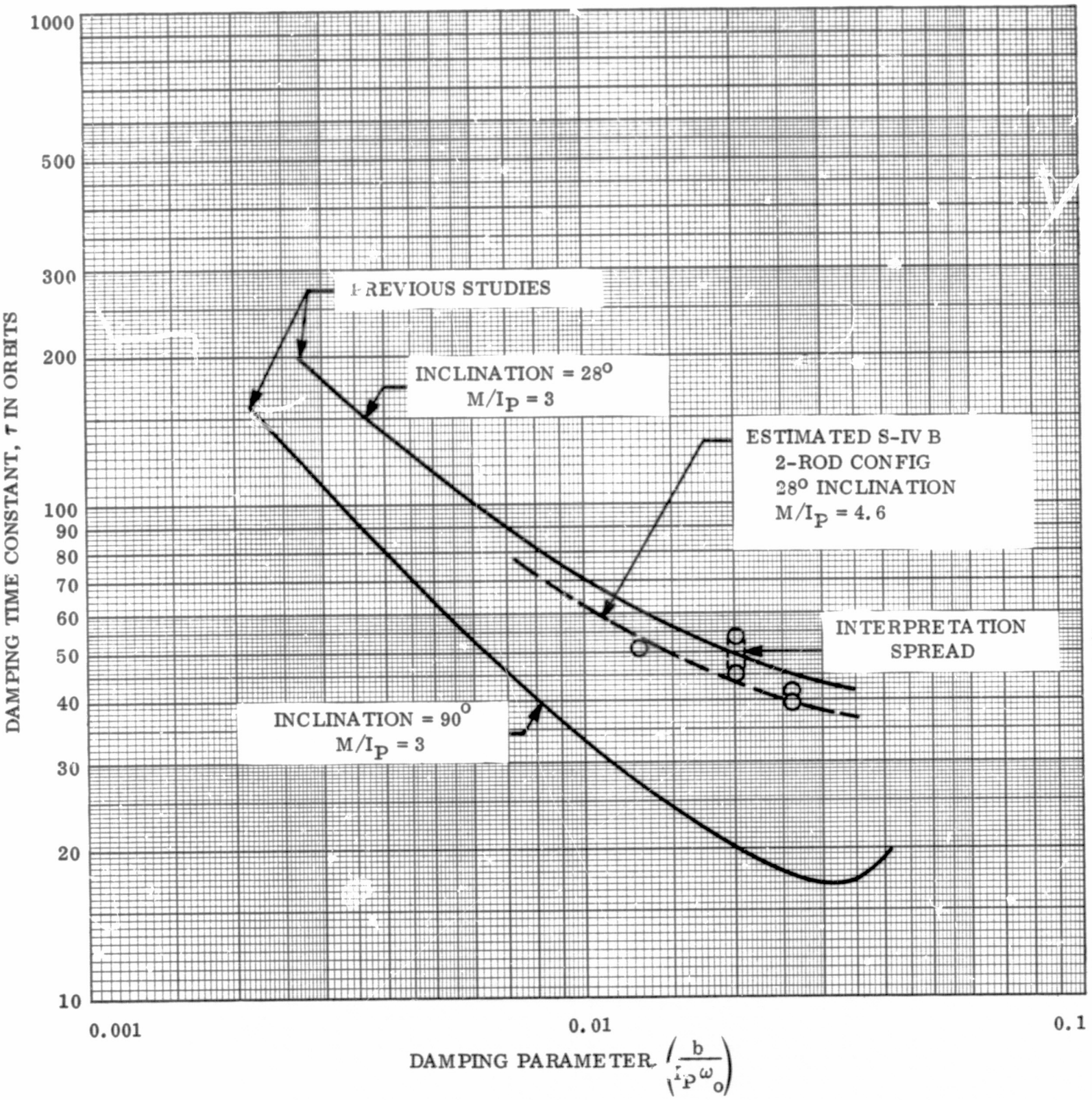


Figure 3-36. Damping Characteristics Three-Axis Horizontal Configuration

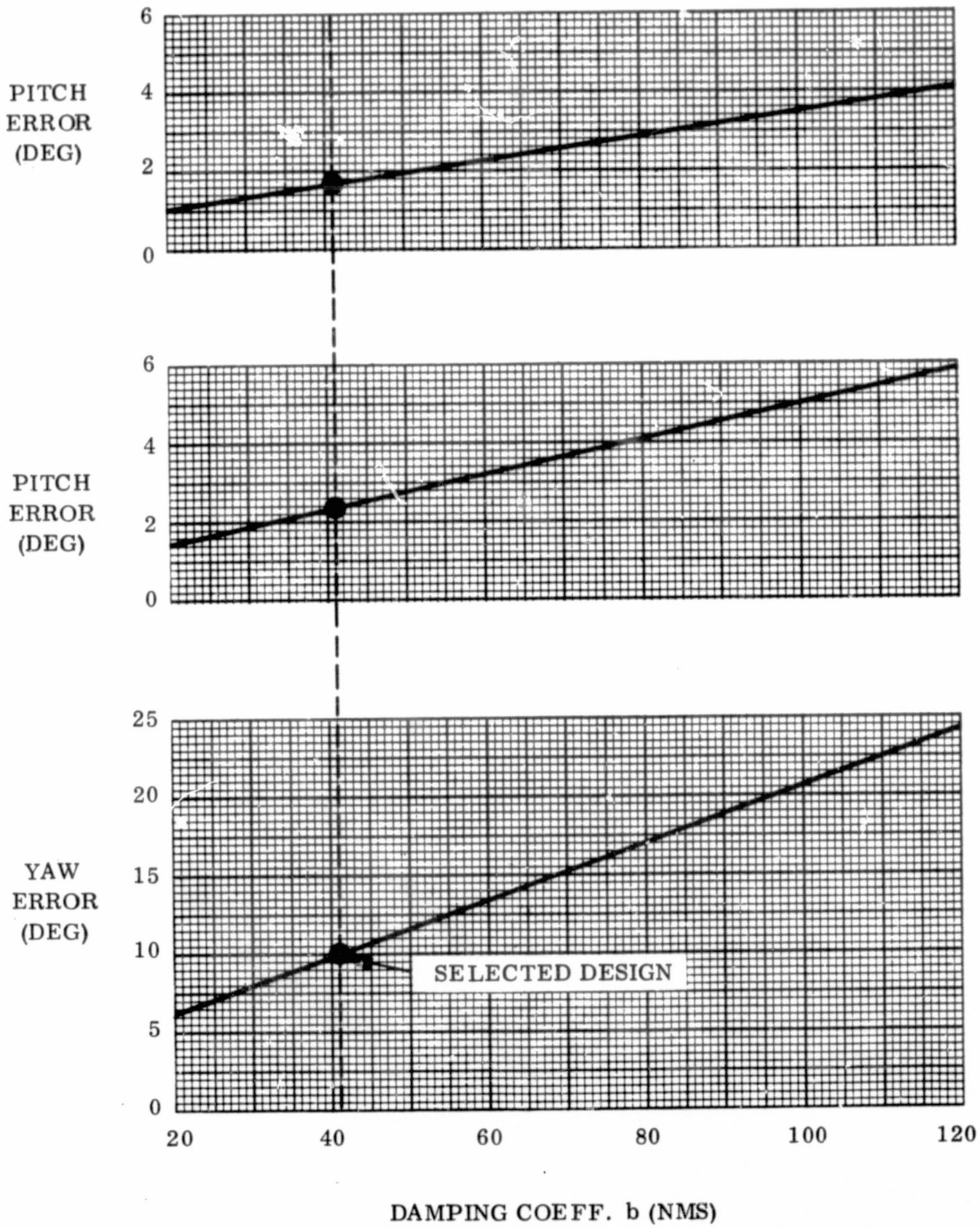


Figure 3-37. Damping Error Versus Damping Coefficients

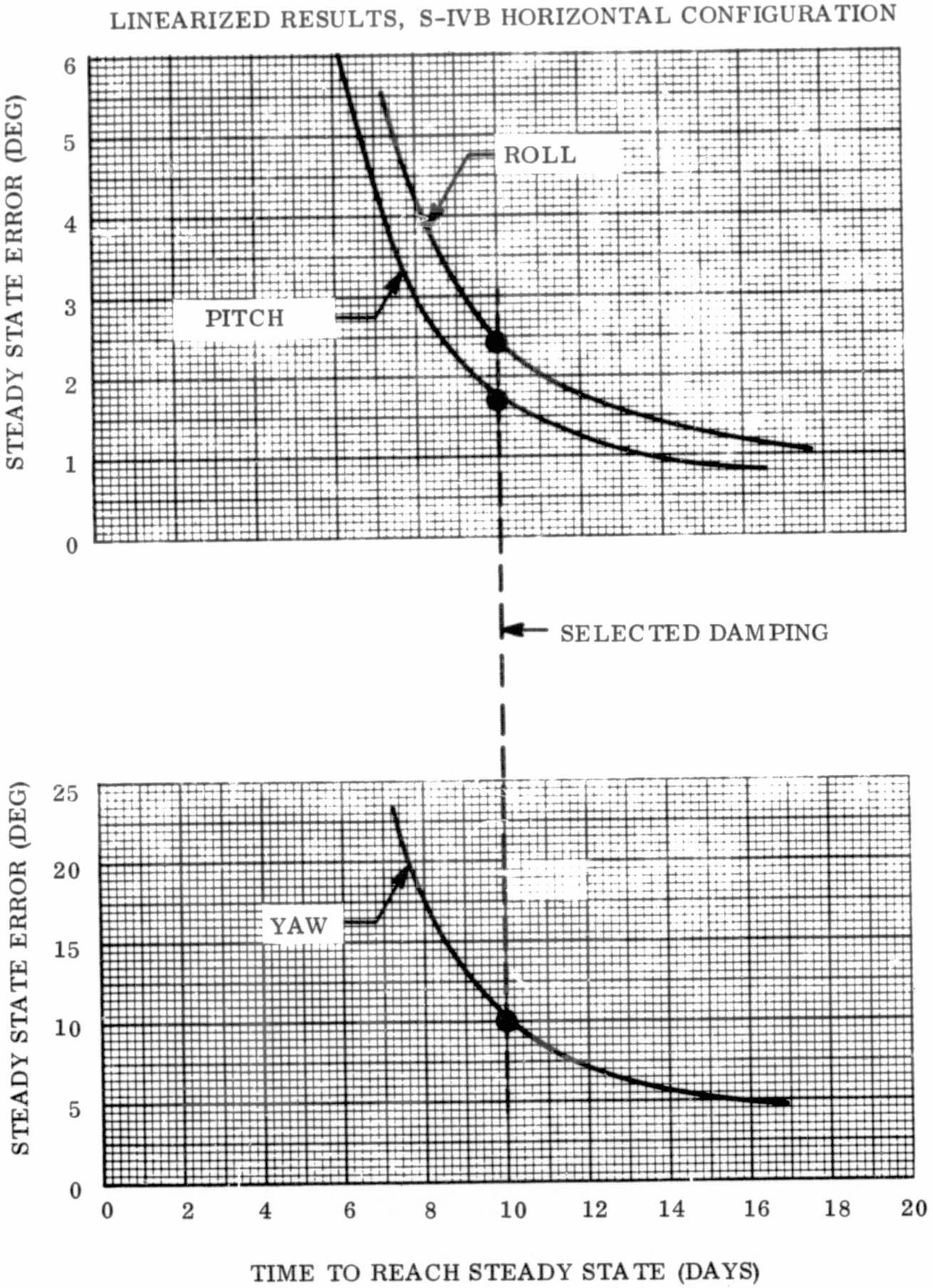


Figure 3-38. Damping Error Versus Time to Reach Steady State

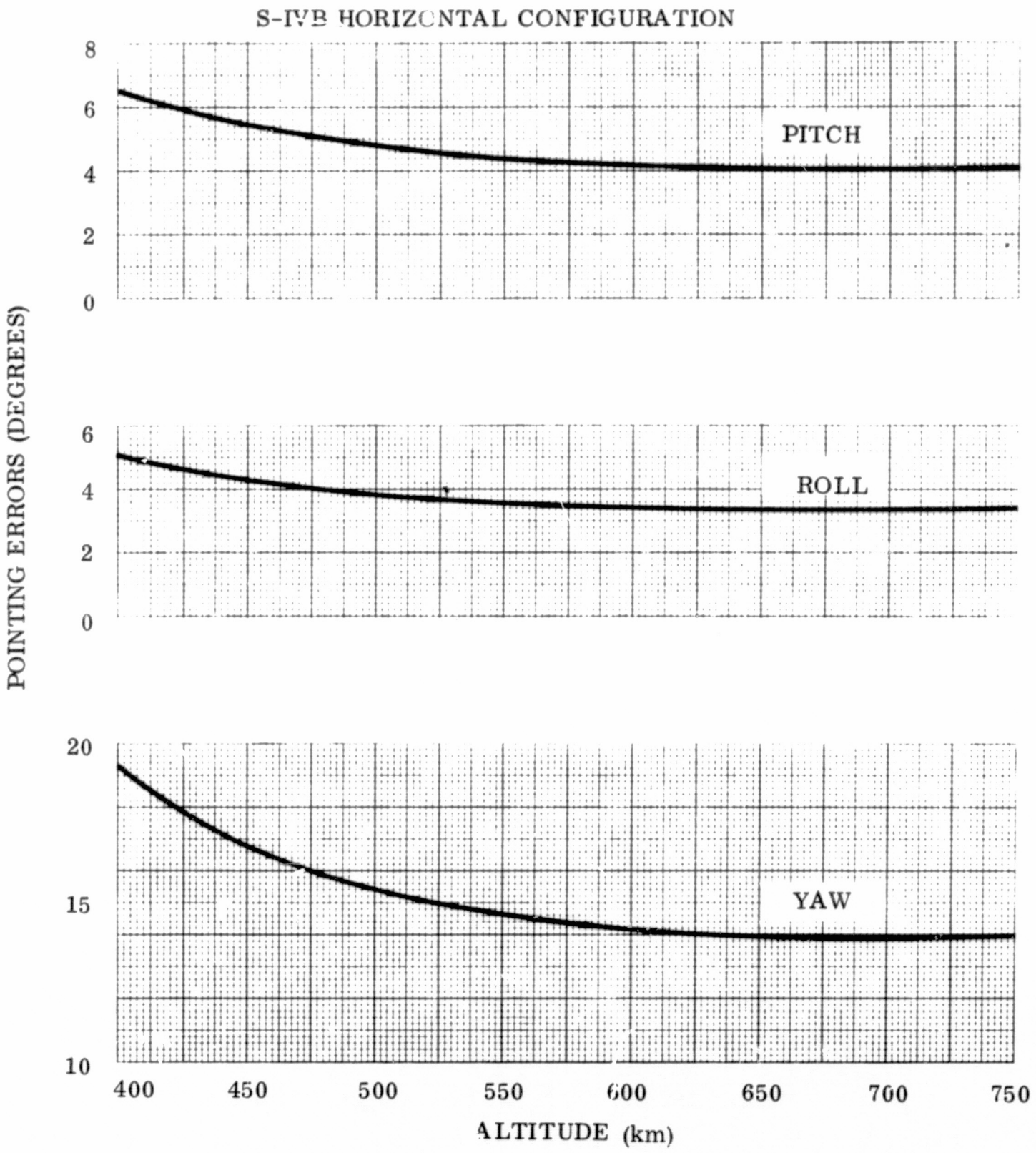


Figure 3-39. Predicted Performance Versus Altitude

SECTION 4

# DESIGN OF A PASSIVE STABILIZATION SYSTEM FOR THE LUNAR EXCURSION MODULE AT SYNCHRONOUS ALTITUDE

## 4.1 DEFINITION OF PROPERTIES

This section defines the nominal characteristics of the LEM vehicle used in the design of the gravity gradient passive stabilization system.

The LEM spacecraft is assumed to include the ascent stage, the experiment rack and all expendables (referred to as the LM-RACK configuration). In the nominal equatorial synchronous orbit, solar arrays are assumed fully deployed. A sketch of the basic vehicle is reproduced in Figure 4-1. The direction of flight is with the "Spar" package facing down and the plane of the "X" rods 8.5 degrees out of the orbit plane.

The mass and inertia characteristics relative to the reference axis system shown on the sketch are as follows:

Weight: 132, 785 newtons (29, 850 lb)

Inertias:

Pitch, $I_z$ . . . . . 166927.62 kg $M^2$ (123119 slug $ft^2$)

Roll, $I_y$ . . . . . 165942.87 kg $M^2$ (122393 slug $ft^2$)

Yaw, $I_x$ . . . . . 217277.67 kg $M^2$ (160256 slug $ft^2$)

Products of inertia assumed negligible.

Center of mass offsets from axes of symmetry:

XCM = 0

YCM = + 12.70 cm (5 inches)

ZCM = + 6.35 cm (2.5 inches)

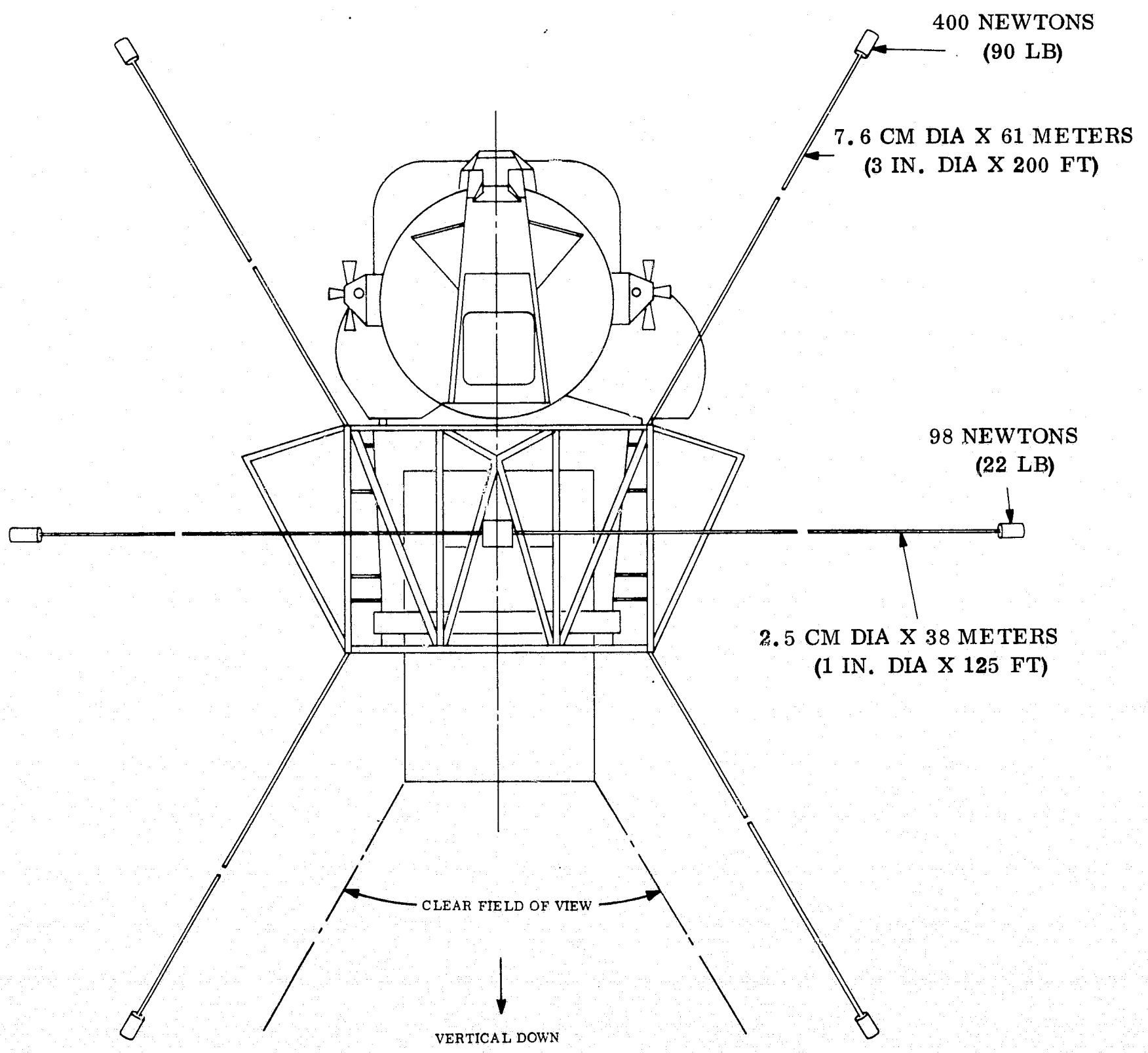


Figure 4-1. LM-RACK Synchronous Configuration

## 4.2 GENERAL APPROACH

For a synchronous orbit application, the magnetically anchored viscous type damper can not be conveniently used because pitch damping is weak and roll disturbances are large because of the characteristics of the magnetic field. Therefore, it is necessary to use a Gravity Anchored Passive System (GAPS). This method of damping satellite motion consists of utilizing a secondary body in the form of a boom or rod attached to the main body by means of a spring and damping mechanism. This secondary boom is nominally oriented in the horizontal plane with one degree of freedom of motion. If it is also aligned at an angle to the body fixed pitch or roll axis, any pitch or roll motion of the satellite will carry the damper rod out of the horizontal plane and allow gravity gradient torques to act upon it. However, the motion of the rod is restricted by the spring so that the relative motion between the two bodies is controlled by the interaction of gravity gradient forces and the spring force. The fact that relative motion does exist allows a damping mechanism to be incorporated. This may be in the form of eddy current damping or magnetic hysteresis damping. Viscous damping is not feasible due to mechanical design limitations.

There are several advantages to the GAPS type system:

a. There exists no self-induced steady state error such as the viscous damper induced error referred to in earlier sections of this document.

b. Relatively fast damping may be incorporated: less than 10 orbits to steady state compared to 30 or 40 orbits for other systems.

For this LM application, the stabilization system has been patterened after the Applications Technology Satellite system ATS-D/E. In addition to a damper boom, there is a four-rod X-boom configuration with the smaller X-angle, nominally bisecting the local vertical. The plane of the X flies nearly in the orbit plane.

## 4.3 CONFIGURATION SELECTION

The procedure followed to arrive at the selected configuration was as follows.

a. Total system inertias and inertia relationships were determined as a function of rod length, tip mass and rod orientation (X half angle).

b. Several of the more attractive combinations of rod length, tip mass, and with inertia relationships which were reasonably close to those of the ATS-D were selected for evaluation in an ATS generated computer routine referred to as the "optic." This is an optimization program designed to find the minimum damping time for a GAPS-type configuration. Based upon the fixed input inertia ratios (i.e., $I_y/I_p$, $I_x/I_p$, $I_{damper}/I_p$), the program defines the required nondimensionalized spring constant and damping coefficient, along with the damper boom orientation, which will result in the minimum damping time.

c. From the results of the "Optic" program, a configuration with a time constant of 3.3 days (10 days to steady state) was selected for evaluation in the large-angle, nonlinear digital simulation program. From the above procedure, the following configuration was selected.

### 4.3.1 GRAVITY GRADIENT RODS

Four 7.6-cm (3-inch) rods in the form of an X are mounted rigidly to the LM vehicle from convenient external surfaces. Each of the four rods are 61 m (200-ft) long and the plane of the X is rotated 8.5 degrees about the spacecraft yaw axis, out of the orbit plane, clockwise looking Earthward. Each of the four rods will carry a 400 newton (90 lb) tip weight.

### 4.3.2 DAMPER BOOM

The damper boom will consist of two 2.5-cm (1-inch) diameter rods, each 38 M (125 ft) long, with tip masses of 98 newtons (22 lb) each. The booms are mounted rigidly to the platform in back-to-back fashion so that when fully deployed they appear and react as one continuous rod. The nonpowered self erecting storage units deploy forming the rod tip masses. The "rod" axis will lie nominally in the roll-pitch plane, but rotated 60 degrees clockwise about the local vertical from a line parallel to the spacecraft roll axis. The damper must have one degree of freedom of motion relative to the spacecraft, but restrained with a spring having a total spring constant of 8222 dyne-cms/radian ($6.064 \times 10^{-4}$ ft-lb/rad). The damper motion will be such as to allow the axis of the damper boom to rotate $\pm 45$ degrees out of the pitch-roll plane and perpendicular to that plane. A damping mechanism will also be incorporated, between the platform and the spacecraft, having a damping coefficient of $2.953 \times 10^{7}$ dyne-cm-secs (2.178 ft-lb-sec).

## 4.3 TOTAL SYSTEMS INERTIAS

The selected configuration has the following moments of inertia when the rods are deployed.

| | | | | |
|---|---|---|---|---|
| Main body: | I pitch | = | 1,139,266 kg $M^2$ | (840,278 slug $ft^2$) |
| | I roll | = | 1,025,399 kg $M^2$ | (756,250 slug $ft^2$) |
| | I yaw | = | 341,799 kg $M^2$ | (252,083 slug $ft^2$) |
| Damper Boom: | I boom | = | 34,178 kg $M^2$ | (25,208 slug $ft^2$) |

## 4.4 NOMINAL PERFORMANCE

The selected configuration was evaluated in the large angle, nonlinear, digital computer program known as the ATS Math Model. This program is similar to the one used for the S-IVB evaluations, but has the capability of simulating a two-body spring-coupled system.

All significant disturbances were included in the simulation: Solar pressure effects relative to center pressure - center of mass offsets, solar heating relative to rod thermal bending effects and vehicle magnetic dipole effects. Solar torque computations were based upon the following surface characteristics:

| Surface | Absorptivity | Specular Reflectivity | Diffuse Reflectivity |
|---|---|---|---|
| Solar Cells | 0.65 | 0.35 | 0.00 |
| Rods | 0.14 | 0.70 | 0.16 |
| Tip Weights | 0.10 | 0.80 | 0.10 |
| All other surfaces | 0.20 | 0.40 | 0.40 |

A vehicle magnetic dipole of 30 amp $m^2$ (30,000 pole cm) was assumed to be oriented on the spacecraft roll axis. This is a worst-case-type orientation relative to yaw performance. The gravity gradient rod characteristics used were those of the 7.6 cm (3-inch) silver-plated copper beryllium rod.

The main body of the LEM is simulated by two cylindrical shapes with the long axis vertical. The cylindrical dimensions used are as follows:

| | Diameter | Length |
|---|---|---|
| Upper | 3.353 meters (11.0 ft) | 5.334 meters (17.5 ft) |
| Lower | 2.073 meters (6.8 ft) | 1.402 meters (4.6 ft) |

The plane of the deployed solar panels is assumed to be at the intersection of the cylinders. These panels are simulated by flat plates with estimated surface characteristics for both sides. Each panel is 13.97 by 2.54 m (45.83 by 8.33 ft). The plane of the panels is perpendicular to the local vertical, two panels centered on a line parallel to the roll axis (forward and aft) and two on a line parallel to the pitch axis (right and left).

The simulation was started at the midnight - spring equinox point and extends for 300 hours (12.5 orbits). The results are shown in Figure 4-2 in terms of the usual Euler angles. A clean once-orbital oscillation is seen on all three axes. Steady state pointing accuracies for this system will be:

Pitch: $\pm 6^{o}$

Roll: $\pm 0.5^{o}$

Yaw: $\pm 2.8^{o}$

Tilt: $6.4^{o}$

up to $1^{o}$ of additional error will be caused by rod nonstraightness.

Figure 4-3 represents a transient performance evaluation of the selected design starting from initially large angles. As may be observed, initial angles are: pitch 45 degrees, roll 20 degrees, and yaw 10 degrees from the nominally preferred orientation. The run represents ten orbits which should have resulted in three time constants; however, it appears that steady state amplitudes have not quite been obtained. Errors at the 10-day point appear to be:

FOLDOUT FRAME /

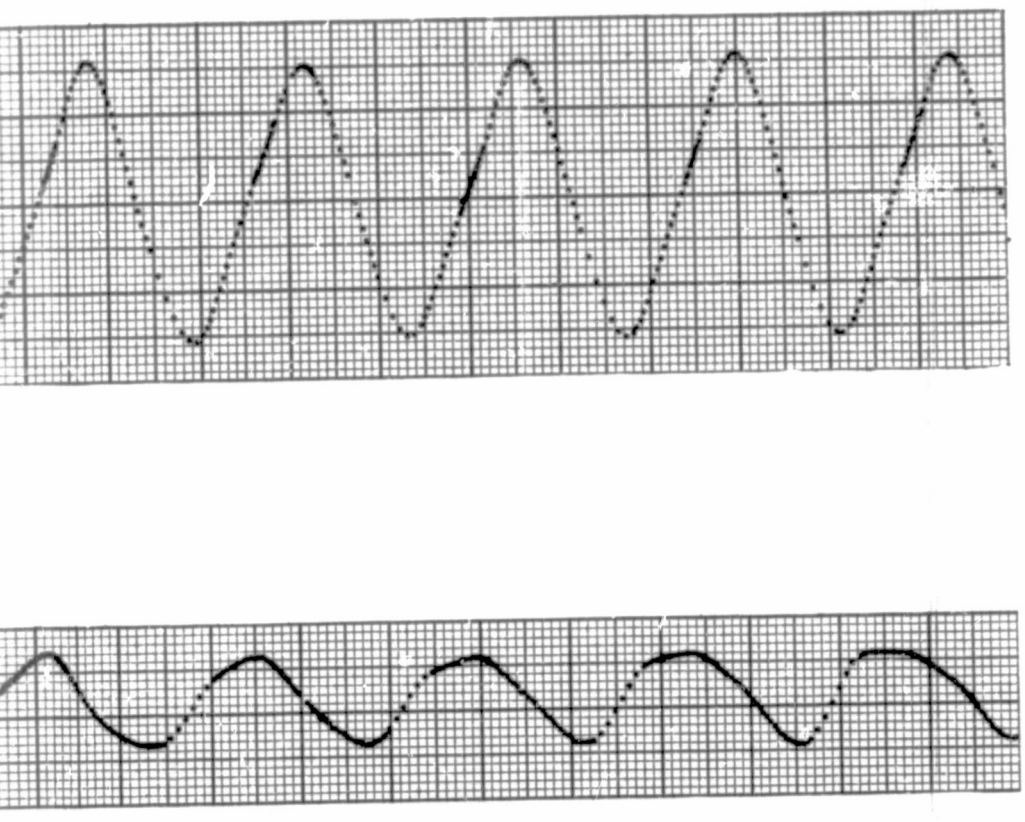

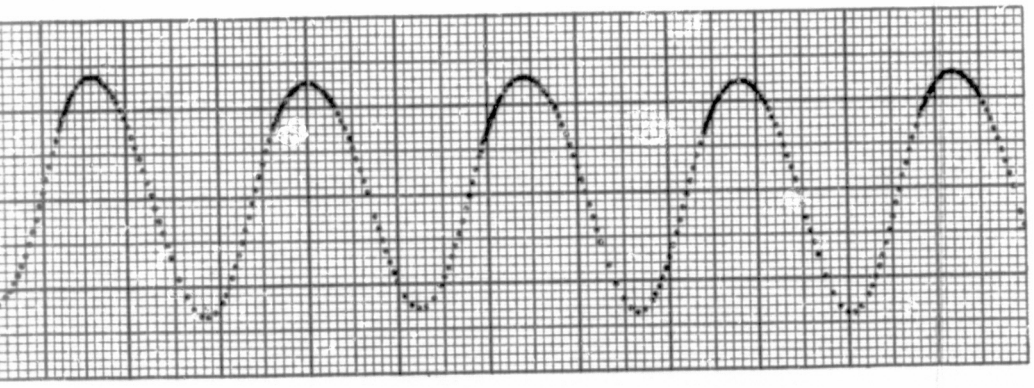

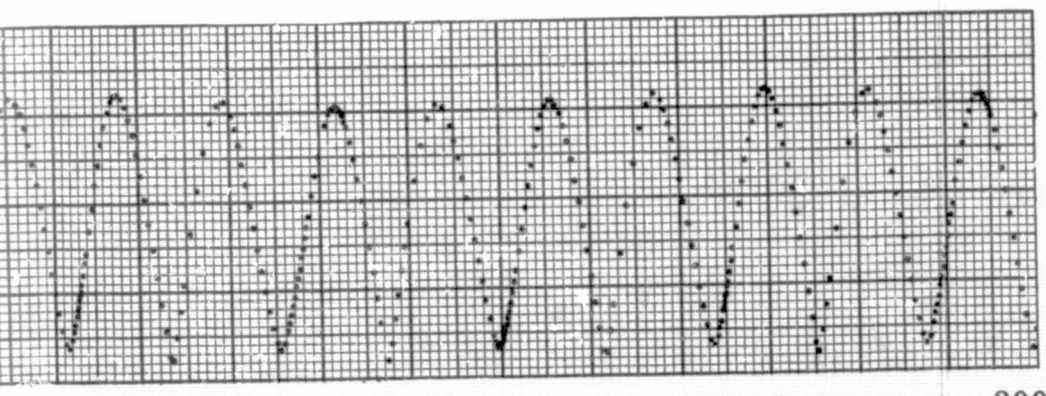

200 300

CONFIGURATION

GRAVITY GRAD. X RODS (4)

LENGTH = 61 M (200 FT) EA.
DIA. = 7.6 CMS (3 IN.)
X HALF ANGLE = $20^{o}$

TIP MASSES ON X RODS (4)

WT. = 368 N. (90 LB) EACH
APPROX. DIA. = 46 CMS (18 IN)

DAMPER RODS (TWO)

LENGTH = 40.25 M (132 FT) EA.
DIA. = 7.6 CM (3 IN)
SPRING CONSTANT = 8222
DYNE-CMS/RADIAN
($6.06 \times 10^{-4}$ FT-LB/RAD)
DAMP. COEFF = $2.953 \times 10^{7}$
DYNE-CMS-SEC
(2.178 FT-LB-SECS)
TIP WTS. = 98 NEWTONS (22 LBS)

INITIAL CONDITIONS

$\theta_p = \theta_r = \theta_y = 0$

$\dot{\theta}_r = \theta_y = 0$

$\dot{\theta}_p$ = ORBITAL RATE

Figure 4-2. LM-RACK Steady State Performance

FOLDOUT FRAME 1

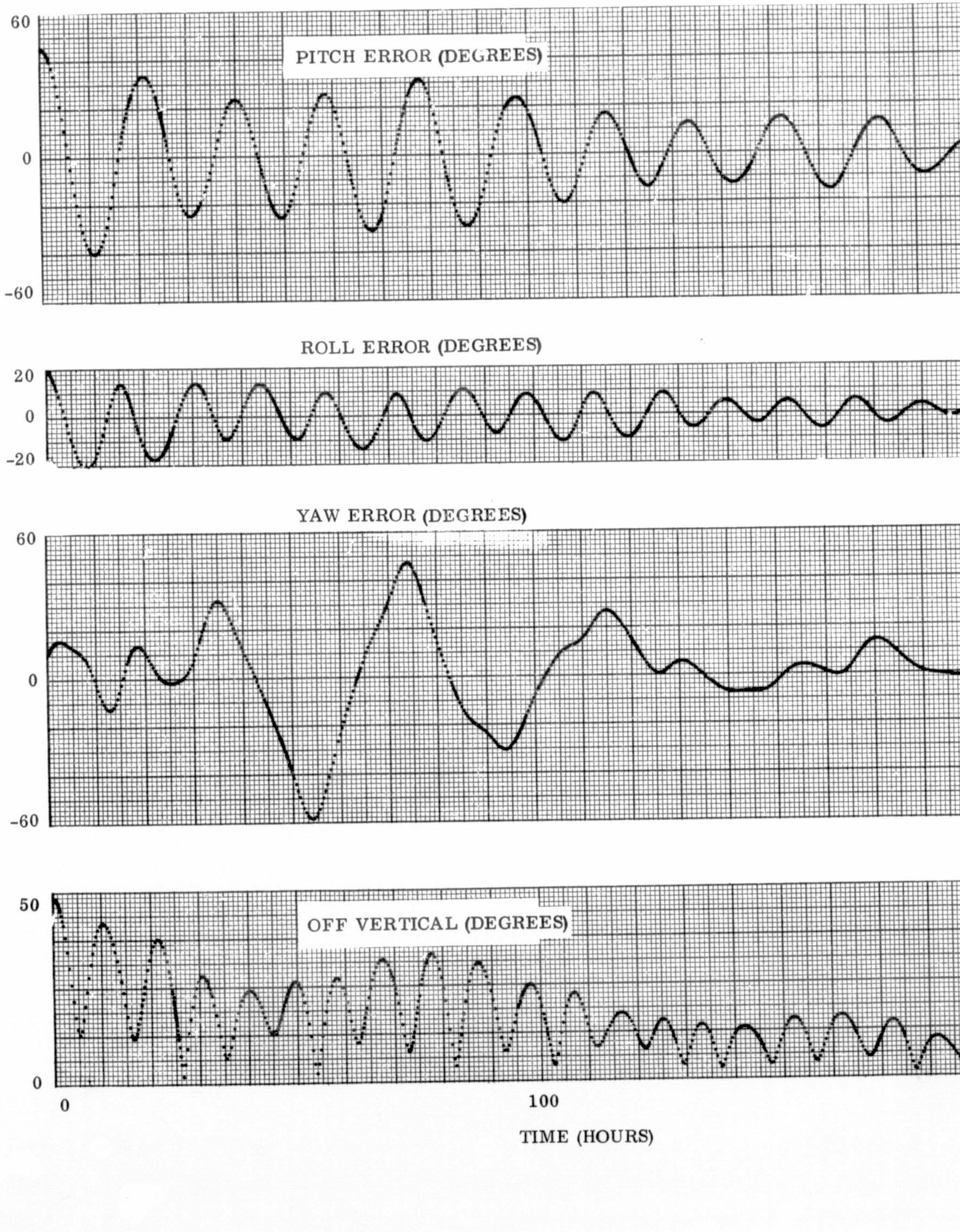

FOLDOUT FRAME 2

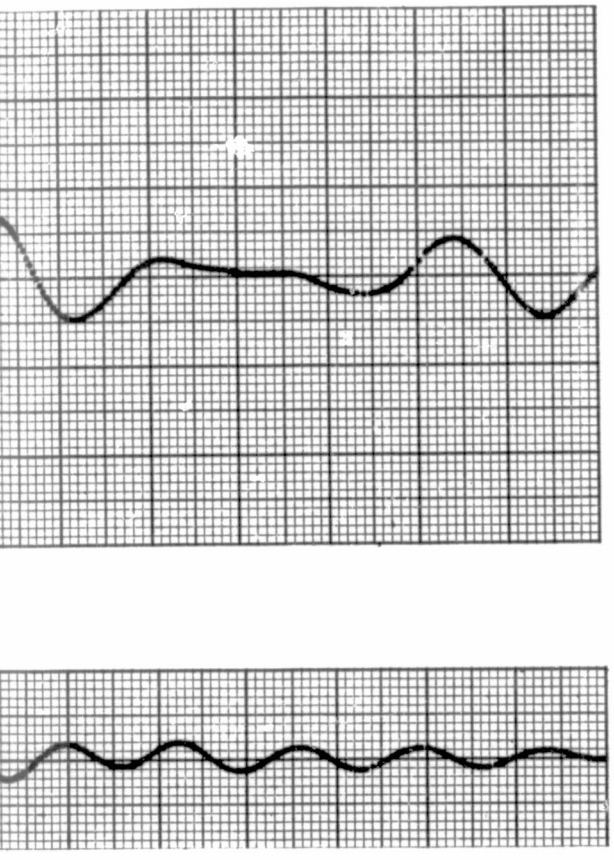

CONFIGURATION IS THE SAME AS FIGURE 4-2 (PRECEDING PAGE)

INITIAL CONDITIONS

$\theta_p = 45^o$

$\theta_r = 20^o$

$\theta_y = 10^o$

$\dot{\theta}_p$ = ORBITAL

$\dot{\theta}_r = \dot{\theta}_y = 0$

200 240

Figure 4-3. LM-RACK Transient Performance

Pitch: $\pm$ 8.5°

Roll: $\pm$ 2.0°

Yaw: $\pm$ 6.0°

Keeping in mind the pointing accuracy requirement is $\pm$ 15 degrees, this will be realized within 160 hours (< 7 days).

## 4.5 PARAMETRIC TRADEOFF STUDIES

For the purposes of predicting performance variation as a function of rod length and tip weight, the linearized error determination program was used. The LEM spacecraft was simulated by 12 flat plates, 8 cylinders, and 7 spheres, including all rods and tip masses. The surface coefficients used are the same as those used for the large-angle, nonlinear predictions. Again a spacecraft magnetic dipole of 30 amp meters$^2$ (30,000 pole cm) was assumed.

The following comparison of the linearized and nonlinearized results for the selected configuration shows good agreement:

| | Nonlinear Results | Linear Results |
|---|---|---|
| Pitch Error | $\pm$6.0° | $\pm$4.9° |
| Roll Error | +0.5° | $\pm$0.6° |
| Yaw Error | +2.8° | +2.6° |

This comparison is made for the case of the sun in the orbit plane, which normally results in "worst-case-type" solar error relative to pitch performance. Maximum roll and yaw solar error will usually exist at the maximum sun angle to the orbit plane. In an equatorial orbit this maximum angle is 23.45 degrees. The linearized evaluation at this angle produces the following errors: pitch 4.1 degrees, roll 2.9 degrees, yaw 5.4 degrees.

Figure 4-4 shows the linearized predicted performance as a function of rod length for various tip masses at the minimum and maximum sun angles. These results have been scaled to agree with the nonlinear performance predictions.

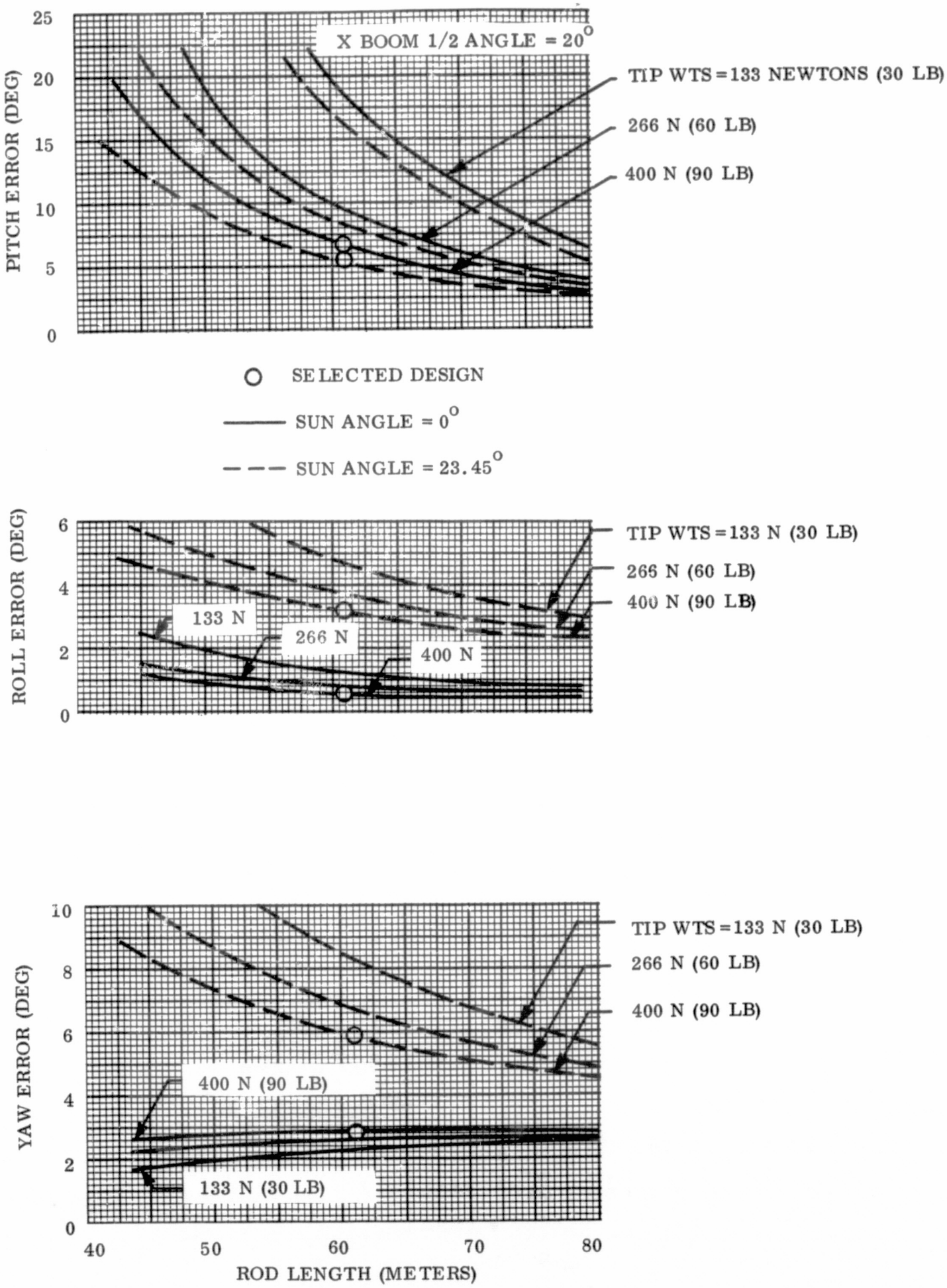


Figure 4-4. LM-RACK Parametric Performance

# SECTION 5

# GRAVITY GRADIENT ROD AND TIP MASS FLIGHT EXPERIMENT

## 5.1 EXPERIMENTAL GOALS

Analysis and experience verified that the gravity gradient forces felt by a body in orbit can be effectively used in attitude control systems. Experience with small unmanned satellites has shown that the use of long extendible rods for obtaining favorable inertia distribution is both feasible and practical. The particular rod configurations suitable in these applications create problem areas which are somewhat unique. As applications are made to larger spacecraft, the required rod lengths and end masses extend into ranges not previously used, with the attendant possibility that the unique problem areas may be emphasized.

The particular areas of concern are caused by the low stiffness of the rod configurations. With the small stiffnesses available, in a 1-g field the applied load on the rod due to gravity acting upon the mass is large compared to the capability of the rod to support the load. These forces then become so overpowering that many effects of smaller magnitude are completely or partially masked by the large body forces. For example, the measurement of straightness of an extended rod is a major undertaking:

a. If the rod is extended vertically upward, any lack of straightness is magnified by the beam column effects of gravity forces.

b. If it is extended vertically downward, the tension due to rod weight tends to minimize lack of straightness.

c. If it is extended horizontally, deflection due to rod weight completely masks the stress-free position and can even cause structural failure.

Thus, the various methods of measuring rod straightness all utilize some type support which can, hopefully, exactly balance the weight but not provide an extra deforming force. From a mechanical standpoint, suspension horizontally in a fluid having the same specific gravity as the rod would appear to be the ideal system. If such a fluid could be found, potential problems of corrosion or damaging surface deposition and availability of

fluid and sufficiently large test tanks still would exist.

In the orbital environment, the force of gravity acting upon the mass of the rod is almost equalized at every location on the rod by the centrifugal force due to orbital rate so that static and dynamic behavior is not completely dominated by the gravity force. Characteristics which are of negligible importance on the Earth are the dominant items in the orbital environment.

Additional variables exist in the area of thermal deformation of rods. Here, in addition to the large gravity forces present at the Earth's surface, experimental problems exist in the elimination of convective heat transfer and simulation of the solar spectrum. Since prediction of the rod position requires an initial knowledge of the straightness and orientation of the rod, the temperature distribution, and a defintion of the structural stiffness constraint, many difficulties exist in experimental validation of analytical predictions. At least two differing formulations for the thermal deformation of rods under known temperature distributions have been published. No definitive ground tests have been performed; some results exist which appear to support the opposing contentions of the two analyses.

Flight experience is limited to the overlapped tube configuration. This configuration is completely lacking in structural continuity at the overlap which results in freedom of the section to breath and warp in addition to the shear, twist, stretch, and bending deformations which would be anticipated in a closed tube.

The digitated rod configuration, which is considered an alternate to the plain overlapped tube, provides an additional shear constraint to the configuration. As a result, the stiffness and structural stability are improved. However, the additional constraint would be anticipated to increase the thermal deformation resulting from the same thermal flux. Additional ground testing is indicated because it is at this location that the test conditions can be controlled and measured most readily and accurately. However, the significant behavior for the intended use may still be obscured. Therefore, some careful measurements are needed in the nearly zero-g, hard vacuum space environment to verify that surface observations are valid.

Of course, when we move from the difficulties of eliminating large order deviations from operating environment inherent in Earth surface environment to the space environment we encounter new problems of measurement, boundary conditions and an inability to control the environment.

The experiments selected and the procedures outlined are chosen to minimize, as far as possible, extraneous disturbances, provide means of nulling out their effect, or provide measurements to remove them analytically.

The experiments will be considered successful if they provide points of data on measured performance of long extendible rods under known conditions of altitude, attitude, body rates, excitation and solar incidence so that a valid comparison with predicted performance can be obtained. The greatest possible separation of modal frequencies, body rates and orbital rates by means of rod/tip weight selection and control of disturbances to the vehicle is advantageous so that isolation and separation of any analytical deficiencies are enhanced.

### 5.1.1 POSSIBLE FLIGHT MEASUREMENTS

The problems inherent in measurement of rod characteristics at earth surface were discussed in the previous paragraph.

Although most of the major flaws in surface experimentation are eliminated in flight experiments since actual environments are experienced, these are replaced by problems inherent in the flight conditions. Two major problems place severe limitations on the amount and quality of data obtainable. These are:

a. Controllability of Conditions

In most cases it is desirable to establish a predetermined attitude and hold it with no disturbance so that careful measurements can be made with respect to a fixed reference. This is not possible. Unintended disturbances will always be present to some degree and measurement must be made in such a manner (usually on a continuous basis over a period of time) that the extraneous effects can be corrected for. In addition, the desired initial conditions cannot normally be anticipated to be achieved exactly so that some loss might be expected from this source.

b. Reference for Measurements

> All measurements must be made with respect to a moving reference system, and the relation to a suitably fixed reference cannot be established with precision. The ability to measure the physical parameters desired (such as deflection) suffers a severe loss in precision relative to ground measurement and the number of coordinates which may be observed is severely curtailed.

The choice of possible experiments must be made with the purpose of achieving measurements which can either verify or provide information to modify either the description of the rod or the description of the environment used in predictions.

The basic parameters which have been considered as potential candidates for isolation by flight experiment are:

A. Rod Characteristics

1. Stiffness
2. Straightness
3. Deflection due to temperature gradient
4. Temperature distribution due to solar flux
5. Rod Damping

B. Environmental Characteristics

1. Aerodynamic drag
2. Solar pressure
3. Gravity gradient
4. Solar spectrum

A fundamental consideration has been that the primary purpose of this experiment is to obtain information about the flexible rod. The environmental effects are considered primarily from the standpoint of their effect on the rod, not as justification for an experiment. In most cases an experiment which did not have the added effects of flexibility would be better for determination of environmental forces.

Practical measurements appear to be limited to:

a. SIVB attitude with reference to the Earth Sun or magnetic to a nominal field

b. SIVB body rates either directly or available by differentiation from attitude measurements

c. Position of rod end mass target relative to the SIVB

d. Temperature distributions measured by thermocouples

e. Time history of planned disturbances

The potential candidate experiments are divided into dynamic experiments and static experiments. These candidate experiments are listed below in Table 5-1.

Table 5-1. Rod Flight Experiment Candidates

| | |
|---|---|
| I. | Dynamic |
| | A. Extension - retraction |
| | B. Thermal impulse |
| | C. Forced vehicle motion |
| | D. Impulse at end mass |
| II. | Static |
| | A. Zero disturbance straightness measurement |
| | B. Aerodynamic drag bending |
| | C. Thermal bending |
| | D. Solar pressure bending |
| | E. Gravity sag |
| | F. Temperature distributions |

The measurements of aerodynamic drag and solar pressure and gravity sag are environmental effects which are not the prime objective of this experiment. The measurement of aerodynamic drag and solar pressure in particular are considered to be undesirable disturbances which should be minimized rather than measured.

Their effect is small and appears at this time to be very difficult to detect.

The aerodynamic drag (II-B) experiment was originally considered primarily because the aerodynamic drag can act as a disturbance to attempts to measure rod straightness and would require measurement to null it out. Measurement of aerodynamic drag is practicable only by measuring very accurately the moments and shears at the root of the rod and it is a function of the altitude and the attitude and geometry of the rod. Measurement of the atmosphere at the particular experimental altitude is not a primary experimental objective, and since straightness indications can be obtained without the shear and moment measurements, it is no longer considered as an individual experiment.

The solar pressure experiment (II-D) is again a secondary result of the presence of solar pressure at all times in which sunlight directly impinges on the rod. It was originally considered that this effect would require measurement to separate bending due to solar pressure from bending due to solar heating. This effect is considered of negligible (unmeasurable) effect within reasonable measurement capability and is eliminated from further consideration.

Gravity sag experiments II-E are considered to be of secondary importance. The bending of an orbiting rod in the gravity field is not a negligible effect; however, it is completely described by the stiffness and mass distribution and orientation of the rod and its altitude. If these quantities are known, there is no lack of confidence in capability for prediction of gravity sag. The quantity in which low confidence exists is the rod stiffness distribution. This characteristic is considered to be verified better by other experiments (I-C or I-D). A specific experiment to measure gravity sag is a possible candidate for a secondary experiment if a long unmanned period in which the control system is off is available. This is required in order to obtain the minimum dynamic motion of the rod possible. This in turn requires the vehicle rod configuration to be gravity gradient stable when the rod is at an acute angle with the Earth vehicle line.

### 5.1.2 EXPERIMENTAL PROCEDURES

Each of the remaining proposed experiments will be discussed and the required measurement specified, then the instrumentation and data will be discussed.

### 5.1.3 STATIC EXPERIMENTS

Rod Straightness - The measurement of rod straightness requires that the rod be placed in a force free field which is also free of the thermal distortion effects. The first requirement can be nearly met by orienting the vehicle so that the rod lies along the velocity vector. The second requirement can be met when the rod is in shadow. This can be met during passage of the vehicle through the umbra or during some parts of the orbit by shadowing the rod with the vehicle. Because the planned orbit plane very nearly includes the Sun-Earth axis, this condition is met at certain portions of the orbit if the rod lies in the orbit plane.

Measurement will be photographic and must be taken for a period at least equal to the period of the lowest natural frequency of the rod so that the mean position can be determined. Vehicle body rates and orientation will also be required as well as a means of illumination because the rod and end mass (target) will be in shadow.

The vehicle control system will be required to bring the vehicle to the proper attitude and stabilize it with minimum disturbance then to be turned off before rod extension and during the period of measurement to prevent external disturbance from affecting data. The geometric configuration must be such that gravity gradient torques do not significantly alter the attitude nor bend the rod during the period required to quiet the system and during the measurements.

The nominal rod location is shown in Figure 5-1.

Thermal Bending - the measurement of thermal bending requires that the rod be placed in a force free field in which the thermal exchange with the solar field is near maximum.

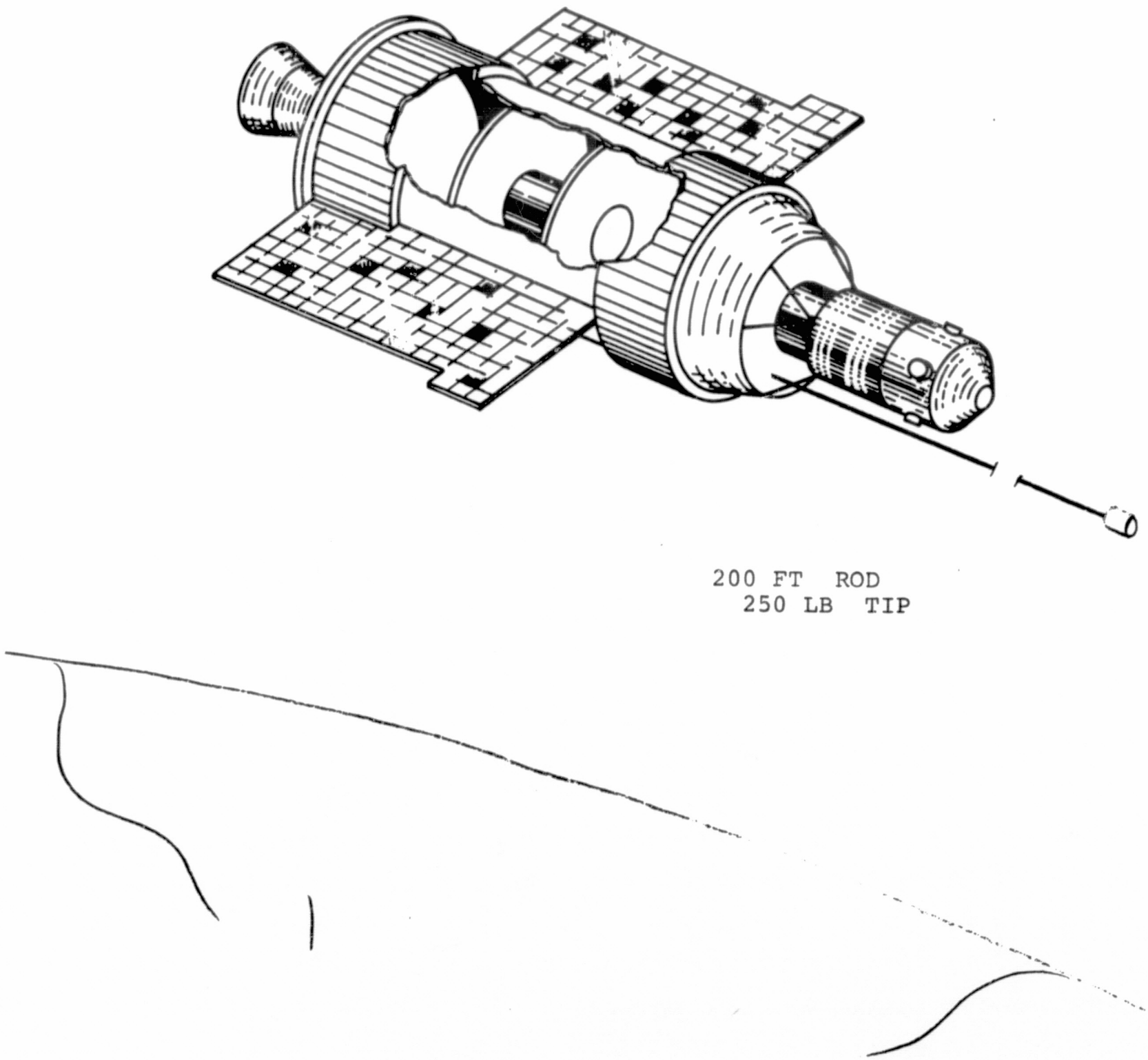


Figure 5-1. Reference Axes for Rod Flight Experiment

This maximum condition is to be sought in order to obtain the largest distortion measurement possible. The first requirement can be very nearly met by orienting the vehicle such that the rod lies in a plane which includes the vehicle center of mass and is perpendicular to the orbital radius vector. Because the anticipated orbit plane very nearly includes the Sun-Earth axis, this condition is met throughout the orbit if the rod is extended perpendicular to the orbit plane and at satellite noon if the rod is in the orbit plane. The attitude and stability requirements are met with the same conditions as the straightness test.

Data should be taken for (1) periods of at least equal to the lowest natural frequency of the rod and (2) at eight points in an orbit to obtain the effect of circumferential sun orientation on thermal deformation. The active control system is off during measurement.

Measurements required are vehicle attitude, and body rates. Orbital position (for sun orientation) and photographic measurement of rod position.

This experiment will be run in conjunction with the thermal impulse experiment discussed later.

Temperature Distribution -This experiment requires a separate rod from all other experiments. It can be performed at any time,but portions should be performed in conjunction with the thermal deformation experiment.

The specimen required is a short (< 10 ft) length of rod identical to the rod used in the other experiments. This rod will be erected with the same orientation as the primary rod experiment during the thermal bending tests. At a sufficient distance from the vehicle at which longitudinal thermal flow is negligible, thermocouples will be mounted in eight (8) circumferential locations. During the thermal bending tests, temperatures from the eight (8) thermocouples will be read. During other periods of the flight when various solar incidence angles are experienced, additional measurement should be made.

This experiment is considered necessary both as an adjunct to the thermal bending experiment and as a complete experiment in its own right because the solar spectrum is known only approximately, the measured absorptivity and emissivity are a function of the incident spectrum, and ground testing has not approached the total solar flux.

### 5.1.4 DYNAMIC EXPERIMENTS

Thermal Impulse - This experiment is set up in conjunction with the static measurement of thermal bending. The phenomenon results from the fact that when the vehicle passes from sunlight into the Earth's shadow the rod reaches a condition of uniform circumferential temperature distribution in a very small fraction of the lowest natural frequencies of the rod. This produces a condition analogous to the simple displacement of the mass in a spring mass experiment, except that instead of a single displacement, the rod is deformed into some shape which is not necessarily the shape of a pure mode. The action is additionally complicated by the adjustment which occurs during passage through the penumbra between full sunlight and full shadow.

Measurements made during the thermal bending experiment just before leaving full sunlight are continued through a period of at least three times the period of the lowest natural frequency of the rod after entry into the umbra. Temperature measurements from the temperature distribution specimen should be obtained during this total period.

The experiment is repeated during emergence from the shadow into sunlight. Here measurements are started at least one natural period before leaving a shadow and continued through three periods after emergence from the penumbra.

Data required are vehicle attitude and body rates and photographic records of rod position. The active control is off and illumination of the end mass target is required. Thermocouple readings from the temperature distribution specimen are required.

Forced Vehicle Motion - In this experiment, the rod system is oscillated at an amplitude sufficient to provide adequate measurement for comparison of the predictions provided the rod system which oscillates it at a sufficient amplitude. Of primary importance is the deflection amplitude rather than the means of excitation although SIVB vehicle motion due to active control is significant as a "simulation" of some possible actual condition.

The experimental procedure for the forced vehicle motion experiment is to stabilize the vehicle in its attitude and with the control system off to erect the rod and allow a period for the rod motion to become steady state and low amplitude. Data are required for time equal to twice the rod fundamental period. At this point, the control system is actuated to develop a roll or pitch torque (as described in the computed examples). The time torque application is quite critical in order to achieve sufficient amplitude for measurement without over-deforming the rod. After the desired impulse has been delivered, the control is turned off and measurement continues for a period equal to three times the fundamental period.

In each case data consist of attitude measurements, body rates and photographic records of rod end mass position. The forced vehicle motion experiment also requires a record of the control actuation.

Computations have been performed using torques about the SIVB body as excitation. The control system has been determined to be adequate for excitation and has the advantage of providing a system in which the actual disturbance can be measured.

Extension and Retraction Experiment - These experiments are not considered as controlled experiments per se since it is not, at this time, considered desirable to deliberately introduce body rates in excess of the minimum possible during the critical extension and retraction maneuvers. The natural motions which are induced during extension and retraction interact with body rates in so significant a manner that it is deemed mandatory that data be acquired during these events for postevent analysis. It is recommended that every extension and retraction should be monitored. Extension and retraction at the full rod length required by the selected stabilization system will also be monitored.

Data required are attitude, body rates and photographic position measurements of the end mass. Records should start, on extension, 1 to 2 minutes before extension, continue through extension and for three times the largest natural period of the rod. During retraction, data recording should begin one period before initiation of retraction continue through the retraction and continue for 15 to 30 seconds after completion of retraction.

### 5.1.5 ROD REQUIREMENTS

The rod used should be identical to that selected for gravity stabilization experiments. This is a digitated 3-inch-diameter beryllium-copper rod. The length and end mass are chosen to provide the lowest natural frequency having a period of approximately 5 minutes to allow completion of measurements in 15 minutes for each experiment. This allows a variation of either the end mass or the length or both from that used in the stabilization experiment. Both length and end mass should approximate a useable system. The weight of the end mass must be sufficient to provide a reflector for obtaining a good photographic image. Other than these constraints, no further rigid requirements exist. Use of an identical rod length with that used in gravity stabilization and a caged damper would offer one attractive choice if appropriate controllable caging does not overly complicate the system. An inert end target of mass equal to the damper mass is considered more practical than a caging device on a damper which will not be used. In this case, the frequency would be adjusted by shortening the rod.

### 5.1.6 ATTITUDE CONTROL SYSTEM

The attitude control system of the vehicle is used to place the vehicle in the desired attitude and stabilize it there before each experiment. It is off during all periods when the rod is extended, except as specified previously. Analysis of rod response to control system action given in Section 5-3 verifies that this is necessary.

### 5.1.7 SENSORS AND SAMPLE TIMES

The sensors for the primary rod experiments consist of vehicle attitude sensors, angular rate sensors and sensors to detect control actuation and a camera mounted to view the rod end mass target.

To obtain the best resolution possible, it is desirable that the photographic image of the rods and timing indicators be obtained on film to be returned to the Earth for development and analysis. If the experiment is to be conducted on an unmanned mission or after all manned periods, the television transmission will be necessary.

Observation of the time histories shown in Section 5.3 indicates that the highest frequency oscillations of measureable parameters has a period of 138 seconds. If there are unanticipated effects which excite higher modes, the measurements should be capable of detecting the effect. The third and fourth modes have periods of approximately 25 seconds. A sampling rate of 5 samples per cycle is adequate for identification of the presence of motion and perform some analytical correlation. This would require a minimum sampling rate of 5 seconds per sample.

The temperature distribution specimen has been previously described and will require thermocouple readings at a rate which will normally not exceed one sample from each thermocouple per minute. An exception will be that during the thermal impulse test the sampling rate should be identical to that for the dynamic system, i.e., a sample every 5 seconds.

## 5.2 SELECTION OF TEST CONFIGURATION

The constraints set for the selection of the extendible rod for use in the rod dynamic flight experiment were as follows:

a. The rod itself is to be the same rod chosen for the passive attitude stabilization experiment. This constraint was imposed, first, to avoid the development of an additional rod size and erection mechanism and, second, to obtain data on the specific rod chosen for stabilization use.

b. The rod length and end mass to be selected to provide a frequency sufficiently high to allow measurement of at least three cycles of oscillation in a short enough time that no extraneous disturbances are likely.

c. The length should be in the general range to be considered comparable to those considered for stabilization use while the end mass must permit an adequate target. Size should be of sufficient magnitude to work the rod structurally.

Judgment indicates that the maximum period reasonable to expect conditions nearly free from external disturbances such as personnel motion, solar incidence change, necessity for control action to prevent excessive attitude drift, etc., is of the order of about 15 minutes of 1/6 of an orbital period. This selection is made subjectively and has not been observed to be limiting in any manner. Since it is considered that three cycles of elastic response are required to establish adequately the pattern of motion and to determine the rate of decay the maximum dynamic period is chosen to be 5 minutes. This, in turn, requires a natural frequency of 0.00333 cps or higher. Initial computations show a cantilever rod of 250 ft and a 200 lb target to exhibit a first mode at 0.00322 cps (T = 5.17 minutes). Data used for this computation are shown in Table 5-2. A listing of the first 20 modal frequency types are shown in Table 5-3.

This rod was attached to a rigid SIVB having mass characteristics shown in Table 5-4. Figure 5-1 shows the configuration and axis definition. For the free-free system, the resulting lowest nonzero natural frequencies were raised to 0.00405 cps (period = 4.12 minutes) for bending about the Z axis and 0.00728 cps (period = 2.29 minutes) for bending

Table 5-2. Extendible Rod Properties

| | | |
|---|---|---|
| Material | | Silver-plated beryllium-copper |
| Diameter | = | 7.6 cm (3 in.) |
| Thickness | = | 0.03 cm (0.012 in.) |
| Section | | Polar Moment of Inertia, $J = 5.8 \times 10^{-8}$ $m^4$ $(6.75 \times 10^{-6}$ $ft^4)$ |
| | | Section Moment of Inertia, $I_{xx} = I_{zz} = 5.2 \times 10^{-8}$ $m^4$ $(6.1 \times 10^{-6}$ $ft^4)$ |
| | | Modulus of Elasticity, $E = 121 \times 10^9 \frac{\text{newton}}{m^2}$ $(2.52 \times 10^9$ $lb/ft^2)$ |
| | | Shear Modulus, $G = 460 \times 10^8 \frac{\text{newton}}{m^2}$ $(9.65 \times 10^8$ $lb/ft^2)$ |

Table 5-3. Rod Modal Characteristics-As a Cantilever

| Mode No. | Frequency (cps) | Period | | Type Deformation | | | |
|---|---|---|---|---|---|---|---|
| | | Minutes | Seconds | Bending About | | Torsion About | Extension Along |
| | | | | X Axis | Z Axis | Y Axis | Y Axis |
| 1 | 0.00322 | 5.17 | 310 | X | | | |
| 2 | 0.00322 | 5.17 | 310 | | X | | |
| 3 | 0.0398 | 0.419 | 25.1 | X | | | |
| 4 | 0.0398 | 0.419 | 25.1 | | X | | |
| 5 | 0.125 | 0.133 | 7.98 | | X | | |
| 6 | 0.125 | 0.133 | 7.98 | X | | | |
| 7 | 0.251 | | 3.97 | | X | | |
| 8 | 0.251 | | 3.97 | X | | | |
| 9 | 0.380 | | 2.63 | | X | | |
| 10 | 0.380 | | 2.63 | X | | | |
| 11 | 0.775 | | 1.29 | | | X | |
| 12 | 2.71 | | 0.368 | X | | | |
| 13 | 2.71 | | 0.368 | | X | | |
| 14 | 5.79 | | 0.172 | | | | X |
| 15 | 7.19 | | 0.138 | | | X | |
| 16 | 13.5 | | | | | X | |
| 17 | 18.6 | | | | | X | |
| 18 | 21.9 | | | | | X | |
| 19 | 26.1 | | | | | | X |
| 20 | 47.6 | | | | | | X |

Table 5-4. Mass Properties of SIVB Workshop

$$I = \begin{bmatrix} 1.162109 \times 10^5 & 1.3625 \times 10^4 & 1.101\,3 \times 10^4 \\ 1.3625 \times 10^5 & 1.181932 \times 10^6 & 3.331 \times 10^3 \\ 1.1013 \times 10^4 & 3.331 \times 10^3 & 1.20837 \times 10^6 \end{bmatrix}$$

All units are Kg - $M^2$

Mass = $2.255 \times 10^4$ Kg

$$I = \begin{bmatrix} 1.195652 \times 10^5 & 1.006131 \times 10^4 & 8.1238 \times 10^3 \\ 1.005121 \times 10^4 & 8.7174342 \times 10^5 & 2.45713 \times 10^3 \\ 8.1238 \times 10^3 & 2.45713 \times 10^3 & 8.912442 \times 10^5 \end{bmatrix}$$

All units are lb-ft-$sec^2$

Mass = 1541.06 lb-$sec^2$/ft

about the X axis. A listing of the 20 lowest frequency modes and their basic characteristics are shown in Table 5-5. The lowest 10 modes were selected for use in analysis. This includes all modes with frequency less than 1 cps, except for the first torsion mode at 0.776 cps. The rate of excitation suitable for this experiment is not rapid enough to excite significantly modes in this frequency range and the higher frequency bending components are included in computations primarily to demonstrate this. Additionally, the torsional mode, as described by the mathematical modeling, does not produce a significant translation of the end-mass target for primary observation.

Table 5-5. Free-Free Modal Characteristics for SIVB Workshop-Rod Configuration

Rod axis lies in XY plane parallel to Y axis

Attachment point relative to SIVB Center of Mass

X = 21.3 ft

Y = 11.25 ft

Z = 0

| Mode No. | Frequency (cps) | Period | | Type Deformation | | | |
|---|---|---|---|---|---|---|---|
| | | Minutes | Seconds | Bending About | | Torsion About | Extension Along |
| | | | | Y Axis | Z Axis | Y Axis | Y Axis |
| 1 | 0.00405 | 4.12 | 247 | | X | | |
| 2 | 0.00728 | 2.29 | 137 | X | | | |
| 3 | 0.0399 | 0.418 | 25.0 | | X | | |
| 4 | 0.0407 | 0.409 | 24.6 | X | | | |
| 5 | 0.125 | 0.133 | 7.98 | | X | | |
| 6 | 0.126 | 0.133 | 7.96 | X | | | |
| 7 | 0.252 | | 3.98 | | X | | |
| 8 | 0.252 | | 3.97 | X | | | |
| 9 | 0.380 | | 2.63 | | X | | |
| 10 | 0.380 | | 2.63 | X | | | |
| 11 | 0.776 | | 1.29 | | | X | |
| 12 | 2.71 | | 0.369 | X | | | |
| 13 | 2.71 | | 0.369 | | X | | |
| 14 | 5.82 | | 0.172 | | | | X |
| 15 | 7.19 | | 0.135 | | | X | |
| 16 | 13.5 | | | | | X | |
| 17 | 18.6 | | | | | X | |
| 18 | 21.9 | | | | | X | |
| 19 | 26.1 | | | | | | X |
| 20 | 47.6 | | | | | | X |

The configuration selected then meets the following criteria for the experiment.

a. Same rod and erection mechanism as used in gravity stabilization experiment

b. Same mounting location

c. Sizeable end mass to provide similar working of the rod structure

d. Length approximates lengths used in gravity stabilization

e. Lowest natural frequency period of 4.12 minutes

## 5.3 ANALYSIS OF ROD RESPONSE TO DISTURBANCE

In order that the experiment may be scaled and checked for feasibility and in order that data obtained during the experiment may be correlated and interpreted, it is necessary to obtain an analytical description of the relation between various causes and effects. This section outlines the equations of motion used for this purpose. First, consider an element of a system which has both mass and inertia. Let the position of the element be

$$X_{i_I} = \begin{bmatrix} X_i \\ Y_i \\ Z_i \end{bmatrix}_I \tag{5-1}$$

measured with respect to an inertial center fixed in space. Now, if the orientation of a body fixed axis is defined by a matrix of direction cosines A, the position of the element is defined as:

$$X_{i_B} = A\, X_{i_I} \tag{5-2a}$$

$$X_{i_I} = A^T X_{i_B} \tag{5-2b}$$

A is a (3 by 3) unitary transformation with the property that

$$A^T = A^{-1} \tag{5-3}$$

$$A^T A = A^1 A \begin{bmatrix} 1 & 0 & 0 \\ 0 & 1 & 0 \\ 0 & 0 & 1 \end{bmatrix} \tag{5-4}$$

$$\overset{o}{A}{}^T = A^T \begin{bmatrix} 0 & -\omega_z & \omega_y \\ \omega_z & 0 & -\omega_x \\ -\omega_y & \omega_x & 0 \end{bmatrix} = A^T(\Omega) \tag{5-5}$$

where $\begin{bmatrix} \omega_x \\ \omega_y \\ \omega_z \end{bmatrix}$ are the rotation rates of the body axes about the body axes $X_B$, $Y_B$, $Z_B$.

Then:

$$\overset{o}{x}_{i_I} = \dot{A}^T x_{i_B} + A^T \dot{x}_{i_B}$$

$$= A^T(\Omega)\, x_{i_B} + A^T \dot{x}_{i_B} \tag{5-6}$$

$$\overset{o}{x}_{i_B} = (\Omega)\, x_{i_B} + \dot{x}_{i_B}$$

The momentum in translation is:

$$h_{T_{i_B}} = M_i \dot{x}_{i_B} \tag{5-7}$$

where

$$M_i = m_i \begin{bmatrix} 1 & 0 & 0 \\ 0 & 1 & 0 \\ 0 & 0 & 1 \end{bmatrix}$$

$m_i$ = mass of i th point

The angular velocity of the element of mass is:

$$\omega_{i_B} = \begin{bmatrix} \omega_{i_x} \\ \omega_{i_y} \\ \omega_{i_z} \end{bmatrix} = \begin{bmatrix} \dot{\alpha}_{i_x} \\ \dot{\alpha}_{i_y} \\ \dot{\alpha}_{i_z} \end{bmatrix} + \begin{bmatrix} \omega_x \\ \omega_y \\ \omega_z \end{bmatrix} \qquad (5\text{-}8a)$$

$$\omega_{i_B} = \dot{\alpha}_1 + \omega \qquad (5\text{-}8b)$$

The angular momentum of the particle is:

$$h_{w_{i_B}} = I_i \, \omega_{i_B} \qquad (5\text{-}9)$$

where

$$I_i = \begin{bmatrix} I_{xx} & -I_{xy} & -I_{xz} \\ -I_{xy} & I_{yy} & -I_{yz} \\ -I_{xz} & -I_{yz} & I_{zz} \end{bmatrix} \qquad (5\text{-}10)$$

Both the translation momentum in Equation 5-7 and the angular momentum in Equation 5-9 are vectors expressed in the body coordinate system.

Equations 5-7 and 5-9 are expressed in the inertial reference frame by:

$$h_{T_{i_I}} = A^T h_{i_{T_B}} = A^T M_i (\Omega) x_{i_B} + A^T M_i \dot{x}_{i_B} \tag{5-11}$$

$$h_{\omega_{i_I}} = A^T h_{\omega_{i_B}} = A^T I_i \dot{\alpha}_i + A^T I_i \omega$$

The rate of change of momentum is:

$$f_{i_I} = \dot{h}_{T_{i_I}} = A^T (\Omega) M_i (\Omega) x_{i_B} + A^T M_i (\dot{\Omega}) x_{i_B} + A^T M_i (\Omega) \dot{x}_{i_B}$$

$$+ 2A^T (\Omega) M_i \dot{x}_{i_B} + A^T M_i \ddot{x}_{i_B}$$

$$f_{i_B} = A\dot{h}_{T_{i_I}} = (\Omega) M_i (\Omega) x_{i_B} + M_i (\dot{\Omega}) x_{i_B} \tag{5-12}$$

$$+ 2 (\Omega) M_i \dot{x}_{i_B} + M_i \ddot{x}_{i_B}$$

$$T_{i_I} = \dot{h}_{\omega_I} = A^T (\Omega) I_i (\dot{\alpha}_i + \omega) + A^T I_i (\ddot{\alpha}_i + \dot{\omega})$$

$$T_{i_B} = A\dot{h}_{\omega_I} = (\Omega) I_i (\dot{\alpha}_i + \omega) + I_i (\ddot{\alpha}_i + \dot{\omega}) \tag{5-13}$$

$$\begin{bmatrix} f_i \\ T_i \end{bmatrix}_B = \begin{bmatrix} (\Omega) M_i (\Omega) + M_i (\dot{\Omega}) & \\ & 0 \end{bmatrix} \begin{bmatrix} x_i \\ \alpha_i \end{bmatrix} + \begin{bmatrix} 2 (\Omega) M_i & 0 & 0 \\ 0 & (\Omega) I_i & (\Omega) I_i \end{bmatrix} \begin{bmatrix} \dot{x}_i \\ \dot{\alpha}_i \\ \omega \end{bmatrix}$$

$$+ \begin{bmatrix} M_i & 0 & 0 \\ & & \\ 0 & I_i & I_i \end{bmatrix} \begin{bmatrix} \ddot{x}_i \\ \ddot{\alpha}_i \\ \dot{\omega} \end{bmatrix} \qquad (5\text{-}14)$$

Let

$$\begin{bmatrix} x_i \\ \\ \alpha_i \end{bmatrix} = \begin{bmatrix} S_{x_i} \\ \\ S_{\alpha_i} \end{bmatrix} q + \begin{bmatrix} R \\ \\ 0 \end{bmatrix} + \begin{bmatrix} d_{x_i} \\ \\ d_{\alpha_i} \end{bmatrix}$$

$$\begin{bmatrix} \dot{x}_i \\ \\ \dot{\alpha}_i \end{bmatrix} = \begin{bmatrix} S_{x_i} \\ \\ S_{\alpha_i} \end{bmatrix} \dot{q} + \begin{bmatrix} \dot{R} \\ \\ 0 \end{bmatrix} + \begin{bmatrix} \dot{d}_{x_i} \\ \\ \dot{d}_{\alpha_i} \end{bmatrix}$$

$$\begin{bmatrix} \ddot{x}_i \\ \\ \ddot{\alpha}_i \end{bmatrix} = \begin{bmatrix} S_{x_i} \\ \\ S_{\alpha_i} \end{bmatrix} \ddot{q} + \begin{bmatrix} \ddot{R} \\ \\ 0 \end{bmatrix} + \begin{bmatrix} \ddot{d}_{x_i} \\ \\ \ddot{d}_{\alpha_i} \end{bmatrix}$$

Since we intend not to consider articulation of the system

$$\begin{bmatrix} \dot{d}_{x_i} \\ \\ \dot{d}_{\alpha_i} \end{bmatrix} = \begin{bmatrix} \ddot{d}_{x_i} \\ \\ \ddot{d}_{\alpha_i} \end{bmatrix} = 0$$

then

$$\begin{bmatrix} f_i \\ T_i \end{bmatrix}_B = \begin{bmatrix} (\Omega^2) + (\dot{\Omega}) & M_i S_{x_i} & (\Omega^2) + (\dot{\Omega}) & M_i N \\ 0 & & 0 & \end{bmatrix} \begin{bmatrix} q \\ R \end{bmatrix}$$

$$+ \begin{bmatrix} 2(\Omega) M_i S_{x_i} & 2(\Omega) M_i & (\Omega) M_i D_i^T \\ (\Omega) I_i S_{\alpha_i} & 0 & (\Omega) I_i \end{bmatrix} \begin{bmatrix} \dot{q} \\ \dot{R} \\ \omega \end{bmatrix}$$

$$+ \begin{bmatrix} M_i S_{x_i} & M_i & M_i D_i^T \\ I_i S_{\alpha_i} & 0 & T_i \end{bmatrix} \begin{bmatrix} \ddot{q} \\ \ddot{R} \\ \dot{\omega} \end{bmatrix} \qquad (5\text{-}15)$$

$$D_i = \begin{bmatrix} 0 & -d_{z_i} & d_{y_i} \\ d_{z_i} & 0 & -d_{x_i} \\ -d_{y_i} & d_{x_i} & 0 \end{bmatrix}$$

$$(\Omega) D_i = D_i^T \omega$$

If we let the following notation represent this indicated expansion of the above terms

$$\Omega = \begin{bmatrix} (\Omega) & & 0 \\ & (\Omega) & \\ 0 & & (\Omega) \end{bmatrix} \quad , \quad D^T = \begin{bmatrix} D_1^T & & 0 \\ & D_2^T & \\ 0 & & D_i^T \end{bmatrix}$$

$$M = \begin{bmatrix} M_1 & & 0 \\ & M_2 & \\ & & \\ 0 & & M_i \end{bmatrix}, \quad I = \begin{bmatrix} I_1 & & 0 \\ & I_2 & \\ & & \\ 0 & & I_i \end{bmatrix}$$

$$S_x = \begin{bmatrix} S_{x_1} \\ S_{x_2} \\ - \\ - \\ - \\ - \\ S_{x_i} \\ - \\ - \end{bmatrix}, \quad S_\alpha = \begin{bmatrix} S_{\alpha_1} \\ S_{\alpha_2} \\ - \\ - \\ - \\ S_{\alpha_i} \\ - \\ - \\ - \end{bmatrix}, \quad N = \begin{bmatrix} n \\ n \\ n \\ \cdot \\ \cdot \\ \cdot \end{bmatrix}, \quad n = \begin{bmatrix} 1 & 0 & 0 \\ 0 & 1 & 0 \\ 0 & 0 & 1 \end{bmatrix}$$

Then a collection of mass elements is represented by the following expansion of Equation 5-15:

$$\begin{bmatrix} f \\ \\ T_B \end{bmatrix} = \begin{bmatrix} (\Omega^2 + \dot{\Omega})\, MS_x & (\Omega^2 + \dot{\Omega})\, MN \\ \\ 0 & 0 \end{bmatrix} \begin{bmatrix} q \\ \\ R \end{bmatrix}$$

$$+ \begin{bmatrix} 2\,\Omega\, MS_x & 2\,\Omega MN & \Omega MD^T N \\ \\ \Omega I\, S_\alpha & 0 & \Omega IN \end{bmatrix} \begin{bmatrix} \dot{q} \\ \dot{R} \\ \omega \end{bmatrix}$$

$$+ \begin{bmatrix} MS_x & MN & MD^T N \\ \\ IS_\alpha & 0 & IN \end{bmatrix} \begin{bmatrix} \ddot{q} \\ \ddot{R} \\ \dot{\omega} \end{bmatrix} \qquad (5\text{-}16)$$

Now, if the transformations $S_x$ and $S_\alpha$ are orthogonal to the rigid body modes, the forces in the deformation coordinates $q$ and the forces and torques at and about the center of mass can be determined by:

$$\begin{bmatrix} F_q \\ F_{c_M} \\ T_{c_M} \end{bmatrix}_H^o = \begin{bmatrix} S_x^T & S_\alpha^T \\ N^T & 0 \\ N^T D & N^T \end{bmatrix} \begin{bmatrix} f \\ \\ T \end{bmatrix}_B \tag{5-17}$$

The transformation obeys the relation

$$\begin{bmatrix} S_x^T & S_\alpha^T \\ N^T & 0 \\ N^T D & N^T \end{bmatrix} \begin{bmatrix} M & 0 \\ & \\ 0 & I \end{bmatrix} \begin{bmatrix} Sx & N & D^T N \\ & & \\ S\alpha & 0 & N \end{bmatrix} = \begin{bmatrix} M_q & 0 & 0 \\ 0 & M_T & 0 \\ 0 & 0 & I_T \end{bmatrix} \tag{5-18}$$

where $M_q$ is the mass associated with the deformation coordinates q, $M_T$ is the total mass, and $I_T$ is the total rigid body inertia about the body axes.

Performing the indicated multiplications and doing some rearranging results in:

$$\begin{bmatrix} F_q \\ F_{CM} \\ T_{CM} \end{bmatrix}_H^{\cdot} = \begin{bmatrix} S_x^T M \Omega^2 S_x & 0 & 0 \\ 0 & M_T(\Omega^2) & 0 \\ N^T DM \Omega^2 S_x & 0 & 0 \end{bmatrix} \begin{bmatrix} q \\ R \\ \int \omega dt \end{bmatrix}$$

$$
+\begin{bmatrix} 2\,S_x^T\,\Omega\,M S_x + S_\alpha^T\,\Omega I\,S_\alpha & 0 & S_x^T \Omega M D^T N + S_\alpha{}^T \Omega I N \\ & 2M_T(\Omega) & 0 \\ N^T D \Omega M S_x + N^T \Omega I S_\alpha & 0 & (\Omega)\, I_T \end{bmatrix} \begin{bmatrix} \dot{q} \\ \dot{R} \\ \omega \end{bmatrix}
$$

$$
+\begin{bmatrix} S_x^T M S_x + S_\alpha^T\, I S_\alpha & 0 & -S_x^T M X \\ 0 & M_T & -M_T \bar{R} \\ 0 & 0 & I_T - N^T D M X \end{bmatrix} \begin{bmatrix} \ddot{q} \\ \ddot{R} \\ \dot{\omega} \end{bmatrix} \qquad (5\text{-}19)
$$

where

$$
-X\,\dot{\omega} = X^T \dot{\omega} = \dot{\Omega} x = \dot{\Omega} S_x q
$$

$$
X = \begin{bmatrix} (x)_1 & & 0 \\ & (x)_2 & \\ 0 & & (x)_i \end{bmatrix} \quad , \quad (x)_i = \begin{bmatrix} 0 & -z_i & y_i \\ z_i & 0 & -x_i \\ -y_i & x_i & 0 \end{bmatrix}
$$

$$
-\bar{R}\,\overset{o}{\omega} = \bar{R}^T \overset{o}{\omega} = \begin{bmatrix} 0 & -R_z & R_y \\ R_z & 0 & -R_x \\ -R_y & R_x & 0 \end{bmatrix}^T \dot{\omega} = \dot{\Omega} \begin{bmatrix} R_x \\ R_y \\ R_z \end{bmatrix}
$$

Equation 5-19 then represents the inertial forces acting throughout the body.

If the dissipative forces can be considered in the form of viscous structural damping, the damper forces can be written:

$$\begin{bmatrix} F_q \\ F_{CM} \\ T_{CM} \end{bmatrix}_{\text{Damping}} = \begin{bmatrix} \begin{bmatrix} S_x \\ S_\alpha \end{bmatrix}^T & C & \begin{bmatrix} S_x \\ S_\alpha \end{bmatrix} & 0 & 0 \\ & 0 & & 0 & 0 \\ & 0 & & 0 & 0 \end{bmatrix} \begin{bmatrix} \dot{q} \\ \dot{R} \\ \omega \end{bmatrix} \qquad (5\text{-}20)$$

The structural constraints between mass points can be complete within the body coordinate system and can be expressed as $\frac{\partial U}{\partial x}$ where U is the internal energy and x is the vector of generalized displacement coordinates, $\begin{bmatrix} x \\ \alpha \end{bmatrix}$, previously defined. For a U which can be expressed as a quadratic in the vector x, the term structurally linear will be applied and $\frac{\partial U}{\partial x}$ reduces to Kx where K is a stiffness matrix and x is again the vector of displacement coordinates. Putting this in format consistent with the inertial and damping terms

$$\begin{bmatrix} F_q \\ F_{CM} \\ T_{CM} \end{bmatrix}_{\text{Constraint}} = \begin{bmatrix} \begin{bmatrix} S_x \\ S_\alpha \end{bmatrix}^T & K & \begin{bmatrix} S_x \\ S_\alpha \end{bmatrix} & 0 & 0 \\ & 0 & & 0 & 0 \\ & 0 & & 0 & 0 \end{bmatrix} \begin{bmatrix} q \\ R \\ \int \omega dt \end{bmatrix} \qquad (5\text{-}21)$$

Any arbitrary system of time dependent forces can be considered to be applied to each or any mass point i. If we write the symbol $\begin{bmatrix} F \\ T \end{bmatrix}$ to represent the generalized force and moment vector

$$\begin{bmatrix} F \\ T \end{bmatrix} = \begin{bmatrix} F_1 \\ T_1 \\ F_2 \\ T_2 \\ \vdots \\ F_i \\ T_i \end{bmatrix}_{\text{APPLIED}}$$

The externally applied forces may be written:

$$\begin{bmatrix} F_q \\ F_{CM} \\ T_{CM} \end{bmatrix}_{APPLIED} = \begin{bmatrix} S_x^T & S_\alpha^T \\ N^T & 0 \\ N^T D & N^T \end{bmatrix} \begin{bmatrix} F \\ T \end{bmatrix}$$

$$= \begin{bmatrix} S_x^T F + S_\alpha^T T \\ N^T F \\ N^T D F + N^T T \end{bmatrix} \qquad (5\text{-}22)$$

If the previous assumption of structural linearity is applied, the particular transformation, $\phi$, of coordinates defining structural modes can be applied. This transformation satisfies the relations

$$\omega_r^2 \, M x_r = K x_r$$

$$x_r = \varphi_r \, q_r \qquad (5\text{-}23)$$

where $\omega_r^2$ is the characteristic solution or eigenvalue of the equation and $\varphi_r$ is a transformation shape vector which will satisfy the equality for any value of the scalar $q_r$, M is a matrix of mass and inertia terms compatible with the displacements and rotations of the vector x and K is the stiffness matrix in the coordinates x. If Equation 5-23 is multiplied through by $\varphi_r^T$ it can be seen that

$$m_r = \varphi_r^T \, M \varphi_r$$

and

$$k_r = \varphi_r^T \, K \, \varphi_r$$

are scalars and the matrix Equation 5-23 reduces to a scalar equation

$$\omega_r^2 \, M_r \, q_r = k_r \, q_r$$

$$\omega_r^2 = \frac{k_r}{m_r} \qquad (5\text{-}24)$$

Now, if $\lambda$ is a diagonal matrix of $\omega_r^2$, $\phi$ is a matrix made up of the $\varphi_r$ vectors and q is the vector of displacement coordinates in each of the r modes, the usual modal equation is obtained

$$\lambda M x = K x$$

$$x = \phi q \qquad (5\text{-}25)$$

$\phi^T M \phi = M^*$, a diagonal matrix of generalized (i.e., modal) masses.

$\phi^T K \phi = K^*$, a diagonal matrix of generalized (i.e., modal) stiffness.

additionally we define

$\phi^T C \phi = C^*$, a matrix of modal damping. We will assume that $C^*$ is a diagonal matrix.

$\phi^T \begin{bmatrix} F(t) \\ T(t) \end{bmatrix} = F^*$, a vector of modal forces.

Gathering Equations 5-19, 5-20, 5-21 and 5-22 together to form Equation 5-26, then rearranging and substituting the modal relations and terminology from Equation 5-25, we get Equations 5-26 and 5-27. (The rigid body mode shapes are given by $\begin{bmatrix} N & D^T N \\ 0 & N \end{bmatrix}$ and have zero eigenvalues, they will not be included in $\phi$ which will be reserved, in this instance, for deformation mode shapes).

$$\begin{bmatrix} F_q \\ F_{CM} \\ T_{CM} \end{bmatrix}_{\dot{H}} + \begin{bmatrix} F_q \\ F_{CM} \\ T_{CM} \end{bmatrix}_{\text{DAMPING}} + \begin{bmatrix} F_q \\ F_{CM} \\ T_{CM} \end{bmatrix}_{\text{CONSTRAINT}} = \begin{bmatrix} F_q \\ F_{CM} \\ T_{CM} \end{bmatrix}_{\text{APPLIED}} \qquad (5\text{-}26)$$

$$\begin{bmatrix} M^* & 0 & -\phi^T \begin{bmatrix} \bar{M} & \bar{0} \\ \underline{0} & \underline{0} \end{bmatrix} \begin{bmatrix} \bar{X} & \bar{0} \\ \underline{0} & \underline{0} \end{bmatrix} \\ 0 & M_T & -M_T \bar{R} \\ 0 & 0 & I_T - N^T \begin{bmatrix} \bar{D} & \bar{0} \\ \underline{0} & \underline{0} \end{bmatrix} \begin{bmatrix} \bar{M} & \bar{0} \\ \underline{0} & \underline{0} \end{bmatrix} \begin{bmatrix} \bar{X} & \bar{0} \\ \underline{0} & \underline{0} \end{bmatrix} \end{bmatrix} \begin{bmatrix} \ddot{q} \\ \ddot{R} \\ \ddot{\omega} \end{bmatrix}$$

$$+ \begin{bmatrix} C^* + \phi^T \Omega \begin{bmatrix} 2\bar{M} & \bar{0} \\ \underline{0} & \underline{I} \end{bmatrix} \phi & 0 & \phi^T \begin{bmatrix} \Omega \bar{D}^T & \bar{0} \\ \underline{0} & \underline{0} \end{bmatrix} \begin{bmatrix} \bar{M} & \bar{0} \\ \underline{0} & \underline{I} \end{bmatrix} N \\ 0 & 2(\Omega) M_T & 0 \\ N^T \begin{bmatrix} \bar{D} \Omega & \bar{0} \\ \underline{0} & \underline{\Omega} \end{bmatrix} \begin{bmatrix} \bar{M} & \bar{0} \\ \underline{0} & \underline{I} \end{bmatrix} \phi & 0 & (\Omega) I_T \end{bmatrix} \begin{bmatrix} \dot{q} \\ \dot{R} \\ \omega \end{bmatrix}$$

$$+ \begin{bmatrix} K^* + \phi^T \begin{bmatrix} \bar{M} & \bar{0} \\ \underline{0} & \underline{0} \end{bmatrix} \Omega^2 \phi & 0 & 0 \\ 0 & (\Omega^2) M_T & 0 \\ N^T \begin{bmatrix} \bar{D} & \bar{0} \\ \underline{0} & \underline{0} \end{bmatrix} \begin{bmatrix} \bar{M} & \bar{0} \\ \underline{0} & \underline{0} \end{bmatrix} \Omega^2 \phi & 0 & 0 \end{bmatrix} \begin{bmatrix} q \\ R \\ \int \omega dt \end{bmatrix}$$

$$= \begin{bmatrix} F^* \\ N^T F \\ N^T D F + N^T T \end{bmatrix} \qquad (5\text{-}27)$$

The form of normalization of modal solutions utilized results in a unit generalized (modal) mass; i.e., $M^*$ = unit matrix. This in turn results in a modal stiffness equal to the eigenvalue for the mode ($K^*$ is a diagonal of $\lambda$) and if damping is expressed in terms of the fraction of critical viscous damping, $\zeta$, the $C^*$ matrix becomes a diagonal of values of $2\zeta\omega$.

Equation 5-27 is conveniently broken into three equations as follows:

$$\ddot{q} + \left\{C^* + \phi^T \Omega \left[\begin{array}{c|c} 2M & 0 \\ \hline 0 & I \end{array}\right] \phi\right\} \dot{q} + \left\{K^* + \phi^T \left[\begin{array}{c|c} M & 0 \\ \hline 0 & 0 \end{array}\right] \Omega^2 \phi\right\} q$$

$$= F^* + \phi^T \left[\begin{array}{c|c} M & 0 \\ \hline 0 & 0 \end{array}\right] \left[\begin{array}{c|c} X & 0 \\ \hline 0 & 0 \end{array}\right] \dot{\omega} - \phi^T \left[\begin{array}{c|c} \Omega D^T & 0 \\ \hline 0 & \Omega \end{array}\right] \left[\begin{array}{c|c} M & 0 \\ \hline 0 & I \end{array}\right] N\omega \qquad (5\text{-}27a)$$

$$M_T \ddot{R} + 2\Omega M_T \dot{R} + (\Omega^2) M_T R = N^T F + M_T \bar{R}\,\dot{\omega}$$

$$\left\{I_T - N^T \left[\begin{array}{c|c} D^T & 0 \\ \hline 0 & 0 \end{array}\right] \left[\begin{array}{c|c} M & 0 \\ \hline 0 & 0 \end{array}\right] \left[\begin{array}{c|c} X & 0 \\ \hline 0 & 0 \end{array}\right]\right\} \dot{\omega} + (\Omega) I_T \omega \qquad (5\text{-}27b)$$

$$= N^T DF + N^T T - N^T \left[\begin{array}{c|c} D\Omega & 0 \\ \hline 0 & \Omega \end{array}\right] \left[\begin{array}{c|c} M & 0 \\ \hline 0 & I \end{array}\right] \phi\,\dot{q} \qquad (5\text{-}27c)$$

$$-N^T \left[\begin{array}{c|c} D & 0 \\ \hline 0 & 0 \end{array}\right] \left[\begin{array}{c|c} M & 0 \\ \hline 0 & 0 \end{array}\right] \Omega^2 \phi\, q$$

Equations 5-27a, 5-27b, and 5-27c describe the body flexible motion, body axis translation, and body axis rotation, respectively.

It can be seen that the body rates, $\omega$, serve to couple inertially the rigid body and flexible body motions. It can be seen that the deformation coordinates enter directly into equation 5-27c in the last two terms and in the X term (which provides the effect of a time varying moment of inertia) in the coefficient to $\dot{\omega}$. The $\omega$ and $\dot{\omega}$ terms are seen to provide the effect of a forcing function to both flexible motion 5-27a and body axis translation 5-27b. Equation 5-27 has been utilized to predict the motion of the vehicle under several conditions.

The terms $\Omega$ and $\omega$ contain the three body angular rates $Q_x$, $Q_y$, and $Q_z$ must be measured and recorded as primary data. (If body rates are not available, careful measurement of body rotation at sufficiently close intervals to allow reasonable approximations of the body rates and accelerations might be used although the effort in analysis of results would be increased significantly). F and M are the applied forces and moments, respectively, and include control thrust, and torque, gravity forces, crew motions and any other applied disturbances. Gravity forces may be computed from the altitude and vehicle attitude relative to the line to the center of the earth, other applied forces must be eliminated during the experiment except when specified and recorded.

The terms q are the scalars which define the magnitudes of deformation in the shapes $\phi$. They are not measured directly but are described along with $\phi$ by the measurement of deflections at selected points.

### 5.3.1 DISCUSSION OF SAMPLE CALCULATIONS

In order to determine the nature of response of the rods to stimuli, sample predictions have been made. A prime objective of these computations was to determine if adequate rod motion could be obtained by actuation of the SIVB control system without overdriving the rods. An additional check was made of limit cycle operation to determine if the control system could be left in automatic mode with the rod in extended configuration.

Results of two sample computations are shown here. In each case, the vehicle is assumed to be initially in an orientation with the X axis perpendicular to the orbit plane with the Y axis (the rod axis) pointing to the center of the Earth. (See Figure 5-1 for axis definition.) The orbit is circular at 400 km (260 mile) altitude.

In Case I, a control torque of 220 ft-lb about the vehicle X axis is applied for 1.5 seconds. The pulse is applied at the start of the computation. Figure 5-2 shows a time history of tip displacements from a straight rod position. The maximum displacement of 16 feet in the desired range indications that the 1.5-second pulse is satisfactory.

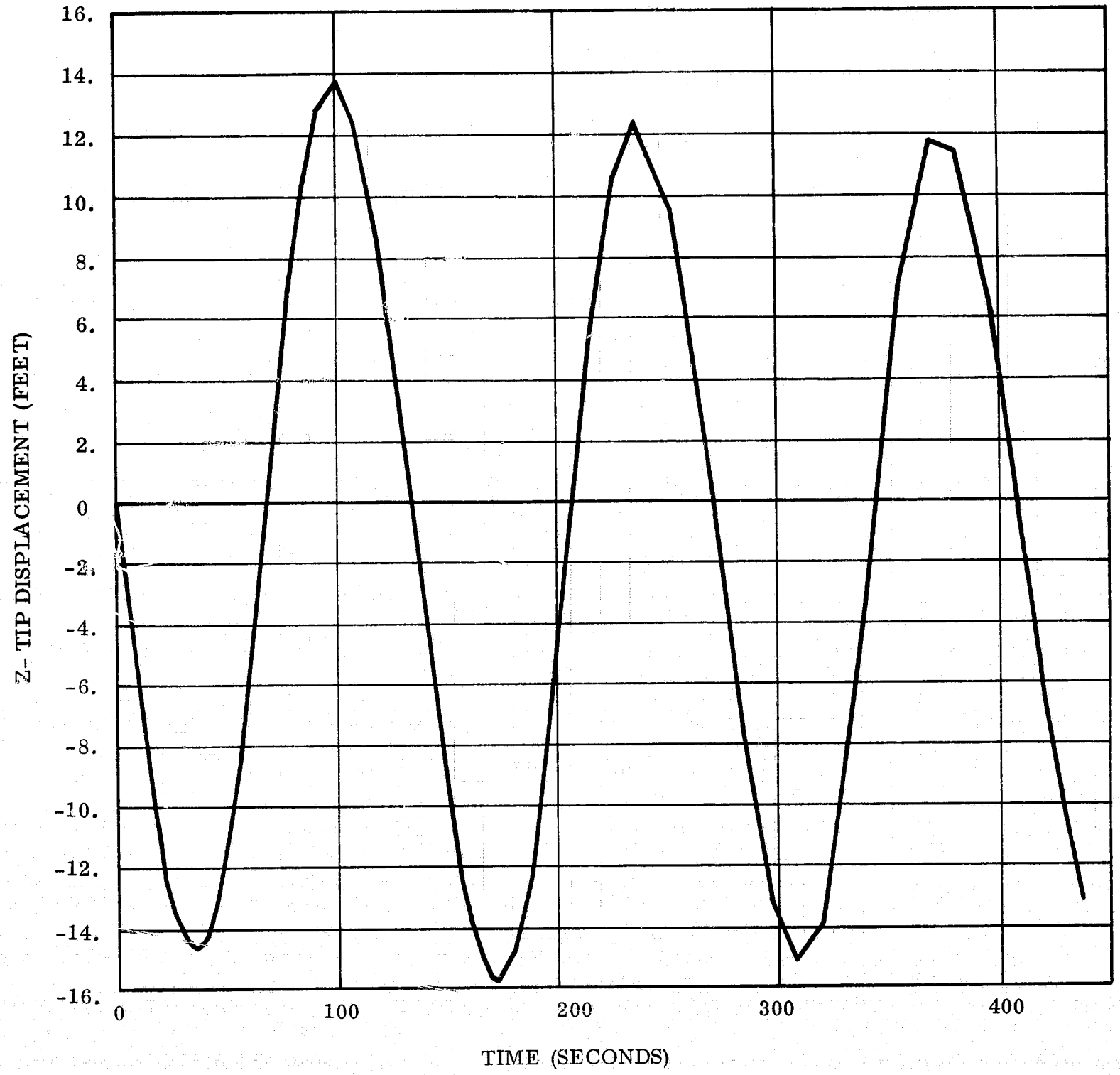


Figure 5-2. Response to Pitch Pulse

The X displacement (displacement parallel to the torque vector) is negligible and is not shown here since the applied forces and induced SIVB motions have negligible admittance to the rod modes with significant X displacement (the odd numbered modes). The modal displacements shown in Figure 5-3 show this, and also that the modal displacement of mode four is negligible.

Higher modes are not shown because they also are negligible disturbed by this motion. The displacements shown are those seen from the SIVB. Since the SIVB vehicle is also moving at the same time, the displacements as observed from the SIVB stage are somewhat different from the pure modal displacement (which are measured from the body axis which includes the center of mass of the deformed system) because of rotation of the SIVB. The displacement of the SIVB body is negligible relative to the end mass, but the rotation has noticeable effect. The component of displacement viewed from the SIVB stage is thus 4.46 times as large as the deflections measured from the body axis.

Figure 5-4 shows the four lowest modal velocities. They are of interest because they show some activity in the higher modes even though the resulting deflections are not measurable.

The SIVB body rotational velocities about the X axis due to flexible disturbance are shown in Figure 5-5. The velocity of the system axis (defined by Equation 5-27c) and the velocity of the SIVB (defined by the complete Equation 5-27) are both shown. The major portion of the angular velocity of the SIVB itself is induced by rod flexibility.

Case II is for a control torque of 770 ft-lb about the SIVB workshop Z axis for 2.5 seconds. Figure 5-6 shows the time history of tip displacements from the straight rod position. Here the displacements on the Z direction are not significant for the same reasons discussed for Case I. The rotations of the SIVB are less significant in this case than in Case I in the contribution to the tip motion as observed from the SIVB. Approximately one-third of the observed tip deflection in the X direction is due to workshop angular displacement. The magnitude of tip displacement shown here is near the maximum considered useful. Therefore the 2.5 second pulse duration should be considered a maximum for this axis.

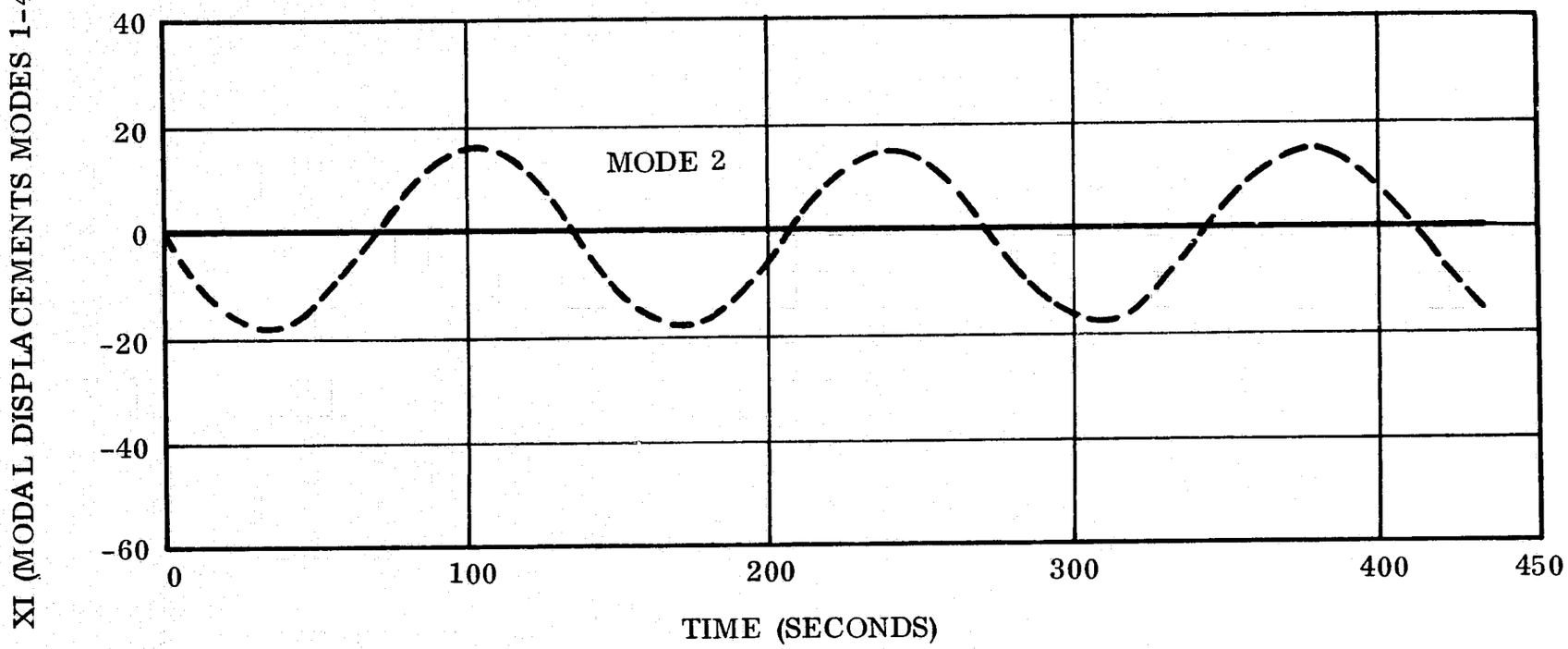


Figure 5-3. Modal Displacements for Pitch Pulse

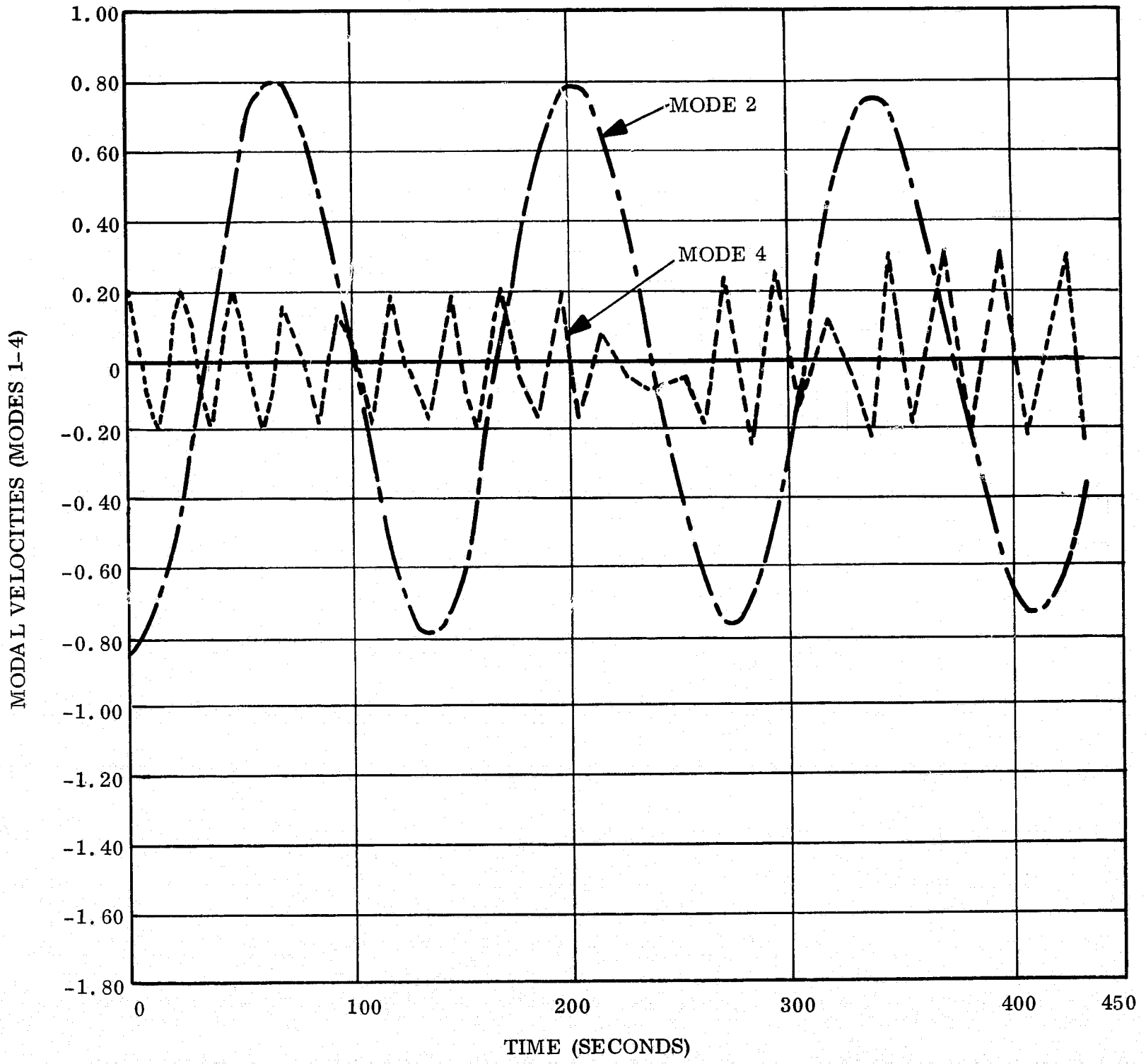


Figure 5-4. Modal Velocities for Pitch Pulse

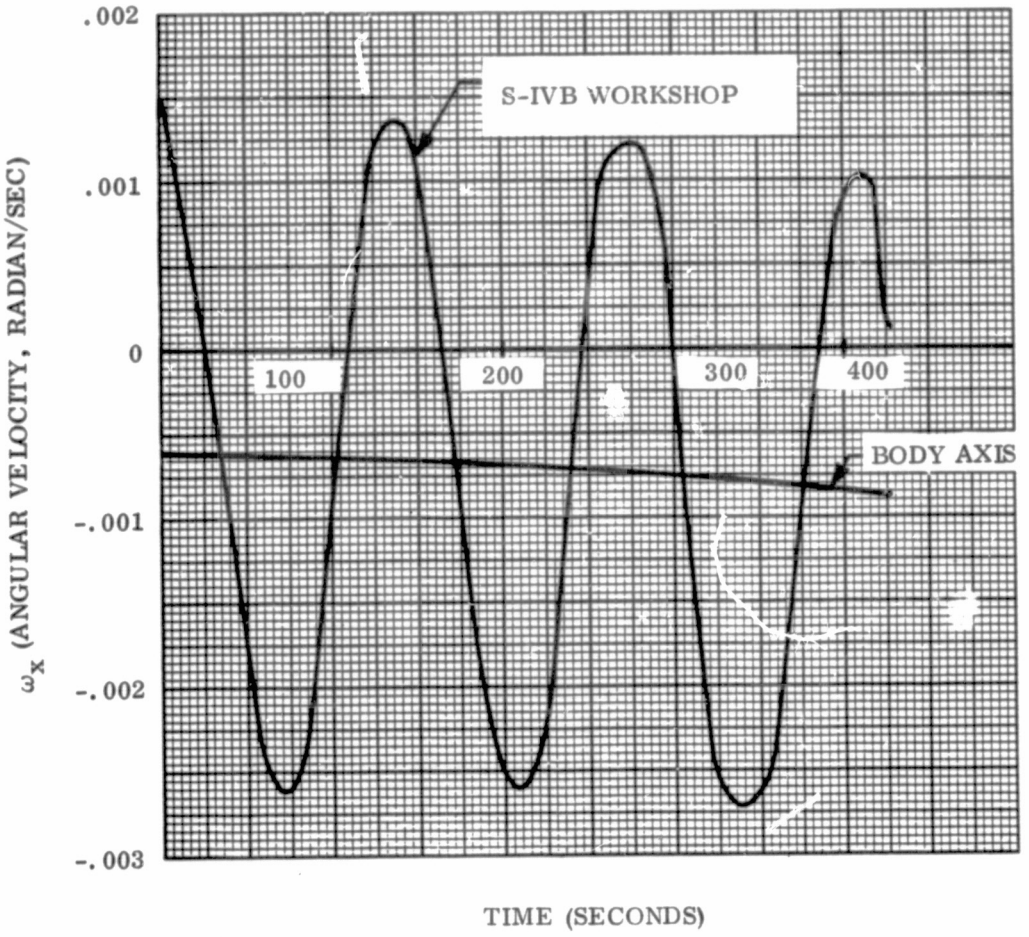


Figure 5-5. Rotational Rates for Pitch Pulse

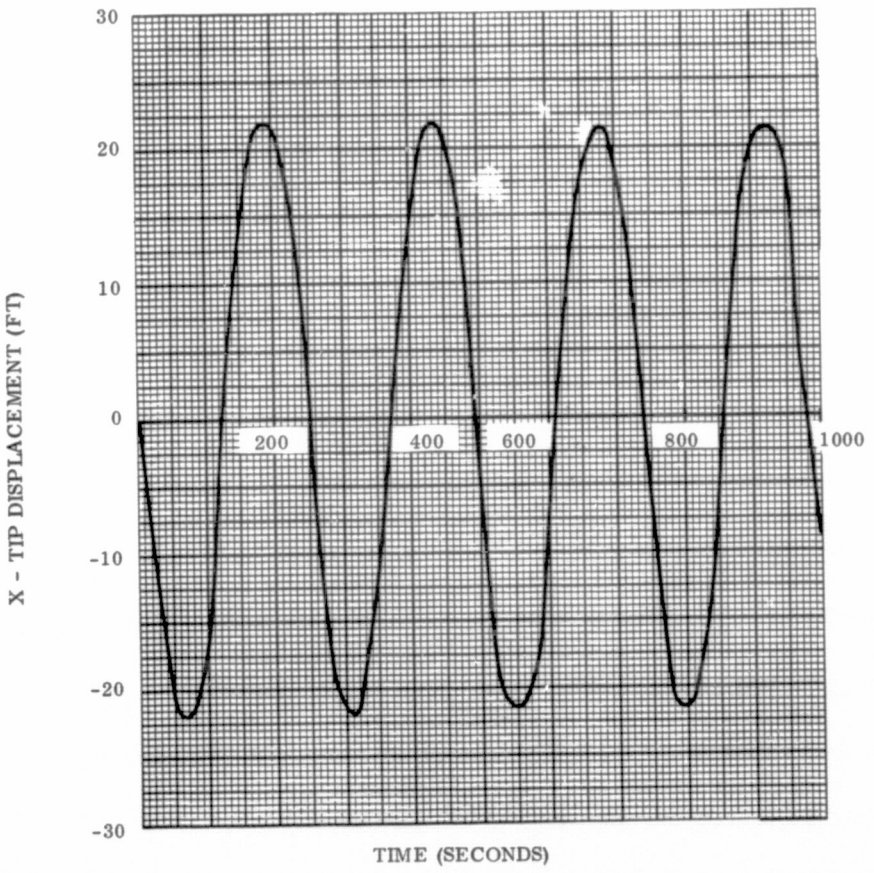


Figure 5-6. Response to Roll Pulse

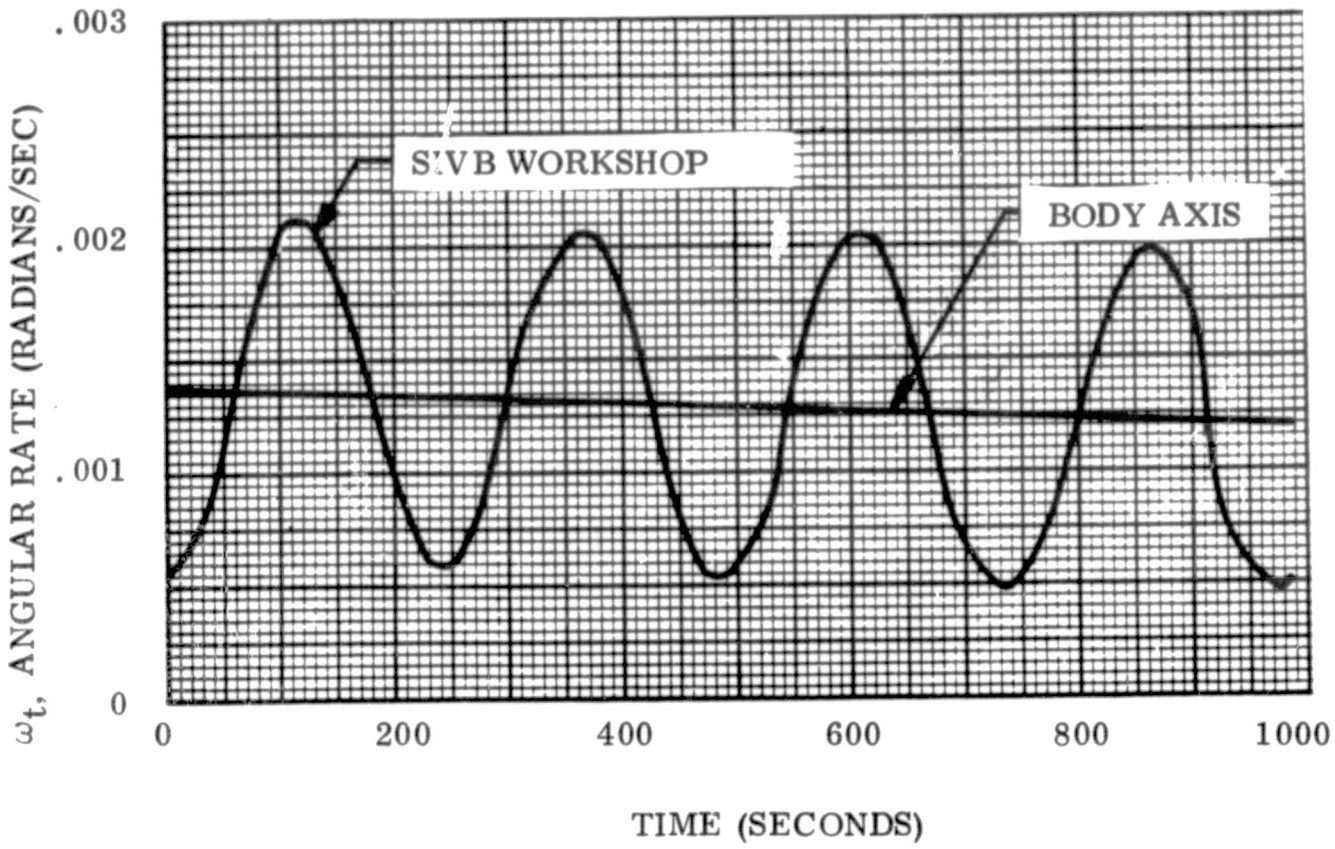


Figure 5-7. Rotational Rates for Roll Pulse

The rotational velocities about the axis in Case II are shown in Figure 5-7. The velocities of the SIVB and the body axis are both shown. Although the flexible effects are not so dominant as in Case I, they are by no means negligible.

Both Cases I and II show tip displacements of about the desired order. Variations in pulse time over a significant range will result in approximately linear variation in tip displacement.

### 5.3.2 LIMIT CYCLE RESPONSE

Case III shows the beginning of a limit cycle condition. A control action is assumed to hold the vehicle in a constant angular orientation about the workshop longitudinal axis with reference to a fixed inertial reference. The vehicle is assumed to be in a planar orbit with the X axis perpendicular to the orbit plane and the Y and Z axes are to be held in a constant orientation. This is done by applying a moment about the X axis of 220 ft-lb.

The limits are set to $\pm$ 5 degrees and the torque shuts off at an angular velocity (body axis) of 0.0017 radian per second. Initial conditions are taken as 4.5 degrees orientation off the desired orientations. No attempt is made to control the rotation about the X and Z axes.

Figures 5-8 and 5-9 show angular orientation, control moments, body rates, tip displacements, and modal responses for this case.

It can be seen that the length of the torque pulse required (the moment impulse with constant moment) to achieve the required change in angular momentum is larger than that selected to provide measurable tip deflections. The case shown indicates excessive rod motion. Although the case taken is a relatively crude approximation to the true control logic, the severity of results are considered conclusive evidence that no possibility of limit cycle action should be permitted.

Because limit cycle action is considered dangerous, the automatic control system mut be deactivated during any period in which the rod is extended and that control thrust be strictly under manual control. This restriction limits the period in which it is permitted for the rod to be extended.

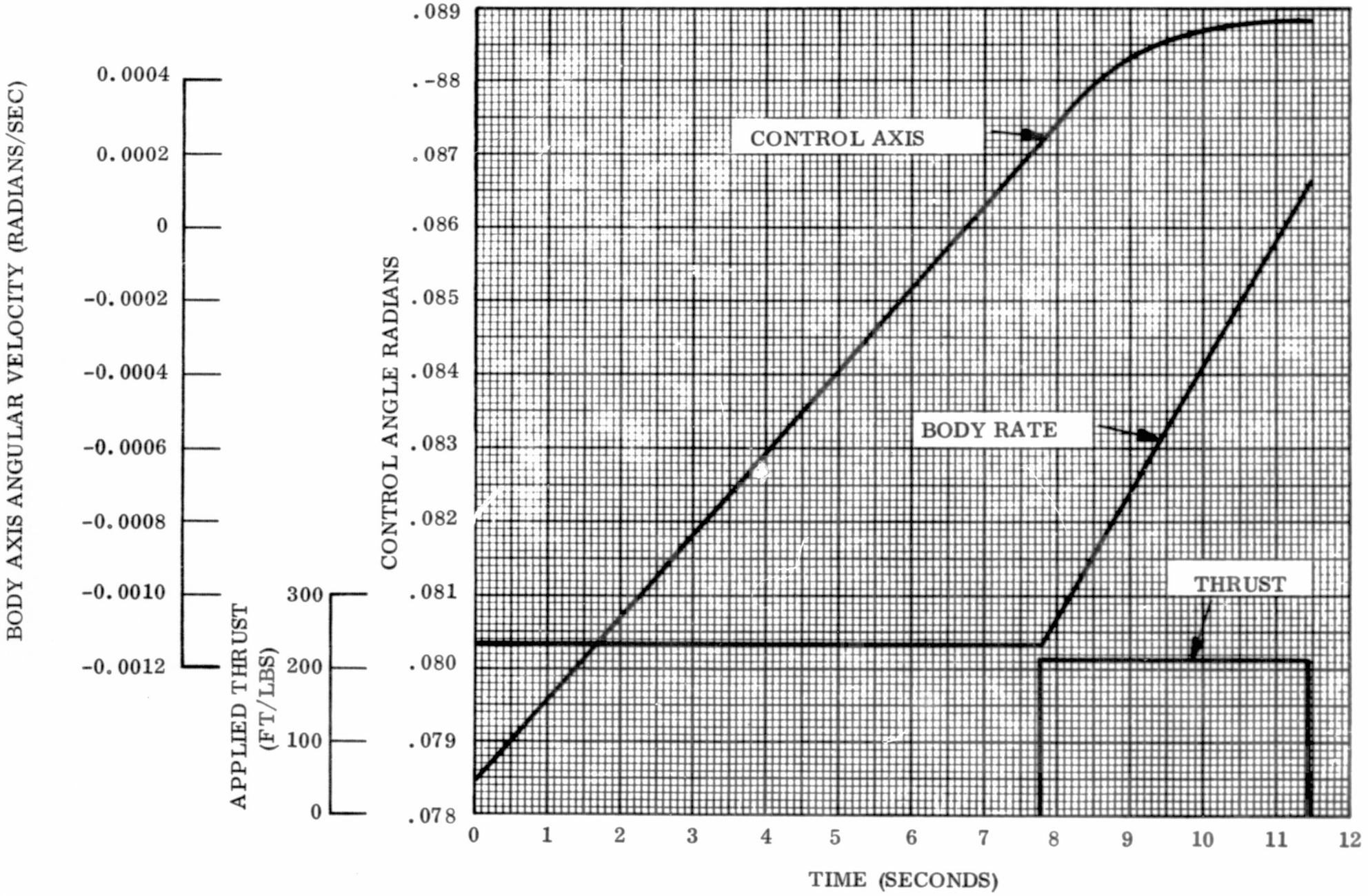


Figure 5-8. Limit Cycle Response

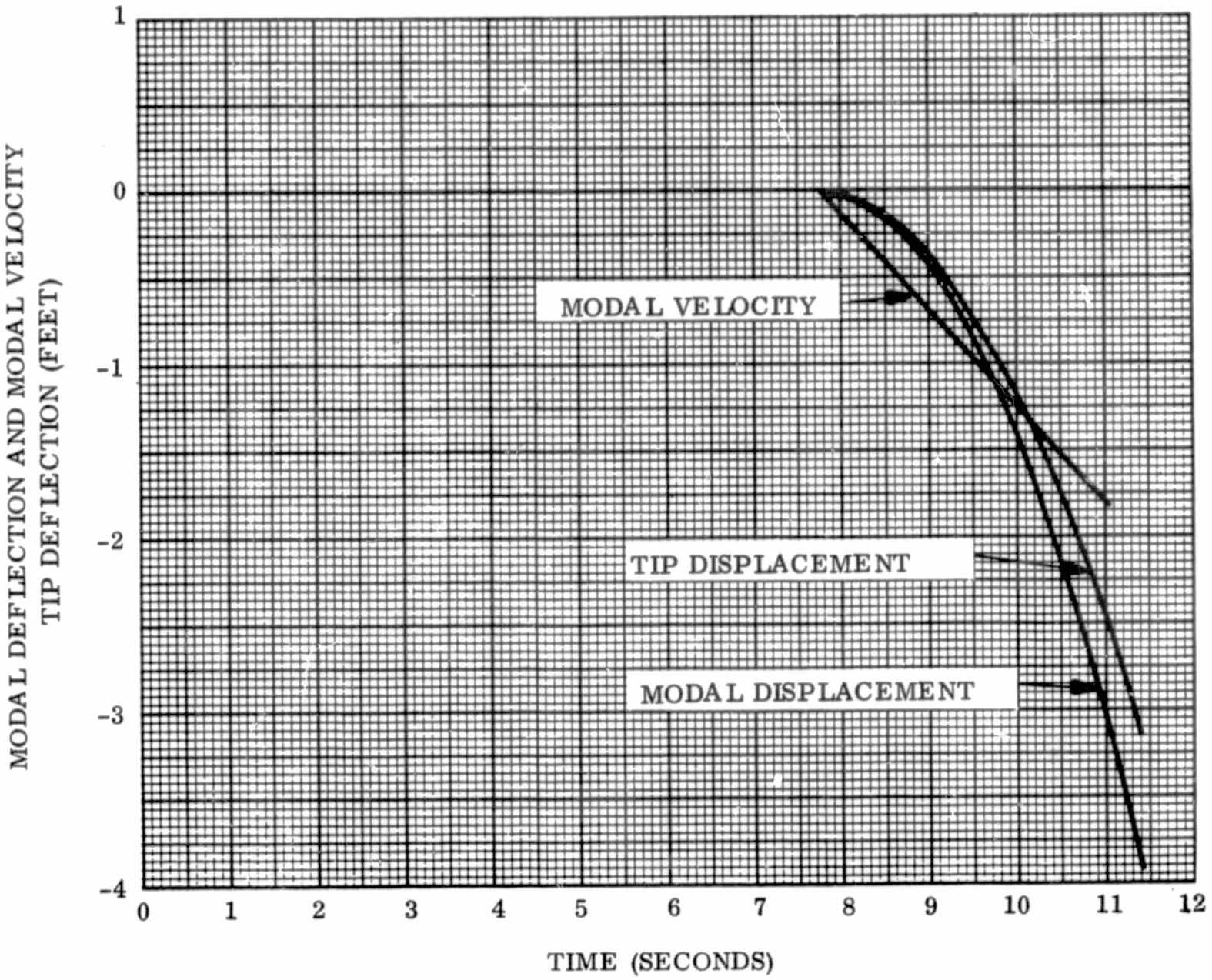


Figure 5-9. Limit Cycle Rod Flexure

# SECTION 6

# COMPONENT DESIGN

This section discusses the functional characteristics and requirements for all of the components required for the six flight experiment designs discussed in Sections 3, 4 and 5. Common components have been selected for all experiments wherever possible, and off-the-shelf components used wherever available, to minimize the development and integration programs required to implement the flight experiments

The stabilization system components required for the S-IVB at 400 km (216 nm) altitude consist of a magnetically anchored spherical damper and a deployable 3-inch-diameter rod. No rod is required on the simplest S-IVB configuration because the natural moments of inertia of the S-IVB provide three-axis stabilization. Designs of the 7.6-cm (3-inch diameter rod and magnetically anchored spherical damper are discussed in detail in Sections 6.1 and 6.2. The 3-inch diameter is also used for the rod structural flight experiment.

The stabilization system for the LM-RACK at synchronous altitude uses the same 7.6-cm (3-inch) diameter rod unit as the low altitude designs. The damper mechanism, however, is different in concept from the spherical damper and is discussed in Section 6.3.

All other components required for implementation of the six flight experiments are available as off-the-shelf items. Requirements for those components are discussed in Section 6.4 through 6.6.

## 6.1 DEPLOYABLE ROD UNIT

A 7.6-cm (3-inch) diameter extendible tubular rod, similar to the type flown in smaller sizes on previous gravity gradient stabilization systems except that a tab lock is used to form a closed seam tube, has been selected for all of the flight stabilization experiment systems and the rod flight experiment. The selection of this type structure is based on the large amount of design, test and flight experience available for this type rod. A comparison of physical characteristics between this rod and other types of tubular extendable members shows that the tubular rod compares favorably in most areas.

A functional description of the rod and erection unit is presented first, followed by discussion of rod requirements and comparison of various rod types. The rod and extension unit specification is included in Appendix E.

### 6.1.1 DEPLOYABLE ROD FUNCTIONAL DESCRIPTION

The extendible tubular rod consists of a tape of silver plated beryllium copper 25-cm (10-inches) wide by 0.03-cm (0.012 inch) thick. This tape is permanently formed into a cylindrical section with a diameter of 7.6 cm (3 inches). The tape is opened to a flat section and rolled onto a drum for storage. A layout design of the rod storage erection unit is shown in Figure 6-1.

The tape storage drum is controlled by a pair of drive belts that provide a positive friction force directly on the tape's outer surface. The drive belt tension is set and maintained by a spring-loaded roller. The drive torque is supplied to the belt by means of a pair of friction drive rollers located 270 degrees apart around the periphery of the tape storage drum. One drive roller acts to turn the drum during rod extension while the other roller drives in the opposite direction during rod retraction. Each roller pulls the drive belt in tension so that the belt remains tight around the storage drum. This not only provides increased drive friction at the drum, but more importantly, holds the tape tightly wound on the storage drum preventing buckling and backwinding as the tape comes off the drum. The two drive rollers are driven from the electric drive motor by a double drive which automatically shifts engagement from one drive roller to the other when the drive reverses rotation.

The tape storage drum rotates on a shaft which is free to ride in a guide slot on the erection unit side plates.

The drum moves to allow for change in diameter as the amount of stored tape varies. The drive belts hold the drum position so that the tape is properly aligned with the deployment guide rollers as it leaves the storage drum. Three sets of guide rollers are mounted to guide the deployment shape of the rod. These guides are positioned to conform to the natural

FOLDOUT FRAME /

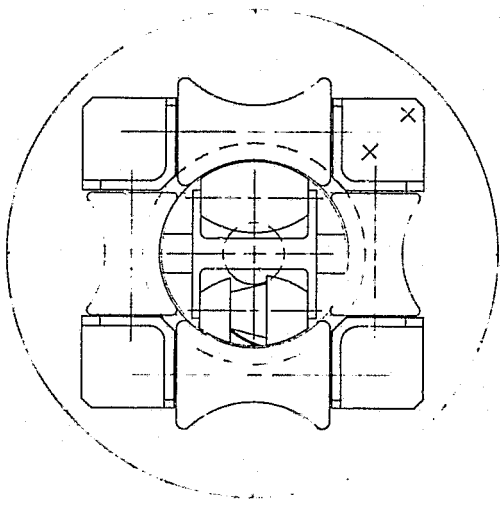

VIEW B-B
SCALE : 1/1

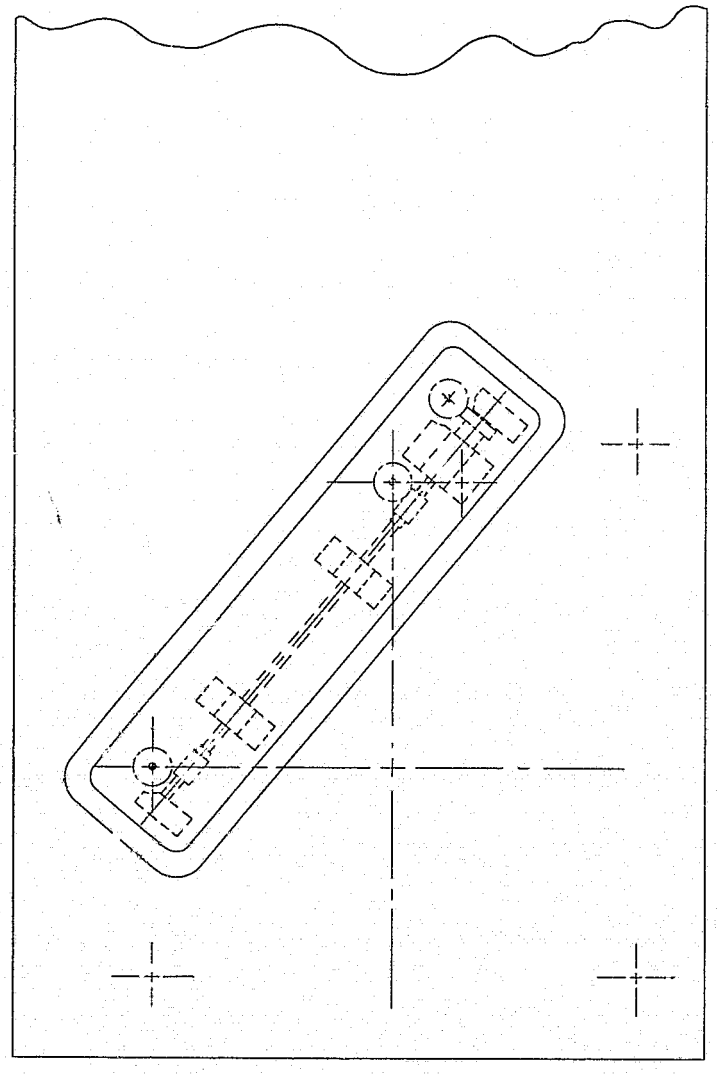

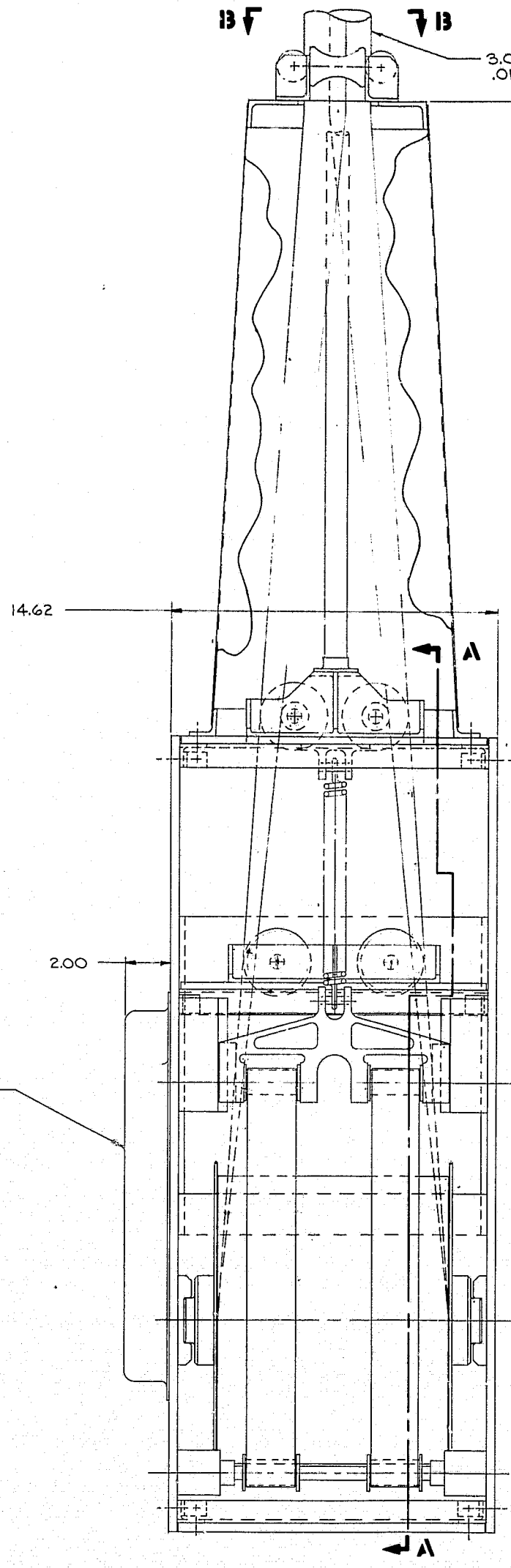

FOLDOUT FRAME 2

3.00 DIA BOOM
.012 THK

54.40
PLOY LENGTH

22.50

63.90

35.50

ERECTION UNIT ASSY

TAPE STORAGE DRUM

TAPE DRIVE SYSTEM

SECTION A-A

FOLDOUT FRAME 3

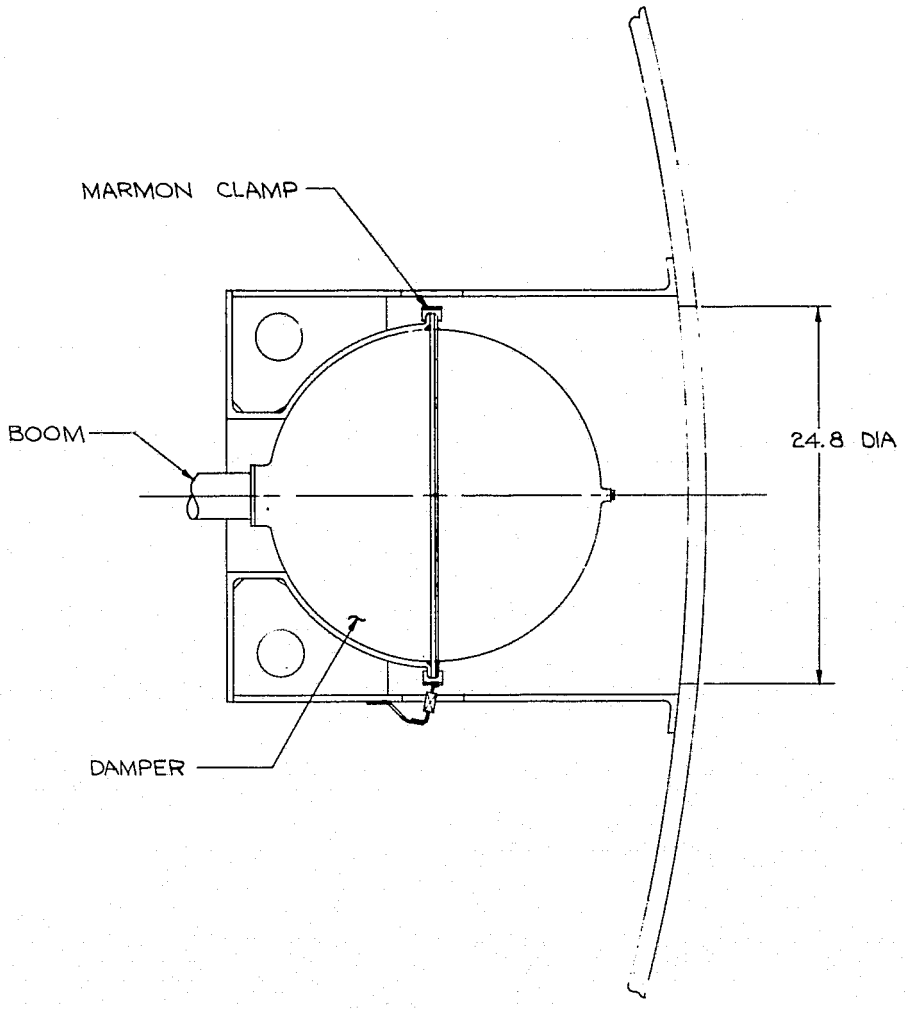


DETAIL SHOWING DAMPER
SCALE: 1/4

ECTION UNIT ASSY

TAPE STORAGE DRUM

APE DRIVE SYSTEM

Figure 6-1. 3-Inch Rod Design

ploy shape that the rod takes between the flat section at the storage drum and the tubular section at the final guide rollers.

The fully formed tubular rod is fastened at the overlap seam by a series of tabs and interlocking slots as shown in Figure 6-2.

The semicircular tab is freed from the surrounding material and assumes a more pronounced curvature so that the tab projects inside the curved rod surface. The slot cut out near the other edge of the tape is located so that as the tube closes the tab clears the tape edge and enters the slot. The amount of overlap material and the free diameter of the cylindrical rod are controlled such that a positive force is exerted trying to push the tab into the slot. The engagement of the tab into the slot occurs between the last two sets of rollers as the rod closes to form a cylindrical section while deploying.

The tab lock feature of this rod provides several important advantages. The locking force between the tab and slot serves to control accurately the rod diameter because the diameter is now established by the geometry and position of the tab and slot rather than the free shape of the tube. The locking forces on the tab and slot sides prevent slipping along the overlap and, thus, greatly increase the torsional stiffness and strength of the rod. Finally, the tab lock feature allows the use of a smaller overlap angle than the normal overlapped tube so that a larger rod diameter results from a given tape width, thus improving bending stiffness to rod weight ratio.

### 6.1.2 ROD REQUIREMENTS AND DESIGN

The function of the deployable rod is twofold: (1) to position accurately a tip weight at a large distance from the spacecraft and (2) to provide sufficient stiffness so that large deflections do not occur in the rod during operation of the stabilization system. The ability of a structure to perform these functions while maintaining minimum weight and stored volume defines the important requirements. These requirements are stated in Table 6-1.

Figure 6-2. 3-Inch Rod Unit

Table 6-1. Deployable Rod Requirements

| | |
|---|---|
| a. | High stiffness-to-weight ratio so that the longest natural period of the deployed structure is as short as possible, while concentrating the total deployed weight in the tip mass. |
| b. | Deploy in as straight and repeatable a position as possible so that the locations of the principal axes of inertia are accurately known. |
| c. | Have low thermal distortion so that the curvature of the rod is minimum. |
| d. | Have high strength so that maximum rod deployment rates and disturbance torques do not cause root bending moments which exceed the allowable and to resist on board disturbance torques such as astronaut motion and active control torques. |
| e. | Have low total weight of rod erection unit. |
| f. | Store in a minimum volume, and reliably deploy over lengths of up to 153 meter (500 feet). |

The actual design values of the selected rod configuration are shown in Table 6-2.

The design values shown in Table 6-2 are arrived at by selection of the smallest diameter extendible rod which will meet the requirements shown in Table 6-1. Requirement No. 1 fixes the bending stiffness of the rod based on the required tip mass and rod length of the gravity stabilization configuration. The stabilization system which provides horizontal orientation of the S-IVB longitudinal axis requires a rod up to (120M) 400 ft long and a 1000 newton (225 lb, tip weight which requires the stiffest rod of any of the configurations. The bending stiffness of the rod, EI = 6600 newton $-M^2$ (16,000 lb-$ft^2$) is selected so that the longest period of oscillation of the rod (first bending mode) is much shorter than any cyclic motion of the spacecraft during the passive stabilization experiment. This assures that the amplitude of rod motion will not become large because of resonance with the rigid body motion of the spacecraft and rod system. The first bending mode oscillatory period is approximately 10.7 minutes while the shortest natural or significant driven period of the rigid body stabilization system is one-half that of the orbit or approximately 45 minutes at 400 km altitude, providing a separation factor of 4.

Table 6-2. Deployable Rod Design Values

| | | |
|---|---|---|
| Rod Length | - | 120 Meters (400 feet) |
| Rod Diameter | - | 7.6 cm. (3 inches) |
| Rod Material | - | Beryllium copper tape 25 cm (10 inches) wide by 0.03 cm (0.012 inch) thick |
| Rod Seam | - | Digitated tabs and slots |
| Rod Weight | - | 880 Newtons (200 lb) |

Rod Stiffness

Bending EI = 6000 Newton - $M^2$ (14,500 lb-$ft^2$)*
Torsion GJ = 276 Newton-$M^2$ (667 lb-$ft^2$)

Rod Allowable Moment

Bending: 270 Newton Meters (200 ft-lb)

Torsion: 65 Newton Meters (50 ft-lb)

Rod Thermal Curvature

Radius of Curvature 500 Meter (1660 ft.)
Curvature 0.012 deg/Meter (0.04 deg/ft)

Rod Straightness Requirement

$2^o$ half cone from nominal straight position

Extension Unit Overall Size

1.5 x 0.4 x 0.28 meters
58 x 16 x 11 inches

Extension Unit Weight

220 Newtons (50 lb)

Extension Unit Power

Extend at 0.03 $\frac{\text{meters}}{\text{sec.}}$ (0.1 ft/sec) 40 watts

Retract at 0.03 $\frac{\text{meters}}{\text{sec.}}$ (0.1 ft/sec) 50 watts

Extension Unit Temperature Limits

Operating: $-50^oF$ to $+100^oF$
Storage : $-50^oF$ to $+150^oF$

*Established by test.

In selecting the rod diameter needed to provide adequate stiffness, the thickness of the rod material was kept as large as possible. The maximum allowable thickness to rod diameter ratio is fixed by the amount of stress which occurs at the tape edge as the tape is flattened for storage on the drum. The stress level is kept below the elastic limit so that repeated deployment of the rod does not change the rod diameter. The maximum material thickness allowable was selected since the distortion due to uneven solar heating is reduced for greater material thickness, because more heat is conducted to the shadowed side of the rod. The small weight reduction possible by using a larger diameter rod of thinner material was not considered worth the additional thermal distortion. A comparison of these factors for a 7.6-cm (3-inch) and 11.0-cm (4-inch) diameter rod is shown in Table 6-3.

The material thickness of the larger rod was selected to give the same stiffness to both rods. The tip weight was selected to give the same deployed moment of inertia considering rod weight. It can be seen that a weight saving of 150 Newtons (35 lb) results for the larger rod while the radius of thermal curvature decreases by a factor of 3.

This large change is due to the decreased heat conduction because of thinner material and the increased heat absorption due to the larger rod diameter.

The selection of rod length and tip weight to provide minimum stabilization pointing errors is discussed in Sections 3 and 4. The selection of rod length includes the effects of rod thermal distortion. The analysis of temperature gradients and resulting rod curvature which were used to select rod length is presented herein.

A thermal analysis was performed to determine the steady state temperature distribution around the periphery of a digitated gravity gradient rod.

To evaluate the maximum thermal gradient, a condition of sun incidence was selected whereby the sun vector is 95 degrees removed from the edge of the overlap. The geometric axis of the rod was considered to be aligned perpendicular to the solar vector. Table 6-4 is a list of detailed physical properties attributed to the rod:

Table 6-3. Comparison of Alternate Rods

| | 7.6-cm (3-inch) Dia | 11.0-cm (4-inch) Dia | 6.0-cm (2.4-inch) BI-STEM | 12.7-cm (5-inch) Truss Boom |
|---|---|---|---|---|
| Rod thickness | 0.03 cm (0.012 inch) | 0.013 cm (0.005 inch) | 0.06 cm (0.024 inch) | 0.5 cm (0.2 inch) |
| Rod length | 120 meters (400 ft) | 120 meters (400 ft) | 120 meters (400 ft) | 120 meters (400 ft) |
| Rod stiffness (EI) | 6600 Newton $-M^2$ (16,000 lb/$ft^2$) | 6600 Newton $-M^2$ | 6600 Newton $-M^2$ | 10,000 Newton $-M^2$ (25,000 lb/$ft^2$) |
| Tape width | 25.4 cm (10 inches) | 34 cm (13.5 inches) | 18 cm (7.1 inches) | 25 cm (10 inches) |
| Rod weight | 890 Newtons (200 lb) | 500 Newtons (112 lb) | 1260 Newtons (284 lb) | 445 Newtons (100 lb) |
| Tip weight | 1000 Newton (224 lb) | 1120 Newtons (252 lb) | 870 Newtons (195 lb) | 1160 Newtons (260 lb) |
| Deployment unit weight | 220 Newtons (50 lb) | 330 Newtons (75 lb) | 150 Newtons (34 lb) | 360 Newtons (80 lb) |
| Total system weight | 2100 Newtons (474 lb) | 1950 Newtons (439 lb) | 2300 Newtons (513 lb) | 1960 Newtons (440 lb) |
| Deployed moment of inertia | 1.9 x $10^6$ N-M-$Sec^2$ (1.4 x $10^6$ ft-lb-$sec^2$) | 1.9 x $10^6$ Newton-M-$Sec^2$ | 1.9 x $10^6$ Newton $-M-Sec^2$ | 1.9 x $10^6$ Newton $-M-Sec$ |
| Thermal curvature radius | 500 meters (1600 ft) | (160 meters) (520 ft) | 1300 meters (4150 ft) | No thermal curvature |
| First bending mode period | 11.1 minutes | 11.1 minutes | 10.9 minutes | 9.0 minutes |

Table 6-4. Rod Thermal Characteristics

| | | |
|---|---|---|
| Rod Diameter | = | 3.0 inches |
| Rod Thickness | = | 0.012 inch |
| Rod Material | = | Beryllium Copper |
| Thermal Conductivity of Rod | = | 63.0 BTU -ft/hr-ft$^2$-$^o$F |
| Optical Properties of Rod Surface: | | |
| Outside Surface | = | $\alpha_s = 0.12$ $\epsilon = 0.04$ |
| Inside Surface | = | --- $\epsilon = 0.05$ |
| Thermal Contact Conductance at Rod Overlap: | | |
| Contact Area | = | 0.0436 ft$^2$ per linear foot |
| Contact Conductance | = | 15.0 Btu/hr-ft$^2$-$^o$F |

The incident solar flux was taken to be 442 Btu/hr-ft$^2$

The results of the thermal analysis showed the temperature distribution around the periphery of the digitated rod to agree closely with the temperatures of a closed tube of the same physical properties. The maximum gradient with the digitated rod is approximately 3$^o$F larger than the gradient obtained with a closed tube. The reason for this similarity is that the contact conductance at the overlap is almost equivalent to the circumferential conductance through the rod itself. Temperature distributions are presented in Figure 6-3. A minimum temperature profile for the digitated rod was also calculated.

The thermal analysis for the digitated rod was performed by utilizing numerical techniques. It included radiant heat exchange at the internal surfaces of the rod. Results showed the internal radiation heat exchange to be insignificant.

For comparison purposes, temperature calculations were also made using a set of closed-form equations which do not include internal radiation and which consider no thermal contact at the overlap. Notice (in Figure 6-3) the effect of the discontinuous overlap on a non-digitated rod of the same physical properties. Where the effect of the overlap is insignificant

LEGEND:

A
1) SIMPLE OVERLAPPED ROD
2) NO INTERNAL RADIATION
3) NO HEAT TRANSFER AT OVERLAP
4) SOLAR VECTOR POSITION PRODUCES MAX. GRADIENT

B
1) DIGITATED ROD
2) WITH INTERNAL RADIATION
3) WITH HEAT TRANSFER AT OVERLAP
4) SOLAR VECTOR POSITION PRODUCES MAX. GRADIENT

C
1) DIGITATED ROD
2) WITH INTERNAL RADIATION
3) WITH HEAT TRANSFER AT OVERLAP
4) SOLAR VECTOR POSITION PRODUCES MIN. GRADIENT

NOTE: TEMP PROFILE OF C SAME AS A SEAMLESS TUBE OF THE SAME PHYSICAL PROPERTIES

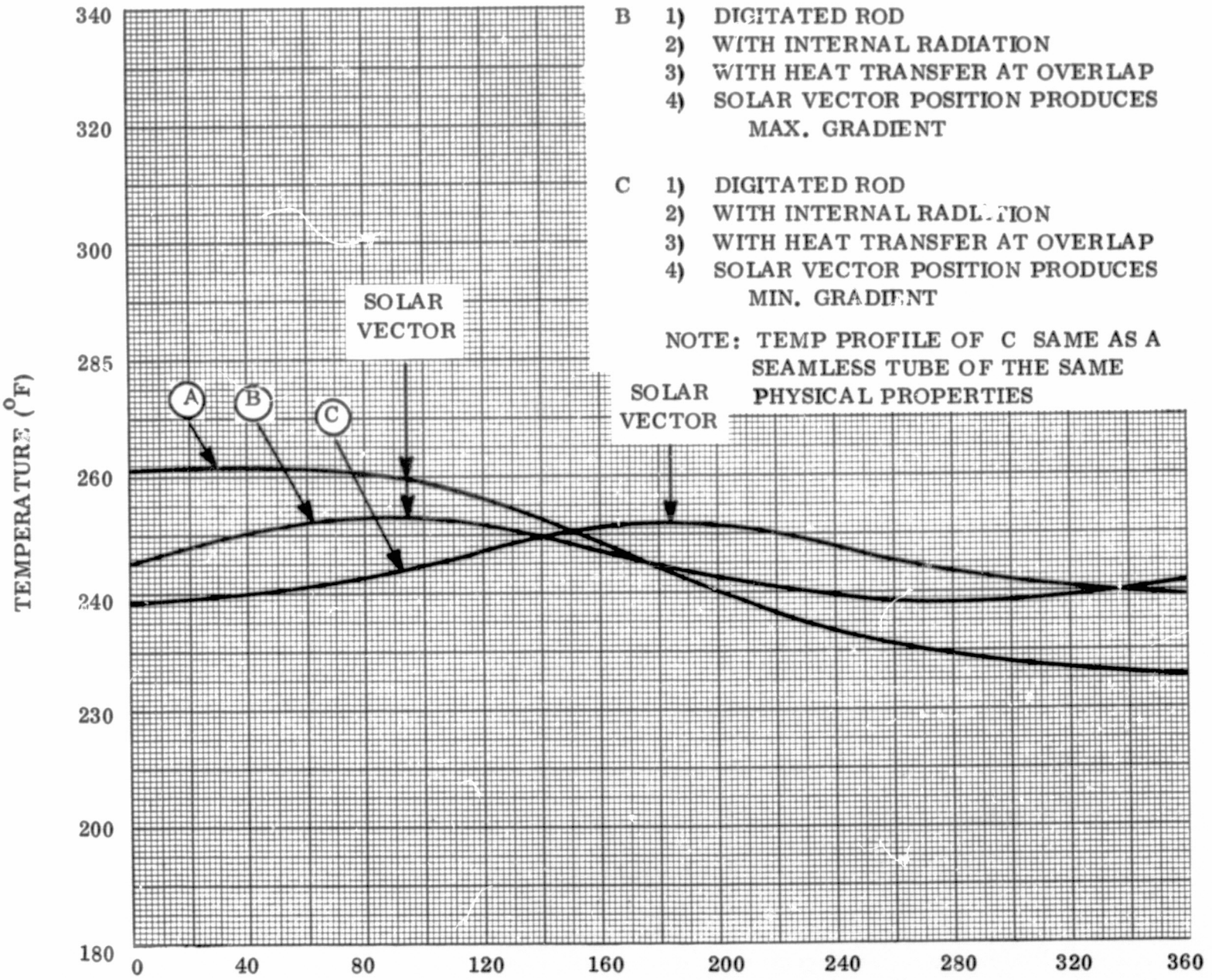


Figure 6-3. Rod Temperature Distribution

(a sun incidence angle of 180 degrees), the results of the closed form solution area almost identical to the results of the numerical analysis.

From Figure 6-3 it can be seen that the maximum thermal gradient for the digitated rod is $16^{O}F$ while the maximum thermal gradient for an equal size overlapped tube is $37^{O}F$.

The distortion which occurs from the $16^{O}F$ thermal gradient calculated above produces a nearly circular curvature in the deployable rod. If several assumptions are made, the shape can be considered truly circular. The first assumption is that the rod length is short compared to the radius of curvature; consequently, the sun incidence angle is constant along the rod length. The true shape of a long rod more nearly approximates a function given by

$$y = R \left[ LN \left( SEC \frac{X}{R} \right) \right]$$

where

Y = displacement from straight position

R = radius of curvature at root

X = distance from root along straight position

The second assumption is that the orientation of the seam remains constant with respect to the solar vector. This assumption is not met over the length of a long rod; however, the worst-case orientation is assumed so that a conservative result (greatest possible curvature) is obtained.

It is assumed in calculating the radius of curvature of the digitated rod, that the tab lock causes the rod to act structurally like a continuous closed tube. The result of this assumption is a smaller radius of curvature than would be obtained for an overlapped rod, with the same thermal distortion can be relieved in an overlapped rod by slipping across the overlap. The radius of curvature for a continuous closed tube with a circumferential temperature gradient of $16^{O}F$ is 500 meters (1660 ft). This radius of curvature in a 122 M (400 ft) long rod cuases the rod tip to move from the nominal straight position by 14.6 meters (48 feet). This transverse displacement corresponds to a 7 degree angle between the straight rod position and the rod root to tip chord.

The basic straightness of the rod cannot be accurately predicted until actual samples are produced in 120-meter (400 ft) lengths. Past experience with beryllium copper rods fabricated by both deHavilland of Canada and General Electric Company has shown the straightness in the 1 and 2 degree range is obtainable in lengths up to 46 meters (150 ft).

The equations used in determining the properties of the digitated tubular rod, are those of a continuous closed section tube and are listed in Table 6-5 for reference.

Table 6-5. Closed Section Tube Formula

| | |
|---|---|
| Bending Stiffness: | $EI = E \pi r^3 t$ |
| Torsion Stiffness: | $GJ = G2 \pi r^3 t$ |
| Maximum Bending Moment: | $M = 0.72 (E/1-u) rt^2$ |
| Maximum Torsion Moment: | $T = 0.54 \pi E/\left[(1-u^2)^{3/4}\right] t^{5/2} r^{1/2}$ |
| First Bending Mode Frequency: | $\omega n = \sqrt{\frac{3\,EI}{1^3 (M_T + 0.23\, M_R)}}$ |
| First Torsional Mode Frequency: | $\omega n = \sqrt{\frac{JG}{(I_R + I_T/3)}}$ |
| Thermal Gradient: $\Delta T = \frac{S' \alpha r^2}{kt}$ | |
| Radius of Thermal Curvature: | $K = \frac{2r}{\epsilon \Delta t}$ |

Symbols

r = rod radius

t = tape thickness

u = Poisson's Ratio = 0.3

1 = rod length

$M_T$ = tip mass

$M_R$ = total rod mass

$I_R$ = rod moment of inertia

$I_T$ = tip moment of inertia

$S'$ = Solar Flux = $470 \frac{Btu}{hr\text{-}ft^2}$

$\alpha$ = absorptivity

k = Thermal conduction = $75 \frac{Btu}{hr = ft\text{-}F^o}$

$\epsilon$ = Thermal expansion = $9.4 \times 10^6 \frac{in./in.}{^oF}$

For Beryllium Copper

$E = (19 \times 10^6\ lb/in.^2)$

$G = (7.3 \times 10^6\ lb/in.^2)$

### 6.1.3 COMPARISON OF VARIOUS ROD TYPES

The digitated tubular rod discussed previously meets all of the design requirements for the stabilization flight experiments; however, there are two other types of rods which offer some advantage in one or more design areas. These rods are discussed herein and compared to the selected rods. Each of these rod types represents a significant departure in design concept from the selected rod, and as such a larger development and flight risk. At their present state of development, the design advantages of these alternate rods do not appear to outweigh the additional development risk.

The three types of booms are listed and compared in Table 6-6. The BI-STEM is an outgrowth of single deployable tube, and consists of two tapes formed into cylindrical shape and stored flat on two adjoining drums. As the tapes extend, they curve with the open sides facing, and one nests within the other leaving a small open segment within each tube.

The advantages of the BI-STEM over the digitated monostem lie in smaller storage volume of the undeployed rod, and greater effective material thickness to rod diameter ratio than can be achieved with the monostem. The BI-STEM advantage in storage volume occurs because of the smaller angular curvature of each of the BI-STEM tapes. Because each tape curves to only about 340 degrees of a circle, the tape width for a 7.5 cm (3 inch-diameter) BI-STEM is about 23 cm (9 inches) compared to 26 cm (10.5 inches) for the same size digitated monostem. The reduced curvature of each BI-STEM tape also decreases the overall length of the deployment unit since the transition from flat to curved shape is shorter, and also because full bending strength is developed by the BI-STEM at a section where the tape is not fully curved. Thus, the final guides of the BI-STEM erection unit are closer to the storage drum than for an equal diameter monostem. A disadvantage of the BI-STEM is that two separate storage drums are required making the erection unit larger in one dimension than a monostem unit and also more complex.

The second potential advantage of the BI-STEM lies in the greater tube wall thickness that can be achieved by nesting tubes. Increased wall thickness on a 7.6-cm (3-inch diameter) rod would tend to reduce the thermal gradient across the tube reducing the amount of thermal

Table 6-6. Alternate Rod Configurations

| Boom Type | Manufacturer | Description | Flight Experience |
|---|---|---|---|
| Digitated STEM | a) General Electric Co.<br>b) deHavilland (SPAR)<br>c) Melpar<br>d) Westinghouse | Same as overlapped tube except tab and slot configuration interlocks to provide torsional rigidity can be perforated | None to date (Development models built) |
| Structural Truss | a) General Electric Co. | Formed of longitudinal stringers and diagonal truss members. Flattens by spring loaded joints. Variable cross section possible. No thermal bending | None to date (No powered erection unit built) |
| BI-STEM | a) deHavilland (SPAR) | Two tapes with double overlap. Shorter storage unit than monostem. Tapes can be stored on common drum. | None to date (Development models built) |

curvature. At the same time, the stiffness and weight of the rod would be increased. Since the rod diameter is selected to meet the stiffness requirement, a comparison of a monostem and BI-STEM of equal stiffness is made in Table 6-3. The maximum allowable thickness of 0.03 cm (0.012 inch inch) is used for each tape making a total wall thickness of 0.06 cm (0.024 inch). From the values shown in Table 6-3 it is apparent that the effect of increasing wall thickness is to moderately increase total system weight, and strongly reduce the effects of thermal bending.

The other alternate rod configuration is also listed in Table 6-6. This truss structure type rod differs markedly from the two previous rods considered, both in physical characteristics and in design of the erection unit. The truss structure consists of four longitudinal stringers tied together by diagonal cross pieces. The truss collapses for storage on a drum by flexing at two diagonal corners of the cross section. The cross section flexes via a spring-loaded pivot joint between the cross member and the longitudinal stringer. The truss collapses flat and rolls onto a drum for storage. Guides for the deployment shape of the truss consist of permanent tube shaped to fit the open truss. This guide transmits loads on the boom through the erection unit to the spacecraft. Sample booms have been made from a varity of materials, including stainless steel music wire and resin impregnated fiberglass rods. A typical set of rod characteristics are shown in Table 6-3 for comparison with the other types of rods.

The principal advantage of the truss boom is the complete absence of distortion due to thermal gradients across the boom. The open structure of the truss prevents significant shadowing and thus eliminates the thermal gradient.

A preliminary configuration based on the 12.7-cm (5-inch) rectangular truss boom is shown in Table 6-3 for comparison with the other rods. The total system weight is somewhat lower for this system, even though the erection unit is heavier. The heavier erection unit results from the large diameter of the storage drum, 62 cm (24 inches) and larger stored volume of the truss caused by the thickness of the truss longitudinal stringers. The stiffness of the truss boom is higher than that of any other type resulting in a shorter first bending mode period, even though the tip weight required is greater.

The erection unit for this rod is in a very early state of design, and no electrically powered or storage drum driven units have been produced. The principal application of the concept thus far has been for ground-based antenna in which deployment is accomplished by pulling the boom out of the storage unit manually.

## 6.2 SPHERICAL MAGNETICALLY ANCHORED DAMPER

The damping requirements of all of the passive gravity stabilization flight experiments at 400 km altitude can best be satisfied by a magnetically anchored damper. This type damper contains a magnetically oriented sphere that is free to rotate about any axis. The rotating sphere is coupled to the gravity-stabilized spacecraft by a viscous fluid which damps the oscillations of both the magnetically oriented sphere and the gravity oriented spacecraft.

The advantage of a damper using a magnetically oriented rotating body is that the magnet can be compactly contained within the damper envelope. Dampers which make use of rotating bodies oriented by the gravity gradient field, or possibly by the solar pressure or aerodynamic pressure field require the deployment of relatively large structures to generate the required orienting torques.

The characteristics of the magnetic field in low altitude orbits are such that a satisfactory balance can be achieved between damping time for transient oscillations of the gravity stabilized spacecraft and the disturbance to the spacecraft which occurs when the magnet turns to follow the earth's magnetic field. This tradeoff is discussed in Section 3.

One orbit condition in which this tradeoff can generally not be satisfactorily made is the synchronous equatorial orbit. The particular environmental magnetic field conditions which prevent the use of the magnetically anchored damper in synchronous equatorial orbit are the small angle between the magnetic field vector and the orbit angular velocity vector, and second the effects of solar magnetic storms which distort the magnetic field vector by large angles (over 60 degrees) for short periods of time (3 to 6 hours). The small angle between the magnetic field vector and the orbit angular velocity vector causes the magnetically anchored damper to be inefficient in damping spacecraft oscillations about the orbit angular velocity vector. The inefficiency results from the fact that this type spacecraft motion

develops viscous torques which tend to turn the magnet primarily about its axis of symmetry where there is no magnetic restoring torque. To overcome the inefficiency, a larger magnet and more viscous fluid coupling must be used. The effect of solar magnetic storms on the local magnetic field in a synchronous equitorial orbit is primarily to rotate the north pointing magnetic field around the orbit velocity vector so that the magnetic vector is nearly radial towards or away from the Earth's surface. This rotation is in a direction to provide the maximum torque on the magnet and thus a large roll disturbance. This combination of effects results in a very poor damping time versus accuracy tradeoff with typical values of damping time to steady state of 100 to 200 days and damper driven errors of from 4 to 6 degrees. For this reason, a gravity gradient anchored damper is selected for the LM-RACK passive stabilization configuration at synchronous altitude. This gravity gradient anchored damper design is discussed in Section 6.3.

This section contains a functional description of the magnetically anchored damper and a discussion of the physical design characteristics for the damper size selected for each configuration. Parametric studies of damper weight versus damping time and steady state error are discussed under each of the flight configuration sections.

### 6.2.1 DAMPER FUNCTIONAL DESCRIPTION

The magnetically anchored damper consists of two concentric spheres separated by a gap which is filled with a viscous silicone oil. The layout design of a 41 cm (16 inch) diameter damper is shown in Figure 6-4. The inner sphere assembly consists of two aluminum hemispheres, a cylindrical permanent magnet, an oil pressure control bellows and several structural parts to locate the magnet and bellows within the inner hemispheres. The outer sphere assembly consists of two aluminum hemispheres and a graphite liner bonded to the inner surface of the aluminum hemispheres.

The inner sphere is suspended concentrically within the outer sphere by the repulsive force generated by the permanent magnet interacting with the diamagnetic graphite liner. This diamagnetic suspension prevents contact and eliminates mechanical friction between the inner and outer sphere. The inner sphere is oriented by magnetic torques which act to align the symmetry axis of the cylindrical magnet to the local external magnetic field.

FOLDOUT FRAME 1

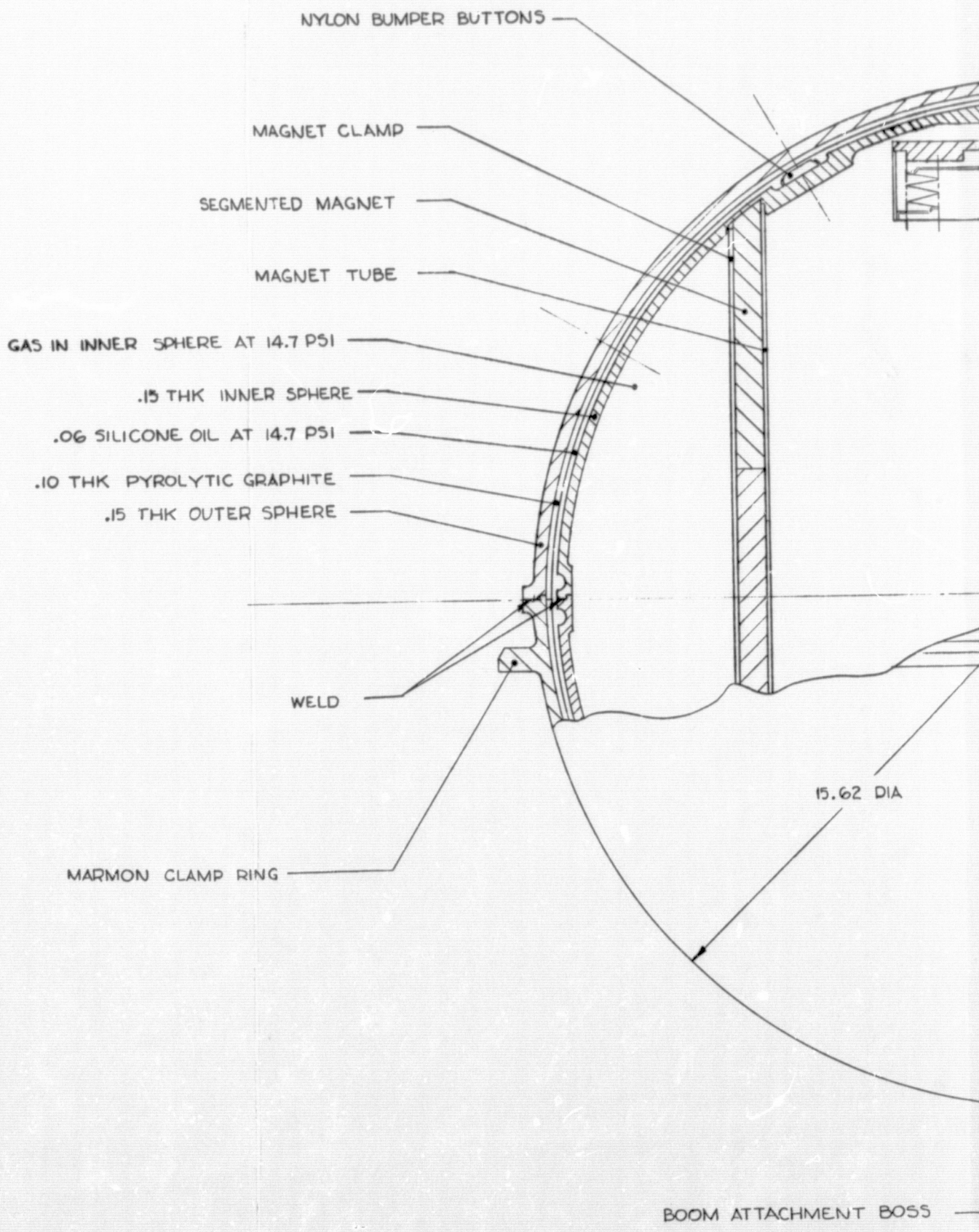

FOLDOUT FRAME 2

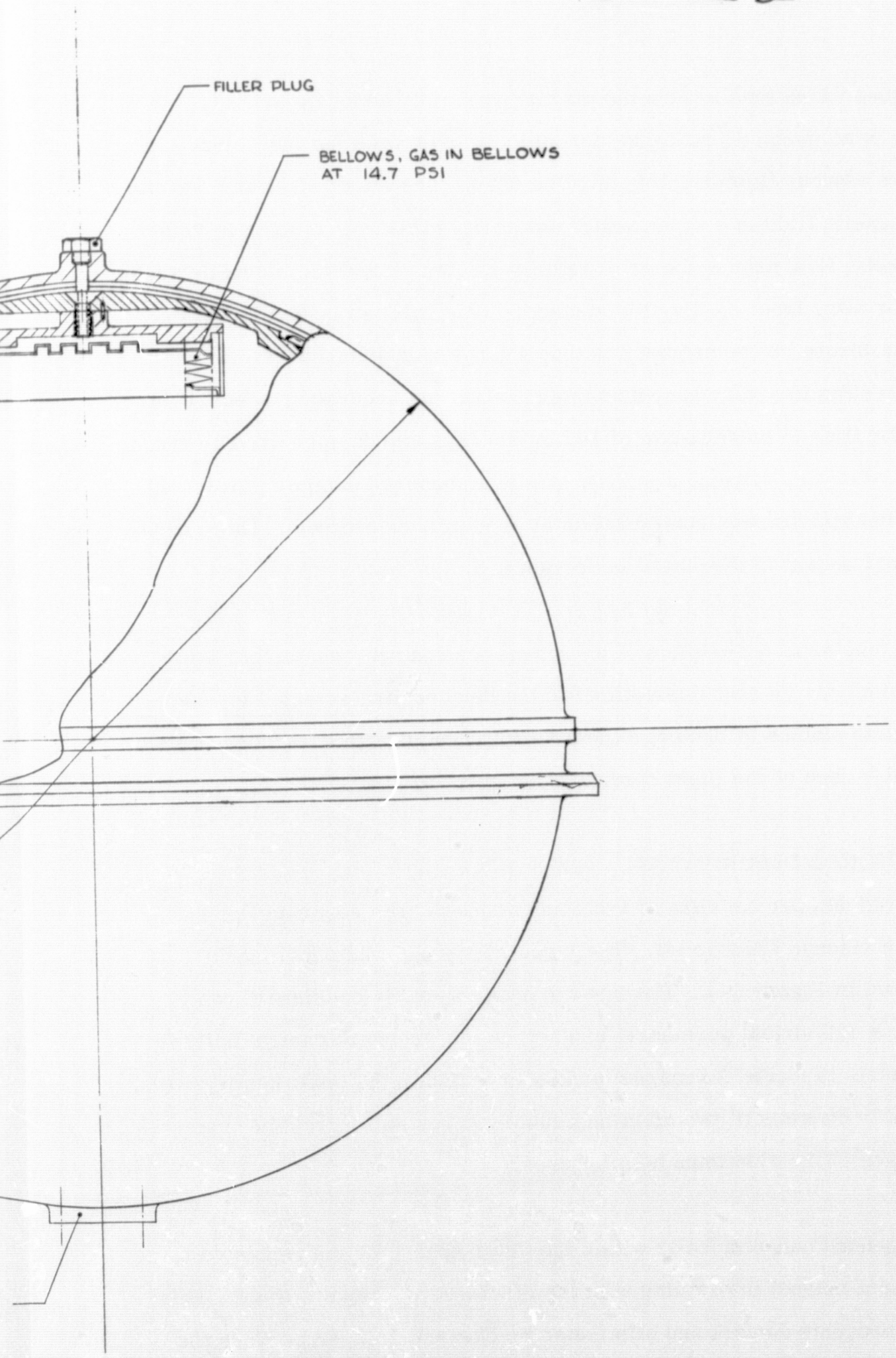


Figure 6–4. Magnetically Anchored Damper

The viscous fluid coupling between the magnetically oriented inner sphere and the outer sphere, which is rigidly attached to the spacecraft, provides damping for both bodies. In practice, the damper inner sphere is greatly over-damped because of the low inner sphere moment of inertia, while the spacecraft is under-damped because of the large inertia and low damping force.

The bellows is included in the inner sphere assembly to provide for volumetric changes in the damping oil with temperature. The cavity in the inner sphere which surrounds the bellows is filled with oil and connected to the oil-filled gap by a passageway. The inside of the bellows is connected to the inner sphere cavity which is pressurized to 14.7 psia with argon. The bellows diameter is selected to provide adequate volumetric change within a short bellows stroke to keep stress levels within the bellows low. A minimal amount of fluid is made possible by keeping the oil cavity small, which also reduces the required stroke for any required temperature range. The inner sphere is balanced and adjusted for neutral buoyancy by the solid aluminum plug opposite the bellows.

Nylon bumper buttons are used on the outside of the inner sphere to prevent contact between the spherical walls of the inner and outer sphere. Contact of these spherical surfaces of nearly identical radius which might occur during ground or launch environment loading would result in nearly all of the oil being squeezed out of a large area and viscous forces might prevent the inner sphere from becoming centered for a long period of time.

The inner sphere magnet (cast Alnico 5) is segmented because the material is difficult to cast in large pieces without warping or cracking. The segments are cast to fit around the magnet tube with ground ends to fit the adjoining segment and the inner sphere. The magnet may be charged either before or after assembly, and in one piece or segments depending on availability of a charging facility large enough to handle the magnet. The inner sphere hemispheres are joined by a weld seam around the diameter. Following welding, the inner sphere is pressurized with helium and sealed at the filling plug. The weld joint is checked for leakage by sniffing in a vacuum environment. A similar leak check is performed after the final pressurizing of the inner sphere with argon.

### 6.2.2 DAMPER DESIGN CHARACTERISTICS

Two damper sizes have been selected in the stabilization configuration designs which will satisfy the damping requirements of all flight experiments at 400 km altitude. The damper selected for the S-IVB two-axis vertical configuration does not serve as a deployable tip weight and is designed to be of minimum weight consistent with providing the required damping level. Therefore, the smallest possible magnet strength is used and a minimum weight damper designed for this magnet strength. The two dampers used as tip weights on the S-IVB horizontal configuration are designed by the minimum tip weight required to provide the necessary moments of inertia for stabilization. This damper design uses the largest possible magnet strength within the allowable damper weight. Table 6-7 shows the design values of the two dampers.

Table 6-7. Design Characteristics for Magnetically Anchored Dampers

| | Small Damper | Large Damper |
|---|---|---|
| Magnet Strength - amp $M^2$ (pole cm) | 2000 ($2 \times 10^6$) | 6000 ($6 \times 10^6$) |
| Magnet Weight - Newtons (lb) | 155 (35) | 470 (106) |
| Total Damper Weight - Newtons (lb) | 356 (80) | 1000 (225) |
| Damping Coefficient Newton-Meter-Sec (ft-lb-sec) | 82 (60 | 82 (60) |
| Damper O.D. - cm. (inches) | 41 (16) | 56 (22) |
| Operating Temperature Range - $^oF$ | -40 to +100 | -40 to +100 |
| Damping Variation with Temperature | 0.8% per $^oF$ | 0.8% per $^oF$ |
| Centering Force - Newtons (lb) | $0.9 \times 10^{-3}$ ($0.2 \times 10^{-3}$) | $1.9 \times 10^{-3}$ ($0.427 \times 10^{-3}$) |
| Bouyancy - Newtons (lb) | $\pm$4.5 ($\pm$1) | $\pm$4.5 ($\pm$1) |

The design of a spherical magnetically anchored damper is primarily an optimization of maximum magnet dipole for minimum overall damper weight. This optimization is made while providing sufficient suspension force to ensure that the inner sphere remains centered during damping operation. Maximization of magnet dipole per unit of magnet weight is obtained by increasing the length and diameter of the cylindrical magnet and decreasing wall

thickness. As the magnet length and diameter increase, however, the diameter of both the inner and outer sphere increase, thus, increasing total damper weight with no increase in magnet dipole. Because no magnets have been fabricated in the sizes required for this application, no test values of magnet dipole per unit magnet weight are available. The magnet design has been performed based on test values from smaller magnets of the same geometry. Magnet efficiencies of ($56,000 \frac{\text{pole cm}}{\text{lb}}$) have been obtained for magnets with a length to diameter ratio (L/D) of 1.4 and a wall thickness to diameter ratio (t/D) of 0.10. Using this magnet efficiency and keeping the same geometric relations results in magnet, inner sphere and total damper weight which increase linearly with dipole.

The resulting weights, and damper sphere diameters are plotted versus magnet dipole in Figure 6-5.

Damper designs of two sizes are required to meet the requirements of all the flight experiment configurations at 400 km. altitude. A magnet strength of $2 \times 10^6$ pole cm is required for the S-IVB vertical configuration while a $6 \times 10^6$ pole cm magnet is required for the S-IVB horizontal configuration.

Selection of the required magnet strength for each configuration is discussed in Section 3.. The layout design of both dampers is the same since the outer sphere diameters are 41 cm (16 inches) and 56 cm (22 inches), respectively, for the $2 \times 10^6$ and $6 \times 10^6$ pole cm dampers.

The requirement for suspension of the inner sphere within the outer sphere is caused by acceleration forces which tend to translate the outer sphere, and because of magnetic forces which tend to translate the inner sphere. Mounting the damper at the end of a long deployed rod will make the magnetic forces on the inner sphere negligibly small compared to the outer sphere acceleration forces. The accelerations of the outer damper sphere are caused by angular acceleration and centrifugal acceleration at the rod tip. The peak force required during tumbling motion at twice orbital rate is $13 \times 10^{-5} \frac{\text{dynes}}{\text{dyne}}$ of unbuoyant weight. Scaling of centering force from test data on smaller magnets results in a conservative estimate of centering force of 190 dynes ($0.42 \times 10^{-3}$ lb) for the large $6 \times 10^6$ pole cm

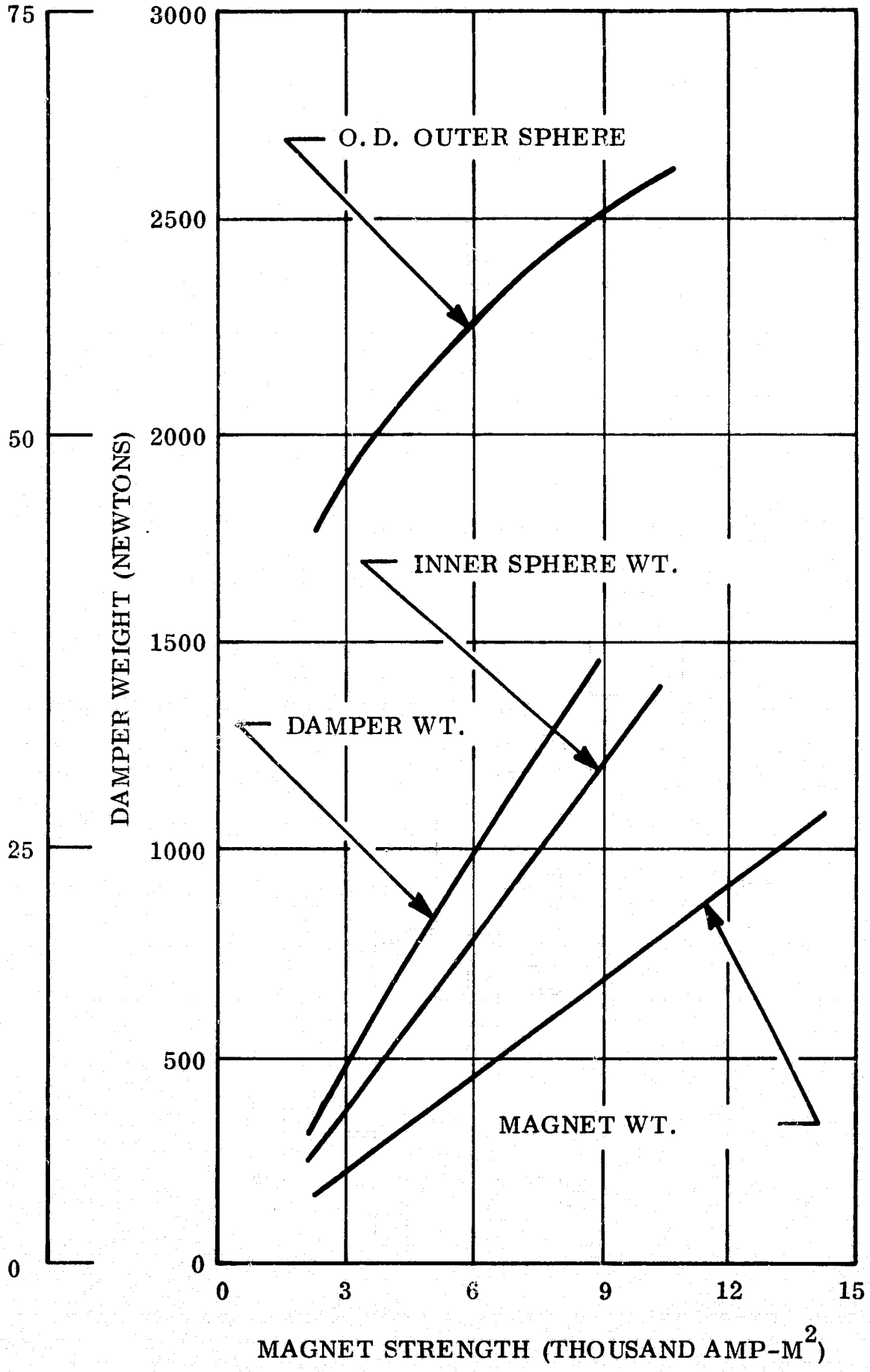


Figure 6-5. Damper Weight and Diameter

damper. By keeping the buoyant weight of the inner sphere to within 4.4 newtons (1 lb), the centering force is three times greater than that required. The centering force scaling has been done based only on the increase in surface area of the magnet face where the magnetic flux is maximum. The calculation of centering force requirements for the $2 \times 10^6$ pole cm damper is based on the effects of nearby magnetic material. The centering force available in the $2 \times 10^6$ pole cm damper will be one of the factors setting the magnetic interface requirements for mounting the damper on the S-IVB. Scaling the small magnet centering force test data in the same manner as described above results in $0.9 \times 10^{-3}$ newtons ($0.2 \times 10^{-3}$ lb) centering force available. Since the damper is mounted relatively near to the spacecraft center of mass the accelerations of the outer sphere require negligibly small centering forces on the inner sphere. Decentering forces due to magnetic materials, as well as other magnetic interference considerations, are discussed in Appendix D.

The buoyancy of the damper inner sphere is adjusted to be as nearly neutral as possible. Neutral buoyancy can be achieved for a single value of damper temperature but will vary with damper operating temperature. Calculations based on change in damping fluid density and inner sphere displacement over the designed operating range of temperature (-40 to $+100^{\circ}$F) show that the deviation from neutral buoyancy will be well within $\pm$4.4 newtons ($\pm$1 lb).

Selection of a damping fluid to provide the design level of damping torque between the inner and outer sphere is based on the predicted operating temperature of the damper in the environment provided by the mounting. Wide ranges in the mean operating temperature of the damper can be compensated by the selection of the oil viscosity. As a typical example, the oil which would be selected to give the design damping level for the 6 million pole cm damper at $100^{\circ}$F is 3500 centistokes; at $-40^{\circ}$F average temperature 500 centistoke oil would be used. These values are based on design damping level of 82 newton-meter-sec (60 ft-lb-sec) for a nominal oil gap of 0.153 cm (0.060 inch). In the final design of a damper for a specific temperature environment, the eddy current damping caused by motion of the inner sphere magnet past the conducting outer sphere is measured and the exact oil viscosity needed to make up the design damping is blended from available oils.

The variation in damping level with cyclic damper temperature is small because of the relatively long thermal time constant of the damper. A damper mounted at a rod tip seeing full illumination for part orbit and full eclipse for part or bit will typically fluctuate in temperature by less than 10 $^{o}$F. The temperature caused variation in damping is 0.8 percent per $^{o}$F resulting in a 8 percent cyclic change in damping level. Because all the gravity stabilization systems are well below critical damping; the cyclic damping variation is averaged over many orbits and thus has little effect on overall system damping time or steady state accuracy.

## 6.3 SINGLE AXIS GRAVITY ANCHORED DAMPER

The previous section of this report has discussed the characteristics of magnetically anchored dampers and points out the particular set of magnetic characteristics existing in a synchronous equatorial orbit which prevent dampers of this type from providing an adequate combination of transient damping and low damper disturbance. This section describes a damper which utilizes the gravity gradient field to orient a secondary body and provide damping of relative motion between the spacecraft and secondary body.

The use of a gravity gradient oriented damper body has the potential for eliminating all errors arising from damper motion, because theoretically both the damper boom and spacecraft could maintain perfect orientation with no relative motion across the damper. In practice, however, solar pressure torques acting on the deployed rods of the damper body cause damper motion. The presence of the damper boom also serves to couple disturbance-driven motion of the spacecraft into axes other than that of the disturbance torque so that damper coupling of errors must also be considered a damper error source. Gravity anchored dampers in general cause less error in the spacecraft stabilization and give more rapid damping at any orbit altitude and inclination than magnetically anchored dampers. The chief disadvantage in gravity anchored dampers lies in the requirement to deploy rods.

This section contains a functional description of the gravity anchored damper used for the LM-RACK stabilization configuration at synchronous altitude. A discussion of design characteristics is also presented.

### 6.3.1 DAMPER FUNCTIONAL DESCRIPTION

The gravity anchored damper consists of two parts which rotate with respect to one another and are separated by a torsion wire suspension so that a single degree of rotational freedom is obtained. One side of the damper contains two deployable rods with tip weights which provide moments of inertia large enough so that significant gravity gradient torques act to orient the damper booms. The rotating damper boom typically has moments of inertia that are 10 percent of the main gravity gradient stabilization system. The other side of the damper is rigidly attached to the spacecraft in a position which locates the damper axis of rotation at a specific angle with respect to the principal axes of inertia of the spacecraft gravity gradient stabilization system. The orientation of the damper axis of rotation is selected such that motion of the spacecraft about any axis will cause rotation across the damper axis and generate damping torques.

The torsion wire suspension serves two purposes: first, to provide freedom of rotation about a single axis with no rubbing contact, and second, to provide a torsional spring restraint which tends to control the position of the damper rods. The null position of the torsion wire spring is such that the damper booms are horizontal. The gravity gradient torques tend to move the damper boom away from horizontal in whichever direction the boom is displaced (statically unstable null) so that the torsion wire spring constant must be greater than the gravity gradient torques, but not so great as to restrict motion of the damper boom.

The damping mechanism for the single axis damper consists of a hysteresis damping element attached to the rotating side and a fixed magnet assembly attached to the stationary side of the damper.

### 6.3.2 DAMPER DESIGN CHARACTERISTICS

The layout design of a single axis hysteresis damper is shown in Figure 6-6. The design characteristics and estimated weight are shown in Table 6-8. The damper consists of a rotor assembly (1), which supports the damping element and damper booms, a housing (2)which supports the permanent magnets (3),and the flexural pivots (4). Torsion wires (5) attached to the flexural pivots support the rotor. The housing also provides the required mounting interface. The damper booms are mounted to the adapter bracket (10). The torsion wire

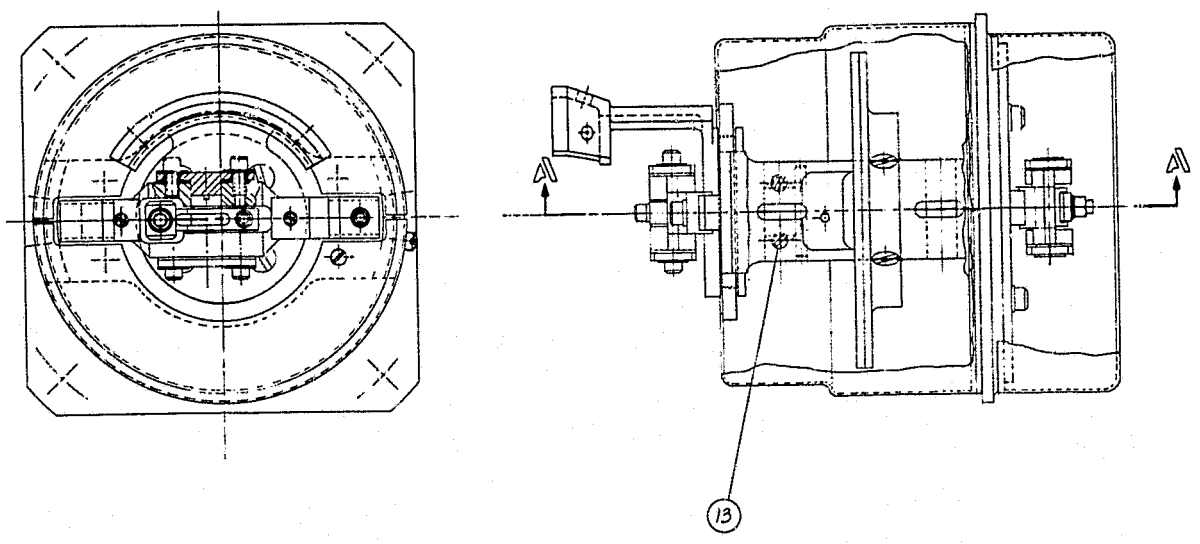


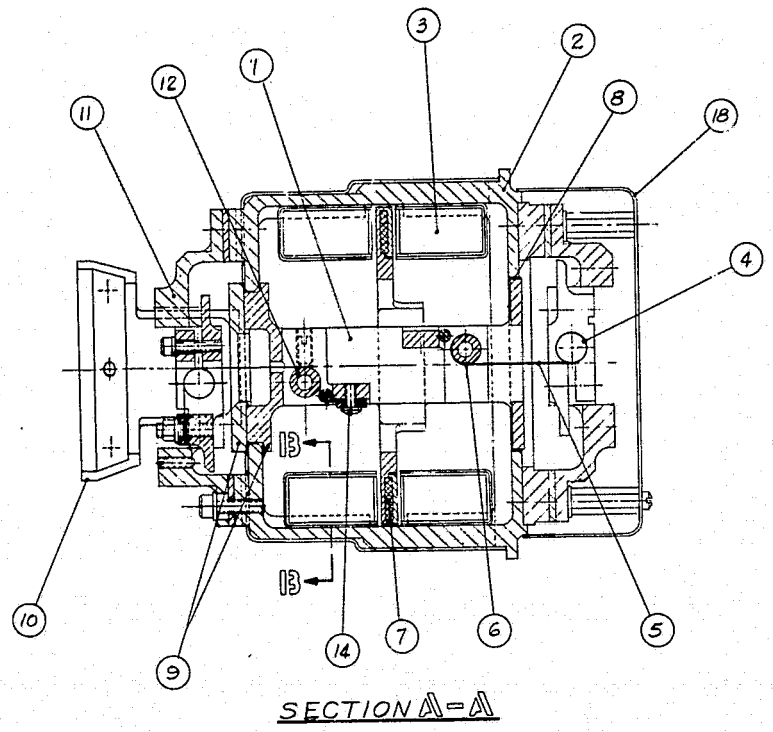


SECTION A-A

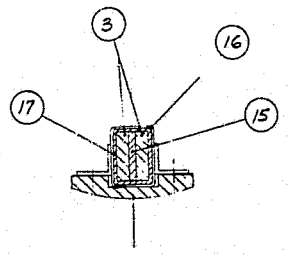


SECTION 13-13

Figure 6-6. Single Axis Hysteresis Damper

Table 6-8. Single-Axis Damper Design Characteristics

| | |
|---|---|
| Torsion Wire Spring Constant | $0.82 \times 10^{-3}$ newton meter/rad<br>$0.61 \times 10^{-3}$ ft lb/rad |
| Damping Constant | $1.19 \times 10^{-5}$ newton meter/degree<br>$0.88 \times 10^{-5}$ ft lb/degree |
| Damper Weight (without booms) | 222 newtons<br>50 lb |
| Damper Size<br>61 dia x 86 long<br>24 dia x 34 long | <br>cm<br>inches |

suspension system consists of two 302 stainless steel torsion wires attached at their inboard ends (6) to the rotor and at their outboard ends to flexural pivots which are attached to the housing. The flexural pivots control wire tension and thereby control the stiffness of the suspension system. The wire suspension system provides sufficient lateral stiffness to withstand externally applied orbit loads and axial/transverse loads imposed by the attractive force between the damping element and the magnets. The maximum axial, radial, and rotational motions of the rotor are constrained by fixed mechanical stops which prevent overstressing of the torsion wire or flex pivots due to ground handling loads. Stops are provided in the axial and radial directions to restrain the rotor within (0.019 inch). Rotational stops are set at plus and minus 45 degrees. Referring again to Figure 6-6, note that the rotor (1) contains the damping and compensating elements (7). The rotor extends out through the housing and provides the attachment to the damper boom assembly. Each end of the rotor has a closely controlled diameter which fits into close fitting holes on the housing (8) to provide precise radial stops. One end of the rotor has two shoulders (9) (one fastened on at assembly) which provide precise axial stops. Angular rotational stops are provided between the damper adapter bracket (10) and the flex pivot bracket (11).

The housing contains the magnet assemblies and flex pivots and provides the required mounting surface to the spacecraft.

The magnet assemblies are mounted on tabs which are part of the fixed structure. Each magnet assembly consists of two magnets (3) fastened to both sides of a magnetic shunt (15). This subassembly is positioned within magnetic shielding (16) so that five sides of the magnets are shielded. Only the surface adjacent to the damping disc is unshielded. Spacers (17) are used to prevent the magnet from shunting to the shielding. Pole pieces are used to ensure flux density uniformity through the damping element.

The damping components consist of hysteresis damping elements. This disc is supported by the torsion wire so that the hysteresis elements pass between the poles of the magnets.

## 6.4 ATTITUDE SENSING COMPONENTS

The components required to sense attitude of the spacecraft during the stabilization flight experiments are all available as off-the-shelf, flight-proven equipment. No special requirements are placed on either the sensors or the spacecraft, except that mounting positions be selected to provide a field of view for the optical sensors and that the sensors be compatible with temperature and load environments present at the selected mounting points. At the time a specific flight experiment design is completed based on an available spacecraft, it may well prove advantageous to use sensors already on board the spacecraft. In particular, infrared Earth sensors for vertical position information, and body rate data from a stable platform, if one is available in the instrument unit, will help to give a complete picture of stabilization performance. This section discusses the selection of attitude sensors from among those available.

Table 6-9 summarizes the weight and power of each of the sensors required for attitude detection.

Table 6-9. Attitude Sensor Weight and Power Summary

| Component | Weight | | Power |
|---|---|---|---|
| | (Newton) | (lb) | (watts) |
| Adcole Solar Aspect Sensor | 27 | 6 | 1 |
| Earth IR Sensor | 53 | 12 | 12 |
| Magnetometer | 22 | 5 | 1 |

6.4.1 SENSOR SELECTION

Instrumentation will be included on the spacecraft to measure the performance of the gravity gradient stabilization subsystems in orbit and to diagnose properly any malfunctions that may occur.

6.4.1.1 Attitude Sensing, 400 km Orbit

The attitude sensing instrumentation necessary for any of the Saturn IV-B configurations in a 400 km orbit has been selected and includes:

a. Solar aspect sensor

b. Earth's horizon sensor

c. A single three-axis magnetometer

Complete three-axis attitude determination can be accomplished when at least two independent reference vectors are simultaneously measured in the spacecraft coordinate system. The combinations of sensors selected (1) fulfills this requirement for the entire orbital period, and (2) facilitates measurement of three reference vectors for better than half of the orbital period. Combinations of present state-of-the-art sensors a and b makes possible calculations of spacecraft attitude to within 1.0 degree in all three axes during that portion or orbit when the satellite is in sunlight, and not near the Earth-Sun line. To facilitate complete three-axis attitude determinations during satellite darkness, and to resolve the ambiguity at the Sun-satellite-Earth line condition, as well as verify accuracy of the other sensors a three-axis magnetometer has been included. Satellite darkness can

eliminate data up to 140 degrees of orbit angle (0.6 hr) while Earth-Sun ambiguity can eliminate up to 60 degrees of orbital angle (0.25 hr)

6.4.1.2 Solar Aspect Sensor

The solar aspect sensor is a flight proven device of high reliability, manufactured by the Adcole Corporation. The sensor is a digital system composed of a single electronics unit and five solar detector assemblies. Each solar detector has a 128-degree by 128-degree rectangular field of view. When the detectors are strategically located on the spacecraft body, the sensor is capable of full $4\pi$ steradian coverage.

Each solar detector is composed of two gray coded reticles, photocells, and housing. The gray coded reticle is a small oblong block of fused quartz with a slit centered along the top surface and a gray coded pattern on the bottom surface. Sunlight enters the eye through the slit, casting a narrow band of illumination across the gray coded pattern. The gray coded reticle pattern provides for the generation of eight bits of information. In any given bit, the band of sunlight will either pass or not pass through the reticle pattern, depending on the angle of the reticle with respect to the sun. Each of the eight bits on the gray coded reticle is superimposed on a photocell. The function of the cells is to detect the presence of light in the apertures at a given angle, and to produce measurable electrical signals correspondingly. An additional wide open bit, with a solar cell under it, is included to compensate the output of the solar cells under the gray code pattern for variations resulting from changes in angle of incidence.

The two eight-bit solar angle measurement and the AGC bit are supplied by each of the five solar detector assemblies to the sensor electronics unit. The electronics unit samples the AGC bit of each detector. The detector most illuminated by the sun is selected and its angular and identity output are introduced to the telemetry system. This sensor has a resolution of $\pm 1/2$ degree and maximum error of $\pm 1$ degree for the worst case sun angle.

6.4.1.3 Earth's Horizon Sensor

A low-altitude four-tracker configurations of the A-OGO horizon sensor, manufactured by the Advanced Technology Division of American Standard, will be used to measure the orientation of the geocenter in the spacecraft coordinate system. The A-OGO horizon sensor employs a four-horizon-point edge-tracking technique to derive instantaneous geocenter orientation information. This information is in the form of analog signals representative of the magnitude and direction of the spacecraft-geocenter vector. Four infrared search-track units (trackers) track points on the Earth's horizon separated 90 degrees in spacecraft azimuth. Signals proportional to the angular displacement of the horizon from the nominal vertical of the spacecraft are generated by each tracker. This is accomplished be detecting the infrared (14 to 15.9 micron) energy in a narrow beam that is caused to oscillate, or dither about the horizon. The beam is produced by an optical telescope and movable mirror. A tracking servo then causes the beam to follow the horizon as the spacecraft moves about.

The A-OGO horizon sensor system is contained in three packages: the central electronic box and two dual-tracker-head assemblies. The central electronic box contains part of the tracking servo circuity for each tracker and necessary system circuity. Each dual-tracker-head assembly contains two trackers that scan in the same vertical plane, but whose fields of view are separated 180 degrees in azimuth. The two heads are mounted orthogonally so that the four scan planes are separated 90 degrees in azimuth.

The only moving parts in the sensor system are the flexure pivots in each of the four positor assemblies used to move the instantaneous field of view. The flexure pivots have an infinite life expectancy at the predicted stress levels. The positor has no bearings or sliding surfaces; hence, the resulting system is essentially static insofar as lifetime and reliability are concerned. The positor drive assembly is an ac electromagnetic drive which scans the field of view back and forth over the image edge.

Considerable redundancy is built into the system because any two trackers could fail and attitude could still be determined in two axes providing the spacecraft altitude is known.

The most severe case of this failure would be if both trackers on the same axis failed. Attitude in the failed axis could then be measured by determining the absolute angle between horizons in the operating axis, and comparing it to the absolute angle for horizon slices on an Earth diameter. The accuracy of the A-OGO horizon sensor is ± 0.1 degree and the field of view for acquisition is ±45 degrees.

6.4.1.4 Magnetometer

The magnetometer will be chosen from among those flight-proven, three-axis magnetometers which have been used on many space programs. Since the accuracy of attitude determined from a magnetometer is less than that available from the two previous systems mentioned, the magnetometer would be used as a primary sensor only in the case of ambiguous solutions from a solar and earth sensor.

6.4.1.5 Attitude Sensing, Synchronous Orbit

The attitude sensing instrumentation necessary for the LEM configuration in a synchronous orbit has been selected and includes:

a. Solar aspect sensor

b. Long-life Earth Sensor

At the synchronous altitude, satellite eclipses will occupy only a small portion of the orbital cycle. Therefore, the loss of solar aspect sensor data can be offset by careful interpolation between attitude points on either side of the eclipse. The ambiguity at the point where the satellite is in the Earth-Sun line cannot be resolved, but this condition occurs only near the vernal and autumnal equinoxes, and is of relatively short duration.

6.4.1.6 Solar Aspect Sensor

The same solar aspect sensor will be utilized at synchronous altitude as is recommended for the 400 km orbit configurations.

### 6.4.1.7 Long-Life Earth Sensor

The long-life Earth sensor, developed by the Advanced Technology Division of American Standard, has been successfully flown on the ATS-2 vehicle and is scheduled to fly shortly on ATS-D and E. The sensor operation and components are very similar to the A-OGO horizon sensor recommended for the 400 km orbit configurations. Rather than dithering on the earth's horizon, the long-life Earth sensor utilizes two orthogonal scan axes that continuously sweep across the entire earth. A mirror suspended on flexure pivots, driven by pulsed electrical coils, causes the narrow field of view of a germanium telescope to scan back and forth in space with a total sweep which covers the earth from edge to edge. A semiconductor bolometer generates an earth pulse and is subsequently reshaped by a Schmitt trigger. If the Earth is centered on this oscillation of the field of view, the output waveform is symmetrical about the zero reference. The Schmitt-trigger output switches positive or negative depending on which side of the zero reference the earth pulse appears. Under these conditions, the Schmitt-trigger output will be positive for the same length of time it is negative, resulting in a zero dc component in the output of the scan axis. If the Earth is displaced from the center of oscillation, the output waveform will be unsymmetrical, resulting in unequal positive and negative output times from the Schmitt-trigger, and thus a dc component. The dc component of each of the two orthogonal sweep axes in telemetered to the ground as geocenter angle position data.

As in the A-OGO horizon sensor, the only moving parts in the long-life earth sensor are the highly reliable flexure pivots in each of the two sweep axes.

In the synchronous altitude configurations, the sensor has a $\pm$21 degree field of view and an accuracy of approximately 0.5 degree in each axis.

# SECTION 7

# FLIGHT EXPERIMENT OPERATIONAL PROCEDURES

The operational requirements for each of the three flight experiments (S-IVB, LM-Rack, Extendible Rod) are described in this section. Operational requirements include:

a. Preflight Experiment System Test Procedure

b. Health Moniter and Experiment Readiness Procedure

c. Flight Experiment Profile

d. Flight Data Collection Profile

e. Data Reduction and Analysis Procedure

In order to avoid repetitive discussion of procedures common to all experiments, a, b, and e above are discussed in common with emphasis on a particular experiment as required. Separate flight experiment and data collection profiles are included for each experiment.

## 7.1 PREFLIGHT EXPERIMENT SYSTEM TEST PROCEDURE

### Experiment Test Requirements

The following information shall be defined and/or documented for each of the flight experiments:

a. Experiment/spacecraft interface definition/requirements (e.g., power, separation planes/force/timing, telemetry, command, etc.)

b. Experiment Critical Functions (ECF) alignment accuracy/precision in each axis, damping factors, etc.

c. Experiment/Mission Profile.

The total experiment test program will be delineated from receipt of the experiment equipment out of final assembly at the factory on through to the time of launch as a part of the spacecraft system. The ground flow profile will show the discrete tests, inspections, configuration, location, time required and purpose. This profile will then provide the basis for scheduling the delivery, installation, test, and launch preparation of the experiment into the spacecraft and will permit identification of specific facilities and manpower requirements peculiar to a given task. Responsibilities for each element of the test profile will be also defined.

A typical ground flow profile is illustrated in Figure 7-1.

Ground test and launch readiness requirements will be identified and documented utilizing the above generated information.

### 7.1.1 GROUND TEST REQUIREMENTS (ACCEPTANCE TEST REQUIREMENTS)

Experiment Critical Functions (ECF) will be reviewed, their critical parameters defined, and the associated critical components identified. Then for each ECF, Experiment Acceptance Test Requirements will be defined to the testing agencies to insure verification of functional operation in the ground, launch and space environments, interface compliance redundant paths (where applicable), negative (taboo) mode operation, and flight readiness.

A recommended set of test requirements shall include:

a. Subsystem functional requirements

b. Electromagnetic compatability requirements

c. Mechanical alignments, weight and balance measurements or calculations

d. Inspection requirements for shipment, installation and flight readiness

e. "Green-line" limits for critical components

f. "Red-line" limits for critical components

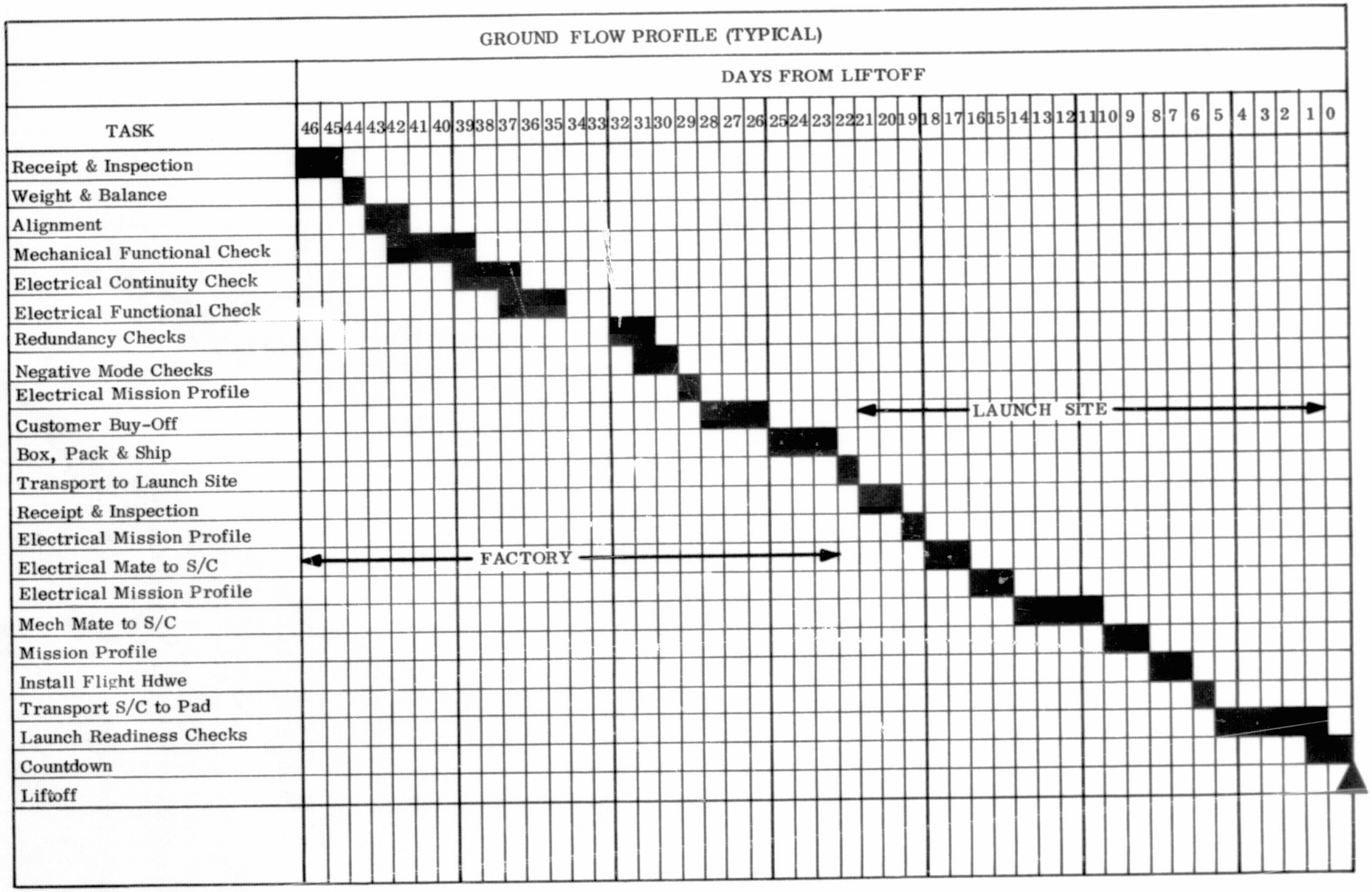


Figure 7-1. Ground Flow Profile

g. Telemetry line/channel/pin assignments, sensor range

h. Command allocation, word structure

i. "Mission profile" definition

j. Test equipment requirements, accuracies, ranges

k. Electrical power, continuity, dielectric strength, battery wet-stand, capacitance

l. Test data requirement for log books, calibration book

m. Method of demonstration of requirement-inspection, calculation, demonstrations and/or qualification

n. Rework requirements-harness, boxes

o. External/internal environmental requirements-operational, storage, shipment and flight

p. Launch readiness requirements - "Hold-Abort" criteria and limitations, thermal conditioning, configuration before gantry removal, initialization requirements

q. Ground environmental test requirements

r. Factory/launch site test requirements for customer buy-off

### 7.1.2 QUALIFICATION TEST REQUIREMENTS

Prime built experiment hardware shall be subjected to and successfully pass a rigorous qualification test program before flight of identical prime experiment hardware. A recommended set of requirements for qualification shall be established for:

a. Temperature (high and low)

b. Vacuum

c. Voltage (high and low)

d. Electromagnetic Interference (EMI)

e. Shock

f. Vibration

g. Life

Where possible in test, combinations of environments shall be made to ensure that the total performance envelope is covered. In no case shall an unqualified component be flown that may in anyway jeopardize the primary mission. Prime-built hardware that has passed the qualification test program shall not subsequently be used as prime flight hardware, since levels of the environments are significantly higher than the anticipated flight levels. In addition, the purpose of qualification is to demonstrate design adequacy and not flight readiness. The qualification hardware shall first have passed the prime acceptance test requirements, thus, "qualifying the acceptance test procedures as well as the design and manufacturing procedures."

### 7.1.3 CUSTOMER OPERATIONAL DOCUMENTATION/REQUIREMENTS

General Electric shall provide the necessary inputs to the following customer operational documentation.

#### 7.1.3.1 System Test Objectives

Define flight experiment objectives. Recommend experiment sequences of events: include definition of significant performance characteristics of experiment hardware as it would affect the mission.

#### 7.1.3.2 Operational Requirements Document (ORD)

A detailed description of all items of an operational nature required from the range by the experiment will be generated. Such specifics as data processing, meteorological services, transportation and all additional related requirements for accomplishing the specific test series in the experiment program will be treated.

#### 7.1.3.3 Planning Estimate (PE)

This will be a brief summary of the general objectives, time phasing and any major range support requirements of the experiment, issued very early in the experiment program.

#### 7.1.3.4 Program Requirements Document (PRD)

The PRD gives the detailed planning information on the test program. Where needed GE shall identify long-lead items and the known requirements as early as possible. Updates of the detailed requirements will be made when necessary.

7.1.3.5 Range Safety Requirements

This document will identify hazards and define the range safety requirements which must be met by the range user. Included in the GE inputs to this document will be:

a. Pad safety Plan

b. Range safety information

c. Communications requests

7.1.3.6 Test Operations Orders

This customer document will contain inputs by GE to define to the tracking stations significant experiment performance characteristics/parameters, telemetry and tracking requirements (frequency of contact, accuracy). These requirements are necessary to permit the controlled conduct of the experiment sequence in orbit.

## 7.2 HEALTH MONITOR AND EXPERIMENT READINESS PROCEDURE

The diagnostic instrumentation required will be obtained in the following manner: Telemetry points will be required to provide experiment subsystem health and diagnostic information. These points will be determined as the hardware design progresses, but are expected to number less than 60. They will include, but not be limited to, measurements of boom-deployment motor current and voltage, strain gauges at the roots of the booms, fluid temperature and pressure on the vehicle-mounted damper, and other housekeeping functions.

## 7.3 FLIGHT EXPERIMENT PROFILE

Flight experiment profiles, showing the sequence of operational events during the passive gravity stabilization experiments, are given in Tables 7-1 through 7-4 for the S-IVB Vertical, S-IVB Horizontal, and LM-RACK Synchronous, stabilization experiments. The operational sequence and time profile for the rod structural flight experiment follows the flight experiment profiles.

The stabilization experiment profiles show the use of the active control system for initial stabilization before the gravity gradient experiment. This is not a requirement for

successful operation of the gravity gradient system, but does ensure that stabilization in the selected orientation is achieved in minimum time.

Table 7-1. S-IVB Vertical Configuration, Flight Experiment Profile

| Event | Time | |
|---|---|---|
| | Begin | Complete |
| 1. Experiment Readiness Check (Evaluate Health Monitors) | 0 hr | 0.5 hr |
| 2. Active Control Positions S-IVB (At Stable Null) | 0.5 | 1.5 hr |
| 3. Activate Experiment Sensors and Record Data (Record Experiment and Health Data) | 1.5 hr | 2.0 hr |
| 4. Deactivate Active Control | 2.0 hr | 2.0 hr |
| 5. Record Position and Rate Data to Evaluate Damping | 2.0 hr | 8 days |
| 6. Record Position and Rate Data to Evaluate Accuracy | 8 days | 16 days |
| 7. Final Health Monitor Check | 16 days, 0 hr | 16 days, 0.5 hr |
| 8. Reactivate Active Control | 16 days, 0.5 hr | - |
| 9. Deactivate Experiment Sensors | 16 days, 1 hr | - |
| 10. Repeat above sequence as possible within flight operations plan | | |

Table 7-2. S-IVB Horizontal Configuration, Flight Experiment Profile

| Event | Time | |
|---|---|---|
| | Begin | Complete |
| 1. Experiment Readiness Check | 0 hr | 0.5 hr |
| 2. Active Control Positions S-IVB (Longitudinal Axis Horizontal) | 0.5 hr | 1.5 hr |
| 3. Activate Sensors and Record Data (Experiment and Health Data) | 1.5 hr | 2.0 hr |
| 4. Deactivate Active Control | 2.0 hr | 2.0 hr |
| 5. *Uncage & Extend Booms | 2.0 hr | 3.0 hr |
| 6. Record Position and Rate Data to Evaluate Damping | 3.0 hr | 8 days |
| 7. Record Position and Rate Data to Evaluate Accuracy | 8 days | 16 days |
| 8. Final Health Monitor Check | 16 days, 0 hr | 16 days, 0.5 hr |
| 9. Change Boom Length by 50 ft to Alter Stabilization Configuration | 16 days, 0.5 hr | 16 days, 1.5 hr |
| 10. Repeat Steps 6, 7, 8 | 16 days, 1.5 hr | 32 days |
| 11. Repeat Steps 9 and 10 at two other Rod Length Increments of 50 Ft. | 32 days | 64 days |
| 12. Reactivate Active Control | 64 days | - |
| 13. Deactive experiment sensors | 64 days, 0.5 hr | - |

*Boom Extension at 0.1 ft/sec from initial conditions of 0.01 degree/sec rate and 10 degree error from the nominal stabilized position and rate will result in between 30 and 45 degrees oscillatory amplitude about the vertical and rates of less than 0.03 degree/sec with respect to vertical.

Table 7-3. LM-RACK Synchronous Configuration, Flight Experiment Profile

| Event | Time | |
|---|---|---|
| | Begin | Complete |
| 1. Experiment Readiness Check | 0 hr | 0.5 hr |
| 2. Active Control Positions LM | 0.5 hr | 1.5 hr |
| 3. Active Sensors & Record Data (Experiment and Health Data) | 1.5 hr | 2.0 hr |
| 4. Deactivate Active Control | 2.0 hr | 2.0 hr |
| 5. *Uncage and Extend Booms | 2.0 hr | 3.0 hr |
| 6. Record Position and Rate Data (Evaluate Damping) | 3.0 hr | 10 days |
| 7. Record Position and Rate Data (Evaluate Accuracy) | 10 days | 30 days |
| 8. Final Health Monitor Check | 30 days, 0 hr | 30 days, 0.5 hr |
| 9. Reactivate Active Control | 30 days, 1 hr | - |
| 10. Deactivate Experiment Sensors | 30 days, 1.5 hr | - |

*Boom Extension at 0.1 ft/sec have initial conditions of 0.1 degree/sec rate and 10 degree error from the nominal stabilized position and rate will result in between 30 and 45 degrees oscillatory amplitude about the vertical and rates of less than 0.004 degree/sec with respect to vertical.

## Table 7-4. Rod Flight Experiment Profile

| Event | | Time | |
|---|---|---|---|
| | | Begin | Complete |
| 1. | Experiment Readiness Check | 0 hr | 0.5 hr |
| 2. | Active Control Positions S-IVB | 0.5 hr | 1.5 hr |
| 3. | Activate Experiment Sensors and Record Data | 1.5 hr | 2.0 hr |
| 4. | Deploy Rod 250 feet for bending test | 2.0 hr | 3.0 hr |
| 5. | Allow Rod Motion to Damp | 3.0 hr | 4.0 hr |
| 6. | Excite Rod and Measure Dynamic Response | 4.0 hr | 5.0 hr |
| 7. | Retract Rod | 5.0 hr | 6.0 hr |
| 8. | Repeat Events 2, 4, 5, 6, 7 | 6.0 hr | 11.0 hr |
| 9. | Active Control Positions S-IVB Delay up to 1.5 hr to achieve proper orbit position | 11.0 hr | 13.5 hr |
| 10. | Deploy Rod 400 feet for Straightness test | 13.5 hr | 15.0 hr |
| 11. | Allow Rod Motion to Damp | 15.0 hr | 16.0 hr |
| 12. | Measure Rod Straightness | 16.0 hr | 16.5 hr |
| 13. | Retract Rod Delay up to 1.5 hr for proper orbit position | 16.5 hr | 19.5 hr |
| 14. | Active Control Positions S-IVB | 19.5 hr | 20.5 hr |
| 15. | Deploy Rod 400 feet for Thermal Bending Test | 20.5 hr | 22.0 hr |
| 16. | Allow Rod motion to Damp | 22.0 hr | 23.0 hr |
| 17. | Measure Rod Bent Position | 23.0 hr | 24.0 hr |
| 18. | Measure Rod Reaction passing through into and out of eclipse | 24.0 hr | 25.5 hr |
| 19. | Retract Rod | 25.5 hr | 27.0 hr |
| 20. | Final Health Monitor Check | 27.0 hr | 27.5 hr |
| 21. | Reactivate Active Control | 27.5 hr | - |
| 22. | Deactivate Experiment Sensors | 28.0 hr | - |

## 7.4 FLIGHT DATA COLLECTION PROFILE

### 7.4.1 DATA COLLECTION

Factors which have been considered in determining the amount of data required from the spacecraft to maintain real-time experiment monitoring and control, and to perform a through postflight evaluation of its performance include the basic frequency of oscillation of the spacecraft about its axes, the number and duration of opportunities for ground station contact with the satellite, the onboard data storage capability, and the capabilities of the ground data processing and analysis programs.

The following assumptions have been made in making the tradeoffs associated with the determination of data collection schedules and techniques:

a. Use of STADAN for Earth-satellite communications

b. Use of essentially the present functional capabilities of ATS/GGTS attitude determination software programs

### 7.4.2 SATURN IV-B EXPERIMENTS

Gravity gradient vehicle motions are sinusoidal in nature. A minimum of five samples per cycle are required to adequately reproduce the wave shape. System simulation studies discussed elsewhere indicate that the shortest period of spacecraft oscillation will be about the roll axis and will be about 50 minutes at 400 km altitude. Since there are two cycles per orbit, a minimum of 10 more or less equally spaced data samples per orbit are required for stabilization subsystem performance determination; however, even these will be insufficient for any but a gross study of boom dynamics. The STADAN net is not adequate to permit sufficient real-time station contacts to perform the stabilization evaluation. Therefore, it appears necessary to include a simple inflight tape recorder for digital data storage when the vehicle is out of station contact. Radiation Inc. built a PCM digital tape recorder for Nimbus and other NASA programs which appears ideal for this purpose. It has more capacity than the Saturn IVB experiment requires and can store 108 minutes of data. This would, therefore, supply continuous coverage that could be read out during one station contact at a speed up of 32 to 1, giving complete data coverage that would permit total experiment evaluation.

It is recommended that the Fort Myers, Quito, Lima, and Santiago STADAN stations be chosen as the primary stations for the Saturn IVB gravity gradient experiment. These stations represent a "fence" across the orbital path and allow contact with the vehicle at least once per orbit. Data could be relayed by these stations to MSFC on a real-time basis via teletype or other existing quick-look communication facilities. Magnetic tape recordings of vehicle telemetry data will be required from the station for detailed postflight analysis of subsystem performance. These stations should also have facilities for receiving and reproducing photographically the output of the onboard television system.

The LEM experiment at synchronous altitude does not present the problem of storing data during the orbital oscillation, because the spacecraft will be in continuous view of one or more stations. Data should be received from the spacecraft approximately once per hour, at least during the initial stages, or until some trend is established that would warrant increasing the frequency of examination or allow it to be decreased.

Data received at the ground station would be recorded, time-annotated, and returned to MSFC and the subsystem contractor for processing and evaluation.

### 7.4.3 EXTENDABLE ROD EXPERIMENT

The rod experiment is to be conducted from a Saturn IVB in a 400 km orbit. Because of the nature of this experiment and the fact that the best measurements of rod dynamics can be obtained from television pictures, it is believed that all the dynamic parts of the experiment should be conducted over a station. This would allow telemetry and television data to be obtained in real time. The starting point of the experiment period should be chosen to provide a maximum number of station contacts during the succeeding four orbits to that all experiment phases can be monitored by STADAN stations. The number of station contacts could be held to one per orbit if a wideband tape recorder, capable of handling TV signals, was procured and used. However, it is felt that the short duration of the experiment and the availability of appropriate equipment at the STADAN stations makes this tradeoff less attractive than maximizing earth/satellite communications.

If at the time of experiment conduction there are astronauts aboard the spacecraft, they could provide assistance on a noninterference (with their summary mission) basis in obtaining film records of boom performance by operating body-mounted cameras aligned with the nominal long axis of the boom.

All data received at the ground station from the spacecraft including video recordings and photographs from a video screen would be returned to MSFC and the subsystem contractor for further processing and evaluation.

## 7.5 DATA REDUCTION AND ANALYSIS PROCEDURE

### 7.5.1 SOFTWARE STATUS

Sufficient software programs and experience are currently in place to perform and evaluate the entire spectrum of Saturn IVB and LEM experimentation. Minimal effort will be required to adapt this knowhow to the specific program requirements.

Several large-scale digital computer programs will be utilized in support of the flight test analysis and evaluation activities. The include systems currently utilized the IBM 7094 computer system for long-term data processing and the General Electric Desk-Side Computer Service (GE 605 computer system) for near-real time data processing.

### 7.5.2 LONG-TERM DATA SYSTEM

The Long-Term Data System will be utilized, to handle, process, and reduce all fight data acquired through the Saturn IVB and LEM flight tests and fowarded to the experimenter at frequent intervals. Telemetry data will be supplied to the experimenter by means of a Raw telemetry Data Tape (RTDT); television data will be supplied by means of 35 mm film. The telemetry data will be processed to provide computer spacecraft attitude information and diagnostic performance data; television data will be processed to provide boom-tip deflection information and spacecraft pointing attitude.

The telemetry data processing portion of the system is divided into three program groupings:

a. Preliminary processing

b. Attitude computation

c. Diagnostic reduction

Each grouping includes those system-component programs which are to be operated concurrently. The three will be operated in the order shown, with an intermediate survey made of the output at the end of each.

7.5.2.1 Preliminary Processing

The first data system run is devoted to preliminary data processing tasks, generally common to both subsequent runs. These include:

a. Data verification and sorting. Each telemetry data frame is checked for telemeter mode before sorting data. The time code associated with each frame is checked for continuity and the telemetry word locations are checked for data file format. The sync bit count is interpreted before each telemetry data word is inserted in the proper data matrix for calibration.

b. Data calibration. Each telemetry function is extracted from the input format and properly converted into appropriate engineering units.

c. Data merge. Ground measurement data is time-correlated with telemetry data for use in subsequent reduction runs.

d. Sensor plots. Attitude sensor data values are plotted (using SC 4020) for manual examination before computation of attitude.

e. Data list. Telemetry function lists are generated over selected intervals of time to be used in subsequent performance analysis (special request basis).

Control capabilities are provided in this run to instruct the system to pass over redundantly provided input data, and to denote time intervals through which data should be listed or otherwise reduced and reported (in hard-copy form).

7.5.2.2 Attitude Computation

The second phase of the data system is devoted to the computation of vehicle attitude. Calculations are based on the attitude sensor data measurements extracted and forwarded by the preliminary processing programs. Computational results are presented on magnetic tape in specified form delivery to NASA and in listed and plotted form for use in subsequent performance analysis.

The techniques for determining vehicle attitude involve comparison of certain reference vectors as defined in an orbit-bound coordinate system to measured position (of these vectors) in a vehicle-bound coordinate system. Consideration of more attitude-related measurements then are (minimally) required to determine attitude allows a computational optimization to improve the accuracy of determination. Further improvement in output data quality is made through comparison of adjacent (in-time) attitude values, considering continuity and smoothness characteristics.

The programs included with this phase of the data system may accordingly be categorized as follows:

a. Initial calculation of attitude, in which preliminary calculation of vehicle attitude is made considering the best minimum combination of measurement data values available.

b. Computation optimization, in which consideration is given to all measurement data values available, adjusting calculated attitude so as to minimize any measurement discrepancies between the various attitude sensors.

c. Attitude value smoothing, in which successive computed attitude values are compared and averaged to produce final determined attitude data. (Vehicle attitude rates are calculated as an inherent step in this smoothing process and are also provided as output data.)

Control capabilities are provided in these programs to block or to deemphasize any questioned input measurement data and to direct the output data-smoothing process as desired.

7.5.2.3 Diagnostic Reduction

The third phase of data system operation involves reduction of telemetry data in providing summarized reports of component operation. The programs included within this portion of the system are:

a. Event condition module. This module interprets all digital event telemetry functions and provides an output report to indicate each event occurrence.

b. Event level module. This module interprets all analog event telemetry functions and provides an output report to indicate each event occurrence.

c. Summary mean/standard deviation module. This module compresses selected analog telemetry functions, providing the mean value and standard deviation of each function as calculated over each file of data handled.

d. Interval mean/standard deviation module. This module compresses selected analog telemetry functions, providing the mean value and standard deviation of each function as calculated over (1) a selected interval of time or (2) a selected number of data samples.

e. Data list module. This module provides a point-by-point report of the value of any selected telemetry function.

f. Record select module. This module collects and integrates the output of the data interpretation modules and provides a summary output of reports from each.

Control capabilities are provided in these programs to allow reduction of data over selected time intervals and to allow establishment of a sample rate in connection with the data listing capability.

Those portions of the data system devoted to reduction of data extracted from television pictures consist of programs to produce boom tip deflection data and vehicle pointing angle data (as measured by the television camera system).

These programs involve:

a. Transfer of measured data from television camera system scale units to spacecraft-bound reference system units.

b. Further transfer of measured data to a selected reference system, if desired

c. Calculation of vehicle pointing angle from earth position measurements

### 7.5.3 SHORT-TERM DATA SYSTEM

The Short-Term Data System provides a capability of determining spacecraft attitude and subsystem "health" status in near-real time, through integration of the General Electric Desk-Side Computer Service (DSCS) at Valley Forge, Pennsylvania, with the NASCOM teletype communication network. Telemetry data is formatted at the tracking stations by an SDS 910 computer (which generates a 5-level Baudot Code paper tape) and transmitted to the Operations Control Center and GE/VF via the NASCOM network. Two separate teletype message formats are utilized:

a. Special Gravity Gradient Message

b. G.G. Class II Data Message

The Special Gravity Gradient Message is utilized when near-real time spacecraft attitude determination is desired. The message contains attitude sensor data sampled every third telemetry main frame (approximately 9 seconds) for approximately 5 minutes (34 data points).

The G.G. Class II Data Message is used to forward to the experimenter one main frame of near-real time telemetry data required for near-real time subsystem "health" monitoring.

### 7.5.4 QUICK-LOOK ATTITUDE DETERMINATION SYSTEM

The Quick-Look Attitude Determination System is used to calculate near-real time spacecraft attitude in support of on-orbit operations. Flight attitude sensor data is transmitted to GE by means of the Special Gravity Gradient teletype message generated by the participating ground stations. The flight data is produced at the GE NASCOM terminal unit in both hard copy and paper tape form. The paper tape is introduced to the terminal unit of the GE Desk-Side Computer Service (DSCS) by the system operator for calculation of spacecraft attitude. Computer attitude (Euler pitch, roll, and yaw) is provided on the DSCS

terminal unit in hard copy and paper tape form. The DSCS generates the paper tape in a format that is compatible with the NASCOM system. The system operator then introduces the resultant paper tape to the GE NASCOM terminal unit for transmission to the Operations Control Center and the ground stations. The cycle can be performed in about 15 minutes.

### 7.5.5 QUICK-LOOK SPACECRAFT HEALTH MONITORING

The already existing GE NASCOM terminal and DSCS facilities enable the gravity gradient experimenter to obtain (and process) near-real time hardware health data directly from the participating ground stations. The hardware health data can be transmitted to the experimenter by means of the G. G. Class II Data Message which is produced at the GE NASCOM terminal in both hard copy and paper tape form. Depending on the units of measurement, the data can be used directly by on-orbit support personnel, or can be introduced into the DSCS for speedy conversion to engineering units. The converted data can again be forwarded to the Operations Control Center, if desired.

### 7.5.6 DATA ANALYSIS AND REPORTING

#### 7.5.6.1 On Line Support

Requirements for support by the subsystem contractor are expected to be similar for all projected experiments. Such support should consist of examination of gravity gradient subsystem health data from the spacecraft to determine if the experiment can be initiated, evaluation of predicted initial conditions to determine if they are within the bounds specified for experiment initiation, to provide any consultation necessary during the initiation/deployment sequency, and to determine if the deployed boom configuration is proper. Perhaps, the most important contribution to be made by the on-orbit support team will be to ensure timely delivery of subsystem telemetry data and orbital and sun ephemeris data as input to the quick-look attitude determination program and then to provide knowledgeable interpretation of the program output to see if the experiment is proceeding as expected. The on-orbit team will also be responsible for the identification of malfunctions anywhere in the subsystem and will participate in contingency planning that can be accomplished to offset the effect of the malfunctions. The on-orbit team should prepare a quick-look report following termination of the experiment which will detail any malfunctions discovered and include preliminary results of the attitude determination studies.

7.5.6.2 Postflight Analysis

In-flight performance of the experiments will be subjected to an in-depth analysis and evaluation to identify system and subsystem performance characteristics (both normal and anomalous), and to provide quantitative and qualitative assessment of flight demonstrated system and subsystem capabilities. This evaluation effort will be planned to consider system performance in stabilizing the spacecraft under flight conditions, and to also consider component hardware performance in supporting system operation. Information and date pertaining to system performance criteria will be generated in a System Capability document to provide standards to which system flight performance may be compared.

7.5.6.3 Initial Capture and Settling

The period of flight immediately following experiment initiation will demonstrate system performance in initially acquiring a preferred spacecraft orientation. As the significant step in initiating capture is boom deployment, capture and settling performance should be evaluated with respect to times, rates, and attitude at deployment. Each attitude parameter should be considered separately in terms of excursion amplitude decay and oscillation frequency, pointing angle, and vehicle yaw characteristics will be of particular importance.

7.5.6.4 Steady-State Performance

Performance characteristics displayed during periods of flight in which no special experiment conditions are imposed will demonstrate the basic capabilities of the stabilization system. Evaluation of performance should include consideration at attitude parameter characteristics such as angular bias, excursion amplitudes, and oscillation frequencies over a complete range of space environment conditions. Solar incidence, magnetic field, and orbit eccentricity profiles will be used in conjunction with associated attitude profiles to assess system response to these changing conditions. System response to dynamic environmental changes, such as magnetic storms or entry/exit from solar eclipse, will be of particular significance.

Spacecraft stabilization under changing operational conditions that may exist during the experiments will be demonstrated periodically throughout flight according to orbit test

scheduling. Characteristics of system performance under these conditions will be assessed, taking into account the components appearing concurrently on each attitude parameter in response to the space environment. Consideration should be given to excursion amplitudes and amplitude decay on each parameter attributable to the operational conditions experienced. (This evaluation will include assessment of system response to gravity gradient system components, as well as other payload experiments and basic spacecraft systems.)

# SECTION 8

# PRELIMINARY RESOURCE ANALYSIS

This section discusses the resource analysis for design, fabrication, and testing of the stabilization components required for the three (3) types of flight experiments. The program shown is complete through qualification of all components, but does not include fabrication and testing for flight components, integration of the experiment into the spacecraft, flight test, or postflight analysis. Five resource analysis plans are outlined; namely,

a. Design Plan

b. Manufacturing

c. Test Plan

d. Schedule Plan

## 8.1 DESIGN PLAN

### 8.1.1 SPHERICAL MAGNETIC DAMPER

#### 8.1.1.1 Engineering Specifications and Test Plans

1. Prepare damper design specification and test specification.

2. Prepare engineering test plan.

#### 8.1.1.2 Analysis

Dynamics

1. Establish dynamic environment for damper during launch phase.

2. Evaluate response of damper to dynamic environment during launch to develop design loadings and component qualification requirements.

3. Provide damper design support to engineering.

4. Provide test planning for dynamic tests. Provide surveillance of tests and analysis of results.

Thermal

1. Provide engineering the analytical support to ensure adequate thermal simulation in design of the damper.

2. Provide test planning for thermal-vacuum environment tests and analyze results.

Weight Control

1. Assemble and supply mass data for all groups concerned.

2. Develop and publish target weight and weight trend current and to effect early weight control action.

Materials

1. Review component specification and all drawings for material applications.

8.1.1.3 Design Magnetically Anchored Damper

Engineering

1. Perform structural design to meet environmental loads.

2. Prepare fit and tolerances design analysis.

3. Design for ease of manufacture.

4. Conduct optimization tests and analysis on the following functional characteristics:

a. Magnetic dipole per lb of damper weight

b. Inner sphere centering suspension force

c. Eddy current and viscuous fluid damping

5. Prepare at least three (3) design concepts in layout form and select one based on evaluation of all pertinent design criteria.

6. Conduct design reviews to permit timely periodic evaluation of design decisions.

7. Contact and evaluate Vendors for purchase of following parts:

a. Magnet

b. Bellows

c. Graphite Hemispheres

8. Prepare Manufacturing drawings.

9. Prepare Engineering Design Report.

Quality Assurance

1. Prepare test equipment specifications and designs for test equipment modifications.

8.1.2 ERECTABLE ROD UNIT

8.1.2.1 Engineering Specifications and Test Plans

1. Prepare rod unit design specification and test specification

2. Prepare engineering test plan.

8.1.2.2 Analysis

2. Evaluate dynamic response to develop design loading for both launch and flight conditions and component qualification test levels.

3. Provide dynamic test planning support, test surveillance, and analysis of results.

Thermal

1. Provide engineering the analytical support to ensure adequate thermal stimulation in design of the rod and erection unit.

2. Provide test planning for thermal-vacuum environment test and analyze results.

Weight Control

1. Assemble and supply mass data for all groups concerned.

2. Develop and publish target weight schedules. Maintain close contact with design to keep weight and weight trend current and to effect early weight control action.

Materials

1. Review component specification and all drawings for material applications.

8.1.2.3 Design Erectable Rod Unit

Engineering

1. Perform structural design to meet environmental loads.

2. Prepare fit and tolerances design analysis.

3. Design for ease of manufacture.

4. Conduct optimization tests and analysis on the following functional characteristics:

   a. Erection Drive Train

   b. Drive Train Bearing and Lubrication

c. Deployed Rod Structural Properties

d. Deployed Rod Straightness

e. Rod Joining Techniques and Properties

5. Prepare at least three (3) design concepts in layout form and select one based on evaluation of all pertinent design criteria.

6. Conduct design reviews to permit timely periodic evaluation of design decisions.

7. Prepare Manufacturing Drawings.

8. Prepare Engineering Design Report.

Quality Assurance

1. Prepare test equipment specifications and designs for test equipment modifications.

## 8.1.3 GRAVITY ANCHORED SINGLE-AXIS DAMPER

### 8.1.3.1 Engineering Specifications and Test Plans

1. Prepare rod unit design specification and test specification

2. Prepare engineering test plan.

### 8.1.3.2 Analysis

Dynamics

1. Establish dynamic environment for damper during launch phase.

2. Evaluate response of damper to dynamic environment during launch to develop design loadings and component qualification requirements.

3. Provide damper design support to engineering.

4. Provide test planning for dynamic tests. Provide surveillance of tests and analysis of results.

Thermal

1. Provide engineering the analytical support to ensure adequate thermal simulation in design of the damper.

2. Provide test planning for thermal vacuum environment tests and analyze results.

Weight Control

1. Assemble and supply mass data for all groups concerned.

2. Develop and publish target weight schedules. Maintain close contact with design to keep weight and weight trend current and to effect early weight control action.

Materials

1. Review component specification and all drawings for material applications.

8.1.3.3 Design Gravity Anchored Damper

Engineering

1. Perform structural design to meet environmental loads.

2. Prepare fit and tolerances design analysis.

3. Design for ease of manufacture.

4. Conduct optimization tests and analysis on the following functional characteristics:

   a. Torsion Wire Design

   b. Hysteresis Material and Segment Shape

   c. Magnet Design and Shielding

5. Prepare at least three (3) design concepts in layout form and select one based on evaluation of all pertinent design criteria.

6. Conduct design reviews to permit timely periodic evaluation of design decisions.

7. Prepare Manufacturing Drawings.

8. Prepare Engineering Design Report.

9. Prepare test equipment specifications and designs for test equipment modifications.

## 8.2 MANUFACTURING PLAN

### 8.2.1 SPHERICAL MAGNETIC DAMPER

Engineering

1. Support Manufacturing in fabrication and assembly of damper prototype and qualification unit.

Quality Assurance

1. Provide receiving inspection for purchased parts, and in process inspection for manufactured parts.

2. Provide engineering and material planning support.

Manufacturing

1. Procure material, fabricate and assemble prototype and qualification damper unit.

2. Institute and follow up make/buy decision process.

3. Provide support for fabrication and assembly.

   a. Master Mechanic

   b. Production Engineering

c. Mechanical Planning

d. Tool Engineering

e. Production Control

8.2.2 ERECTABLE ROD UNIT

Engineering

1. Support Manufacturing in fabrication and assembly of rod and erection prototype and qualification units.

Quality Assurance

1. Provide receiving inspection for purchased parts, and in process inspection for manufactured parts. Inspection of metallurgical condition of tape material and rod straightness will be emphasized.

2. Provide engineering and material planning support.

Manufacturing

1. Procure material, fabricate, and assemble prototype and qualification rods and erection units.

2. Initiate and follow up make/buy decisions. Make/buy decision on formed rod will be key event in rod fabrication.

3. Provide support for fabrication and assembly:

   a. Master Mechanic

   b. Production Engineering

   c. Mechanical Planning

   d. Tool Engineering

   e. Production Control

### 8.2.3 GRAVITY-ANCHORED SINGLE-AXIS DAMPER

Engineering

1. Support manufacturing in fabrication and assembly of damper prototype and qualification units.

Quality Assurance

1. Provide receiving inspection for purchased parts, and in process inspection for manufactured parts.

2. Provide engineering and material planning support.

Manufacturing

1. Procure material, fabricate, and assemble prototype and qualification rods and erection units.

2. Institute and follow up make/buy decisions.

3. Provide support for fabrication and assembly:

   a. Master Mechanic

   b. Production Engineering

   c. Mechanical Planning

   d. Tool Engineering

   e. Production Control

## 8.3 TEST PLAN

### 8.3.1 SPHERICAL MAGNETIC DAMPER

Quality Assurance

1. Plan and conduct the following tests on both prototype and qualification dampers:

   a. Functional (dipole, damping, centering force)

   b. Vibration, Acceleration, and Shock

   c. Temperature

   d. Thermal Vacuum

Engineering

1. Evaluate test results and implement design changes as required

2. Conduct failure analysis as required

3. Document design and test history in final engineering report.

Analysis

1. Support engineering in interpretation of test results and failure analysis as required.

8.3.2 ERECTABLE ROD UNIT

Quality Assurance

1. Plan and conduct the following tests on both prototype and qualification rod and erection units:

   a. Functional (erection/retraction, straightness)

   b. Vibration, Acceleration and Shock

   c. Temperature

d. Thermal Vacuum

2. Reduce and document test results

Engineering

1. Evaluate test results and implement design changes as required.

2. Conduct failure analysis as required.

3. Document design and test history in final engineering report.

Analysis

1. Support engineering in interpretation of the test results and failure analysis as required.

### 8.3.3 GRAVITY-ANCHORED SINGLE-AXIS DAMPER

Quality Assurance

1. Plan and conduct the following tests on both prototype and qualification dampers:

   a. Functional (damping, suspension restraint)

   b. Vibration, Acceleration, and Shock

   c. Temperature

   d. Thermal Vacuum

2. Reduce and Document Test Results.

Engineering

1. Evaluate test results and implement design changes as required.

2. Conduct failure analysis as required.

3. Document design and test history in final engineering report.

Analysis

1. Support engineering in interpretation of test results and failure analysis as required.

## 8.4 SCHEDULE PLAN

The schedule plan shown in this section contains key events for design, development, fabrication and test of the three stabilization components. A separate schedule plan is shown for each component.

MILESTONE SCHEDULE

Spherical Damper (NAME)

ENGINEERING PROPOSAL/PROGRAM

PAGE ___ OF ___

FORM 1-9511 REV. (2-61)

| "B" LEVEL OPER. NO. | OPER. NAME | PREPARED BY | DATE | APPROVED BY | DATE | ISSUE NO. |
|---|---|---|---|---|---|---|
| | | | | | | |

| TASK NO. | SUB-TASK NO. | DESCRIPTION OF DETAIL MILESTONES | ELAPSED TIME SCHEDULE |
|---|---|---|---|
| 95b | | | (INDICATE YEARS) |
| | | | (SPECIFY CATEGORY) MONTHS/ |
| 1.0 | | Design: Dynamic Analysis | |
| | | Thermal Analysis | |
| | | Functional Optimization | |
| | | Layout Design | |
| | | Prototype Dwg. | |
| | | Qual. Unit Dwg. | |
| 2.0 | | Manufacturing: Engineering | |
| | | Procurement | |
| | | Tooling | |
| | | Proto. Fabrication | |
| | | Qual. Fabrication | |
| 3.0 | | Test: Prototype | |
| | | Qualification | |
| | | | |
| | | | |

1 2 3 4 5 6 7 8 9 10 11 12 13 14 15 16 17 18 19 20 21 22 23 24 25 26 27 28 29 30

△ START ▽ COMPLETE ▭ TIME PERIOD OF WORK

95b ⇩ MAJOR ITEM EVENT (REPORT, HARDWARE DELIVERY, FLIGHT TEST, ETC.) – INDICATE ITEM NAME NEXT TO ARROW.

Figure 8-1. Spherical Damper Schedule

MILESTONE SCHEDULE
Erectible Rod (NAME) ENGINEERING PROPOSAL/PROGRAM

FORM 1-9511 REV. (2-61)

PAGE ___ OF ___

| "B" LEVEL OPER. NO. | OPER. NAME | PREPARED BY | DATE | APPROVED BY | DATE | ISSUE NO. |
|---|---|---|---|---|---|---|
| | | | | | | |

| TASK NO. | SUB-TASK NO. | DESCRIPTION OF DETAIL MILESTONES | ELAPSED TIME SCHEDULE (INDICATE YEARS) (SPECIFY CATEGORY) MONTHS/ 1 2 3 4 5 6 7 8 9 10 11 12 13 14 15 16 17 18 19 20 21 22 23 24 25 26 27 28 29 30 |
|---|---|---|---|
| 95c | | | |
| 1.0 | | Design: Dynamic Analysis | |
| | | Thermal Analysis | |
| | | Functional Optimization | |
| | | Layout Design | |
| | | Prototype Dwg. | |
| | | Qual. Unit Dwg. | |
| 2.0 | | Manufacturing:Engineering | |
| | | Procurement | |
| | | Tooling | |
| | | Proto.Fabrication | |
| | | Qual. Fabrication | |
| 3.0 | | Test: Prototype | |
| | | Qualification | |
| | | | |
| | | | |

95c △ START ▽ COMPLETE ▭ TIME PERIOD OF WORK

MAJOR ITEM EVENT (REPORT, HARDWARE DELIVERY, FLIGHT TEST, ETC.) – INDICATE ITEM NAME NEXT TO ARROW.

Figure 8-2. Erectable Rod Schedule

MILESTONE SCHEDULE
Single Axis Damper — ENGINEERING PROPOSAL/PROGRAM
(NAME)

FORM 1-9511 REV. (2-61) — PAGE ___ OF ___

| "B" LEVEL OPER. NO. | OPER. NAME | PREPARED BY | DATE | APPROVED BY | DATE | ISSUE NO. |
|---|---|---|---|---|---|---|
| | | | | | | |

| TASK NO. | SUB-TASK NO. | DESCRIPTION OF DETAIL MILESTONES | ELAPSED TIME SCHEDULE |
|---|---|---|---|
| 95d | | | (INDICATE YEARS) |
| | | | (SPECIFY CATEGORY) MONTHS/ |
| | | | 1 2 3 4 5 6 7 8 9 10 11 12 13 14 15 16 17 18 19 20 21 22 23 24 25 26 27 28 29 30 |
| 1.0 | | Design:Dynamic Analysis | |
| | | Thermal Analysis | |
| | | Functional Optimization | |
| | | Layout Design | |
| | | Prototype Dwg. | |
| | | Qual. Unit Dwg. | |
| 2.0 | | Manufacturing:Engineering | |
| | | Procurement | |
| | | Tooling | |
| | | Proto. Fabrication | |
| | | Qual. Fabrication | |
| 3.0 | | Test: Prototype | |
| | | Qualification | |
| | | | |
| | | | |

△ START ▽ COMPLETE ▭ TIME PERIOD OF WORK

95d ⇩ MAJOR ITEM EVENT (REPORT, HARDWARE DELIVERY, FLIGHT TEST, ETC.) – INDICATE ITEM NAME NEXT TO ARROW.

Figure 8-3. Single Axis Damper Schedule

## APPENDIX A

## S-IVB MASS/INERTIA AND AERODYNAMIC DATA TRANSFORMATIONS

The mass and inertia properties of the S-IVB configuration to be used in the study (S-IVB Stage, Instrument Unit, Air Lock, Multiple Docking Adapter) were received from MSFC and are reproduced below:

Table A-1. Mass and Inertia Data

| | | |
|---|---|---|
| Wt. | $0.495820 \times 10^{5}$ lb | (1541.058 slugs) |
| X | $0.42834 \times 10^{3}$ in. | (35.695 ft) |
| Y | $0.519999999 \times 10^{1}$ in. | (0.433 ft) |
| Z | $-0.259999999 \times 10^{1}$ in. | (-0.2167 ft) |
| $I_{xx}$ | $0.162109021 \times 10^{6}$ kg-$m^2$ | (119565.13 slug-$ft^2$) |
| $I_{yy}$ | $0.119847985 \times 10^{7}$ kg-$m^2$ | (883950.90 slug-$ft^2$) |
| $I_{zz}$ | $0.119181699 \times 10^{7}$ kg-$m^2$ | (879036.7 slug-$ft^2$) |
| $I_{xy}$ | $-0.174242866 \times 10^{5}$ kg-$m^2$ | (-12851.36 slug-$ft^2$) |
| $I_{xz}$ | $+0.184811460 \times 10^{4}$ kg-$m^2$ | (+1363.0959 slug-$ft^2$) |
| $I_{yz}$ | $-0.132197614 \times 10^{5}$ kg-$m^2$ | (-9750.367 slug-$ft^2$) |

These moments of inertia are defined for a set of reference axes shown in Figure A-1.

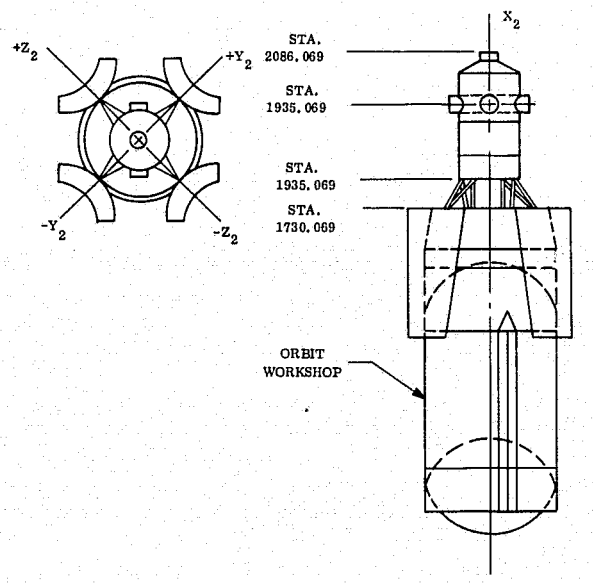


Figure A-1. Mass and Inertia Reference Axes

These moments and products of inertia are used to define the inertia dyadic as follows:

$$I_{xx} = \Sigma\, m\,(Y^2 + z^2)$$

$$I_{xy} = -\Sigma\, m\, XY$$

$$\Phi = \begin{bmatrix} I_{xx} & I_{xy} & I_{xz} \\ I_{yx} & I_{yy} & I_{yz} \\ I_{zx} & I_{zy} & I_{zz} \end{bmatrix}$$

In order to use the mass/inertia characteristics supplied by Marshall Space Flight Center as inputs to the General Electric computer program, they were transformed to a new set of body fixed reference axes. This transformation is made in two steps for simplicity. First the mass/inertia data is transformed to the reference axes used for the aerodynamic data, shown in Figure A-2. This transformation is shown as $[A]$ below. The second transformation is used to refer both mass/inertia and aerodynamic data to the set of body fixed axes used in the GE computer program. The set of body fixed axes, used in the GE computer program, is oriented with respect to an orbit reference frame set by three Euler angles: pitch ($\theta_p$), roll ($\theta_r$), yaw ($\theta_y$) in sequence, as shown in Figure A-2. In order to keep the values of these Euler angles below 90 degrees when the S-IVB is at stable null, the S-IVB and aerodynamic reference axes are rotated by -90 degrees about $Y_3$ (J2 gimbal down), and + 90 degrees about the new position of $X_3$ (offset solar panel away from direction of flight). The new position of the S-IVB with respect to the GE body axes set is shown in Figure A-2. The transformation from the aerodynamic body axes to the GE body axes is given by $[B]$. The method of transformation and numerical results are given below.

$$\begin{bmatrix} X_1 \\ Y_1 \\ Z_1 \end{bmatrix}$$ reference axes of Figure A-3 (GE computer program)

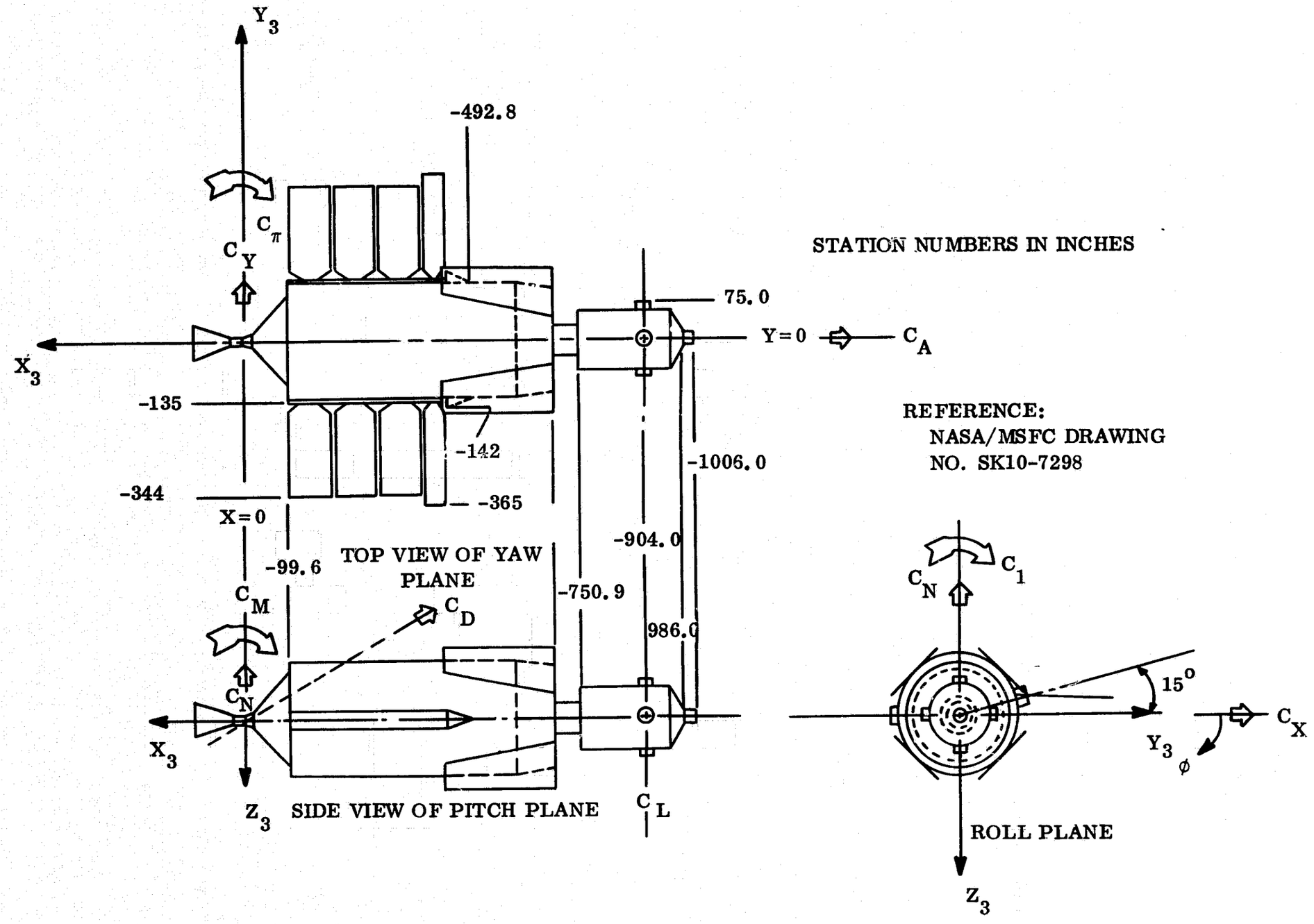


Figure A-2. Aerodynamic Body Reference Axes

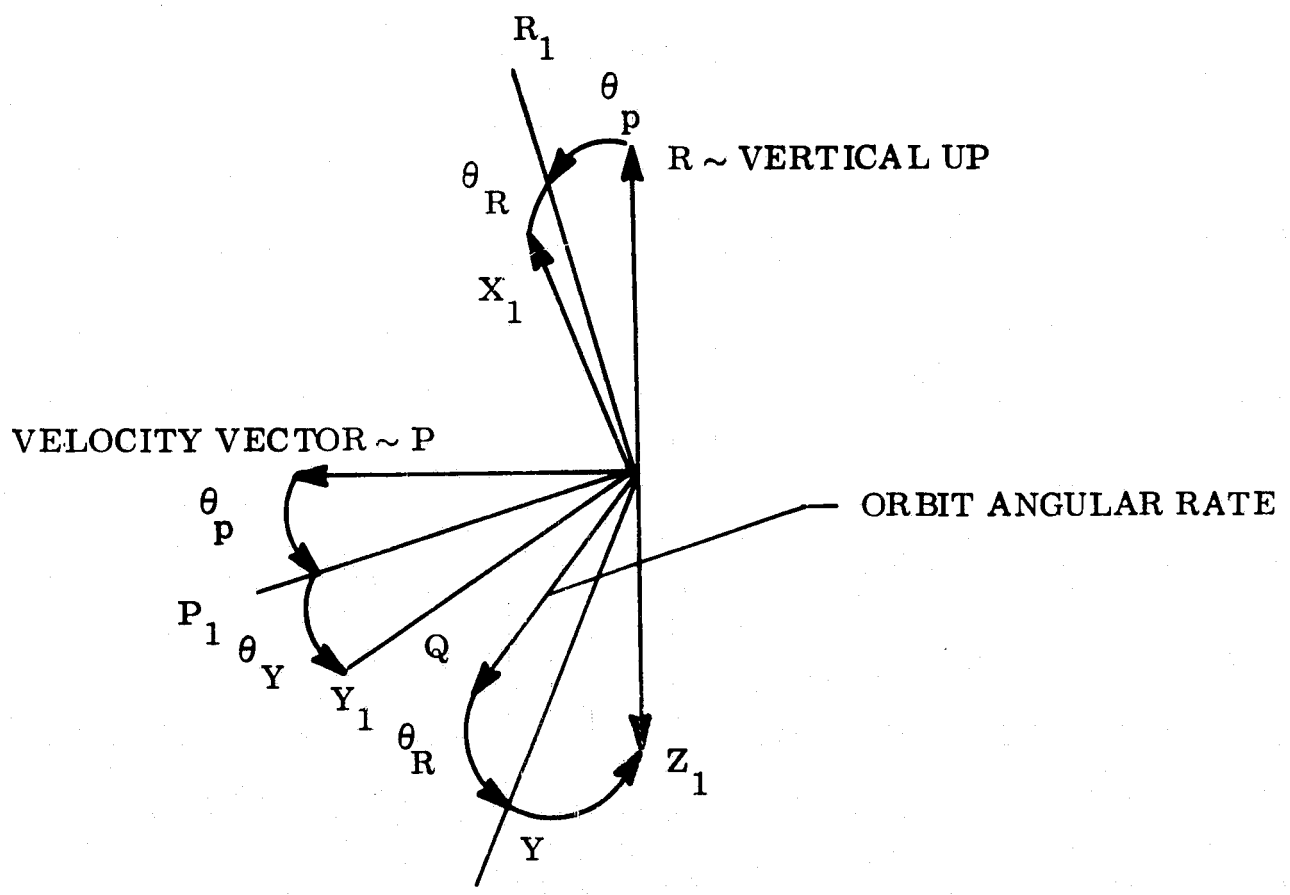


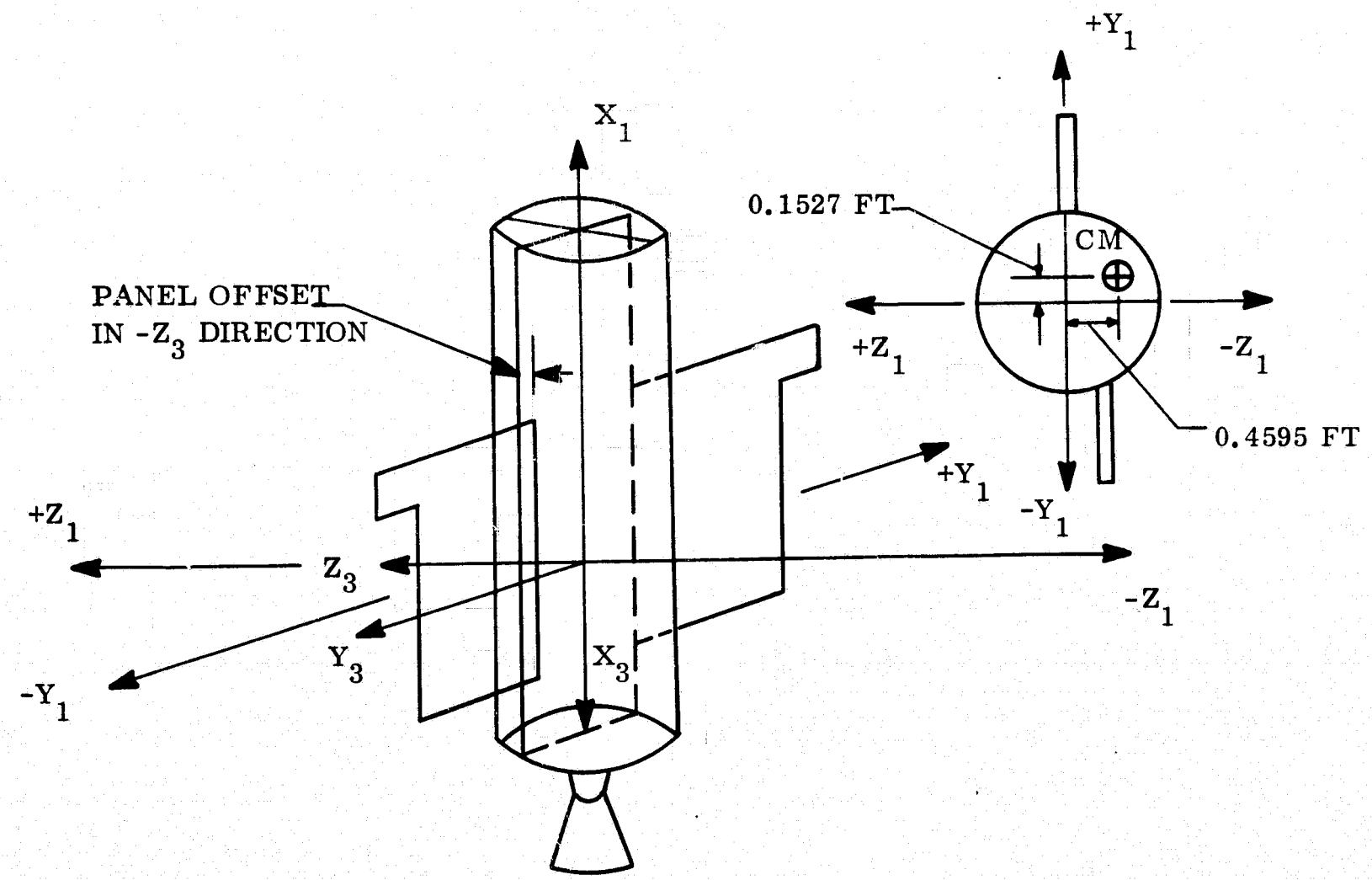


Figure A-3. General Electric Body Axes

$$\left.\begin{matrix} X_2 \\ Y_2 \\ Z_2 \end{matrix}\right]$$ reference axes of Figure A-1 (mass data)

$$\left.\begin{matrix} X_3 \\ Y_3 \\ Z_3 \end{matrix}\right]$$ reference axes of Figure A-2 (aero data)

$$\begin{bmatrix} X_1 \\ Y_1 \\ Z_1 \end{bmatrix} = [T] \begin{bmatrix} X_2 \\ Y_2 \\ Z_2 \end{bmatrix}$$

$$\begin{bmatrix} X_3 \\ Y_3 \\ Z_3 \end{bmatrix} = [A] \begin{bmatrix} X_2 \\ Y_2 \\ Z_2 \end{bmatrix}$$

$$\begin{bmatrix} X_1 \\ Y_1 \\ Z_1 \end{bmatrix} = [B] \begin{bmatrix} X_3 \\ Y_3 \\ Z_3 \end{bmatrix}$$

$$[A] = \begin{bmatrix} -1 & 0 & 0 \\ 0 & -0.707 & -0.707 \\ 0 & -0.707 & -0.707 \end{bmatrix}$$

$$[B] = \begin{bmatrix} -1 & 0 & 0 \\ 0 & -1 & 0 \\ 0 & 0 & +1 \end{bmatrix}$$

$$[T] = [B][A] = \begin{bmatrix} 1 & 0 & 0 \\ 0 & +0.707 & +0.707 \\ 0 & -0.707 & +0.707 \end{bmatrix}$$

then,

$$\Phi_1 = [T][\Phi_2][T]^{-1}$$

$$\Phi_1 = \begin{bmatrix} Ixx & +0.707\ (I_{xy} + I_{xz}) & -0.707\ (I_{xy} - I_{xz}) \\ +0.707 \leftarrow (I_{yx} + I_{zx}) & 0.5\ (I_{yy} + 2I_{yz} + I_{zz}) & 0.5\ (I_{zz} - I_{yy}) \\ -0.707 \leftarrow (I_{yx} - I_{zx}) & 0.5\ (I_{zz} - I_{yy}) & 0.5\ (I_{yy} - 2I_{yz} + I_{zz}) \end{bmatrix}$$

$$\Phi_1 = \begin{bmatrix} 119565 & -8123 & +10049 \\ -8123 & 871746 & -2457 \\ +10049 & -2457 & 891246 \end{bmatrix} \quad \text{Slug-ft}^2$$

The center of mass offsets are transformed in a similar manner as shown below:

$$\begin{bmatrix} X_1 \\ Y_1 \\ Z_1 \end{bmatrix} = [T] \begin{bmatrix} X_2 \\ Y_2 \\ Z_2 \end{bmatrix}$$

$X_1$ 35.695 ft

$Y_1$ = +0.1527 ft

$Z_1$ -0.4595 ft

These inertia and center of mass transformations were performed and are applicable to the two axis, local vertical configuration. For the configurations involving a different S-IVB orientation, only the transformation from the aerodynamic body axes to the GE body axes must be altered. This is the transformation [B] previously discussed.

For the local vertical, three-axis configuration (plane of the solar panels perpendicular to the orbit plane) this matrix becomes:

$$[B] = \begin{bmatrix} -1 & 0 & 0 \\ 0 & 0 & -1 \\ 0 & -1 & 0 \end{bmatrix}$$

From the aerodynamic reference frame this represents a -90 degree rotation about the $Y_3$ axis (J2 gimbal down). The $[T]$ matrix then becomes:

$$[T] = \begin{bmatrix} 1 & 0 & 0 \\ 0 & 0.707 & -0.707 \\ 0 & 0.707 & 0.707 \end{bmatrix}$$

again,

$$\Phi_1 = [T][\Phi_2][T]^{-1}$$

then,

$$\Phi_1 = \begin{bmatrix} I_{xx} & 0.707\ (I_{xy} - I_{xz}) & 0.707\ (I_{xy} + I_{xz}) \\ 0.707\ (I_{xy} - I_{xz}) & 0.5\ (I_{yy} - 2I_{xz} + I_{zz}) & 0.5\ (I_{yy} - I_{zz}) \\ 0.707\ (I_{xy} + I_{xz}) & 0.5\ (I_{yy} - I_{zz}) & 0.5\ (I_{yy} + 2I_{xz} + I_{zz}) \end{bmatrix}$$

$$\Phi_1 = \begin{bmatrix} 119565 & -10049 & -8123 \\ -10049 & 891246 & 2457 \\ -8123 & 2457 & 871746 \end{bmatrix} \quad \text{Slug -ft}^2$$

In metric system

$$I_{xx} = 162,109 \text{ kg-m}^2 \qquad I_{xy} = -13625 \text{ kg-m}^2$$

$$I_{yy} = 1,208,370 \text{ kg-m}^2 \qquad I_{xz} = -11013 \text{ kg-m}^2$$

$$I_{zz} = 1,181,932 \text{ kg-m}^2 \qquad I_{yz} = +3331 \text{ kg-m}^2$$

The center of mass offsets are transformed:

$$\begin{bmatrix} XCM_1 \\ YCM_1 \\ ZCM_1 \end{bmatrix} = [T] \begin{bmatrix} XCM_2 \\ YCM_2 \\ ZCM_2 \end{bmatrix} = [T] \begin{bmatrix} 35,695 \\ 0.433 \\ -0.217 \end{bmatrix} = \begin{bmatrix} 35,695 \\ +0.4595 \\ +0.153 \end{bmatrix} \quad \text{ft}$$

For the velocity vector (horizontal) configuration the $[B]$ transformation is:

$$[B] = \begin{bmatrix} 0 & 0 & -1 \\ 1 & 0 & 0 \\ 0 & -1 & 0 \end{bmatrix}$$

From the aerodynamic reference frame this represents no rotation, merely a redefinition of axes.

$$[T] = \begin{vmatrix} 0 & 0.707 & -0.707 \\ -1 & 0 & 0 \\ 0 & 0.707 & 0.707 \end{vmatrix}$$

The final inertia dyadic is:

$$\Phi_1 = \begin{bmatrix} 891246 & 10049 & 2457 \\ 10049 & 119565 & 8123 \\ 2457 & 8123 & 871247 \end{bmatrix} \quad \text{Slug-ft}^2$$

and,

$$X_1 = +0.4595 \text{ ft}$$

$$Y_1 = -35.696 \text{ ft}$$

$$Z_1 = +0.153 \text{ ft}$$

# APPENDIX B

## EVALUATION OF S-IVB PERFORMANCE WITH ROTATED SOLAR ARRAY

An additional S-IVB configuration with solar panels positioned perpendicular to the longitudinal axis was evaluated by means of the large angle, nonlinear computer simulation. The spacecraft orientation is identical to that of the two-axis local vertical configuration. A new set of aerodynamic force and moment coefficients and mass/inertia data was supplied by MSFC and incorporated in the computer simulations. These particular evaluations, both steady state and transient, were made without any form of damping in order to evaluate the rate of error build-up.

Figure B-1 shows the results of the steady state performance run wherein initial angles were set to zero as well as initial roll and yaw rates; initial pitch rate was equal to orbital. After 24 hours (15 orbits) performance remains stable, but amplitudes are increasing. Amplitudes and biases appear to be:

Pitch: $\pm 0.75^{o}$ on a $-0.25^{o}$ bias

Roll: $\pm 1.5^{o}$ on a $\pm 0.75^{o}$ bias

Yaw: $\pm 11.0^{o}$ on a $-7.0^{o}$ bias

The transient performance evaluation assumed $10^{o}$ position errors on all axes and 0.01 deg/sec rates about all axes (on pitch: orbital + $0.01^{o}$/sec). The results, shown in Figure B-2, are quite different than the steady state run. Yaw goes unstable in the eighth orbit and remains so for the remainder of the fifteen-orbit simulation.

### B.1 LINEARIZED STABILITY ANALYSIS

A generalized stability analysis was performed for a gravity gradient stabilized satellite under the influence of disturbing torques about all three axes. This analysis considered the influence of the aerodynamic stiffness coefficients upon the total system stability. The damping coefficients necessary to insure stability were then determined for the specific configurations of interest.

Euler's rotational equation of motion was written. The body angular rates, in terms of Euler angles and their derivatives, were then substituted into the dynamic equation and equated to the external disturbance torques. These disturbance torques were considered to be gravity gradient (restoring torque), aerodynamic, and those due to damping devices. The Euler angles were assumed to represent constant bias angles plus some differential angles; small angle approximations were then made in the trigonometric expressions for these differential angles.

The steady state bias angles were obtained by inspection of the large angle dynamics program computed solutions. Aerodynamic stiffness coefficients were then calculated by using linear approximations for the rate of change of torque about an axis as a function of the variation of each Euler angle.

The complete system equations may be written in the following matrix form (with the $A_{IJ}$ terms being intermediate variables).

$$\begin{bmatrix} T_X \\ T_Y \\ T_Z \end{bmatrix} = \begin{bmatrix} A_{11} & A_{12} & A_{13} \\ A_{21} & A_{22} & A_{23} \\ A_{31} & A_{32} & A_{33} \end{bmatrix} \begin{bmatrix} \theta_Y \\ \theta_R \\ \theta_P \end{bmatrix} \qquad (1)$$

where $T_{X, Y, Z}$ are the constant torque terms about the yaw, roll, and pitch body axes

$\theta_{Y, R, P}$ are the differential yaw, roll, and pitch angles

The $A_{IJ}$ intermediate variables will now be defined in terms of a second set of intermediate variables, $T_{1, 2, 3}$ (with the $D^N$ term denoting the Nth order differential operator, and $\dot{\eta}$ being orbital rate).

FOLDOUT FRAME /

FOLDOUT FRAME 2

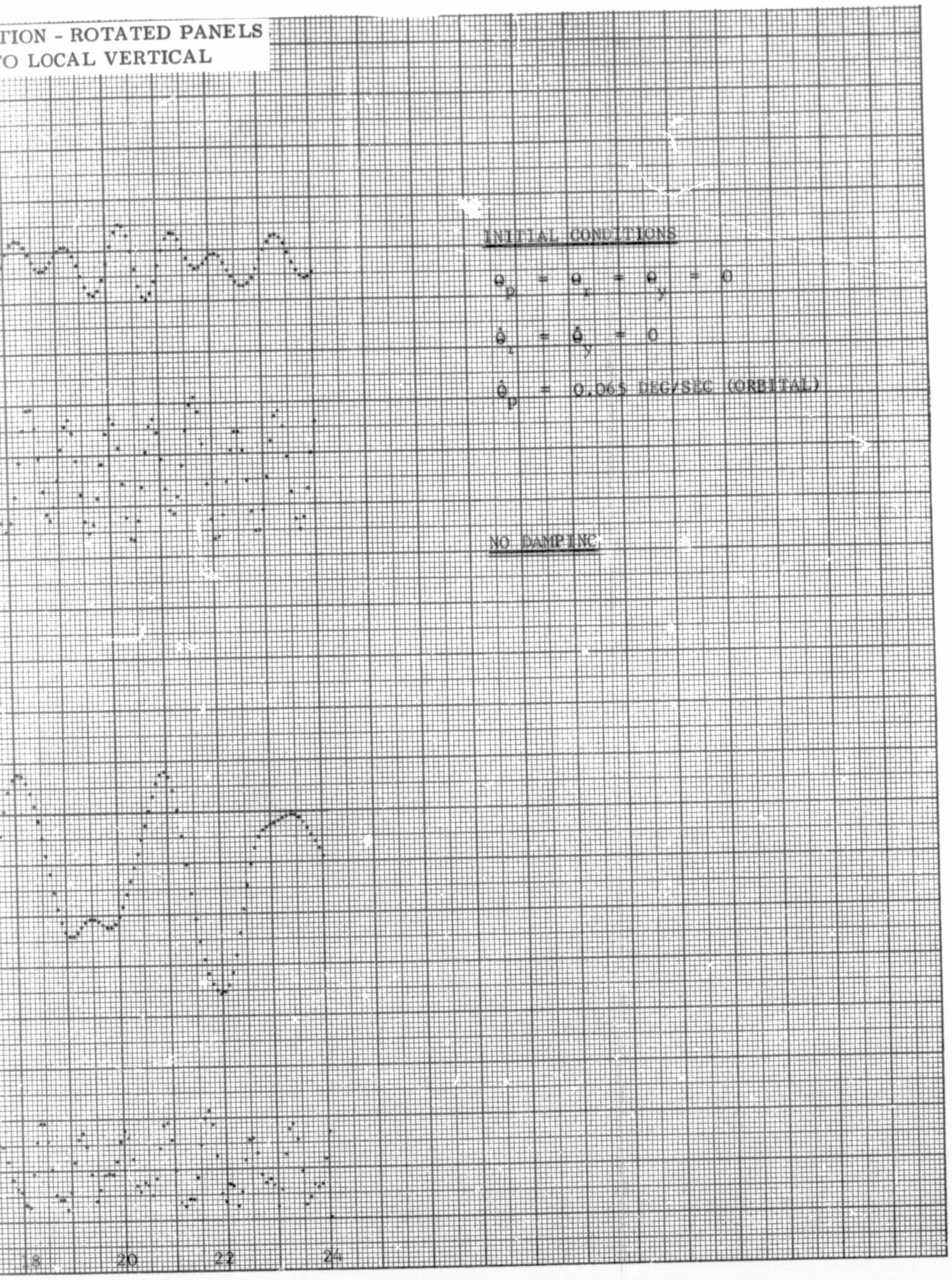


Figure B-1. S-IVB Vertical, No Damping Performance

FOLDOUT FRAME 1

S-IVB TWO-AXIS VERTICAL CONFIG
SOLAR PANELS PERPENDICUL

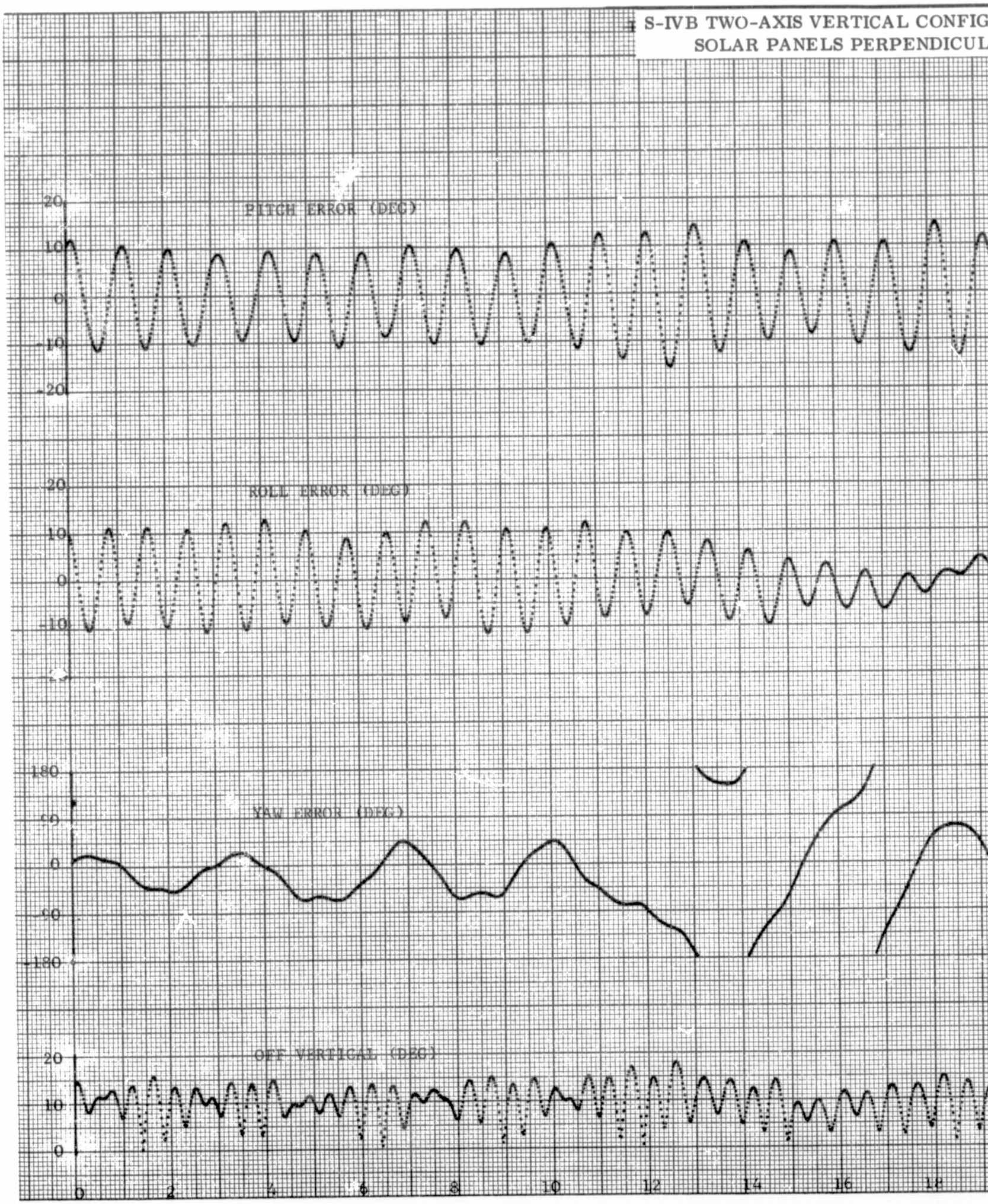


TIME - (HOURS)

FOLDOUT FRAME 2

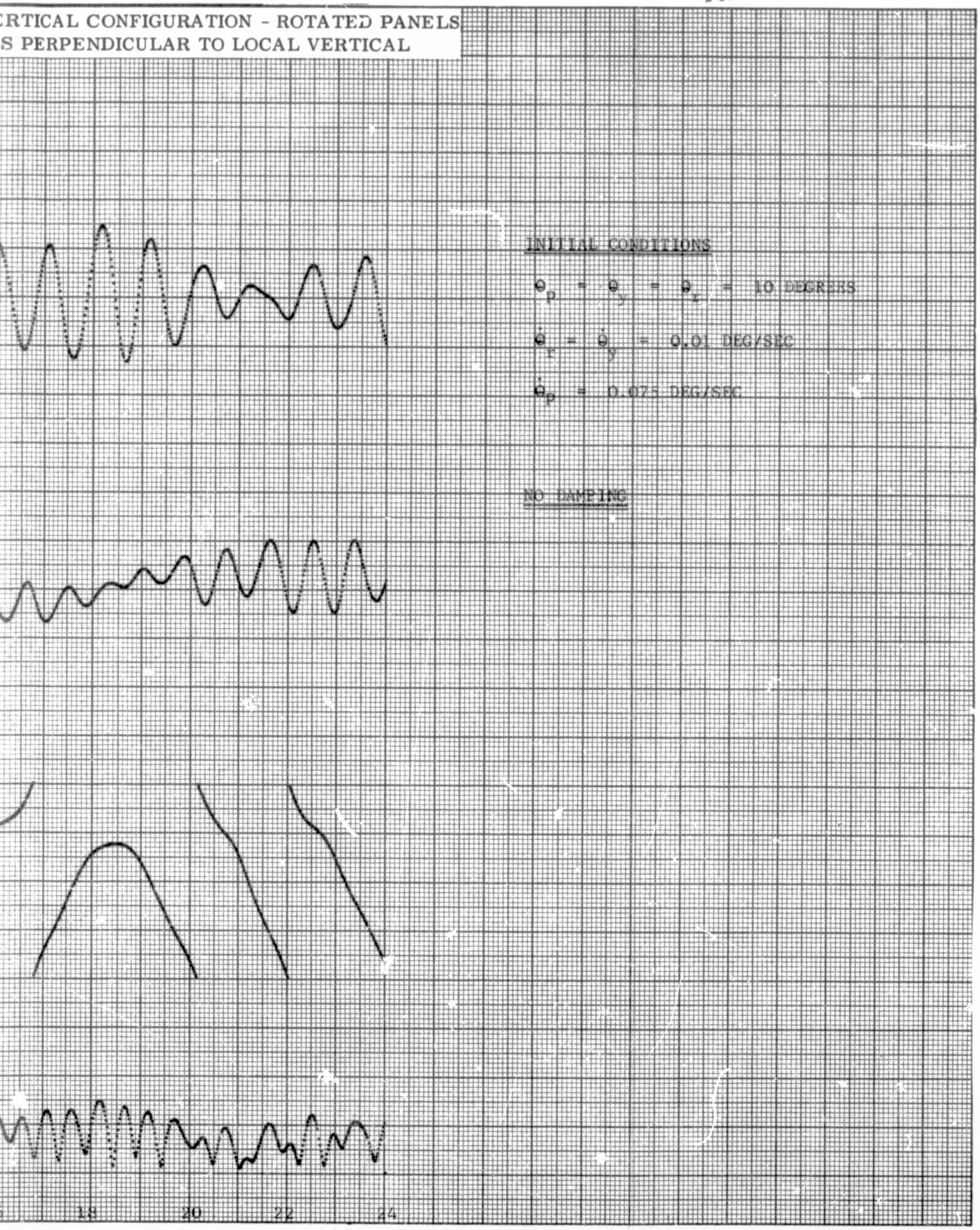


Figure B-2. S-IVB Vertical, No Damping Transient Performance

$$A_{11} = T_{111}D^2 + T_{112}\dot{\eta}D + T_{113}\dot{\eta}^2$$

$$A_{12} = T_{121}D^2 + T_{122}\dot{\eta}D + T_{123}\dot{\eta}^2$$

$$A_{13} = T_{131}D^2 + T_{132}\dot{\eta}D + T_{133}\dot{\eta}^2$$

$$A_{21} = T_{211}D^2 + T_{212}\dot{\eta}D + T_{213}\dot{\eta}^2$$

$$A_{22} = T_{221}D^2 + T_{222}\dot{\eta}D + T_{223}\dot{\eta}^2 \qquad (2)$$

$$A_{23} = T_{231}D^2 + T_{232}\dot{\eta}D + T_{233}\dot{\eta}^2$$

$$A_{31} = T_{311}D^2 + T_{312}\dot{\eta}D + T_{313}\dot{\eta}^2$$

$$A_{32} = T_{321}D^2 + T_{322}\dot{\eta}D + T_{323}\dot{\eta}^2$$

$$A_{33} = T_{331}D^2 + T_{332}\dot{\eta}D + T_{333}\dot{\eta}^2$$

Finally, the intermediate $T_{i,2,3}$ variables are defined in terms of the following system parameters.

$I_{xx}$, $I_{yy}$, $I_{zz}$ are the yaw, roll, and pitch principal moments of inertia

$B_X$, $B_Y$, $B_Z$ are the damping coefficients of the damper

$\theta_{YS}$, $\theta_{RS}$, $\theta_{PS}$ are the steady state yaw, roll, and pitch bias angles

$K_{AXP}$ is the partial derivative of the aerodynamic torque about the X axis with respect to $\theta_P$, with $\theta_R$ and $\theta_Y$ held constant, $\left.\frac{\partial T_{AX}}{\partial \theta_P}\right|_{\theta_R,\theta_y}$ (i.e., stiffness coefficient).

The $T_{1,2,3}$ variables are now defined (with $C\theta$ = COSINE $\theta$, $S\theta$ = SINE $\theta$)

$$T_{111} = I_{XX}$$

$$T_{112} = B_X/\dot{\eta}$$

$$T_{113} = (I_{ZZ} - I_{YY})\ C2\theta_{YS} \left\{ C^2\theta_{RS} - 3 \left[ (S\theta_{RS} C\theta_{YS} - S\theta_{YS} C\theta_{PS} S\theta_{RS}) \cdot (S\theta_{YS} C\theta_{PS} S\theta_{RS} - S\theta_{PS} C\theta_{YS}) + (C\theta_{YS} C\theta_{PS} S\theta_{RS} + S\theta_{YS} S\theta_{RS}) \cdot (S\theta_{PS} S\theta_{YS} + C\theta_{YS} C\theta_{PS} S\theta_{RS}) \right] \right\} + K_{AXY}/\dot{\eta}^2$$

$$T_{121} = 0$$

$$T_{122} = -C\theta_{RS} (I_{XX} + I_{YY}\ C2\theta_{YS} - I_{ZZ}\ C2\theta_{YS})$$

$$T_{123} = (I_{ZZ} - I_{YY}) \left\{ -2S\theta_{RS}\ C\theta_{RS} S\theta_{YS} C\theta_{YS} - 3 \left[ (C\theta_{YS} C\theta_{RS} C\theta_{PS}) \cdot (S\theta_{YS} C\theta_{PS} S\theta_{RS} - S\theta_{PS} C\theta_{YS}) + (S\theta_{YS} C\theta_{RS} C\theta_{PS}) \cdot (S\theta_{PS} S\theta_{YS} + C\theta_{PS} S\theta_{RS} C\theta_{YS}) \right] \right\} - B_X\ C\theta_{RS}/\dot{\eta} + K_{AXR}/\dot{\eta}^2$$

$$T_{131} = -I_{XX} S\theta_{RS}$$

$$T_{132} = C^2\theta_{RS} S2\theta_{YS} (I_{ZZ} - I_{YY}) - B_X S\theta_{RS}/\dot{\eta}$$

$$T_{133} = (I_{ZZ} - I_{YY}) \left\{ C^2\theta_{RS} S2\theta_{YS} - 3 \left[ (C\theta_{PS} S\theta_{YS} - C\theta_{YS} S\theta_{PS} S\theta_{RS}) \cdot (S\theta_{YS} C\theta_{PS} S\theta_{RS} - S\theta_{PS} C\theta_{YS}) - (S\theta_{PS} S\theta_{RS} S\theta_{YS} + C\theta_{PS} C\theta_{YS}) \cdot (S\theta_{PS} S\theta_{YS} + C\theta_{YS} C\theta_{PS} C\theta_{PS} S\theta_{RS}) \right] \right\} + K_{AXP}/\dot{\eta}^2$$

$$T_{211} = 0$$

$$T_{212} = C\theta_{YS} C\theta_{RS} (I_{XX} + I_{YY} - I_{ZZ})$$

$$T_{213} = (I_{XX} - I_{ZZ}) \Big\{ S\theta_{RS} C\theta_{RS} S\theta_{YS} + 3 \Big[ C\theta_{PS} C\theta_{RS} (S\theta_{PS} C\theta_{YS} - S\theta_{YS} C\theta_{PS} S\theta_{RS}) \Big] + K_{AYY} \dot{\eta}^2 + B_Y C\theta_{YS} C\theta_{RS} \dot{\eta}$$

$$T_{221} = I_{YY} C\theta_{YS}$$

$$T_{222} = (I_{XX} - I_{ZZ} - I_{YY}) S\theta_{YS} S\theta_{RS} + B_Y C\theta_{YS} \dot{\eta}$$

$$T_{223} = (I_{XX} - I_{ZZ}) \Big\{ - C\theta_{YS} C2\theta_{RS} - 3 \Big[ (C\theta_{YS} C^2\theta_{PS} C^2\theta_{RS} - S\theta_{RS} C\theta_{PS}) \cdot (S\theta_{PS} S\theta_{YS} + C\theta_{YS} C\theta_{PS} S\theta_{RS}) \Big] \Big\} + K_{AYR} \dot{\eta}^2 - B_Y S\theta_{YS} S\theta_{RS} \dot{\eta}$$

$$T_{231} = I_{YY} S\theta_{YS} C\theta_{RS}$$

$$T_{232} = -2 (I_{XX} - I_{ZZ}) S\theta_{RS} C\theta_{RS} C\theta_{YS} + B_Y S\theta_{YS} C\theta_{RS} \dot{\eta}$$

$$T_{233} = -3 (I_{XX} - I_{ZZ}) \Big[ C\theta_{PS} C\theta_{RS} (C\theta_{PS} S\theta_{YS} - C\theta_{YS} S\theta_{PS} S\theta_{RS}) - S\theta_{PS} C\theta_{RS} (S\theta_{PS} S\theta_{YS} + C\theta_{YS} C\theta_{PS} S\theta_{RS}) \Big] + K_{AYP} \dot{\eta}^2$$

$$T_{311} = 0$$

$$T_{312} = (I_{YY} - I_{ZZ} - I_{XX}) S\theta_{YS} C\theta_{RS}$$

$$T_{313} = (I_{YY} - I_{XX}) \Big\{ - S\theta_{RS} C\theta_{RS} C\theta_{YS} + 3 \Big[ C\theta_{PS} C\theta_{RS} (S\theta_{YS} S\theta_{PS} + C\theta_{YS} C\theta_{PS} S\theta_{RS}) \Big] \Big\} + K_{AZY} \dot{\eta}^2 - B_Z S\theta_{YS} C\theta_{RS} \dot{\eta}$$

$$T_{321} = -I_{ZZ} S\theta_{YS}$$

$$T_{322} = (I_{XX} - I_{YY} - I_{ZZ}) C\theta_{YS} S\theta_{RS} - R_Z S\theta_{YS} \dot{\eta}$$

$$T_{323} = (I_{YY} - I_{XX}) \Big\{ -S\theta_{YS} C2\theta_{RS} - 3 \Big[ (C^2\theta_{PS} C^2\theta_{RS} S\theta_{YS} - S\theta_{RS} C\theta_{PS}) \cdot (S\theta_{YS} C\theta_{PS} S\theta_{RS} - S\theta_{PS} C\theta_{YS}) \Big] \Big\} + K_{AZR} \dot{\eta}^2 + B_Z S\theta_{RS} C\theta_{YS} \dot{\eta}$$

$$T_{331} = I_{ZZ} C\theta_{YS} C\theta_{RS}$$

$$T_{332} = -2\, S\theta_{RS} C\theta_{RS} S\theta_{YS} (I_{YY} - I_{XX}) + B_Z C\theta_{YS} C\theta_{RS}/\dot{\eta}$$

$$T_{333} = -3 (I_{YY} - I_{XX}) \Big[ -S\theta_{PS} C\theta_{RS} (S\theta_{YS} C\theta_{PS} S\theta_{RS} - S\theta_{PS} C\theta_{YS})$$

$$-C\theta_{PS} C\theta_{RS} (S\theta_{RS} S\theta_{PS} S\theta_{YS} + C\theta_{PS} C\theta_{YS}) \Big] + K_{AXP}/\dot{\eta}^2 \qquad (3)$$

The complete system stability, as a function of the aforementioned parameters, was then verified by calculating the roots of the characteristic equation. This characteristic equation was obtained by taking the determinant of the $A_{IJ}$ matrix given in Equation 1. A digital computer program was written to calculate these roots. This program was then utilized to determine the minimum damping coefficient that would insure system stability.

The parameter values inserted into the stability program were the following:

$I_{XX} = 0.119348 \times 10^6$ ft-lb-sec$^2$

$I_{YY} = 0.871503 \times 10^6$ ft-lb-sec$^2$

$I_{ZZ} = 0.891708 \times 10^6$ ft-lb-sec$^2$

$\theta_{RS} = 0$ degrees

$\theta_{PS} = 0$ degrees

$\theta_{YS} = 20.5$ degrees

$K_{AXR} = 1.133 \times 10^{-3}$ rad/sec

$K_{AXP} = 0$ ft-lb/degree

$K_{AXY} = 0.6 \times 10^{-5}$ ft-lb/degree

$K_{AYR} = -3.0 \times 10^{-4}$ ft-lb/degree

$K_{AYP} = -2.8 \times 10^{-5}$ ft-lb/degree

$K_{AYY}$= 5.2 x $10^{-4}$ ft-lb/degree

$K_{AZR}$= 0 lb-ft/degree

$K_{AZP}$= 1.8 x $10^{-5}$ lb-ft/degree

$K_{AZY}$= 6.0 x $10^{-4}$ lb-ft/degree

The computed roots of the characteristic equation for the 4.8 ft-lb-sec damping coefficient are the following:

| Root No. | Real Part | Complex Part |
|---|---|---|
| 1 & 2 | -2.221917E-05 | ±1.3066151E-04 |
| 3 & 4 | -3.343309E-06 | ±1.8087101E-03 |
| 5 & 6 | 1.4495072E-11 | ±2.1584948E-03 |

This damping coefficient is the value at which the real parts of roots 5 and 6 become zero and represent the amount of damping needed to make the systems stable.

# APPENDIX C

# DAMPING OF THE S-IVB BY USE OF A SINGLE-AXIS GRAVITY-ANCHORED DAMPER

## C.1 SUMMARY AND CONCLUSIONS

Damping of the S-IVB spacecraft can be accomplished using a damper boom, mounted to the spacecraft. Relative motion is damped in a damping mechanism utilizing rate or hysteresis damping. Optimizing the damper, assuming rate damping, indicates maximum damping can be achieved with a damper size of approximately 2 percent of the pitch moment of inertia. The time constant of this subsystem is approximately eight orbits. Smaller booms can be used if longer time constants are acceptable.

## C.2 Discussion

The primary gravity gradient studies performed for the S-IVB have been made assuming the magnetically anchored rate damper supplied the required damping. There is, however, a different class of damper which can also be used to damp a gravity gradient spacecraft. This type damper consists of a gravity gradient rod and tip mass (to provide a large moment of inertia) mounted to the spacecraft by means of a rotational joint and spring. Relative motion between the damper and the spacecraft is damped either by a rate damping technique (eddy current, viscous fluid, etc.) or by a hysteresis technique.

The simplest damper of this type is a single-axis damper consisting of a boom (two rods and tip masses), mounted through a single spring to the spacecraft (Figure C-1 and C-2). This type of damper has been analyzed and developed for the ATS spacecraft. Damping of all three axes is obtained by mounting the damping axis of the damper skew to the principal axes of the spacecraft (but normal to the axis of minimum moment of inertia, the local vertical). This type of system provides excellent damping characteristics if the moment of inertia relationships of the main spacecraft are optimized in conjunction with the spacecraft damper parameters.

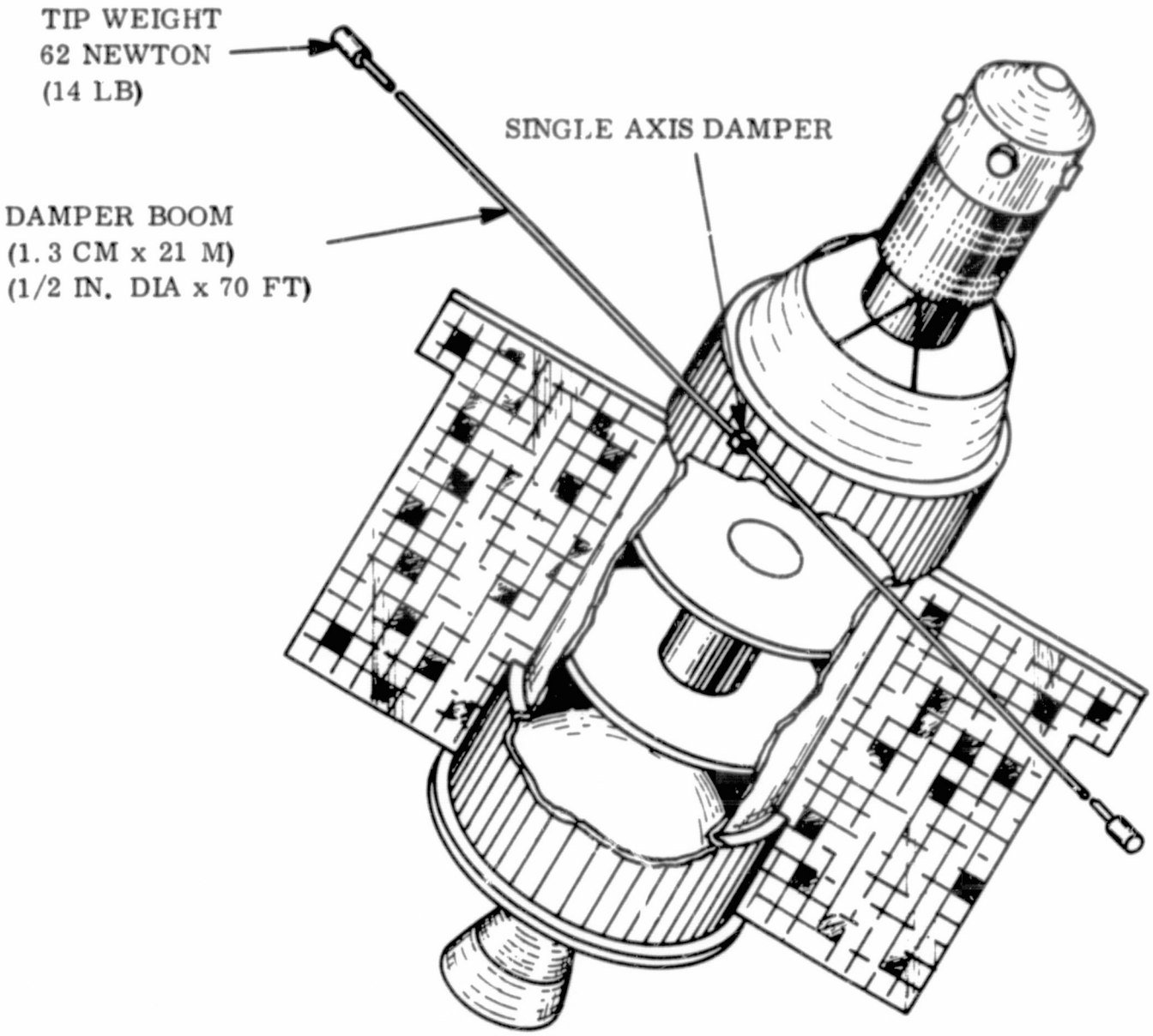


Figure C-1. S-IVB Single Axis Damper Configuration

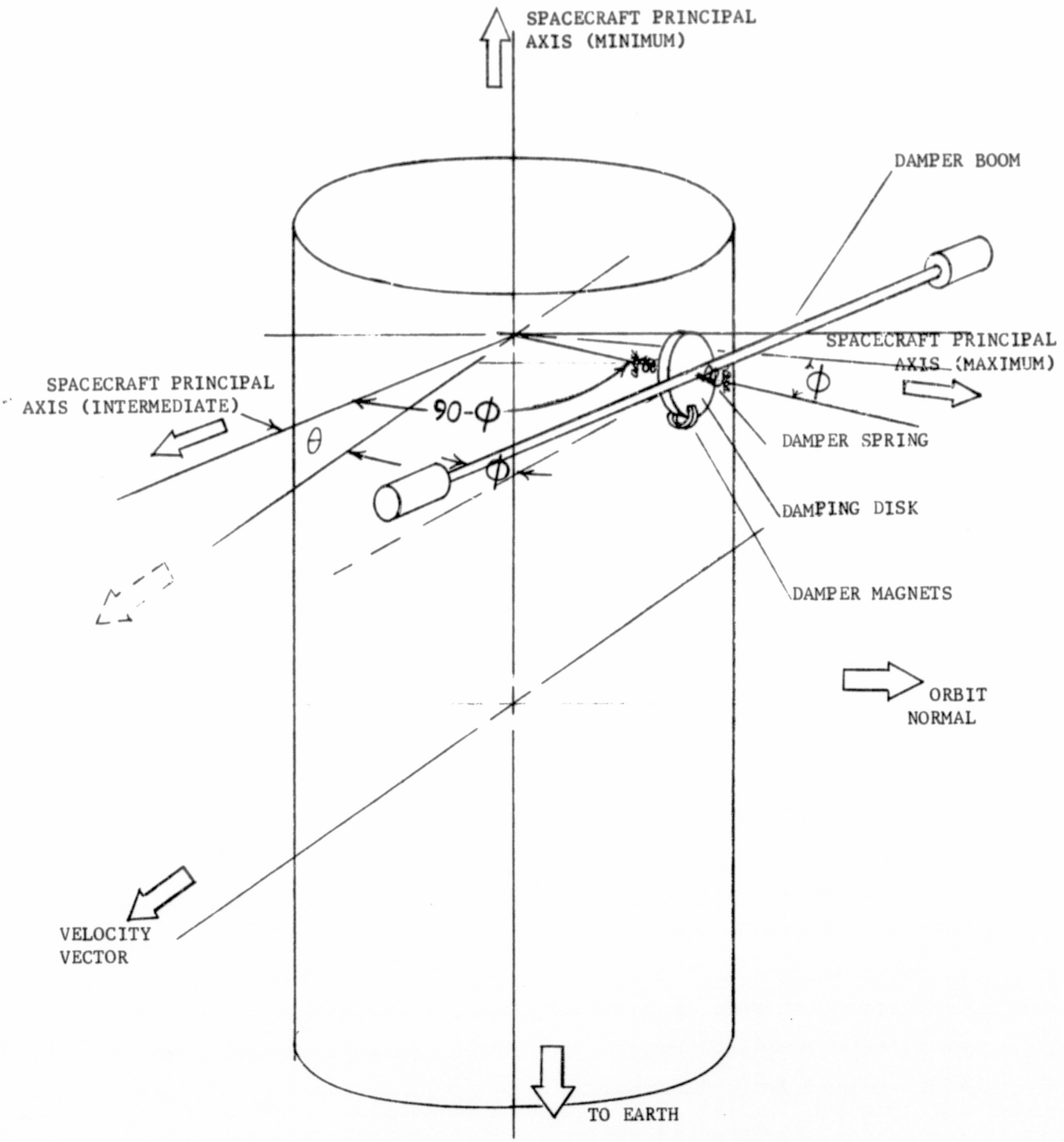


Figure C-2. S-IVB Single Axis Damper Angles

Typically, in the design of this type of spacecraft the moment of inertia ratios (roll to pitch and yaw to pitch) are parameters which can be controlled. For the S-IVB, however, the moments of inertia of the spacecraft are known, and a damper must be added to the known spacecraft. The S-IVB spacecraft is nearly a dumbbell configuration (i.e., the two largest moments of inertia are nearly equal), with only 2.3 percent difference between the pitch and roll moments of inertia. To utilize this small value, only a small damper can be used and the design effort centered on dampers wherein the moments of inertia are not much larger than two percent of the spacecraft pitch moment of inertia.

In the selection of the damper, there are six parameters (nondimensionalized) of interest: three moment of inertia ratios (roll to pitch, yaw to pitch, and damper to pitch), the spring constant, the damping coefficient, and the angle ($\phi$) at which the damper is mounted to the spacecraft. Since the moment of inertia ratios of the spacecraft are defined (roll/pitch = 0.977, yaw/pitch = 0.134), only four parameters remain. The design procedure is to optimize these parameters to obtain the best damping. External disturbances are not considered for this type of study.

For this study, the damper boom moment of inertia was considered to be the independent variable, and values to 3 percent of the spacecraft pitch moment of inertia were considered. The spring constant, damping coefficient, and orientation angle were then optimized using the characteristic equation of the system (eighth order). A review of the results indicated that an optimum damper size existed, and an optimization run was made to determine the size. The results are shown in Figure C-3. The optimum damper is slightly less than 2 percent of the pitch moment of inertia.

The damping coefficients, spring constants, and orientation angles for variations in damper boom size are shown in Figures C-4, C-5 and C-6. The angle at which the spacecraft flies ($\theta$) is shown in Figure C-6, and defined in Figure 1.

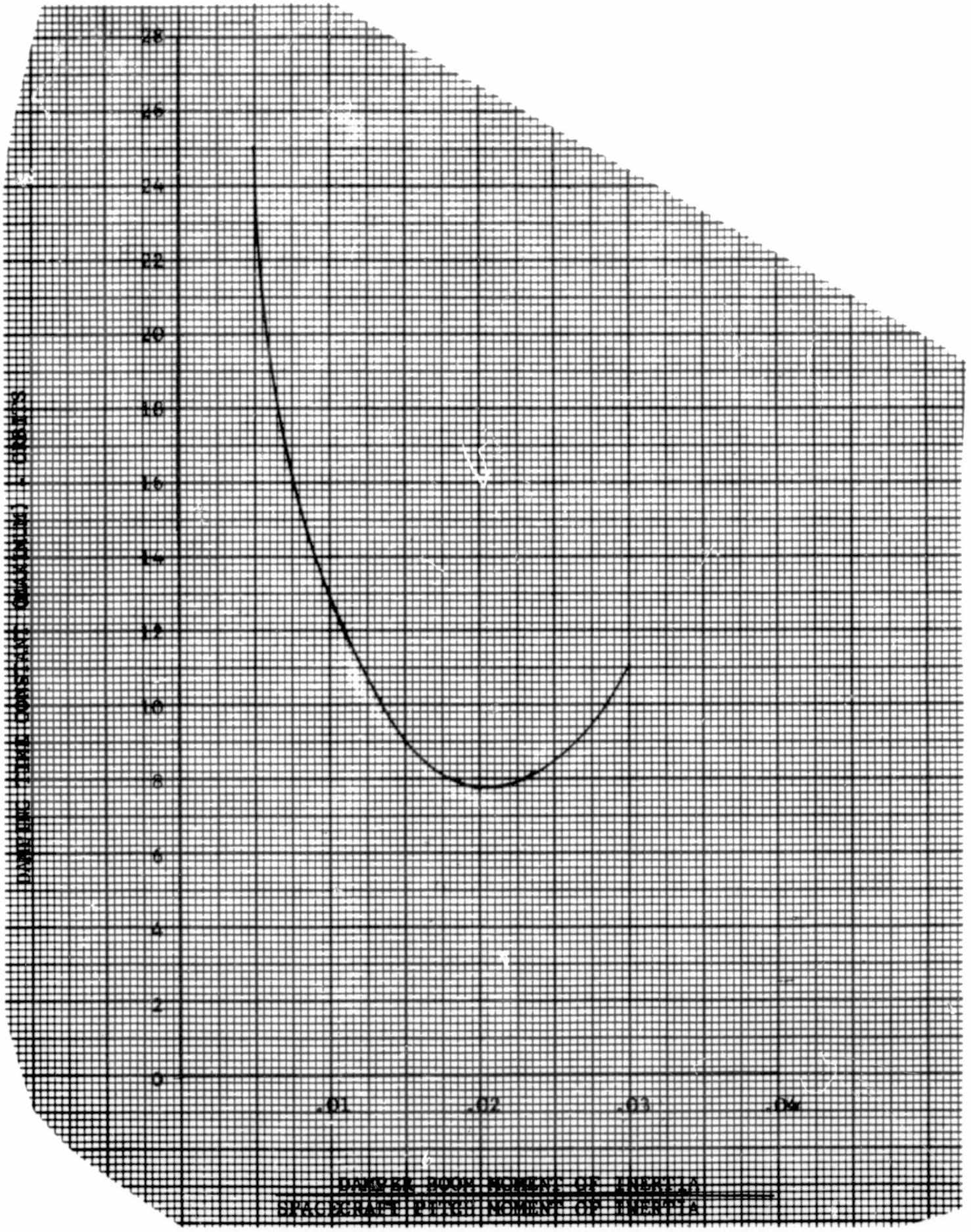


Figure C-3. Damper Boom Optimization

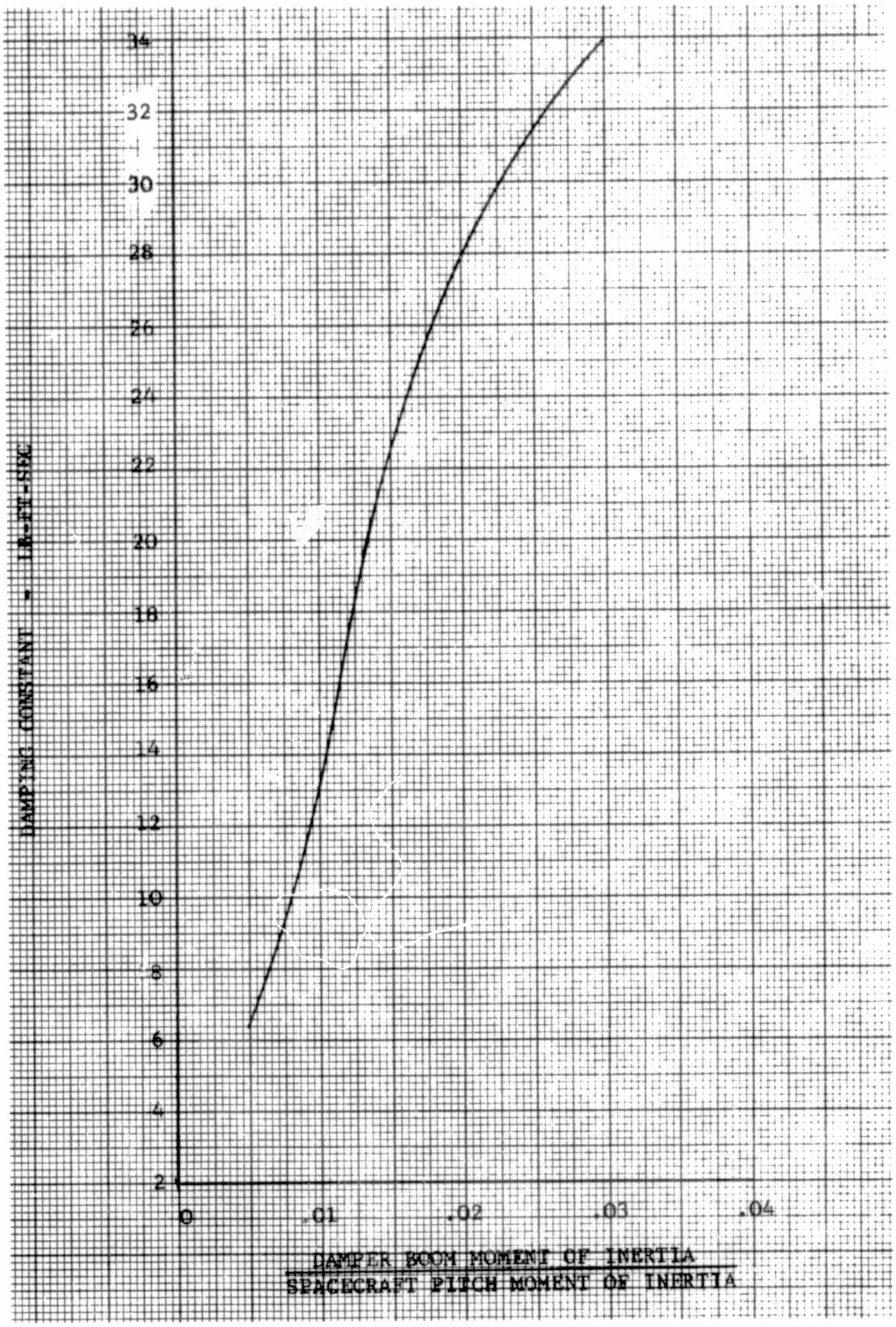


Figure C-4. Variation in Damping Constant

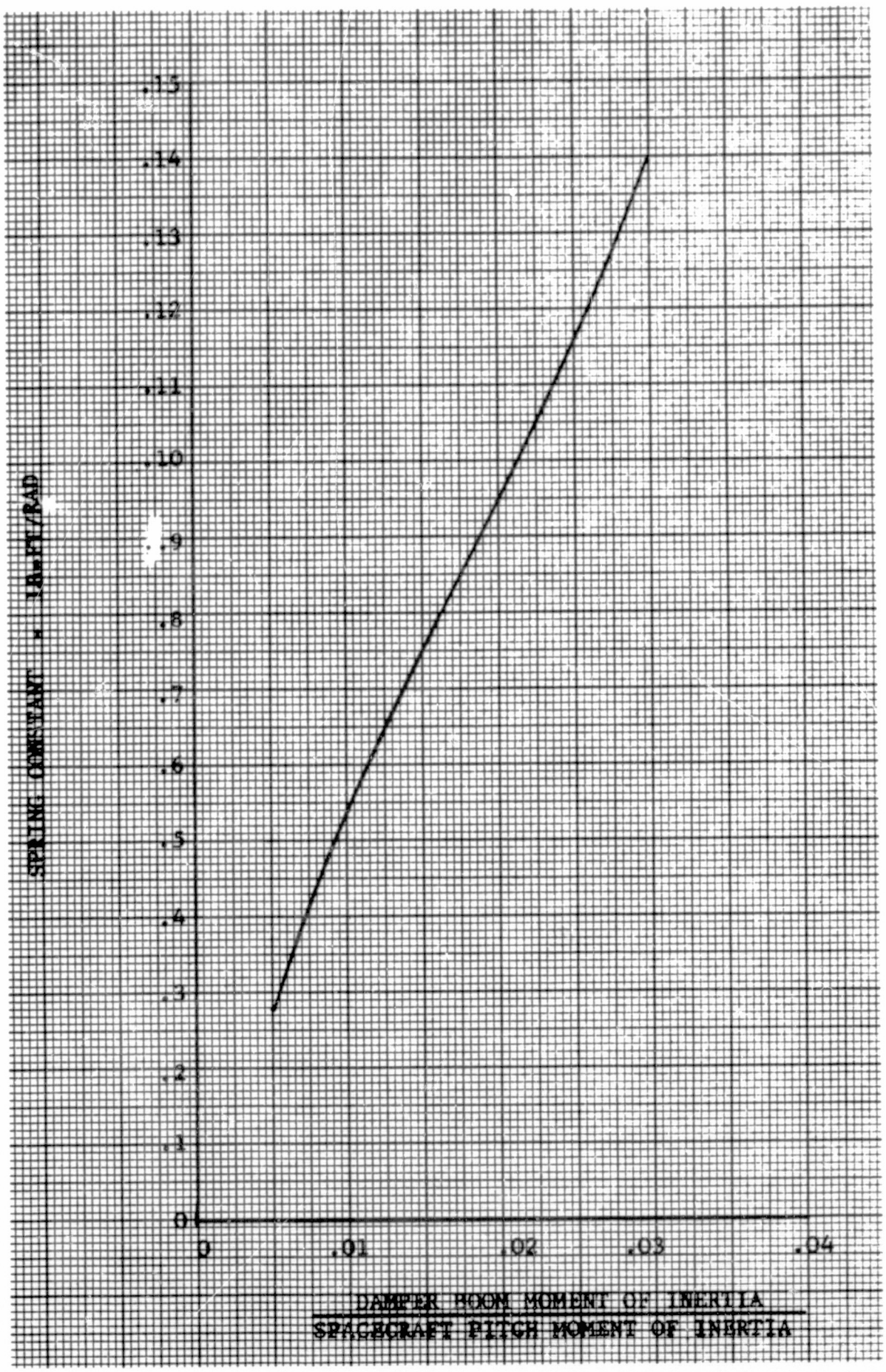


Figure C-5. Variation in Spring Constant

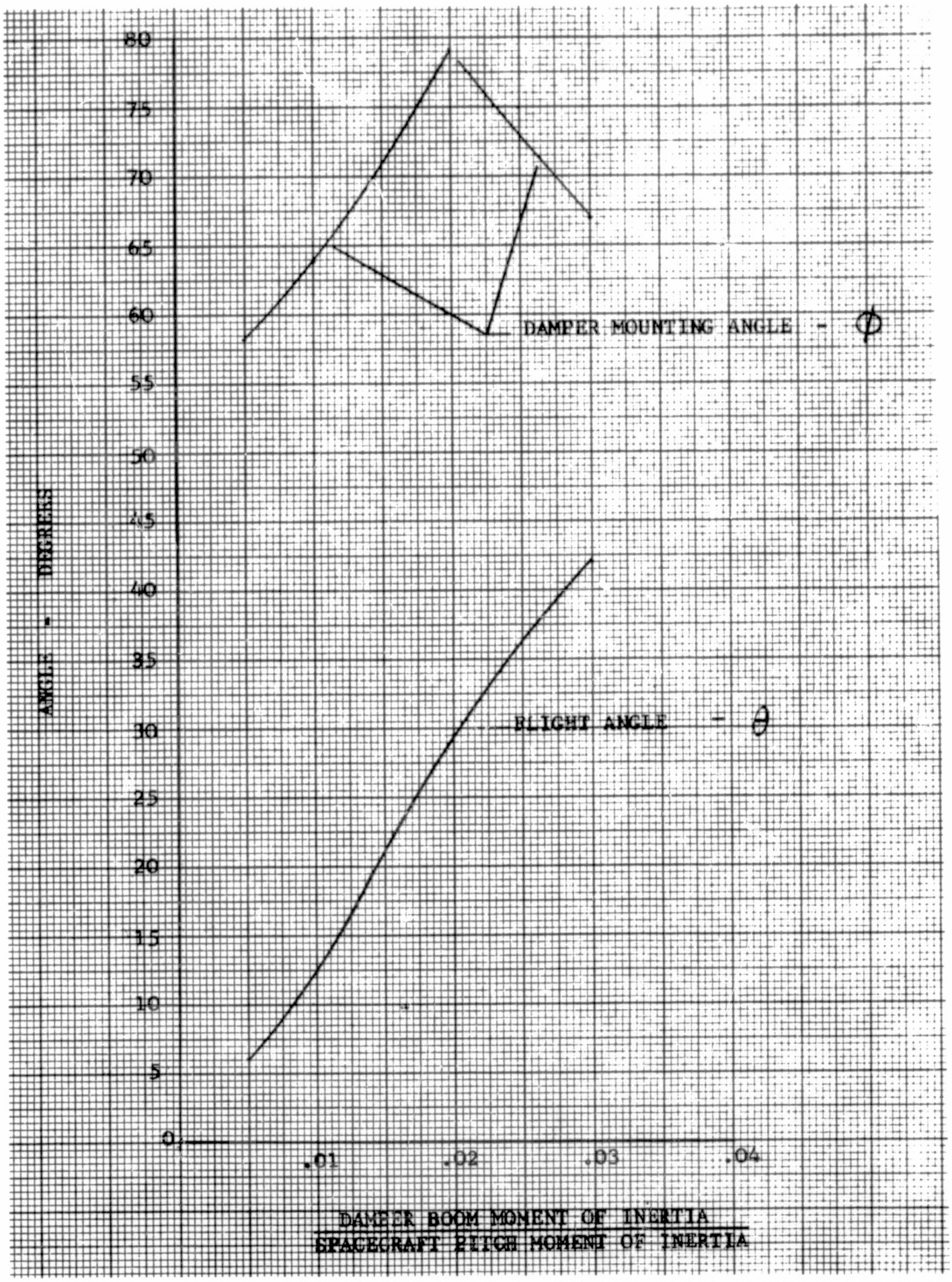


Figure C-6. Damper and Flight Angle

Hysteresis damping is also possible, the only change to the system being the substitution of hysteresis damping for rate damping. GE has developed and patented a bow-tie hysteresis damper which is a significant improvement over normal hysteresis damping. The system damps to steady state more rapidly than conventional hysteresis damping, and provides a smoother overall performance. This damper has already replaced the original hysteresis dampers on ATS-D and ATS-E It has the advantage of being lighter, in general, than an eddy current damper.

# APPENDIX D

## MAGNETIC CHARACTERISTICS OF LARGE DAMPER MAGNETS

The spherical viscous dampers specified for use on the S-IVB spacecraft are large compared to those of other previous applications. Since large magnets are required, certain aspects become important and need consideration. Typical areas of question are:

a. The strength of the magnetic field in the immediate vicinity of the magnet and how it decreases with distance from the magnet

b. The magnetic field induced in various components or "black boxes" present in the field of this magnet.

c. The torque and decentering force imposed on the damper magnet in the presence of a magnetic material in proximity to it.

In order to answer these questions without a detailed knowledge of the specific magnetic characteristics of the S-IVB spacecraft or components within the immediate vicinity of the instrumentation unit, the following information is presented:

Figure D-1 shows the magnetic field intensity in oersteds as a function of distance from the center of the magnet on a line coincident with the magnetic north-south axis. Two curves are shown: one for the smaller damper magnet recommended for the two axis local vertical configuration, 2000 amp meters$^2$ ($2 \times 10^6$ pole cms), and one for the 6000 amp meters$^2$ ($6 \times 10^6$ pole cms) magnet applicable to the three-axis horizontal configuration.

The internal field intensity and flux can be estimated for a component (or structure, etc.) which is in the magnetic field of the damper by the use of Figure D-2. Knowing the length to diameter ratio (1/d) of the component and its permeability ($\mu$), the intensity of the internal field (Hi) as a function of the external field ($H_o$) can be determined from the graph. $H_o$ is read from Figure D-1. The internal magnetic flux (Bi) can then be determined from the equation:

$$Bi = \mu Hi$$

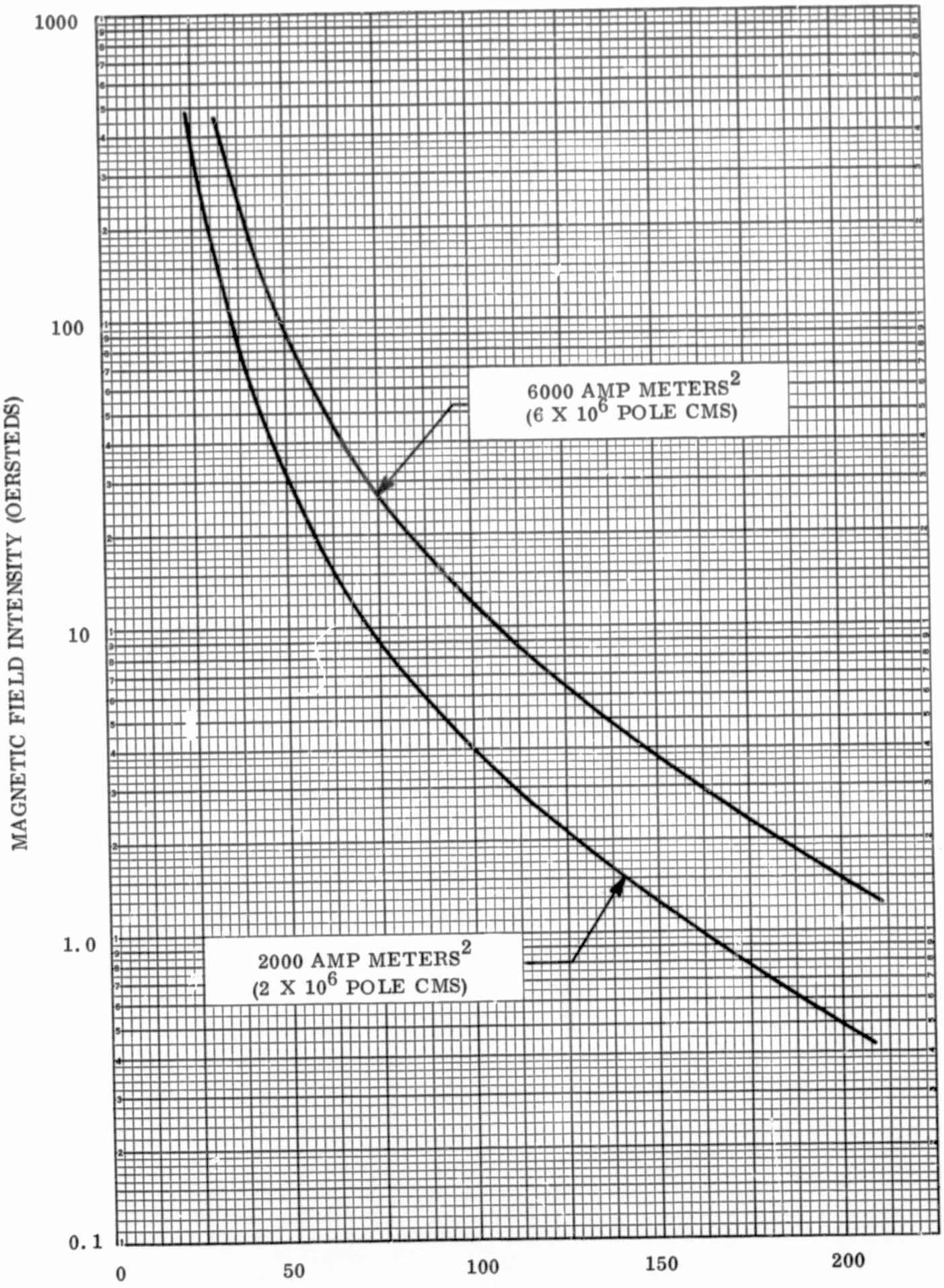


Figure D-1. Magnetic Field Intensity

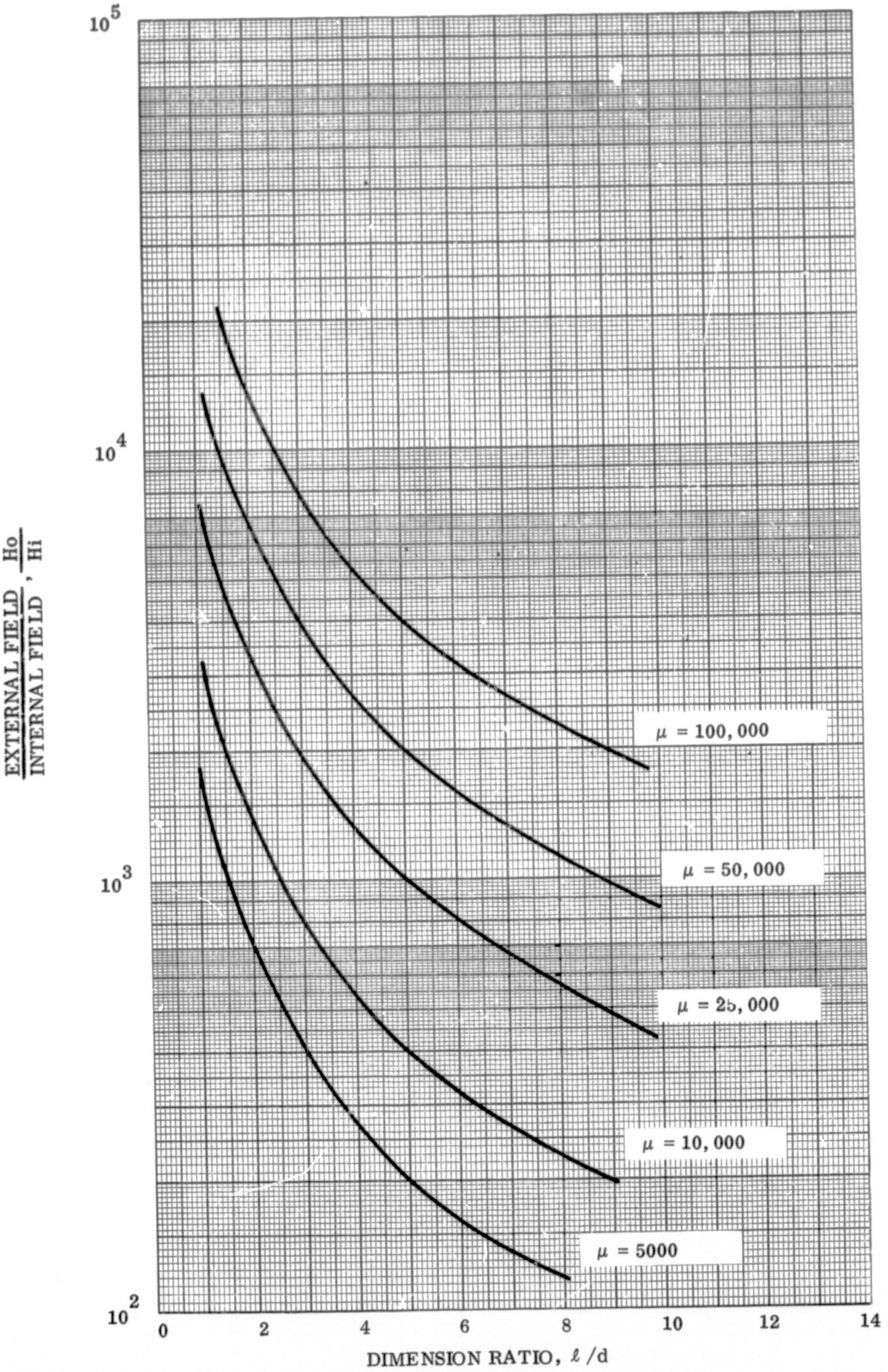


Figure D-2. Effect of External Magnetic Field

Figure D-2 is generally applicable, but nonlinearities in $\mu$ particularly in the high and low values of Bi, make extrapolation of the curves suspect.

Figure D-3 shows the torque that would be exerted on the 2000 amp meters$^2$ ($2 \times 10^6$ pole cm) damper magnet as the result of a magnetic material at a distance of 80 inches or less from the center of the magnet. The torque in terms of dyne-cms per cubic centimeter of magnetic substance is shown as a function of distance from the center of the magnet for lines of constant "effective permeability" of the substance.

The torque necessary to displace the $2 \times 10^3$ amp meter$^2$ magnet by 1 degree from the earth's magnetic field is $7 \times 10^3$ dyne cm. Torques of this value or less are insignificant in the operation of the damper.

Figure D-4 shows effective permeability as a function of geometry.

Figure D-5 shows peak decentering force on the damper magnet as a function of effective permeability. The centering force capability of the 2000 amp meter$^2$ damper is 90 dynes.

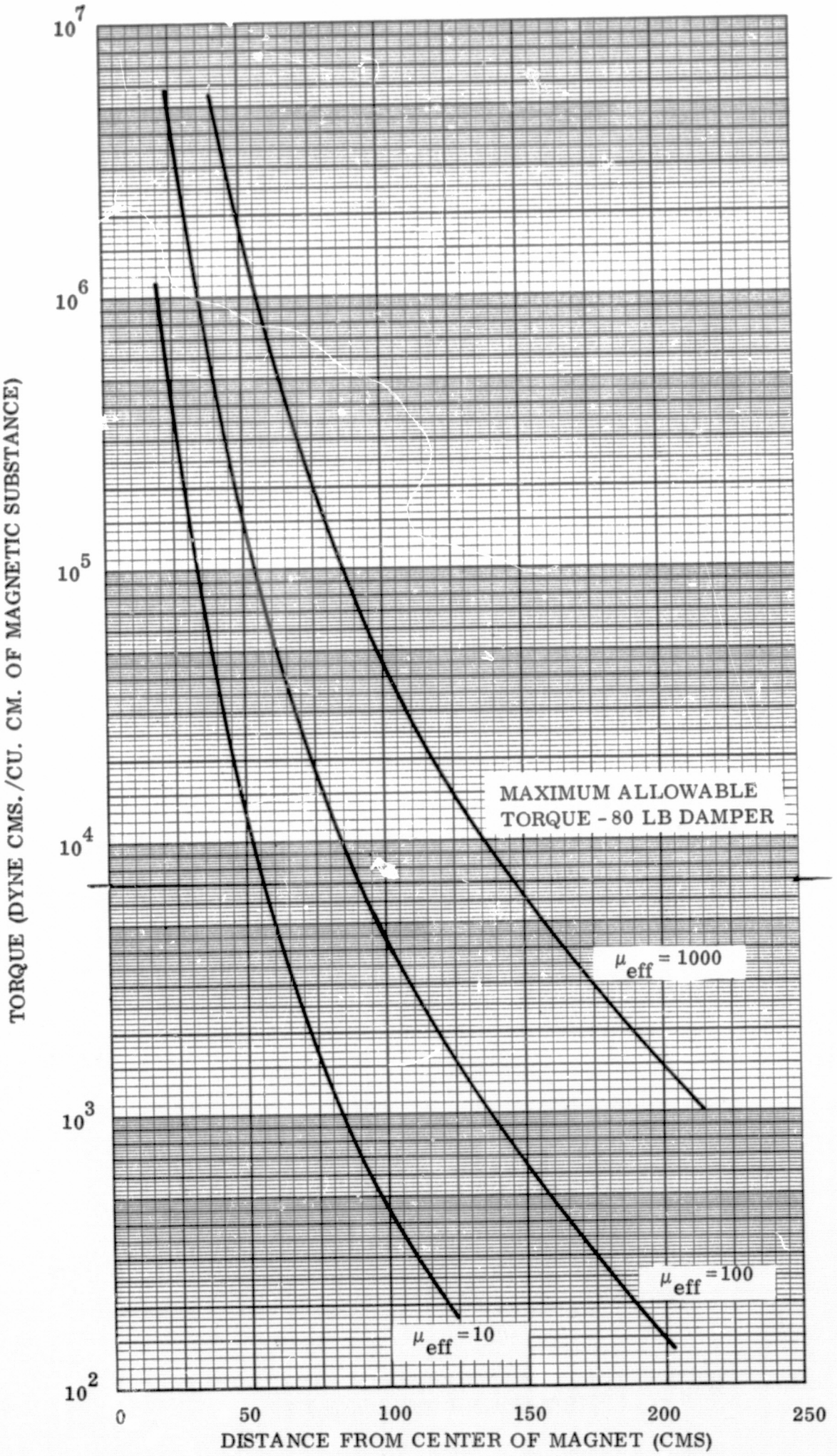


Figure D-3. Disturbance Torque on the Magnetic Damper

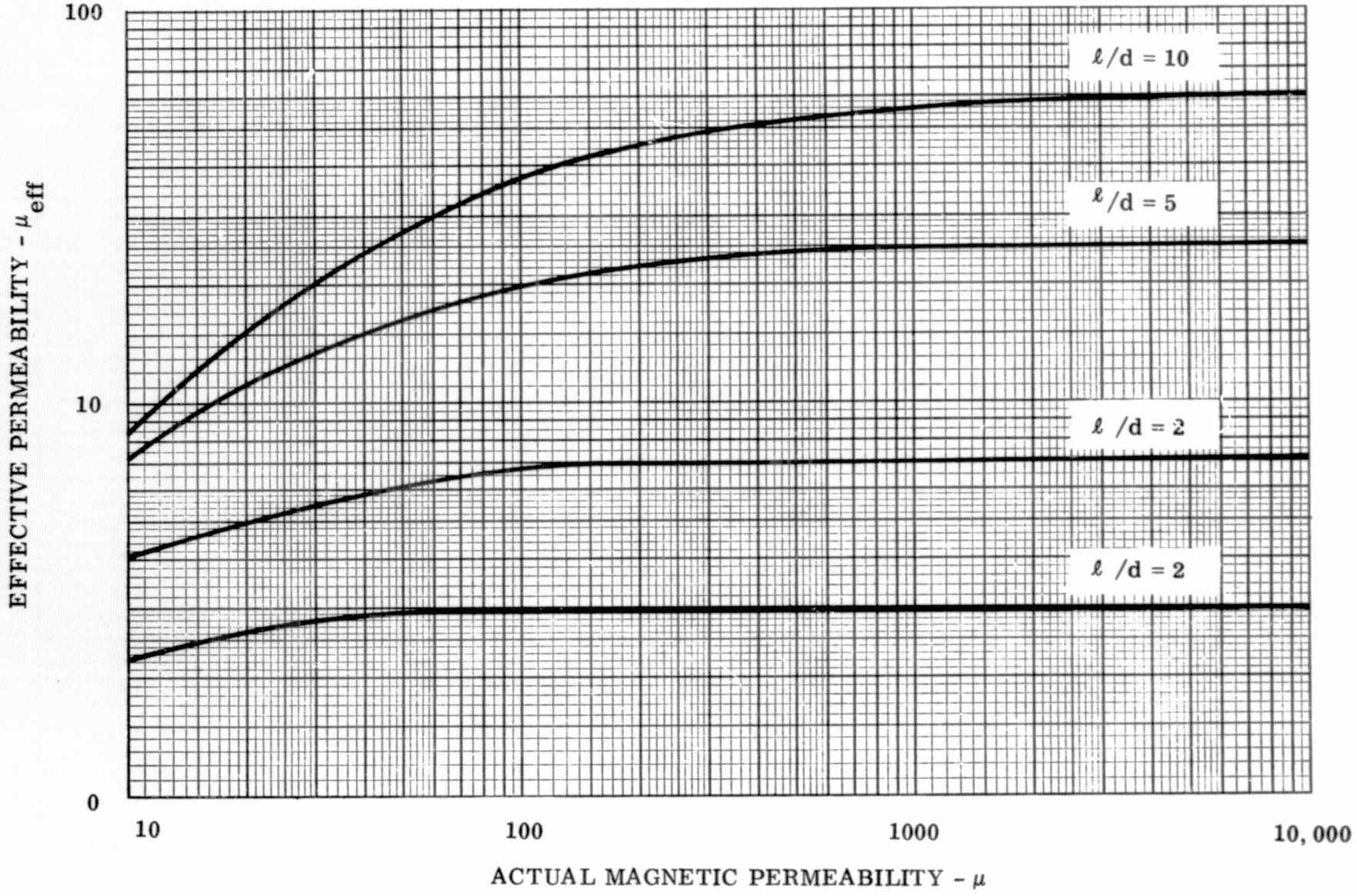


Figure D-4. Effective Permeability

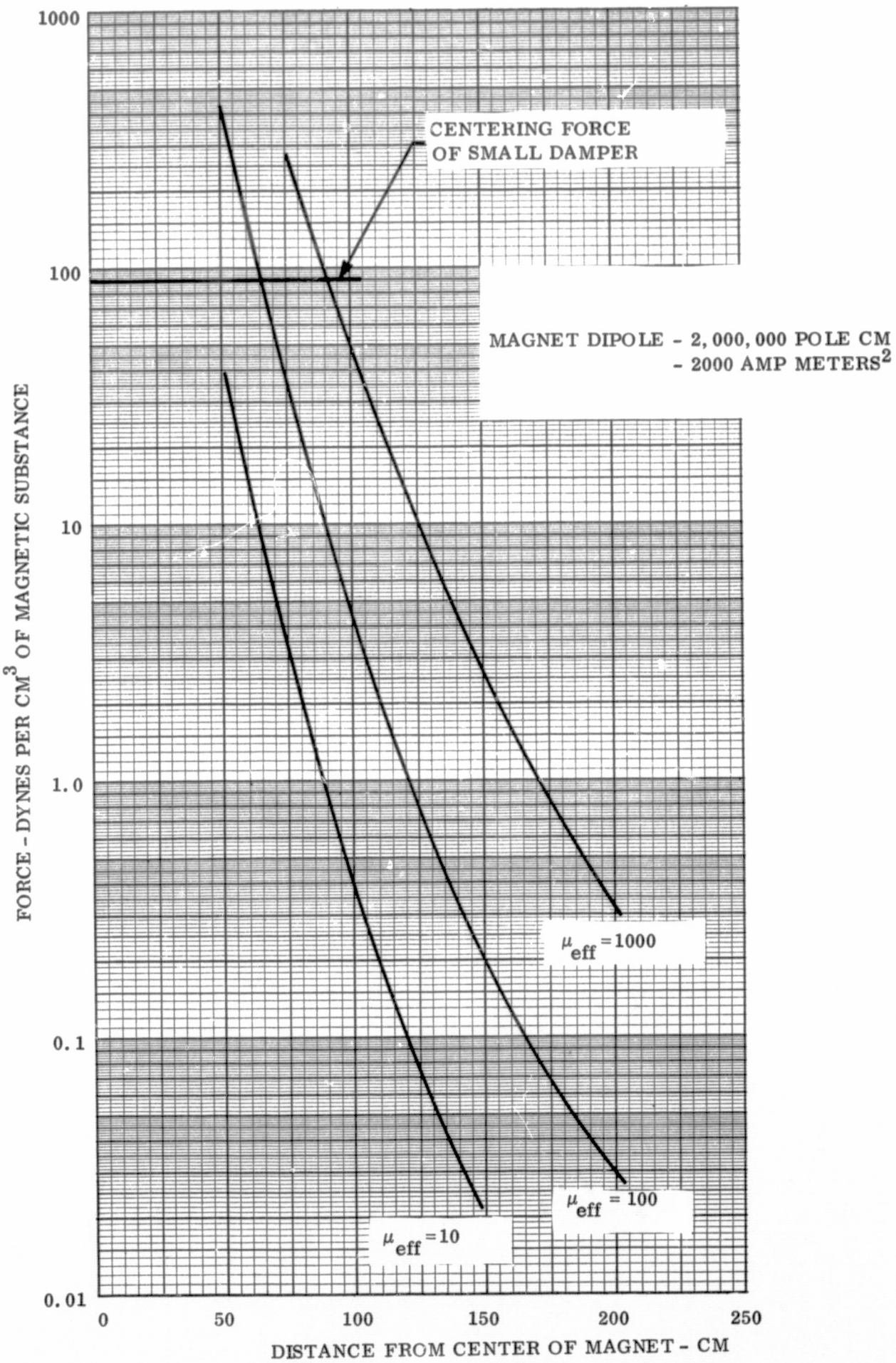


Figure D-5. Decentering Force on the Magnetic Damper

SATURN IV-B

GRAVITY-GRADIENT BOOM SYSTEM

## 1.0 SCOPE

This specification covers the design, fabrication, and test requirements for a Gravity-Gradient Boom System consisting of gravity gradient rod deployers. The deployers shall provide moments of inertia necessary for vehicle stabilization after attainment of the desired orbit. The gravity gradient rod deployer involves an erectable, retractable rod and shall hereafter be referred to as the Assembly.

The Assembly consists of a housing and support structure containing an erection unit with a storable extendable appendage (SEA), associated torque transmission system, deployment motor, deployment sensor and a damper type tip mass.

## 2.0 APPLICABLE DOCUMENTS

The following documents of the issue in effect on the date of release of this specification form a part of this specification to the extent defined herein:

### 2.1 Government Documents

Specification

Military

| | |
|---|---|
| MIL-S-7742 | Screw Threads, Standard Optimum Selected Series, General Specification for |
| MIL-126600 | Interference Control Requirements; Aeronautical Equipment |
| MIL-G-70327 | Drawings, Engineering and Associated Lists |
| MIL-M-7866 | Powder for Dry Film Lubricant ($MoS_2$) |

NASA

| | |
|---|---|
| | Environmental Qualification and Acceptance Test Specification for Saturn IV B Components |
| MSFC PROC-256 | Electrical Fabrication, Procedure for |
| GSFC-HB-3 | Spacecraft Operations at A.M.R. |
| NPC-200-3 | Inspection System Provisions for Suppliers of Space Materials, Parts, Components and Services |

STANDARDS

Military

| | |
|---|---|
| MIL-STD-202 | Test Methods for Electronic and Electrical Component Parts |
| MIL-STD-447 | Definitions of Interchangeable, Substitute and Replacement Items. |
| MIL-STD-831 | Test Reports, Preparation of |

DRAWINGS

Military

| | |
|---|---|
| MS 20995 | Wire Lock |
| MS 33540 | Safety Wiring, General Practices for |
| MS 33586 | Metals, Definition of Dissimilar |
| AND 10476 | Washers, Limitations on Usage of Lock |

MANUAL

Air Force

| | |
|---|---|
| T. 0.00-25-203 | Standard Functional Criteria for Design and Operation of Clean Rooms |

2.2 Non-Government Documents

STANDARDS

General Electric

| | |
|---|---|
| 118A1526 | Identification and Markings |

| | |
|---|---|
| 146A9560 | Preparation for Delivery of Commercial Shipments, General Requirements for |
| SVS | Use of Standards, Parts, Processes for Saturn IV B |
| | Approved Parts List, Project Saturn IV B |
| | Approved Materials and Processes Saturn IV B |
| 171A4167 | Adhesive and Sealant, RTV Silicone Rubber: Process for Application of |
| 147A1835 | Surface Treatment for Adhesive Bonding of Metallic and Non-metallic Surfaces |
| SI 217260 | Vendor Quality Control Instructions |
| 118A1600 | Finishes and Coatings |

DRAWINGS

General Electric

| | |
|---|---|
| 47J214522 | Boom Assembly - SCD |
| 895D724 | Electro Explosive Pressure Cartridges |
| | Damper Assembly, SCD |
| | Actuator Assembly, SCD |

2.3 Order of Precedence

In the event of conflict between this specification and the documents referred to herein, this specification shall govern.

## 3.0 Requirements

### 3.1 General Description

The Assembly shall have available, for experimental purposes, variable moments of inertia as a function of SEA length.

The Assembly shall have the capability to extend its SEA to any desired precise length up to and including 400 feet, stop its SEA at a predetermined length, retract its SEA to any desired precise length in excess of 150 feet. Mechanically adjustment of its SEA to any desired precise length shall be possible by means of electrical input of suitable polarity at the interface connector.

The following requirements apply:

## 3.2 Detail Design Requirements

The requirements delineated by this specification, unless otherwise noted, apply to all prototype and flight units.

### 3.2.1 Extendable Booms

All booms will be of tubular cross section split longitudinally so that the cross section may be flattened and rolled up for storage. The "free" edges of the split tube will overlap and digitate upon deployment to increase strength.

#### 3.2.1.1 Extended Length

400 ft. $\pm$ 3/4 ft.

Extended length of booms shall be measured from the center of the erection unit storage drum to its tip mass C.G.

#### 3.2.1.2 Diameter

booms - 3 in. $\pm$ 1/8 in.

#### 3.2.1.3 Wall Material

The boom material will be beryllium copper (berylco 25 or equivalent); silver plated on its outside diameter.

#### 3.2.1.4 Wall Thickness

Basic wall - 0.012 $\pm$ .0012

#### 3.2.1.5 Strip Width

10.000 $\pm$ .025

#### 3.2.1.6 Wall Overlap (Ref)

#### 3.2.1.7 Finish

The polish of the outside surface of the boom rods shall produce the lowest solar absorptance obtainable and shall not exceed a value of 0.15. Emissivity is not to be less than 0.05.

Suitable protection from sea level environments is to be provided the components in order to preserve the low absorptivity until deployment in orbit.

3.2.1.8 Straightness and Coordination

The entire length of the erected booms shall be within the volume described on the Figure 1 straightness envelopes regardless of the percentage of total boom length extended.

The center of gravity of each boom/tip mass assembly shall always lie within the confines of the straightness envelope of Figure 1, regardless of the percentage of total boom length extended.

3.2.1.9 Alignment

Each Boom Assembly will be externally identified by a GE approved method such that the centerline described in Figure 1 can be located in a three dimensional field.

3.2.1.10 Tip Mass

Each boom is to be provided with mass secured to its tip.

Each tip mass shall consist of a mount, a damper assembly and associated mounting hardware.

3.2.1.10.1 Damper

The damper shall conform to GE source control drawing

3.2.1.10.2 Damper Mount

The damper mount shall conform to GE source control drawing 47J214522.

3.2.2 Erection Units

The erection units shall consist of a spool or cassette on which the flattened tube may be rolled up and stored. Means shall be provided for unwinding the stowed boom and guiding it as it assumes its circular cross section. A method of stopping extension of the primary booms at a predetermined distance shall be required. The erection units shall be capable of retraction of the booms to any desired fine length in excess of 50' and adjustment at any desired length by means of electrical input of suitable polarity at the boom system interface connector. Extension, retraction, and adjustment of each primary boom pair is to be mechanically coordinated within the tolerance of paragraph 3.2.1.1.1. Each erection units is to be powered by a single electrically reversible DC type motor.

3.2.2.1 Caging, Release and Launch

The erection unit is to provide means of caging the tip mass associated with that boom during boost, and is to provide for timely release and launch of tip mass at the time of boom erection. The means of launching the tip mass is to be provided in such a way as to restrict loads on the tape to those which will not cause tape failure.

The uncaging of the tip mass is to be triggered by squib activated cable cutters and a release mechanism arrangement (marmon clamp).

The thrusters shall each employ a squib capable of producing enough gas pressure to release tip mass even if the other squib does not ignite.

The maximum no-fire current for each bridge wire circuit shall conform to paragraph 3.3.10. The minimum all-fire current shall conform to paragraph 3.3.10.

The cable cutters and squibs shall meet all the range safety requirements for Category "A" Ordnance Devices as delineated in NASA/GSFC specification HB-3, "Spacecraft Operations at A.M.R."

The release assembly shall conform to GE Drawing 47J214522. Mounting and activation of this assembly shall be as depicted on GE Drawing 47J214522.

3.2.2.2 Deployment Rates

| Extension | Retraction |
|---|---|
| 1.5 in/sec maximum | 1.5 in/sec maximum |
| 0.9 in/sec minimum | 0.6 in/sec minimum |

(when driven by deployment motor)

3.2.2.3 Deployment Accuracy

The erection units of the primary and damper booms shall be capable of repeatedly deploying the boom to the straightness and length tolerance of paragraph 3.2.1.

3.2.2.4 Stability

Throughout the duration of the mission, the erection units shall restrict changes in erected boom length to within $\pm$ 3/4 inch (exclusive of temperature effects

on the boom) as long as the motor circuit is open. The diameter of all erected boom is to remain within manufacturing tolerance.

3.2.3 Deployment Motor

Each deployment motor shall satisfy the following requirements:

Rated Voltage: 28 VDC + 2 VDC -6 VDC

| OPERATING CONDITION | APPLIED VOLTAGE (VDC) | MAXIMUM CURRENT (AMP) | |
|---|---|---|---|
| | | ARMATURE | BRAKE & FIELD |
| Normal Load | 28 | 1.5 | .75 |
| Stall at normal load and Initial Surge* | 28 | 12.0 | .75 |
| Max. Stall and Surge | 30 | 16.0 | 1.0 |

* Duration of initial surge - 3 seconds maximum.

NOTE: At no time, under any combination of operational and environmental conditions shall the total current of each extension motor exceed 27.0 amp maximum.

3.2.4 Telemetry

The electrical interconnection for the telemetry shall conform to GE SCD 47J214522.

3.2.4.1 Deployment Sensor

Each erection unit shall be equipped with a potentiometer type sensor capable of monitoring the extended length of the boom of that assembly.

Range: 0 to 500 feet

Accuracy: ± 15 inches (on position of each boom after ground calibration)

Input: -5 ± 0.01 VDC (being provided by GE)

Output: 0 to -5 volts (full scale range)

Output Impedance: 10,000 ohms maximum

3.2.4.2 Event Monitors

The boom system is to be equipped with microswitch type event monitors to detect the following functions:

(a) Boom full extension. Each monitor shall be coordinated to indicate simultaneously with the set of cutoff switches associated with that boom.

Each micro-switch is to be equipped with a center tap, one normally closed contact, and one normally open contact.

| | |
|---|---|
| Input (by GE): | -5 $\pm$ 0.01 VDC on N.O. contact, instrument ground on N.C. contact, return to telemetry on center tap. |
| Maximum Current: | 1 milliamp |
| Contact Resistance: | The contact resistance of each contact shall not exceed 50 milliohms. |

3.2.5 Motor Cut-off

A set of power limit switches is to be provided which will automatically cut-off extension motor power upon the reaching of fully extended length. The set of switches shall be coordinated to cutoff simultaneously with the telemetry full extension indication associated with that boom.

3.2.6 Magnetic Dipole

It is the design goal that the primary boom have a magnetic dipole of less than 350 pole-cm. The dipole magnitude and orientation of each component shall be measured and recorded. Measurements shall be made in both the active and passive condition on the assembly. Active condition of the Assembly for the purposes of this test shall be interpreted as meaning that the tip mass is removed from the structure.

3.3 Design and Construction

The boom system shall be designed and constructed in accordance with Drawings 47J214522 and shall conform to all requirements of this specification.

3.3.1 Interchangeability

All boom assemblies having the same manufacturer's part number shall be interchangeable as defined in MIL-STD-447. Changes in the vendor's part number shall be in accordance with Specification MIL-D-70327.

3.3.2 Electrical Connectors

Electrical connectors shall be specified on the GE source control drawing 47J214522.

3.3.3 Electronic Component Parts

Electronic component parts shall be selected from Drawing as specified by specification SVS , whenever the design dictates the use of parts within the category covered by the selected parts list.

MSFC PROC-256 shall be used as a guide in fabrication of all electrical parts.

3.3.4 Threads

Threads shall conform to Specification MIL-S-7742.

3.3.5 Screw Thread Locking Devices

All mating threaded parts shall be positively locked by safety wiring, selflocking devices, locking compound or other approved methods. Safety wire, if used, shall be in accordance with Standard MS 20995 and shall be installed in accordance with Standard MS 33540. Star washers and simple jamnuts shall not be used. Use of lockwashers shall be governed by the limitations set forth in Standard AND 10476.

3.3.6 Materials

3.3.6.1 Dissimilar Metals

Contact between dissimilar metals, as defined by Standard MS 33586, should be avoided. Where it is necessary that dissimilar metals be assembled in intimate contact with each other, an interposing insulating or mutually compatible material shall be used.

3.3.6.2 Fungus

Materials shall be inherently fungus inert or shall be treated by an approved method to resist fungus growth.

3.3.6.3 Selection

Material shall be selected from Drawing or shall have specific GE-MSD approval.

3.3.6.3.1 Magnetic Materials

Usage of all magnetic materials shall have GE-MSD approval.

3.3.6.4 Metals

Metal parts shall be inherently corrosion resistant or shall be protected against corrosion by means of chemical or electrolytic finishes and treatments which are not deleterious to the required function of the part.

3.3.6.5 Lubricants

Unless otherwise specified, dry film lubricant per MIL-M-7866 shall be utilized in the torque transmission gear trains of the assembly.

3.3.7 Finishes

Unless otherwise specified herein, all finishes shall be in accordance with GE Standard 118A1600.

3.3.8 Mounting

3.3.8.1 Damper Interface

GE drawing 47J214522 defines the mechanical interface with the damper assembly.

3.3.8.2 Vehicle Interface

GE drawing 47J214522 defines the electrical and mechanical interface with the vehicle.

3.3.9 Wiring

3.3.9.1 Circuit Isolation, Continuity and D. C. Resistance

The electrical wiring circuits of the assembly shall be isolated from each other and from frame ground as specified on GE Drawing 47J214522 and shall have the proper continuity and D. C. resistance.

3.3.9.2 Bridgewire Resistance

The electrical bridgewire resistance of the electro-explosive pressure cartridges shall conform to GE drawing 895D724.

3.3.9.3 Insulation Resistance

The insulation resistance of all wiring shall not be less than 10 megohms with 100 VDC applied between each pin isolated from frame ground and frame ground itself.

3.3.9.3 (continued)

The insulation resistance of each electroexplosive cartridge shall not be less than two (2) megohms when tested at 100 VDC for five (5) seconds. Insulation resistance shall be measured between the shorted bridge circuits and ground (case) and between bridgewire circuits.

3.3.9.4 Radio Interference Suppression

In the design of the boom system component, Specification MIL-I-26600 is to be used as a guide in the suppression of radio interference.

3.3.10 Ordnance Devices

All ordnance devices used in the boom system shall have minimum no-fire characteristics as follows for each bridge wire:

(a) 1 amp for 5 minutes (DC)
(b) 1 watt for 5 minutes (DC)

The probability of firing due to the above conditions shall be 0.001 or less at a confidence level of 95%.

The minimum all-fire current for each bridge wire shall be no greater than 3 amps (DC). The design firing current shall be no greater than 5 amps (DC).

The design shall allow ease of disassembly of all ordnance devices, both mechanically and electrically, in order to facilitate shipment of the ordnance device to the launch complex in a container separate from the boom system, while maintaining the integrity of the boom system assembly involved. Said disassembly may take the form of removal of the ignitor or removal of the entire ordnance activated device.

3.3.11 Weights

The boom system components shall not exceed weights of:

| | |
|---|---|
| Erection Unit (without tip mass ) | 300# max. |
| Each tip mass | 225# max. |
| Total ½ system | 525# max. |

3.3.12 Structural Integrity

All boom system components are to be designed to survive all loads imposed by the environments and performance tests delineated in section 4, considering initial spacecraft spin rates of $1^{o}$/sec about any axis. In any case, every boom must be capable of sustaining a 0.5 ft-lb bending moment without damage.

## 3.4 Performance

Each assembly shall be performance tested to meet the applicable portions of paragraph 3.2. Upon delivery of the minimum all-fire current to the electroexplosive pressure cartridges (squibs), the delivery of the full range of power to the deployment motor, for erection units, the appropriate device shall perform the desired function. Potentiometer calibration curves shall be supplied with each assembly for operation of the assembly while in orbit. Margins of safety (ability of motors to operate beyond the range of specified input voltages) should also be supplied with these calibration curves. Calibration curves should be the operating parameter vs telemetry output voltage.

### 3.4.1 Tip Mass Release

After uncaging of the damper by delivery of the minimum all-fire current to the electroexplosive pressure cartridges (squibs) application of specification voltages to the deployment motor shall result in uncaging and release of tip mass in the Assembly.

### 3.4.2 Deployment.

All deployment tests shall be full length deployments. Initial starts should be at low voltage for all full length deployments. Enough tests shall be conducted to obtain sufficient correlation between the telemetry sensor monitor and extended length at minimum and maximum rated deployment motor voltages for both extension and retraction. Enough tests shall be conducted to establish the adequacy of the coordination of the motor cutoff and telemetry switches for each erection unit at full extension with minimum and maximum rated deployment motor voltages.

## 3.5 Service Conditions

The boom system components shall be designed to be capable of meeting the requirements of 3.4 under any natural combination of the conditions specified in 3.5.1 after exposure to any natural combination of the conditions specified in 3.5.2.

3.5.1 Operating

The boom system components shall be designed to be capable of satisfactory operation while exposed to the following conditions or any natural combination of these conditions.

3.5.1.1 Radiation

Total accumulative radiation shall be $1.8 \times 10^5$ RADS (air)

3.5.1.2 Temperature

$-7^{\circ}$ C to $+ 49^{\circ}$C

3.5.1.3 Pressure

$10^{-10}$ mm Hg.

3.5.2 Non-Operating

The boom system components shall be capable of satisfactory operation after prolonged exposure to the following conditions or any natural combination of these conditions.

3.5.2.1 Temperature

$-30^{\circ}$ C to $+ 60^{\circ}$ C

3.5.2.2 Pressure

1 atmosphere to $10^{-10}$ mm Hg

3.3.2.3 Humidity

90% $\pm$ 3% at $+ 30^{\circ}$ C $\pm 2^{\circ}$ C

3.5.2.4 Vibration

(including damper caging mechanism with linear actuators and squibs)

Each assembly except the component qualification assembly will be subjected to the sinusoidal and random vibration environments delineated in Tables 1 and 2 at the points where the assembly is attached to the spacecraft structure.

The component qualification assembly will be subjected to the sinusoidal and random vibration environments delineated in Tables 3 and 4 at the points where the assembly is attached to the spacecraft structure.

3.5.2.5 Acceleration

Each component qualification assembly will be subjected to the accelerations specified in section 4.

3.6 Life

The boom system components shall be designed to meet the life requirements of 3.6.1 and 3.6.2.

3.6.1 Operating

The boom system shall be capable of operating for the cycles specified herein. These numbers of cycles are representative of the cycles accumulated during all operational checks and full mission life of 3 years in orbit.

| | |
|---|---|
| Extensions and retractions | 50 cycles |
| Tip mass caging and uncaging | 50 cycles (at least 3 pyrotechnic) |
| Damper uncaging | 50 cycles (at least 3 pyrotechnic) |

3.6.2 Storage

The boom system components shall be capable of meeting the requirements of 3.6.1 after a one-year period under the following environmental storage conditions:

(in storage containers compatible with the spacecraft as required)

| | |
|---|---|
| Temperature | $70^{o}$ F $\pm$ $10^{o}$ F |
| Humidity | 50% relative or less |

3.7 Drawings

Drawings format shall be in accordance with the requirements of Specification MIL-D-70327.

3.8 Nameplates and Markings

The boom system components shall be marked in accordance with a nameplate drawing approved by GE.

3.9 Serial Number

Each boom system erection unit shall be identified by a vendor assigned serial number according to the requirements of GE SI No. 217260, paragraph 4.4.

3.10 Workmanship

The boom system components shall be constructed in a thoroughly workmanlike manner. Particular attention shall be paid to neatness and thoroughness of soldering, wiring, impregnation of coils, marking of parts and assemblies, plating, painting, riveting, machine screw assemblage, welding, brazing and freedom of parts from burrs and sharp edges.

3.11 Cleanliness

Materials and parts shall be manufactured in such a manner as to provide freedom from residual contaminates, such as corrosion inhibiting oils, greases, dust and dirt particles, and machining chips which might contaminate the boom system prior to and after launching. "Clean Room" facilities consistent with Class III or IV requirements of Document T.O. 00-25-203 are recommended practice for obtaining the desired level of cleanliness, but are not mandatory.

## 4.0 QUALIFICATION AND ACCEPTANCE TESTS (QUALITY ASSURANCE PROVISIONS)

To insure satisfactory quality, compliance with the requirements of Section 3 of this specification shall be demonstrated by subjecting each unit to the tests and procedures defined herein. The control requirements of Specification NPC 200-3 shall apply.

4.1 Classification of Tests

The inspection and testing of the boom system shall be classified as follows:

4.1.1 Acceptance Tests

Each boom system, except the system for component qualification, shall be subjected to the tests herein, in the order shown.

4.1.2 Qualification Tests

A boom system for component qualification shall be subjected to the tests herein, in the order shown.

4.2 General

Selection of test items, test facilities, standard test conditions, test reports and procedures in the event of failures shall be in accordance with Specification S2-0102.

4.2.1 Test Reports

Test reports shall be prepared and submitted for each qualification and acceptance unit. MIL-STD-831 shall be used as a guide in preparing test data.

4.3 Examination of Product

4.3.1 Visual and Mechanical Inspection

Each boom system component shall be visually and mechanically inspected to determine that the materials, finish, reflectivity, adhesion, design, workmanship, construction, weight, dimensions and markings conform to the applicable drawings and to the requirements of this specification. Reflectivity and adhesion shall be conducted on samples obtained from installed booms prior to obtaining proper length.

4.3.2 Circuit Isolation, Continuity and DC. Resistance

The assembly shall conform to the electrical requirements of GE Drawing 47J214522 as specified in Section 3, when measured with a voltmeter or ohmmeter.

4.3.3 Bridge Wire Resistance

The electroexplosive pressure cartridges utilized in each assembly shall conform to the bridge wire resistance requirements of GE Drawing 895D724 as specified in Section 3.

4.3.4 Insulation Resistance

The boom system shall conform to the requirements of Section 3 when measured in accordance with Method 302 of Standard MIL-STD-202.

4.3.5 Straightness and Alignment

Straightness and alignment measurements to determine the satisfaction of the requirements of Section 3 are to be made in a simulated zero "g" facility, such as a water flotation tank, while each boom is mounted to the erection unit in which it will be delivered and the erection units are in the structure in which they will be delivered. A plot of extended boom centerline in three dimensions relative to fiducial marks on the erection unit is to be delivered as part of the inspection record of each boom. The centerline is to be plotted a minimum of four times to an accuracy of $\pm$0.2 inches. Measurements shall be taken with booms extended to full length, 75%

full length, 55% full length and 35% full length and shall be at maximum extended length, 75% extended length, 40% extended length and 10 feet for each of the above extended lengths, for the Qualification component. All other components will have measurements taken with booms extended to full length only.

4.3.6 Magnetic Dipole

The boom system components shall conform to the magnetic dipole requirements specified in Section 3 by establishing a known magnetic field with helmholtz coils and measuring the component dipole with a magnetometer or gaussmeter.

4.4 Performance

When performance is to be monitored prior to, during, or after the acceptance and qualification environmental tests, each assembly shall be subjected to tests to insure compliance with the performance characteristics of this specification, unless modified herein.

Unless otherwise specified herein, tests may be conducted without the use of a GE approved test track and without tip weights attached. Sequence of tests is optional.

4.4.1 Deployment

a. Electroexplosive Actuation and Damper Uncaging
b. Tip mass release and launch
c. Deployment rate
d. Deployment telemetry monitor (pot calibration)
e. Deployment Length (full)
f. Motor deactivation telemetry monitor
g. Motor deactivation

4.5 Acceptance Tests Sequence

| | | |
|---|---|---|
| a. | Physical Inspection | Per Par. 4.3, except 4.3.5 and 4.3.6 |
| b. | Performance | Per Par. 4.4.1 |
| c. | Vibration | Per Par. 4.7.2 (Random only) |
| d. | Physical Inspection | Per Par. 4.3 |
| e. | Thermal vacuum/performance | Per Par. 4.7.3 4.4.1.a<br>4.4.1.b<br>4.4.1.e (3 ft.max.) |
| f. | Performance | With No Test Track: Per Par. 4.4.1.b<br>With Test Track: Per Par. 4.4.1 except 4.4.1.a |
| g. | Physical Inspection | Per Par. 4.3 |

4.6 Qualification Tests Sequence

| | | |
|---|---|---|
| a. | Physical Inspection | Per Par. 4.3 Except 4.3.6 |
| b. | Performance | Per Par. 4.4.1 |
| c. | Humidity | Per Par. 4.7.4 |
| d. | Physical Inspection, reflectivity and adhesion | Per Par. 4.3 Except 4.3.5 and 4.3.6 |
| e. | Vibration | Per Par. 4.7.2 |
| f. | Physical Inspection | Per Par. 4.3 except 4.3.5 and 4.3.6 |
| g. | Acceleration | Per Par. 4.7.5 |
| h. | Physical Inspection | Per Par. 4.3 Except 4.3.5 and 4.3.6 |
| i. | Thermal vacuum performance | Per Par. 4.7.3 4.4.1.a<br>4.4.1.b<br>4.4.1.e (3 ft.max.) |

| | | With Test Track | With No Test Track |
|---|---|---|---|
| j. | Performance | Per Par. 4.4.1 except 4.4.1.a | Per Par. 4.4.1.b |
| k. | Physical Inspection | Per Par. 4.3 | |

4.7 Test Methods

4.7.1 Configurations

For the purposes of paragraph 4.7 the configuration described in this paragraph shall be referred to as a component.

One boom with erection unit (stowed condition) mounted to the associated drive train, tip mass, release mechanism, and support structure.

4.7.2 Vibration

Attachment of the component to the vibration generator shall be made a rigid fixture.

Vibration shall be applied in each of three orthogonal directions, one direction being parallel to the thrust axis. The component shall be placed in non-operational condition normal to boost insertion phase during the vibration test.

Any indication of instability in performance of the component during any phase of the vibration schedule shall be reported. As a minimum, the report shall state the frequency or frequency bandwidth where instability and resonance were detected and the axis of the subassembly found to be most sensitive to vibratory excitation.

For the purpose of controlling vibration applied to the test article, a calibrated accelerometer shall be attached rigidly on the fixture near the component structure, trued with the axis of applied vibration. As an alternate to a recording accelerometer, the X-Y plot record of the control accelerometer may be sufficient for the permanent record of vibration in this direction. For recording in the other two directions, two recording accelerometers - oriented so that their axes are mutually perpendicular to the control accelerometer - shall be located on the fixture near the interface, between the fixture and the component.

4.7.2.1 Vibration Schedule

Vibration schedules are as follows:

Acceptance - as specified in Tables 1 and 2

Qualification - as specified in Tables 3 and 4

4.7.2.2 Sinusoidal Vibration Records

The three recorder accelerometer signals shall be recorded continuously during all sinusoidal tests. Due care shall be exercised to calibrate the overall system for frequency response and amplitude linearity characteristics to values of 1.25 times the maximum expected to be recorded during tests.

Permanent records shall be made, properly identified, and retained to demonstrate conformance with this specification.

4.7.2.3 Random Vibration Records

During the random vibration tests, the signal from the control accelerometer shall be passed through a spectrum analyzer having the following characteristics:

a. Filter bandwidth not to exceed 25 cps below 100 cps or 50 cps above 100 cps.

b. Averaging time (seconds) at least 75 divided by the filter bandwidth (cps).

c. If a tape loop is used for analysis, the sample length (seconds) shall be at least 150 divided by the filter bandwidth (cps).

Permanent records shall be made during the specified random vibration tests and properly labeled to demonstrate conformance with this specification.

4.7.2.4 Sinusoidal-Swept Frequency

This portion of the test shall be conducted by sweeping the applied frequency once through each range specified in the schedule. The rate of change of frequency shall be as follows:

Acceptance - 4 octaves per minute

Qualification - 2 octaves per minute

4.7.2.5 Random Motion Vibration

Gaussian random vibration shall be applied with the "g-peaks" clipped at three times the root-mean-square acceleration specified in the schedule. With the component installed the control accelerometer responses shall be equalized such that the specified power spectral density (PSD) values are within $\pm 3$ db throughout the frequency band as determined by the analysis specified in 4.7.2.3. The filter roll-off characteristic above 200 cps shall be at a rate of 40 db/octave or greater.

4.7.3 Thermal Vacuum

The component shall be attached to a mounting fixture in a manner which simulates the attachment of the component to the spacecraft structure, including heat capacity and thermal conductivity. If this is not possible, the component shall be mounted in such a manner that it is thermally isolated from its mounting fixture. The mounting fixture for this purpose shall be designed to minimize interference of radiation paths from

the radiant sources to the component.

The component shall be installed in the test chamber in such a way that it will not be exposed to any abnormally hot or cold source. Thermocouples shall be attached to the component in sufficient number and at such locations where the highest and lowest component temperatures are expected to occur. Component pressure and temperature sensors shall be monitored during thermal vacuum.

4.7.3.1 Low Temperature Vacuum

Exposure temperatures are as follows:

| | | |
|---|---|---|
| Acceptance | - | as specified in paragraph 3.5.1.2 |
| Qualification | - | $10^{\circ}$ C $\pm$ $2^{\circ}$ C below paragraph 3.5.1.2 minimum temperature |

Exposure period (after stabilization) are as follows:

| | | |
|---|---|---|
| Acceptance | - | 12 hours |
| Qualification | - | 24 hours |

With the component non-operating the pressure and temperature of the chamber shall be decreased until the mounting surface temperature sensor on the component surface registers the appropriate exposure temperature, and the pressure sensor registers $1 \times 10^{-5}$ mm Hg or lower. The temperature of the chamber shall then be stabilized.

Stabilization shall be assumed when indication from each thermocouple attached to the component does not change by more than $2.0^{\circ}$ C per hour. The chamber controls shall be held fixed and the primary boom operated periodically during the appropriate exposure period. The temperature of the component shall be monitored continuously during the exposure period.

The performance of the assembly shall be in accordance with paragraph 4.5 or 4.6, whichever is applicable. The cyclically-operated component (on-off orbital operation) cold start capability shall be demonstrated at least three times during the exposure period. The cycle of operation shall be preceded by returning to stabilized conditions at the minimum temperature specified above.

4.7.3.2 High Temperature Vacuum

Exposure temperatures are as follows:

| | | |
|---|---|---|
| Acceptance | - | as specified in paragraph 3.5.1.2 |
| Qualification | - | $10^{\circ}$ C $\pm$ $2^{\circ}$ C above paragraph 3.5.1.2 maximum temperature |

Exposure period (after stabilization) are as follows:

| | | |
|---|---|---|
| Acceptance | - | 12 hours |
| Qualification | - | 24 hours |

At the conclusion of the low temperature vacuum exposure, the chamber temperature shall be increased until the mounting surface temperature sensor on the component registers the appropriate exposure temperature and the chamber pressure is $1 \times 10^{-5}$ mm Hg or lower, whereupon the test specimen shall be placed in non-operating mode and the temperature of the chamber stabilized.

stabilization shall be assumed when indication from each thermocouple does not change by more than $2.0^{\circ}$ C per hour. When stable conditions have been achieved, the chamber temperature controls shall be held fixed, and the primary boom operated periodically during the appropriate exposure period. The components shall have their temperature monitored continuously during the exposure period.

The performance of the assembly shall be in accordance with paragraph 4.5 or 4.6 whichever is applicable. The component shall be placed in a non-operating mode while returning the component to ambient conditions.

4.7.4 Humidity (Qualification)

The component shall be installed in a temperature humidity chamber where the atmospheric conditions in the immediate vicinity of the component is as follows, and in which the air is constantly circulated by a fan:

| | |
|---|---|
| Temperature | $30^{\circ}$C $\pm$ $2^{\circ}$C |
| Humidity - relative | 90% |

4.7.5 Acceleration (Qualification)

The component shall be attached to a mounting fixture in a manner which simulates the actual mountings of the component to the spacecraft structure.

The differing acceleration levels imposed by the centrifuge across the component being tested shall not vary from the specified acceleration by more than ± 10%. The acceleration specified shall be applied at the c.g. of the component and shall not vary at the c.g. by more than ± 1.0 g or ± 5%, whichever is greater. The duration of the exposure shall be three minutes.

Thrust

The mounting fixture shall be attached to the acceleration equipment (centrifuge) so that the component may have the acceleration applied in the thrust axis (Z-Z) (See Figure 3). The applied acceleration shall be 13.0 g ± 1.0 g in the thrust axis.

Spin

The mounting fixture shall be attached to the acceleration equipment (centrifuge) so that the component may have the acceleration applied in the spin axis (X-X) (See Figure 3). The expected spin rate during ground testing is 120 rpm.

Resultant r

The mounting fixture shall be attached to the acceleration equipment (centrifuge) so that the component may have acceleration applied in the direction of the resultant "(A)" of the acceleration due to thrust (Z-Z) and spin (X-X). (See Figure 3). The magnitude of the acceleration to be applied in this direction shall be determined by the formula:

$$A = \sqrt{A_t^2 + (.0000426\ r\ N^2)^2}$$

where:

A = resultant acceleration for the component in "g's"

$A_t$ = 13.0 "g's" (1.5 times maximum expected thrust acceleration of the apogee motor)

r = radius in inches from the spin axis of the spacecraft to the c.g. of the component.

N = 150 rpm (maximum spin rates expected in flight in revolutions per minute)

## 5.0 PREPARATION FOR DELIVERY

5.1 Each boom system component shall be prepared for delivery in accordance with Specification 146A9560.

General Electric Company
Spacecraft Department
Valley Forge Space Technology Center
Box 8555
Philadelphia, Pennsylvania 19101

Specification
Issued:

# MAGNETIC ANCHORED VISCOUS DAMPER ASSEMBLY

## SATURN IV B

PREPARED BY: _____ DATE: _____
R. Knipe, Dev. Eng. Mech. Des.
Electromechanical Control Equipment Eng.

APPROVED BY: _____ DATE: _____
E. J. Buerger, Manager
Electromechanical Control Equipment Eng.

REVIEWED BY: _____ DATE: _____
R. C. McGinn, Engineer
Quality Control and Test

APPROVED BY: _____ DATE: _____
P. Weygandt

ISSUED BY: _____ DATE: _____
Print Control & Reproduction

General Electric Company
Spacecraft Department
Valley Forge Space Technology Center
P. O. Box 8555
Philadelphia, Pennsylvania 19101



# MAGNETIC ANCHORED VISCOUS DAMPER ASSEMBLY

SATURN IV B

## 1.0 SCOPE

1.1 This specification covers the design, fabrication and test requirements for a magnetic anchored viscous damper.

## 2.0 APPLICABLE DOCUMENTS

2.1 Documents - The following documents of the exact issue shown form a part of this specification to the extent of being a guide and to the extent specifically stated herein.

MILITARY

| | |
|---|---|
| MIL-D-5028 | Preparation of Manufacturer Drawings and Data Lists |
| MIL-D-5480D 5 February 1959 | Reproduction of Engineering and Technical Data |
| MIL-I-45208A | Inspection System Requirements |
| MIL-D-70327 27 March 1962 | Engineering Drawings and Associated Lists |
| MIL N-25027B | Nut, Self Locking |
| MIL E-5272 | Environmental Testing, Aeronautical and Associated Equipment |
| MIL-S-22473B | Sealing Compounds, Retaining, Single Component, Anaerobic |
| MIL-I-8500 | Interchangeability of Parts |

STANDARDS

| | |
|---|---|
| MIL-STD-30A | Associated Lists, Lists of Material, Data List, Index List |
| MIL-STD-31 1 April 1959 | Numbering and Coding of Engineering Drawings, Associated Lists and Documents |
| MIL-STD-143A | Specifications and Standards Order of Preference |
| MS 33588 | Nuts and Plate Nuts, Self Locking Design and Usage |

STANDARDS (continued)

| | |
|---|---|
| MS 33586 | Metals, Definition of Dissimilar |
| MS 35540 | Safety Wiring, General Practices for |
| MS 20995 | Wire, Lock |
| MIL-STD-129B | Marking for Shipment and Storage |

OTHER

| | |
|---|---|
| ANA Bulletin 438 | Age Controls of Age Sensitive Elastomeric Items |

SPECIFICATIONS

| | |
|---|---|
| 171A4211 Rev. B | Pyrolytic Graphite |
| 171A4161 | Application of D4D Thermal Control Coating |
| 118A1526 | Identification Marking |

DRAWINGS

(Later)

## 3.0 REQUIREMENTS

3.1 Qualification - The qualification of the damper shall be in accordance with the tests specified in Section 4 of this document.

3.2 General Description - The multi-axis passive damper consists of two concentric spheres separated by a damping fluid. A permanent magnet installed in the inner sphere provides an anchoring torque referenced to the earth's magnetic field, and supplies a centering action through repulsion of a diamagnetic (pyrolytic graphite) liner in the outer sphere.

3.3 Design and Construction

3.3.1 Materials - Materials shall be selected using MIL-STD-143 as a guide. Selection shall be made with special attention being given to the requirements of temperature, temperature change, thermal conductivity, vibration, loads compatibility, and other environmental conditions. Attention shall also be given to reliability, reparability, and lightweight construction. When necessary to use other than standard materials, the manufacturer shall base his selection on tests to prove suitability for the intended purpose.

3.3.1.1 Metals - All metals used in the construction of the damping unit shall be of a corrosion-resistant type, or shall be suitably protected to resist corrosion during the normal service life of the system, when in storage or during service use. Dissimilar metals as defined by MS 33586, shall not be used in intimate contact with each other unless suitably protected against electrolytic corrosion. Zinc and cadmium shall not be used as materials in alloys, in solders, in surface coatings or platings or in any other manner.

3.3.2 Protective Treatment - When materials are used in the construction of the damping unit that are subject to deterioration when exposed to climatic and environmental conditions likely to occur during service usage, they shall be protected against such deterioration in such a manner that they will not crack, chip, or scale with age or extremes of climatic and environmental conditions.

3.3.3 Installation - The installation requirements and mounting directions shall be in accordance with GE/SD drawing number (later). This drawing will define the required space envelope and mounting provisions.

3.3.4 Interchangeability - The requirements of MIL-I-8500 shall not apply; however, removable components shall be replaceable with like components to the degree practicable.

3.3.5 Construction - All components of the damping unit shall be constructed to withstand the strains, shock vibration, pressures, load factors, and other conditions incident to shipping, storage, installation and service use.

3.3.5.1 Load Factors - The damping unit shall be designed to withstand accelerations of 4.6g in both directions along the three orthagonal axes. Five (5) periods of five (5) minutes each shall be completed in each direction.

3.3.5.2 Locking of Parts - All threaded parts shall be locked by safety wire, by self-locking nuts conforming to MIL-N-25027, or by other approved methods. Safety wire shall be installed in accordance with MS 33540 and shall conform to MS 20995. The safety wire shall be non-magnetic (aluminum). Self locking nuts shall be used in accordance with MS 33588; they shall not be used where loosening or disengagement of the nut could result in the nut or other parts entering the canister or other structure. Any threaded parts locked in place with a sealing compound shall be in accordance with MIL-S-22473B.

3.3.5.3 Age Controls - All components containing synthetic rubber or other developed seal material parts shall be identified and dated in accordance with ANA Bulletin 438. The use of tags is not permissible.

3.3.5.4 Cleanliness - The presence of even minute particles of ferrous material in the damper can degrade centering performance. Prior to assembly all parts except graphite hemispheres shall be ultrasonically cleaned where possible, and all assembly work shall be performed under standard clean room conditions.

3.3.6 General Requirements - The damper unit shall meet the physical requirements of the following paragraphs.

3.3.6.1 Volume - The total volume of the complete unit shall be the lowest consistent with the specified damping requirements of paragraph 3.5 and with paragraph 3.3.3.

3.3.6.2 Weight - The damper weight shall not exceed 224 pounds. The damper shall be weighed and tagged after final assembly.

3.3.6.3 Mounting Arrangement - The unit shall be fabricated in a manner that allows ease of installation in the vehicle. The exact mounting arrangement shall be in accordance with Drawing No. (later)

3.3.6.4 Leakage - The unit, subjected to the temperature and pressure extremes of paragraphs 3.4.1 and 3.4.2, shall show no evidence of leakage of its viscous fluid. The unit shall meet the requirements of paragraph 4.2.2.

3.3.6.5 Inner Sphere Assembly - Prior to the installation of the bellows into the inner sphere, a pressure vs stroke plot shall be established by test. The pressure required to position the bellows at its midpoint ($P_B$) shall be recorded. The inner sphere assembly shall be evacuated and then filled with one atmosphere of argon gas. The atmospheric pressure shall be recorded.

3.3.6.6 Storage - The unit shall be packaged for storage in a manner such that inadvertent storage in an adverse environment (i.e., extremes of temperature and high magnetic fields) will not degrade performance of the unit by more than 5 percent in 6 months.

3.3.6.7 Life - The unit shall have an operational life of one year.

3.3.6.8 Magnetic Fields - The unit shall not be moved through or placed in magnetic fields (either AC or DC) greater than 10 oersteds peak.

3.3.6.9 Internal Pressure - At no time shall a pressure differential greater than 15 psi be applied across the bellows. Thus, all bellows and weld joint leak tests shall be limited to 15 psi pressure differential. After welding, each subassembly shall not be pressurized higher than 15 psi for any reason. The subassemblies shall be tagged stating so. The tags are to be removed prior to assembly into another subassembly or after filling (par. 4.2.6).

3.3.6.10 Serial Number - The damper shall be assigned a serial number and marked per 118A1526 Class 21.

3.3.6.11 Thermal Coating - A thermal coating of D4D shall be applied per 171A4161.

3.3.6.12 Handling - Special precautions shall be exercised in handling the large segmented magnet before and after it is assembled into the inner sphere. These precautions are in addition to that specified in 3.3.6.8. The purpose is to prevent the forces of attraction from damaging the graphite or other parts due to direct loads or draging loads resulting from the damper being moved while the magnet is being attracted to stationary iron. The magnet shall be prevented from coming closer than two inches from any iron.

3.3.6.13 Buoyancy - By removing material from the buoyancy adjustment plug, the inner sphere shall be made neutrally buoyant to $\pm$ .05 lb. at room temperature in damper fluid of the specific gravity to be used.

3.4 Operating Environment - In general, MIL-E-5272 shall apply with particular emphasis on the following requirements. The damper shall operate under these conditions and meet the requirements of Paragraph 3.5.

3.4.1 Vacuum - The unit shall be capable of operating at any pressure between 30.5 inches of mercury and $8 \times 10^{-10}$ inches of mercury.

3.4.2 Temperature - The unit shall be capable of operating over the temperature range of -30°F to 135°F. But will meet the damping tolerances only at the temperature specified in 3.5.1.

3.5 Performance - The performance requirements are defined in the following subparagraphs.

3.5.1 Damping Coefficient - The combined damping coefficient shall be 60 $\pm$8% foot-pounds per radian per second at a component temperature of (later).

3.5.1.1 Eddy Current Damping - The eddy-current damping coefficient shall be approximately (later) foot-pounds per radian per second with the inner sphere centered within the outer sphere. The exact value of eddy current damping shall be established by testing.

3.5.1.2 Viscous Damping - After establishing the exact value of the eddy-current damping coefficient, the proper blend of silicone oil shall be used so that the combined damping coefficient is 60 ft. lbs./rad/sec at (later) $^{o}F$. The desired viscosity of the oil can be obtained from the following:

$$\mu = \frac{3\ t\ b}{8\ R^4}$$

where $\mu$ = viscosity, centipoise
$b$ = damping coefficient, dyne-cm/rad/sec
$t$ = gap, cm
$R$ = sphere radius, cm

The corresponding viscosity at 75°F (or room temperature) may be established from a viscosity-temperature curve for SF-96 silicone fluid.

3.5.2 Magnetic Dipole - The magnetic moment of the unit shall be 6,000,000 pole cm minimum.

3.5.3 Centering Force - Displacement of the inner sphere in the presence of earth's gravity environment can be restricted to avoid "sticking" and to comply with the damping coefficient limitation of paragraph 3.5.1. The centering force levels must comply with the following minimum requirements at maximum allowed deflections (with damper at room temperatures).

Minimum axial force = 100 dynes
Minimum radial force = 40 dynes

## 4.0 QUALITY ASSURANCE PROVISIONS

To insure satisfactory quality, compliance with the requirements of Section 3 of this specification shall be demonstrated by subjecting the damper assembly to the tests and procedures defined herein. The central requirements of Specification MIL-I-45208 shall apply.

4.1 Classification of Tests

4.1.1 Component Qualification Unit - The damper assembly shall be subjected to the following environmental and performance tests.

4.1.2 Examination of Product - The damper assembly shall be visually and mechanically inspected to determine that the materials, finish, workmanship, construction, weight, dimensions, and markings conform to the applicable drawings and to the requirements of this specification.

4.2 Prequalification Testing - The initial performance of the unit shall be verified by tests performed on the component parts prior to final assembly.

4.2.1 Diamagnetic Susceptibility - Pyrolytic graphite hemispheres in accordance with specification 171A4211 shall be used. The uniformity of the susceptibility of the graphite hemispheres shall be surveyed to locate any substantial areas of substandard performance. The repulsion force for a predetermined magnet dipole and gap shall be measured.

4.2.2 Leak Tests - The leak rates of the individual parts, seals, and weld joints shall be measured with mass spectrometer equipment. The following maximum leak rates of helium at 14.7 psi shall apply; the requirements of paragraph 3.3.6.9 shall be met.

a) Bellows - $1 \times 10^{-7}$ atm cc/sec
b) Inner sphere weld - $5 \times 10^{-8}$ atm cc/sec
c) Inner sphere assembly - $2 \times 10^{-7}$ atm cc/sec (argon instead of helium)
d) Outer sphere assembly - $2 \times 10^{-7}$ atm cc/sec (argon instead of helium)
e) Outer sphere weld - $5 \times 10^{-8}$ atm cc/sec.
f) Fill plug - no visual leaks of damping fluid after thermal-vacuum test.

4.2.3 Magnetic Moment - After final assembly, but before filling, the magnet shall have its dipole measured (inner sphere locked to the outer sphere). The requirements of paragraph 3.5.2 shall be met.

4.2.4 Centering Force - The centering force on the magnets two principal axis (axial and radial) shall be measured after assembly but before filling the unit.

4.2.5 Damping Fluid - The silicone damping fluid shall be certified for viscosity, viscosity/temperature gradient and cleanliness prior to filling the unit. The viscosity of the fluid shall be governed by the damping requirements of paragraph 3.5.1.

4.2.6 Filling - The filling operation shall be accomplished under vacuum conditions to avoid the formation of gas bubbles. After gravity fill is complete, the unit shall be opened to atmospheric pressure for damping tests. Prior to environmental testing, the damping unit shall be pressurized. The damper is to be pressurized until the bellows is at its midpoint at 75°F. The unit shall be sealed and lockwired at this condition.

4.2.7 Damping Coefficient - The damping coefficient shall be measured on a rate table and shall meet the requirements of paragraph 3.5.1. Eddy-current damping tests shall be performed prior to filling the damper with damping fluid. Tests may be made at room temperatures and results extrapolated in accordance with damping fluid data obtained in paragraph 4.2.5. The damping torque shall be measured at approximately 0.5 deg/sec and 1.0 deg/sec. in both directions. The computed damping coefficient shall meet requirements of paragraph 3.5.1.

4.2.8 Buoyancy - After filling the damper the buoyancy of the inner sphere shall be measured. The requirements of paragraph 3.3.6.13 shall be met.

4.3 Environmental Testing - Verification of the required operational performance of the damping unit shall be obtained by the following general plan. The unit shall be subjected to the following environment and shall then meet the requirements of paragraph 4.4.

The longitudinal axis is any axis parallel to the marmon clamp ring and should be designated by a scribe mark on the ring. The lateral axis is also parallel to the ring and at 90 degrees to the longitudinal axis. The third orthogonal axis is defined as the normal axis.

4.3.1 Acceleration - The damping unit shall be subjected to steady-state accelerations, of both polarities, along the three axes of the input triad for a period of not less than five (5) minutes. The steady state accelerations shall be the limit values as specified in paragraph 3.3.5.1.

4.3.2 Shock - After completion of all other requirements of paragraph 4.3, the damper shall be installed in the shock test machine and then subjected to shock testing as follows:

| Level | Duration | Pattern |
|---|---|---|
| 35g | 10 milli-sec | 3 axes triangular |
| 35g | 7.1 milli-sec | 1/2 sin wave |
| 35g | 5 milli-sec | rectangular |

One shock will be administered in each direction along each of the three axes for each pattern.

4.3.3 Vibration - The damping unit shall be subjected to transient vibration tests at a sweep rate of one minute per octave along each of the 3 axes as follows:

| Frequency | Intensity |
|---|---|
| 10 - 100 cps | 2.9 g |
| 100 - 280 cps | .0046 double amplitude displ. |
| 280 - 2000 cps | 20g peak |

4.3.4 Thermal/Vacuum - The damper shall be subjected to one cycle of temperature in a vacuum chamber at a pressure level of 1 X $10^{-5}$ mm/hg. The temperature cycle shall be in approximate accordance with the following profile. The temperature of the damper sphere will constitute the control temperature.

(Profile later)

4.4 Performance Testing - Verification of the required operational performance of the damping unit shall be obtained by the following tests.

4.4.1 Visual External Inspection - Immediately on removal of the unit from the vacuum chamber inspect the damper for evidence of silicone fluid leakage. There shall be no evidence of fluid leakage. Silicone fluid must be distinguished from any oil contamination from the vacuum pump if present.

4.4.2 Damping - Remove the seal cap and measure the damping coefficient of unit at an input rate of 1 deg/sec. in two directions of rotation. The coefficient shall meet the limits of paragraph 3.5.1.

4.4.3 Centering Force - After thoroughly removing the fluid from the damper, (NOTE: Retain fluid for future inspection) the centering force gradient shall be measured on two axes (axial and radial to the magnet). The performance shall meet the requirements of paragraph 3.5.3.

4.4.4 Magnetic Moment - The magnetic moment shall meet the requirements of paragraph 3.5.2.

# APPENDIX F

## ROD STRESS DURING EXTENSION

The influences of rod strength on spacecraft separation rates, deployment rates and retraction rates are discussed. The solutions to the problems are not rigorous, but can be classified as "engineering solutions" applicable in identifying the magnitude of significant problems and aiding in the establishment of system constraints. In general, numerical rather than closed form solutions are presented since the problems are non-linear in nature. The deployment of rods from a spacecraft having angular rates imposes bending moments on the rod due to centrifugal, Coriolis, and angular accelerations. Solutions are obtained that relate the tolerable combinations of spacecraft rate and rod extension rate based on the other physical parameters of the system. The problems associated with extension and retraction rates are generally related to the buckling phenomena that exist when a long slender rod with a tip mass is stopped or started at a finite length. The technique used to investigate this problem is to assume transfer of the kinetic energy of the tip mass into flexural strain energy of the rod in its buckled mode as determined by utilizing the differential equation of the deflection shape along with boundary conditions of axial and transverse inertial forces of the tip mass at the free end. Expressions are developed for determining the maximum bending moments and excursions. The results of the investigation indicate that careful consideration must be given when specifying allowable spacecraft separation rate errors, and erection and retraction rates in order to preclude structural problems.

This Appendix examines the systems constraints placed on spacecraft by structural aspects of long flexible rods with attached tip masses. Specifically the problems encountered with deployment and retraction are discusses. Generally speaking the majority of spacecraft that have such a system are gravity gradient stabilized and have anywhere from one to six such rods in the stabilization system. The intent of this section is to expose some of the perculiarities of long flexible rod systems and to present the results of analyses performed so that preliminary systems requirements that are influenced by structural limitations can be set with some degree of reality. The general solution to the majority of problems encountered are, unfortunately, time dependent and non-linear. Closed form solutions are

available in some cases when simplifying assumptions are made. The numerical solutions that are required can be set up without great difficulty and are especially suited for the desk side, time sharing, computer systems now in popular use with many aero-space organizations.

Table F-1. Symbols for Rod Dynamic Equations

$H_o$ = angular momentum vector

$I_o$ = inertia matrix about the center of body fixed coordinate axes

$\bar{\omega}$ = spacecraft angular velocity vector

$\bar{r}_\ell$ = position vector of tip mass in body fixed coordinate axes

$m_\ell$ = mass of tip mass

$\bar{S}_\ell$ = position vector of tip mass in inertial fixed coordinate axes

$\bar{a}$ = position vector from center of body fixed coordinate axes to base of deployable rod (Figure 1)

$\theta_1$, $\theta_2$ = angles locating $\bar{a}$ and deployment axes with respect to body fixed coordinate axes (Figure 1)

n = number of rods deployed

M = bending moment at base of rod

r, $\ell$ = deployed length of rod (Figure 1 or 4)

x, y, z = body fixed coordinate axes

Subscripts

$\ell$ = 1, 2, 3, n defines particular rod and tip mass

i, j, k = unit vectors corresponding to directions of x, y, z body fixed coordinates

Spacecraft Separation Rates

The deployment of rods from vehicles having spin and tumbling rates imposes bending moments on the rod due to centrifugal, angular, and Coriolis accelerations. In order to evaluate these effects it is best to simplify the problem by considering the case of symmetrical deployments and where the angular momentum vector coincides with one of the principle axes and remains fixed in the inerital frame of reference until the deployment is completed. With these assumptions extremely complex motions are avoided and the effects of the various parameters on the maximum root bending moments can best be evaluated. The system under consideration is shown in Figure F-1. The motion of the satellite will be described in reference to a set of body fixed coordinate axes (x, y, z) with an origin that coincides with the geometric and mass center of the spacecraft system. The angular momentum of the system can now be expressed vectorially as

$$\bar{H}_o = I_o \cdot \bar{\omega} + \sum_{\ell=1}^{n} \bar{r}_\ell \times m_\ell \dot{\bar{r}}_\ell \qquad (1)$$

and

$$\frac{d}{dt} \bar{H}_o = \frac{d}{dt} (I_o \cdot \bar{\omega}) + \bar{\omega} \times \sum_{\ell=1}^{n} \bar{r}_\ell \times m_\ell \dot{\bar{r}}_\ell + \sum_{\ell=1}^{n} \bar{r}_\ell \times m_\ell \ddot{\bar{r}}_\ell \qquad (2)$$

where

$$\frac{d}{dt} (I_o \cdot \bar{\omega}) = \dot{I}_o \cdot \bar{\omega} + I_o \cdot \dot{\bar{\omega}} + \bar{\omega} \times (I_o \cdot \bar{\omega})$$

and

$$\dot{I}_o \cdot \bar{\omega} = \sum_{\ell=1}^{n} \bar{r}_\ell \times (\bar{\omega} \times m_\ell \dot{\bar{r}}_\ell) + \sum_{\ell=1}^{n} \dot{\bar{r}}_\ell \times m_\ell (\bar{\omega} \times \bar{r}_\ell)$$

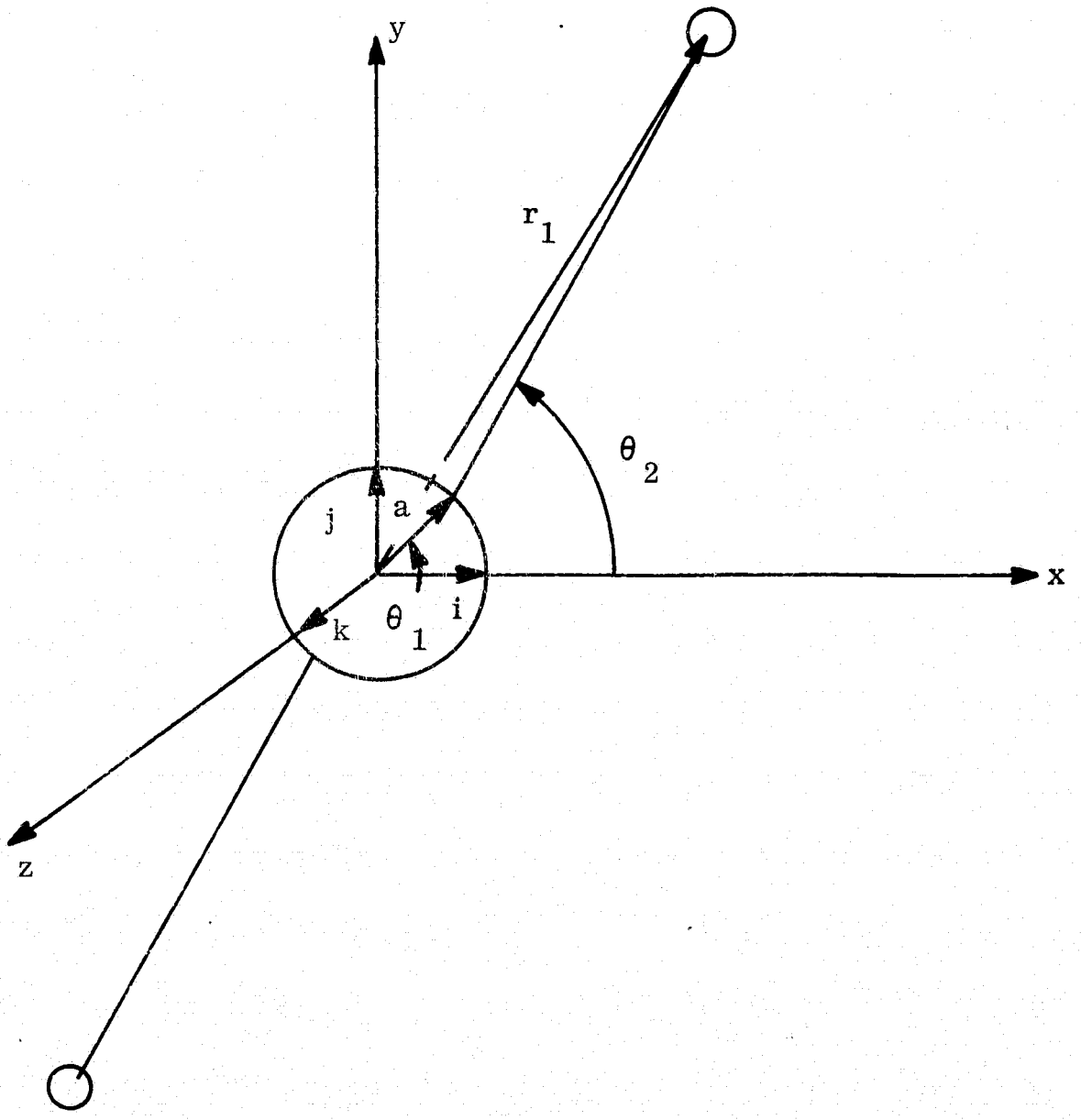


Figure F-1. Rod Deployment Model

The acceleration of the tip mass will be

$$\frac{d^2 S_\ell}{dt^2} = \ddot{\bar{r}}_\ell + \bar{\omega} \times (\bar{\omega} \times \bar{r}_\ell) + \dot{\bar{\omega}} \times \bar{r}_\ell + 2\bar{\omega} \times \dot{\bar{r}}_\ell \qquad (3)$$

and the bending moment applied to the base of the rod is

$$M = m_\ell \bar{r} \times \frac{d^2 S_\ell}{dt^2} = m_\ell \bar{r} \times \left[ \ddot{\bar{r}}_\ell + \bar{\omega} \times (\bar{\omega} \times \bar{r}_\ell) + \dot{\bar{\omega}} \times \bar{r}_\ell + 2\bar{\omega} \times \dot{\bar{r}}_\ell \right] \qquad (4)$$

Using the assumptions noted earlier, the following expressions for bending moments are obtained

for:

$$\omega_R = \omega \text{ (SPIN RATE)}$$

and

$$\omega_i = \omega_j = 0$$

$$M_k = m\Big[ \omega^2 ( a \cos\theta_1 + r \cos\theta_2) + \dot{\omega} (a \sin\theta_1 \, r \sin\theta_2) + 2\omega (\dot{r} \sin\theta_2) \Big] \, r \sin\theta_2 + m \Big[ -\omega^2 (a \sin\theta_2 + r \sin\theta_2) + \dot{\omega} ( a \cos\theta_1 + r \cos\theta_2) + 2\omega (\dot{r} \cos\theta_2) \Big] \, r \cos\theta_2$$

where

$$\omega = \frac{Ho}{n \; m \left[ (a^2 + r^2) + 2ar \cos(\theta_1 - \theta_2) \right] + I_o}$$

$$\dot{\omega} = \frac{-2\, r\, \omega \left[ r + a \cos (\theta_1 - \theta_2) \right] n\, m}{n\, m \left[ (a^2 + r^2) + 2ar \cos (\theta_1 - \theta_2) \right] + I_o}$$

Equation (5) expresses the bending moments developed for the deployment of n symmetrical rigid rods as a function of geometry, mass properties and system rates and is applicable when the initial angular momentum vector coincides with the spin axes. If we assume that the spacecraft is a point mass ($a = \theta_2 = 0$), the equation for bending moment reduces to

$$M = \frac{2\, r\, \dot{r}\, I_o\, m\, \omega_o}{(n\, m\, r^2 + I_o)^2} \qquad (6)$$

$$\omega = Ho/(n\, m\, r^2 + I_o)$$

The maximum moment will be

$$M_{max} = \frac{0.6495\, \dot{r} \sqrt{I_o\, m}\, \omega_o}{n} \qquad (7)$$

and the maximum moment will occur when

$$r = \frac{I_o}{n\, m} \qquad (8)$$

Equation (7) is a much simplified expression for the maximum bending moment. It is very useful in determining the approximate magnitude of the expected loading as well as indicating the degree to which erection rate, spin rate, tip mass, and vehicle inertia affect the maximum loads.

In order to estimate the magnitude of the problems anticipated on the S-IVB configuration, the following values were substituted in equation (7)

$m = 91\ KG = 6.22\ Slugs$

$I_o = 1,208,370\ KG\text{-}M^2 = 891,241\ Slug\text{-}Ft^2$

$r = 0.03\ M/sec = 0.1\ Ft/Sec$

$\omega_o = 0.0017\ rad/sec$

The maximum root moment becomes two foot pounds which is two orders of magnitude less than the critical failure load. Therefore, it is concluded that vehicle rates will not adversely affect the structural integrity of the rods for the anticipated deployment speeds and mass properties. Based on the large safety factor, the requirement for more exact analysis, considering the effects of non-symmetric deployment of flexible rods, is not considered necessary.